



UNIVERSITÀ DEGLI STUDI DI MILANO

FACOLTÀ DI SCIENZE E TECNOLOGIE

Dipartimento di Chimica

Corso di Dottorato di Ricerca in Chimica Industriale

XXXI Ciclo

***NOVEL Pt(II) AND Ir(III) COMPLEXES FOR NON-LINEAR
OPTICAL, LUMINESCENT AND BIOMEDICAL APPLICATIONS***

Mattia Fontani

R11405

Tutor: Chiar.ma Prof.ssa DOMINIQUE MARIE ROBERTO

Co-tutor: Prof.ssa CLAUDIA DRAGONETTI

A.A. 2017/2018

	AIM OF THE THESIS	1
I.	SECOND-ORDER NON-LINEAR OPTICAL PROPERTIES OF Pt(II) AND Ir(III) COMPLEXES	4
1.1.	Introduction to non-linear optics	4
1.2.	In solution studies and measurements of quadratic hyperpolarizability (β)	9
1.2.1.	Electric Field Induced Second Harmonic generation	9
1.2.2.	Hyper-Rayleigh Scattering	11
1.2.3.	Solvatochromic method	12
1.3.	Improvement of the second-order NLO properties in organic molecules	12
1.4.	Solid state measurement of quadratic hyperpolarizability	17
1.5.	Device building up	17
1.6.	Second-order NLO properties of metallorganic compounds	19
1.6.1.	Organometallic NLO-phores: response-structure correlation	19
1.6.2.	Second-order NLO properties of Pt complexes	25
1.7.	Novel Fullerene Platinum Alkynyl complexes	30
1.7.1.	Synthesis of the compounds 23-29	31
1.7.2.	Photophysics and second-order NLO measurements of compounds 23-29	33
1.7.3.	Conclusions	38
1.8.	Second-order non linear optics in Iridium complexes	39
1.9.	Novel neutral homo- and heteroleptics Ir(III) NLO-phores	43
1.9.1.	Conclusions	44
1.10.	Anionic Ir(III) NLO-phores	45
1.10.1.	Synthesis and characterization	46
1.10.1.1.	Synthesis of the anionic Iridium (III) complexes	46
1.10.1.2.	Characterization of Iridium derivatives	47
1.10.2.	EFISH measurements	48
1.10.3.	Conclusions	48
1.11.	References	50
II.	LUMINESCENCE IN Ir(III) COMPLEXES	61
2.1.	Introduction to luminescence	61
2.2.	Application of luminescent materials in solid state lighting	64
2.2.1.	OLED (Organic light-emitting diode) devices	66
2.3.	Organometallic complexes for luminescence	69
2.3.1.	Ir(III) complexes for luminescence	71

2.4.	Two novel luminescent homoleptic Ir(III)-NHC complexes	75
2.4.1.	Electrochemical studies and DFT calculations	76
2.4.2.	Photophysics	78
2.4.3.	Device fabrications	84
2.4.4.	Conclusions	89
2.5.	Two novel luminescent tetrahydrocurcumin bis(cyclometalated phenylpyridine) Ir(III) complexes	89
2.5.1.	Synthesis and characterization	90
2.5.1.1.	Synthesis of the neutral heteroleptic iridium (III) complexes	90
2.5.1.2.	Characterization	91
2.5.2.	Device fabrications	92
2.5.3.	Conclusions	93
2.6.	Promising applicability of the novel luminescent tetrahydrocurcumin bis(cyclometalated phenylpyridine) Ir(III) complex in the photodynamic therapy (PTD)	93
2.6.1.	Photodynamic therapy: introduction and state of art of antitumoral coordination compounds	93
2.6.2.	Curcuminoids and their complexes	99
2.6.3.	Two novel curcuminoid bis(cyclometalated phenylpyridine) Ir(III) complexes	101
2.6.3.1.	Photophysics studies	102
2.6.3.2.	Internalization studies	104
2.6.3.3.	Conclusions	110
2.7.	References	112
III.	EXPERIMENTAL SECTION	122
3.1.	General comments	122
3.2.	Synthesis of complexes	126
3.2.2.	Synthesis of compound 23 and 24	126
3.2.3.	Synthesis of complexes 25, 26 and 27	129
3.2.3.1.	Synthesis of complex 25	129
3.2.3.2.	Synthesis of complex 26	131
3.2.3.3.	Synthesis of complex 27	132
3.2.4.	Synthesis of compound 28 and complex 29	134
3.2.4.1.	Synthesis of compound 28	134
3.2.4.2.	Synthesis of complex 29	137

3.2.5.	Synthesis of the neutral heteroleptics Ir(III) complexes 56 and 57	138
3.2.5.1.	Synthesis of the complex 56	139
3.2.5.2.	Synthesis of the complex 57	140
3.2.6.	Synthesis of the anionic heteroleptics Ir(III) complexes 60_1 – 65_1	141
3.2.6.1.	Synthesis of the complex 60_1	141
3.2.6.2.	Synthesis of the complex 61_1	142
3.2.6.3.	Synthesis of the complex 62_1 and 62_2	142
3.2.6.4.	Synthesis of the complex 63_1 - 63_3	144
3.2.6.5.	Synthesis of the complex 64_1	147
3.2.6.6.	Synthesis of the complex 65_1	148
3.2.7.	Synthesis of the neutral homoleptic Ir(III) complex 59	148
3.2.8.	Synthesis of the neutral heteroleptics Ir(III) complex 70	151
3.3.	X-ray Crystallography of complex 58 and 59	151
3.4.	DFT calculations of complexes 58 and 59	154
3.5.	OLEDs fabrication	155
3.6.	Internalization studies	156
3.7.	References	159

AIM OF THE THESIS

Organometallic complexes with second-order non linear optical (NLO) and/or luminescent properties are of increasing interest as new molecular materials. They can provide indeed an additional flexibility, compared to purely organic compounds, given by active electronic charge-transfer transitions between the metal and the organic ligand; these transitions can be tuned in function of the metal nature, its oxidation state and coordination sphere.

My PhD thesis, which belongs to this research field, is developed in two principal lines:

1. Organometallic complexes characterized by second-order NLO properties;
2. Luminescent complexes.

The first line was dedicated to the synthesis of novel Platinum (II) and Iridium (III) complexes and to the evaluation of their second-order NLO response in solution by means of the Electric-Field Induced Second Harmonic (EFISH) generation technique. In particular, *push-pull* Platinum (II) complexes containing a Platinum (II) σ -acetylide moiety, acting as donor group, combined with a fullerene, acting as acceptor group, through a π -conjugated bridge have been investigated. In addition, since it is known that an increase of the π -conjugated bridge often leads to an enhancement of the second-order NLO response, the effect of the nature of the π -delocalized linker was studied.

Dealing with Iridium (III) organometallic compounds, both anionic and neutral complexes have been synthesized and examined. The investigation on Iridium (III) anionic complexes is particularly interesting, since, to my knowledge, no second-order NLO study has been carried out on this class of compounds so far. My aim was that of investigating the effect on the second-order NLO response produced by a variation of both organic bidentate C^N and ancillary ligands on the iridium centre.

Neutral Ir(III) complexes were mainly synthesized for luminescent studies, but since they could have also interesting second-order NLO features, their NLO response was also evaluated. These complexes can be divided in two classes:

- i. Neutral heteroleptic complexes in which the metal centre bears two cyclometallated phenylpyridines and a curcuminoid ligand (curcumin and tetrahydrocurcumin). Both these compounds showed a good NLO response in solution. Besides, the complex with curcumin demonstrated also satisfying second-order NLO properties in the solid state.

- ii. Neutral homoleptic complexes in which the metal centre bears three NHC-ligands. These complexes, result of my work in the laboratory of Prof. Eli Zysman-Colman of the St. Andrews University (Scotland, UK), showed a fair second-order NLO response.

The second line of my project involves luminescent Ir(III) neutral complexes. Two Ir(III) homoleptic complexes, bearing three NHC-ligands, demonstrated to possess remarkably optoelectronic properties and so were used to fabricate different OLEDs devices. In this dissertation all the fabricated devices will be presented. Remarkably, one of them resulted to be the best performing deep-blue emitting Ir(III) complexes-based OLED device reported so far.

The novel heteroleptic Ir(III) complex bearing tetrahydrocurcumin and two phenylpyridines was used for the preparation of another OLED device. It was shown that the introduction of two electronwithdrawing Fluorine atoms on the phenylpyridine ligands leads to a blue-shift of the emission; In fact, the complex bearing the unsubstituted phenylpyridines is a green emitter, while the one with the fluorinated phenylpyridines emits in the blue region of the visible spectrum.

Thanks to its remarkable and peculiar properties, the above heteroleptic Ir(III) complex bearing tetrahydrocurcumin and two cyclometallated phenylpyridines resulted to have promising features for applications in combined bio-imaging and Photo-Dynamic Therapies (PDT). The last part of this thesis indeed reports all the internalization studies about this complex, carried out in the IFOM-IEO biological institute in Milan.

I. SECOND-ORDER NON-LINEAR OPTICAL PROPERTIES OF Pt(II) AND Ir(III) COMPLEXES

1.1. Introduction to non-linear optics

Optics started to be applied since the ancient Egyptians and Mesopotamian civilizations, who first developed lenses. Further in Rome and Greece lenses were made by filling with water glass spheres. The most early theories can be found in Greek physicists and philosophers; the word *optics* derives indeed from the ancient Greek ὀπτική (optiké), which means “vision, seeing”.

Nowadays optics is that portion of physics studying light properties and how it behaves and interacts with matter.¹

Non-linear optics (NLO) is more recent and can be individuated with the invention of laser by Peter Franken in the 60s years of the last century.² Since that moment a huge number of scientific discoveries concerning non-linear optics have been made.³

NLO deals with those optical phenomena involving the interaction between a strong oscillating electromagnetic field (light for example) with particular molecules or bulk materials; after this interaction a second new electromagnetic field is emitted, which differs from the first one (the incident one) in phase, frequency or other optical properties.

The interaction between electromagnetic fields and molecules or materials produces a polarization in these latter. If the incident radiation is weak, it propagates itself linearly and the electrons polarize harmonically near the nuclei; this induces the generation of a wave characterized by same phase and intensity of the first one. In this situation when the external electric field hits molecules the polarization can be expressed as:

$$\vec{P} = \mu_0 + \alpha\vec{E} \quad \text{Eq. 1}$$

Where μ_0 is the dipole moment of the molecular ground state, α is the linear polarizability tensor, while \vec{E} is the external electric field.

Further, if the external electromagnetic field is strong enough, such as a laser beam, the radiation doesn't propagate in the medium linearly and electrons around the nuclei get a anharmonic polarization; the new wave such generated differs with respect to the incident one in phase, frequency, amplitude or other features.⁴

In these conditions the polarization can be described by a power series:

$$\vec{P} = \mu_0 + \alpha\vec{E} + \beta\vec{E}^2 + \gamma\vec{E}^3 + \dots \quad \text{Eq. 2}$$

Where β and γ are the non-linear quadratic and cubic hyperpolarizability tensors, respectively, which second and third order non-linear effects can be attributed to. Since β and $\gamma \ll \alpha$, it's easy to understand the reason why NLO was not studied before the invention of lasers and their application with strong electric fields. In order to observe a non-linear optical response, indeed, it is fundamental that the incident field has a minimum energy: $\vec{E} \geq 10^8\text{-}10^9$ V/cm. Only such powerful electric fields are able to perturb the electronic levels of a molecule or a material. The more the order of the non-linear optical effect increases, the less the hyperpolarizability tensors are in value; the efficiency (η) of a non-linear process is expressed as:

$$\eta \approx \frac{1}{\lambda_{laser}} \left(\frac{\vec{E}_{laser}}{\vec{E}_{atom}} \right)^{n-1} \quad \text{Eq.3}$$

Since $E_{laser} > E_{atom}$, for most of materials the effects higher than the third order ones have low efficiencies, therefore cannot be observed.

For materials, hence at macroscopic level, the polarization induced by a strong external electromagnetic field is given by:

$$\vec{P} = \vec{P}_0 + \chi_{(1)}\vec{E} + \chi_{(2)}\vec{E}^2 + \chi_{(3)}\vec{E}^3 + \dots + \chi_{(n)}\vec{E}^n \quad \text{Eq.4}$$

where \vec{P}_0 is the material static dipole, while $\chi_{(1)}$, $\chi_{(2)}$, $\chi_{(n)}$ are the linear, second, n-order electrical susceptibilities, respectively ($\chi_{(1)} = \sum \alpha$, $\chi_{(2)} = \sum \beta$, ...). The susceptibility terms from $\chi_{(2)}$ to $\chi_{(n)}$ characterize the non-linear optical response of the material. While in linear phenomena \vec{P} is proportional to the electric field intensity, in the case of higher order non-linear phenomena, for example second or third order, the relationship between \vec{P} and \vec{E} is not linear anymore, but is quadratic and cubic, respectively.

The perturbation or polarization, \vec{P} , induced by the external electric field, \vec{E} , can be represented as in Fig. 1⁽⁵⁾:

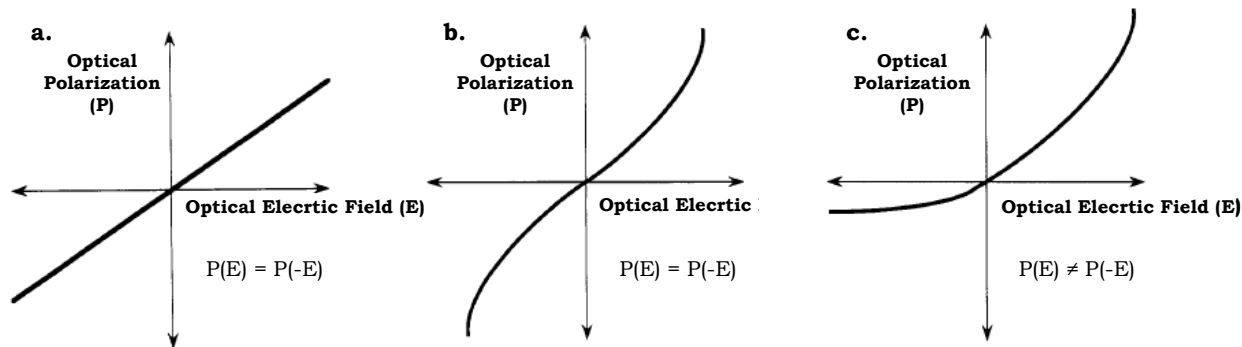


Figure 1. Representation of the polarization in (a) linear, (b) centrosymmetric non-linear, (c) non centrosymmetric non-linear materials.

From a graphical point of view it is possible to observe the linear response of the polarization when the applied electric field is relatively weak (Figure 1a). Different are the cases when the applied field is stronger, in which the response is non-linear indeed. Both β and $\chi_{(2)}$ go to zero in centrosymmetric molecules or materials, respectively (Figure 1b); this because for symmetry properties, the power series of \vec{P} cannot include even terms, such as β (or $\chi_{(2)}$). It's possible to better understand this by observing that if a positive field (+E) is applied to a molecule (or a material as a consequence) the second order non-linear term β (or $\chi_{(2)}$ if a material) induces a polarization of $+\beta E^2$ (or $+\chi_{(2)} E^2$); on the other hand, if the molecule (or the material) is irradiated by a negative electric field (-E), the response, reasonably, is $-\beta E^2$ (or $-\chi_{(2)} E^2$). Being the molecule (or the material) centrosymmetric, $\vec{P}_{ind}(+\vec{E}) = \vec{P}_{ind}(-\vec{E})$ and this leads to an overall β (or $\chi_{(2)}$) value equal to zero. This is not true for γ and $\chi_{(3)}$, which are the first non zero terms in the centrosymmetric media power series; with a positive applied field (+E), the response is γE^3 (or $+\chi_{(3)} E^3$ in the case of a material), while if the applied field is negative (-E), the response will be $-\gamma E^3$ (or $-\chi_{(3)} E^3$). The same is not valid for non centrosymmetric molecules or materials, for which the power series contains either even and odd terms; this means $\vec{P}_{ind}(+\vec{E}) \neq \vec{P}_{ind}(-\vec{E})$.

It follows that to obtain molecules or bulk materials with high second-order NLO response, high values of β or $\chi_{(2)}$ are required, respectively.

Oudar et co-workers in 1977 first gave a theoretical explanation of the electronic factors controlling the quadratic hyperpolarizability.⁶ In their studies on nitroanilines, they discovered that β can be splitted in two terms:

$$\beta = \beta_{CT} + \beta_{add} \quad \text{Eq.5}$$

Where β_{CT} is related to charge-transfer processes between a donor and an acceptor in the molecule, while β_{add} concerns interactions between the π -conjugated system and other

substituents. Since quadratic hyperpolarizability of a molecule is created by polarizable electrons mobility, under the action of a strong electric field \vec{E} associated with a powerful incident radiation, it follows that it is dependent on electronic transitions which, being associated with a significant electronic mobility, are of high CT character. If we consider a monodimensional molecule, its second-order NLO response will be mostly affected by one CT process, oriented along one axis (e.g. z); in this situation the β_{add} contribution is marginal, and can be neglected. β_{CT} therefore can be defined according to:

$$\beta_{\text{CT}} = \beta_{\text{zzz}} = \frac{3}{2h^2 c^2} \frac{\nu_{eg}^2 r_{eg}^2 \Delta\mu_{eg}}{(\nu_{eg}^2 - \nu_L^2)(\nu_{eg}^2 - 4\nu_L^2)} \quad \text{Eq.6}$$

where z is the axis of the CT transition direction, h is the Planck's constant, while c is the light speed in the vacuum, ν_{eg} (cm^{-1}) the frequency of the CT transition, r_{eg} the transition dipole moment, $\Delta\mu_{eg}$ the difference between excited state (μ_e) and ground state (μ_g) molecular dipole moments, and ν_L the frequency of the incident radiation. Equation 6 is the so-called "two level" model, used to estimate the frequency dependent quadratic hyperpolarizability for specific types of second-order NLO chromophores, characterized by a single dominant CT transition.

Using in the Eq.6 a frequency equal to zero, it's possible to calculate β_0 , the static quadratic hyperpolarizability, a helpful way to assess the basic second-order NLO properties of a molecule. β_0 is then expressed as:

$$\beta_0 = \beta_\lambda \left[1 - \left(\frac{2\lambda_{\text{max}}}{\lambda} \right)^2 \right] \left[1 - \left(\frac{\lambda_{\text{max}}}{\lambda} \right)^2 \right] \quad \text{Eq.7}$$

where β_λ is the quadratic hyperpolarizability value at the laser wavelength while λ_{max} is the absorption wavelength of the CT transition controlling the NLO response.

The molecular quadratic hyperpolarizability β can be expressed both in the cgs ($\text{cm}^4 \text{statvolt}^{-1} = \text{esu}$) or in the SI ($\text{C m}^3 \text{V}^{-2}$) unit systems (the conversion from the SI to the cgs system is given by the relation $10^{-50} \text{C m}^3 \text{V}^{-2} = 2.694 \times 10^{-30} \text{esu}$). From the "two-level" model it is possible to deduce the dipolar electronic requirements that a molecule has to satisfy in order to show an important second-order NLO response. It must be noncentrosymmetric, with CT transitions with large $\Delta\mu_{eg}$ and r_{eg} and at relative low energy (excited state and ground state must be close in energy).

It's possible to achieve this, for example, by separation of an electron-donor and an electron-acceptor fragments with a π -conjugated polarizable spacer, as occurs in classical 1D dipolar *push-pull* organic systems.⁴

Multipolar systems, like octupolar molecules, have also been deeply investigated.⁷ These systems may have a higher transparency and an easier non centrosymmetric disposition of molecules in

crystals and bulky materials. However, the vector component of β is erased and only the octupolar component is left.

Molecules and materials with high second-order NLO response are of great interest for a lot of NLO processes. These can be distinguished in two main categories:

1. Conversion of frequency (Figure 2): when the applied electromagnetic radiation interacts with the NLO-active material, a new beam coming out from the material is generated. This latter differs in frequency from the incident one. This event can be observed for instance in the *Second Harmonic Generation*,⁸ a process arising by the combination of two incident waves, with a ω frequency, which interact with the NLO-active molecules or material, to generate a third wave with a 2ω frequency, called second harmonic.

Other phenomena of the same group are *optical rectification*, made by simply polarizing the material, thus generating a static electric field,⁹ or *sum or difference frequency generation* where two incident radiations are combined by sum or difference, with the production of a third output beam.

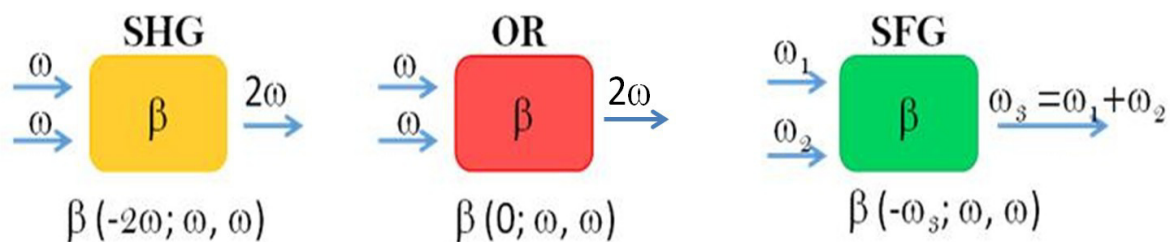


Figure 2. Schematic representation of wave combination phenomena.

2. Refraction index modulation: the interaction between a laser radiation and an NLO material, in the presence of an electric field, which is able to induce a refraction index variation, can modulate the propagation rate of the laser pulse, not its frequency. If the applied field is an electric one, we can talk about electro-optical effects.¹⁰ In several materials the correlation between the variation in refractive index and the intensity of the electric field is linear. This variation is called *linear electro-optic effect*, also known as *Pockels effect*.¹¹ Since this effect can be also expressed as $\chi^{(2)}$ (i.e. second-order non-linear susceptibility), it can take place only for non-centrosymmetric materials. Differently, in those materials which are centrosymmetric, such as liquids and glasses, the lowest-order change in the index of refraction has a quadratic dependence with the strength of the electric field; this latter effect is better known as *quadratic electro-optic effect*, or *Kerr electro-optic effect*.¹² These phenomena can be taken in advantage by devices like modulators and optical switches.

1.2. In solution studies and measurements of quadratic hyperpolarizability (β)

In order to define in solution the experimental value of β in molecules, two techniques are commonly used: the Electric Field Induced Second Harmonic generation (EFISH) and Hyper-Rayleigh Scattering (HRS).

1.2.1. Electric Field Induced Second Harmonic generation

The EFISH technique has been largely used to determine experimentally the value of the quadratic hyperpolarizability in NLO-active polar molecules (Figure 3).¹³

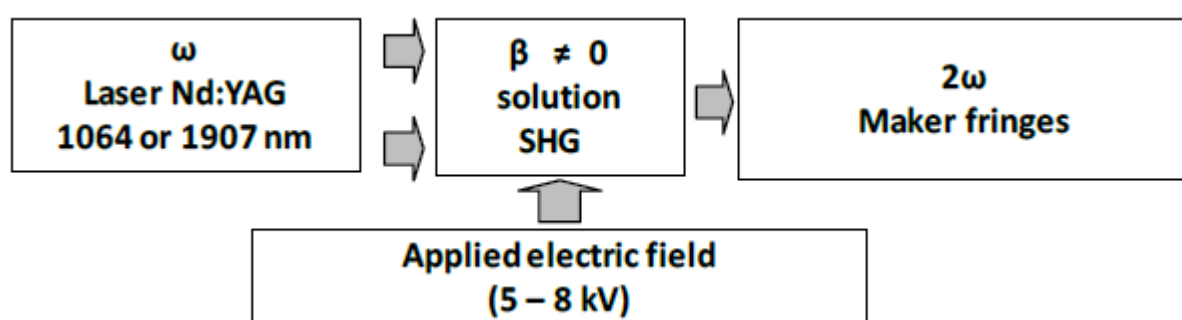


Figure 3. Schematic representation of an EFISH apparatus.

It is suited for neutral dipolar molecules and allows to evaluate the product $\mu\beta_\lambda$, where μ is the molecular dipole moment of the ground state while β_λ is the projection along the dipole moment axis of the vectorial component of the quadratic hyperpolarizability tensor, β_{ijk} , working with a pulsed laser of wavelength λ . μ can be determined separately, either with theoretical methods or experimental techniques (such as the Guggenheim method¹⁴); accordingly, β can be easily calculated from $\mu\beta_\lambda$, through EFISH measurements.

To avoid β overestimation, it is important to choose an incident radiation which second harmonic is far from any molecule electronic absorption. A Nd:YAG laser incident beam operates at a wavelength of 1064 nm; it can be coupled with a hydrogen Raman cell, which is able to shift the laser fundamental wavelength from 1064 to 1907 nm. Practically, once the compound is dissolved in the proper solvent (usually CH_2Cl_2 , CHCl_3 or DMF), all the molecules are aligned in the same direction by a strong electric field ($\sim 30 \text{ KW/cm}$), which is necessary to get the solution centrosymmetry lost.

A laser beam at ω frequency is then pointed through the measure cell in presence of the electric field and, while the detection is occurring, the cell is shifted orthogonally to the beam. The cell

(Figure 4) has a wedge shape, it is made up by two quartz windows, separated by the opportune angle and settled on a stainless steel support.

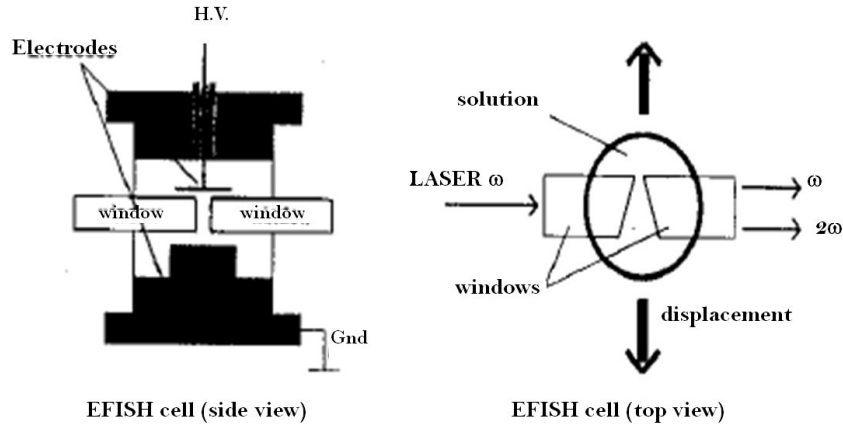


Figure 4. Scheme of a EFISH cell.

When the cell is translated orthogonally to the laser beam, the latter has to cover a path that will be different depending on time. This leads to interferences which are represented by the *Maker fringes*, which come from the interference between the harmonic and the fundamental wave into the medium. β is then determined, plotting the intensity of the second harmonic as function of the position.

In output two radiations are released: the incident one, with ω frequency, and the second harmonic, which has a 2ω frequency; this latter arises from the laser-sample interaction. Therefore the incident radiation is removed by a filter, in order to collect only the 2ω radiation, which is sent to the photomultiplier.

The Maker fringes periodicity and the amplitude are related to $\Gamma(x)$, which is the solution macroscopic susceptibility, defined in the following Equation 8:¹⁵

$$\Gamma(x) = \frac{1}{l_c(x)} \left[A \sqrt{\frac{I^{2\omega}(x) E(0)}{I^{2\omega}(0) E(x)}} + B \right] \quad \text{Eq 8.}$$

Where A and B are constants which depend on the solvent, $I^{2\omega}(x)$ is the harmonic at concentration x (while 0 is referred to the solvent) and E(x) is the electric field intensity. Given the Equation 9:

$$\gamma_{EFISH} = \frac{M}{\rho N_a f x} [(1 + x)\Gamma(x) - \Gamma(0)] \quad \text{Eq. 9}$$

where M is the compound molecular weight, N_a is the Avogadro's number, x the compound molar fraction, ρ the solvent density and f is a correction factor of the electric field, is possible to calculate $\mu\beta$ (product of the ground state dipole moment by the projection of the vectorial part of the quadratic hyperpolarizability tensor along the direction of the dipole moment axis) through Equation 10:

$$\gamma_{EFISH} = \frac{\mu\beta(-2\omega; \omega, \omega)}{5kT} + \gamma(-2\omega; \omega, \omega, 0) \quad \text{Eq. 10}$$

Where the ratio $\mu\beta(-2\omega; \omega, \omega)/5kT$ is the dipolar orientation contribution, while $\gamma(-2\omega; \omega, \omega, 0)$ is a third order electronic contribution of the incident beam wavelength and it is often negligible for molecules with a low electronic polarizability. $\mu\beta$, can thus be calculated directly by using the γ_{EFISH} value.

The EFISH technique affords some advantages, such as:

- i. Good sensitivity;
- ii. Precise methodic of calculation;
- iii. Direct determination of the product $\mu\beta$.

Nevertheless, it includes also drawbacks, which are:

- i. Employment only with dipolar and neutral compounds and tight ion-pairs;
- ii. The measure of μ should be obtained with another method;
- iii. The obtained β value is only the projection of the vectorial part of the quadratic hyperpolarizability tensor along the direction of the dipole moment axis;
- iv. For some compounds, such as highly polarizable ones, the third order term (γ) is not negligible sometimes.

Despite this, the EFISH technique is the most largely employed to obtain the β value of dipolar neutral organic compounds and metal complexes.

1.2.2. Hyper-Rayleigh Scattering

The HRS technique¹⁶ can be used to calculate β for dipolar, octupolar, neutral and, since it doesn't require the application of a strong electric field, also charged compounds (like salts).

The base of the HRS process can be found in the incoherent harmonic diffusion of the incident laser, as underlined Persoons and his colleagues.¹⁷

A strong advantage in this methodology, respect to the EFISH technique, is that it is possible to determine β , without determination of μ and γ . Moreover, since the measure provides the sum of

dipolar and octupolar contributions of the quadratic hyperpolarizability tensor, it results more complete.

As a drawback, in HRS experiments, the laser radiation can be too intense, producing some spurious signals, which can be misunderstood from the harmonic emission; it is also possible that the sample fluorescence interferes with the second harmonic signal¹⁸.

1.2.3. Solvatochromic method

This method allows to obtain the value of β along the direction of the predominant charge transfer, β_{CT} .¹⁹ It takes advantage of the shift of the emission or absorption band of a compound, when this latter is dissolved in solvents with different polarity, particularly when are used a variety of solvents with a wide range of refraction index and dielectric constant. It's possible to get β_{CT} by the application of the two-states model, described above; when the dipole moment axis and the CT transition have the same direction, β_{CT} and β_{EFISH} are the same.

1.3. Improvement of the second-order NLO properties in organic molecules

The Oudar's two-states model already underlined some of the requirements that molecules have to satisfy to show a satisfying second-order NLO response, therefore it can be exploited as a guideline to design better second-order NLO chromophores.

Traditionally inorganic crystals such as KH_2PO_4 or LiNbO_3 have been adopted, thanks to their high efficiency, nevertheless their synthesis is not simple, and the response requires relatively long time. Thus, in the last two decades a lot of research has been dedicated towards second-order NLO organic systems, since they provide many good points, such as high NLO properties, quicker response, cheaper production and great design flexibility.²⁰

To increase the second-order NLO properties a molecule should have strong electron donating and electron withdrawing groups to improve the system polarizability and a suitable π -conjugated linker, which promotes the electron transfer, thus providing the typical functionalities of an optimum *push-pull system*.

Oudar and Chemla first explored the second-order NLO properties of nitroanilines, which have been considered archetype compounds for a great number of push-pull system from then on.^{6a} they observed that β could be modulated, depending on the position of the amino group (strongly electron-donating) and the nitro group (strongly electron-withdrawing) on the phenyl ring. In the case of *ortho*- and *para*-nitroaniline, β showed an impressive enhancement with respect to *meta*-nitroaniline (see Table 1): this arises from an intramolecular charge transfer from the donor to the

acceptor group, through the π -delocalized bridge, made by the benzene. The enhancement of the NLO properties both for *ortho*- and *para*-nitroaniline (especially for this latter) is linked to a more efficient intramolecular charge transfer, in contrast to the *meta*- isomer.

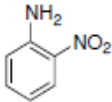
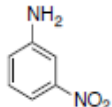
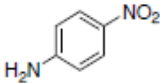
Chromophore	β_{exp} (10^{-30} esu ^a)
	10.2
	6
	34.5

Table 1. Experimental values of β of nitroanilines. ^a 1 esu (electrostatic unit) = 1cm/statvolt; 1 statvolt = 299.79 volt.

Such behavior, when a substitution is performed with this kind of groups with opposite electronic effects, has been proved to be general.²¹ It has been shown by Marder et al. how monosubstituted benzenes have lower β values, respect to *para*-disubstituted ones which benefit from the synergic effect of donor and acceptor groups, resulting in higher values of first hyperpolarizability.²² On the other hand, when more groups are present on the same ring, the final result can be self-defeating: there can be alterations of geometry, hybridization or conjugation, which could lead to a lower delocalization and thus a reduced optical non-linearity.

Beyond focusing on the electronic features of substituents, it's worth to consider also the extension of the π -conjugated system. It has been shown how stilbenes and styrenes are characterized by higher β values than the corresponding benzenes:²³ focusing on organic systems, for instance, β grows with the length of the π -conjugated system and it depends also on the spacer electronic properties. If an acceptor substituent is bound to the vinyl position of a stilbene, the increase of β is much greater than that obtained if the same acceptor group is linked to the stilbene phenyl position.

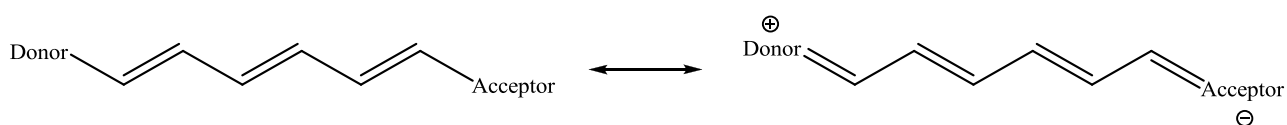
Beyond studying nitroanilines, Oudar and co-workers observed also the second-order NLO properties of differently substituted stilbenes.^{6a} Since *cis*- and *trans*-stilbenes with no substituents are not polar, they don't exhibit second-order NLO properties, as expected. On the other hand, by considering substituted stilbenes, it can be observed that their β values are one order of magnitude greater than those of the corresponding benzenes; this is clearly due to the longer π -spacer. The

high β value of 4-nitro-4'-dimethylaminostilbene is due to the presence of both strong electron-withdrawing and electron-donating groups.

On going from *trans*-stilbenes to diphenylacetylenes,²³ with a triple bond instead of a double one as a linker between the two phenyl rings, β decreases of almost 50%. This is probably due to the *p* orbital electronrichness in the hybrid *sp* orbital of the acetylenic carbon, because of the σ orbital low energy; this causes a mismatch with the *p* orbital of the neighbour *sp*²-hybridized phenyl carbon, hence a less efficient π delocalization. Furthermore, the aromaticity is lost, when the two phenyl rings are linked by a triple bond. The π delocalization, indeed, is more effective in *trans*-stilbene-like structures, where all carbons have the same *sp*²-hybridization, allowing a better orbitals interaction and so a higher electron flow.

It can be said in general that the conjugation efficiency comes from the π electrons delocalization, which is directly bound to features like bond equivalence and planarity. Planarity together with small torsional angles enable a more effective orbitals overlap, thus promoting donor-acceptor charge-transfers in the molecule. A clear example for this can be found in fluorenes, which being more rigid than biphenyls, present higher values of β . Obviously, the dependence with torsional angles becomes more important, considering bigger systems with a higher conjugation degree, since they can provide much more torsional opportunities.

A second element to take in account in evaluation of a system π -conjugation is the *bond-length alternation* (BLA, i.e. the average length difference between single and double bonds when the molecule is in the ground state). The values of the quadratic hyperpolarizability maximizes for a combination of acceptor and donor groups for a determined conjugated linker.²⁴ The ground state stems from a combination of two resonance forms:



When the donor and acceptor groups are weak, the ground state wavefunction is mostly represented by the neutral resonance, while the molecule has a high degree of BLA. On the other hand, when the donor and the acceptor are stronger, as the contribution of the charged resonance form to the ground state wavefunction increases, BLA drops down. In other cases, when resonance and coulombic factors are balanced, the contribution of the two resonances forms is equal both for the excited and the ground state. In this case the molecule shows no BLA; such situation is known as *the cyanine limit*, since it refers to the cyanine molecule structure. From the neutral polyene to the cyanine limit, it can be observed first an increase of β , with a positive peak

for the intermediate structure, then a drop towards negative values (the cyanine limit) (Figure 5). At this stage, the more β decreases, the more the dominant resonance structure will be the charged one, until it reaches a negative peak, increasing again afterwards.²⁵ The conscious combination of donor-acceptor with the appropriate linker, in order to change the energy balance of the two resonance forms, enable to design promising compounds with high second-order NLO features. However it should be kept in mind that, if the π -conjugated chain contains more than 9 carbons, the increase of β with the chain length is not observed anymore and a plateau is reached.

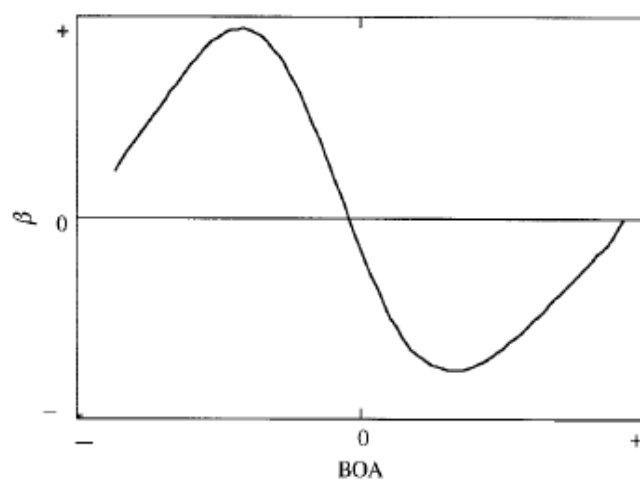


Figure 5. Plot of β vs. BOA (bond-order alternation, i.e. difference in π -bond order in adjacent C-C bonds) of a simple D-A polyene polarized to increasing extents by application of an electric field along the molecule dipole vector.

It's also possible to enhance the quadratic hyperpolarizability of those systems presenting phenyl units in their conjugated structures, by changing phenyl rings with different groups, resembling more polyenes.²⁶ The amount of β increase or decrease with respect to the corresponding stilbene, depends on the position and the nature of the heterocyclic ring in the overall molecular structure (Table 2).

Chromophore	β_{exp} (10^{-30} esu)
	73
	83
	98

Table 2. Experimental values of quadratic hyperpolarizability of 4-nitro-4'-dimethylamino-stilbene and derivatives with five-membered heterocyclic rings; measurements performed in dioxane.

Usually, replacing a phenyl ring on the donor with heteroaromatic rings like furan, pyrrole or thiophene, leads to an enhancement of β . Pyrrole has better effects than thiophene and furan. On the contrary, if the heterocycle is present on the acceptor side, the opposite trend is observed.²⁷ β values of many molecules including a thiophene instead of a benzene has been exhaustively studied.²⁸ It turned out that thiophenes provide better conjugation than benzenes; interestingly there is an important $\mu\beta$ enhancement when both phenyl rings are replaced in a stilbene-like system.²⁹

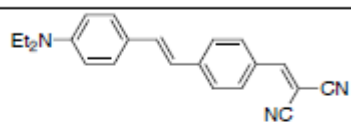
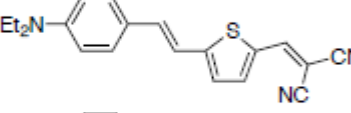
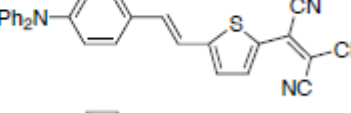
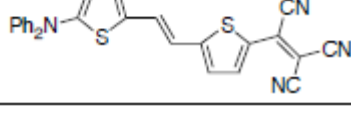
Chromophore	$\mu\beta_{\text{exp}}$ (10^{-48} esu)
	1100
	1300
	3250
	10200

Table 3. $\mu\beta$ values obtained in dioxane referred to different push-pull systems presenting the effect of thiophenes introduction.

In table 3 are shown $\mu\beta$ values of stilbene derivatives where one or both the phenyl rings are substituted with thiophene. By observing the numbers, it is clear that the donor/acceptor groups effect is relevant also when the molecule skeleton presents heteroaromatic rings. First, those compounds including a tricyanovinyl acceptor have a much higher $\mu\beta$, if compared with those bearing a dicyanovinyl;³⁰ moreover, although the diphenylamino group is a weaker donor than the diethylamino, it seems to confer to the molecule a better stability, when employed in a device.³¹ Nowadays electro-optic polymers are made using an organic molecule: disperse red one ($\beta_0 = 50 \cdot 10^{-30}$ esu).³² Anyway it must be kept in mind that the molecules are thought to be integrated in a device, hence their features of stability, solubility, processability and easy synthetic route are important.³³

1.4. Solid state measurement of quadratic hyperpolarizability

The most commonly used technique to study the second-order NLO response of bulk materials was developed by Kurtz and Perry.³⁴ With this method in a fast and simple way it is possible to perform an initial investigation of the material NLO properties by measuring the intensity of the radiation second harmonic, thus obtaining an early indirect evaluation of $\chi^{(2)}$ magnitude order. This technique requires the sample being in a crystalline powder form. The typical source of radiation is a pulsed Nd:YAG Q-switched laser, which irradiates a section of the sample of about 0.2 mm; the second harmonic emission light is then collected by a photomultiplier and confronted with a reference, for instance quartz or urea.

The so-obtained results are semi-quantitative, since they are affected by particles size; hence, to carry out qualitative measurements, it's possible to make a thin film of the powder with undetermined granulometry on a microscope slide. For quantitative determinations the procedure is more complicated; particles with a determined size, usually between 75 and 150 μm , are chosen by an opportune sieve and then introduced in a quartz cell with a known thickness. Through a vibrator the particles are packed, while their size is controlled by an optical microscope.

1.5. Device building up

The main issue to overcome in a device fabrication is that the second-order NLO active molecules tend to crystallize in a centrosymmetric way, in order to balance the overall dipole moment, disposing the molecules dipoles in an antiparallel way. To solve this problem generally pre-organized materials, for instance poled films, inorganic or organic frameworks linked to a support and Langmuir-Blodgett films, can be used.

NLO-active molecules are first dispersed in a polymeric film; an increase of the temperature beyond the film glass transition point, under application of a strong electric field, makes all the dipoles molecules be oriented in the same direction of the applied field; after a rapid cool down of the temperature the film becomes more rigid and all the dipole molecules should stay oriented in that same direction. Unfortunately, the problem of this method is the time stability, which is sometimes not very durable due to the disorientation of the molecules in absence of the electric field.³⁵

The most commonly employed technique to quantify the non-linearity of a solid material is called "Maker fringes"³⁶ by the name of its creator. In this experiment, the intensity of the second harmonic wave, generated by the sample, is correlated to the fundamental radiation incident angle and is referred and compared to that of a well know standard, such as a quartz crystal wafer.³⁷ The fundamental incident light can be generated by a 1064 nm Q-switched Nd:YAG laser. During the

measurement the sample is rotated around the Y-axis, in order to increase the incident radiation optical pathway through the sample (Figure 6).

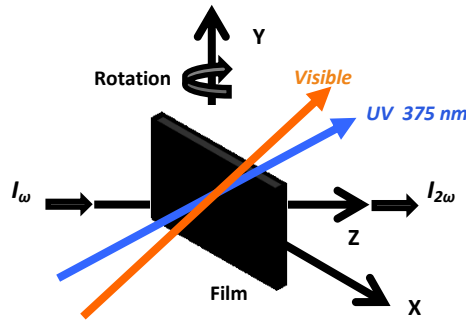


Figure 6. Set-up photoswitch experiment and Maker Fringe (XYZ is the macroscopic coordinate system).

In the Second Harmonic Generation, since the laser beam and the second harmonic wave generated by the sample do not have equal speed, their phase is not always the same: constructive and destructive interferences can occur, which provoke an increase and a decrease of the generated second harmonic, respectively. The resulting SHG signal thus appears like a periodic function, with minimum and maximum values, generating those peaks, known as “fringes”. To quantify the periodicity of this effect, the *coherence length* shall be used; it is calculated by scanning the Maker fringes minima positions, which have a wider range of θ (incident angle) with respect to the maxima, so they can be determined more accurately. Even if there is a slight difference in the angle between the second harmonic wave and the fundamental beam, it is small and can usually be neglected.

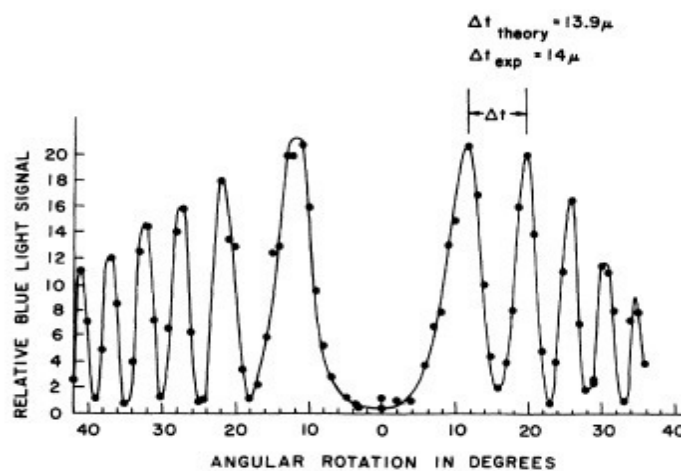


Figure 7. Blue light generation vs inclination of quartz platelet, reported by Maker et al.³⁶ The rotation axis is orthogonal to the laser beam and parallel to the crystal Z axis.

The standard expression^{37b} used to fit the SHG intensity in a Maker fringe experiment considers the film absorption coefficient at the harmonic frequency. In this equation the intensity of the SHG is proportional to the square of the effective non-linear optical coefficient, $(d_{\text{eff}})^2$ which is dependent from both the incident and the SH beams polarizations.³⁸ By considering the $C_{\infty v}$ symmetry, the expected one for poled films, and the beams polarizations, d_{eff} can be written as the following expression:

- For s \rightarrow p configuration $d_{\text{eff}} = d_{31} \sin \vartheta_2$ Eq. 11

- For 45 \rightarrow p configuration $d_{\text{eff}} = d_{15} \sin \vartheta_1$ Eq. 12

- For p \rightarrow p configuration $d_{\text{eff}} = 2d_{15} \sin \vartheta_1 \cos \vartheta_1 \cos \vartheta_2 + \sin \vartheta_2 (d_{31} \cos^2 \vartheta_1 + d_{33} \sin^2 \vartheta_1)$ Eq. 13

where d_{ij} are the non-linear optic coefficient tensor components, θ_1 and θ_2 are the refraction angles into the poled film for the incident and the SH beam, respectively, with refractive indices n_{ω} and $n_{2\omega}$ ($\sin \theta_m = \sin \theta / n_{m\omega}$, $m=1,2$). p and s indicate the beam polarization in the parallel and orthogonal plane, respectively, to the incident one. Between the components of the non-linear optic coefficient and the susceptibility tensor exists the relation: $2d_{ij} = \chi_{ij}^{(2)}$. The Maker fringe measurements are then fitted using the previously reported equations, in order to evaluate the three non-zero coefficients of the second-order susceptibility tensor for a poled film $\chi_{33}^{(2)}$, $\chi_{31}^{(2)}$ and $\chi_{15}^{(2)}$. The estimated error for these data is lower than 20%.

1.6. Second-order NLO properties of metallorganic compounds

1.6.1. Organometallic NLO-phores: response-structure correlation

In the last two decades, organometallic complexes have become of increasing interest as a new class of promising NLO-phores, since they can offer extra electronics advantages from the NLO response point of view, if compared to the traditional organic compounds :Low-energy CT transitions, such as Metal-to-Ligand CT (MLCT), are present with important values of quadratic hyperpolarizability, i.e. β ;

- i. d and/or f electrons confer a better polarizability and increase the number of low-energy excited states;
- ii. The metal centre can have different oxidation states, with the chance to modulate the electronic distribution of the fundamental and excited states, thus the NLO response;

- iii. A wide choice of ligands, geometries and coordination sphere, provide a further opportunity of NLO-response modulation.

Thanks to their versatility, metals and their coordination complexes have become very palatable in this field; depending on the metal nature, its oxidation state and ligands surrounding, they can indeed play both as electron-acceptor or electron-donor species, or even act as bridging unit between donor and acceptor fragments.⁴

Many organometallic complexes have been studied for their second-order NLO properties;³⁹ among them some classes have been further examined thanks to their interesting response. One early example can be found in metallocenes, in particular ferrocenes examined first by Green et al.⁴⁰ Their donor features have indeed made these compounds one of the most deeply and exhaustively studied class of organometallic compounds for NLO applications.⁴¹ Ferrocenes are characterized by a moderate donor ability, similar to that of a methoxy-phenyl group (see Table 4), due to its low metal ionization energy and easy oxidation.

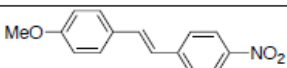
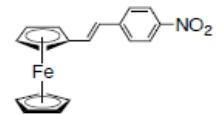
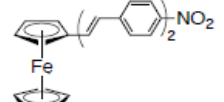
Chromophore	β (10^{-30} esu)
	28 ^a
	31 ^a
	403 ^b

Table 4. Two examples of second-order NLO-active ferrocenyl complexes, in comparison with stilbene. (a) $\beta_{1.91}$, EFISH in dioxane; (b) $\beta_{1.08}$, HRS in dichloromethane.

By considering the redox potentials and the binding energies, one might expect to observe higher β values. When there is less effective π binding between the metal and the ligands, the donor ability of the metal decreases.⁴² In a same way to what learned for purely organic compounds, increasing the π -bridge length, hence the system conjugation, leads to a red-shift of the CT absorption bands, with a consecutive increase of the quadratic hyperpolarizability.⁴³ It has also to be pointed out that, if the double bond is in *Z* conformation instead *E*, β decreases. One more interesting characteristic of this class of compounds, for the point of view of NLO applications, is their ability to crystallize by their own in non-centrosymmetric structures, which confers to them a relatively high Second Harmonic Generation, since the acceptor units are usually bulky species.⁴⁴

Ruthenocene compounds show a smaller β if compared with related ferrocenes. When iron is replaced by ruthenium, a blue shift of the absorption bands is observed; therefore β decreases, since in ruthenium ionization energy is higher than in iron.⁴⁵

It is interesting that metallocenes NLO properties can be tuned, and eventually impressively increased, by changing their function. Lately, in fact, multi-layer sandwich complexes (general formula V_nBz_{n+1} ; where $n = 1,2,3,4$ and Bz = benzyl group) have been developed and used as π delocalized bridge in push pull systems, thus formed donor-(V_nBz_{n+1})-acceptor.⁴⁶ It came out that β values of these compounds rised with the increase of the layers number; an impressive value of $\beta_0 = 6638 \cdot 10^{-30}$ esu was reached for $V_3Bz_4-(CN)_3$.

Another class of compounds, i.e. alkylphosphine-M- σ -acetylide complexes with transition metals of groups 8, 10, 11, have been widely studied as second-order NLO chromophores by Humphrey and co-workers.⁴⁷ As in metallocenes, this family of compounds can include cyclopentadienyl rings in the structure and the metal in general acts as donor group. Their second-order NLO properties can be explained on the basis of MLCT transitions. The biggest β values in these complexes have been achieved with Ru(II), but also Ni(II) and Au(I) showed quite high results. In comparison with metallocenes, σ -acetylides, thanks to their almost linear structure M-C \equiv C-R provided by the triple bond, confer a better orbitalic coupling between the d metal orbitals and the σ -acetylide π^* orbital, then a larger second-order NLO response. Occurring in plane, these MLCT transitions emerge to be more efficient than those of the metallocenes.

Recently, complexes where ruthenium bears two alkynyl moieties have been synthetized.⁴⁸ In such systems, the ruthenium plays the role of a π -bridge between the acceptor and the donor, thus the NLO properties can be suitably tuned by changing the two alkynyl ligands.

An exhaustively explored family of compounds, taking advantage of the double nature of the metal as donor or acceptor, are metal complexes bearing pyridine and carbonyl units as ligands,⁴⁹ as shown in Figure 8.

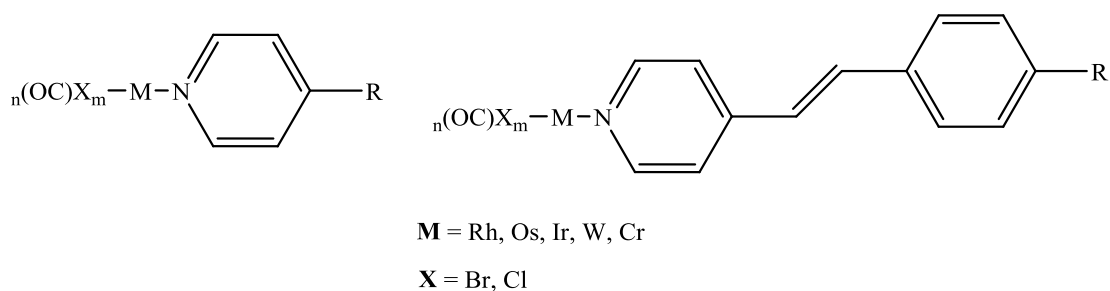


Figure 8. Schematic structure of the metal-pyridine-carbonyl complexes investigated.

Absorption spectra of compounds like those above are characterized by dominant ILCT (Intra-Ligand-Charge-Transfer) bands. These bands are shifted towards the red with respect to those of the free ligands; in the case of the stilbazole, where there is more π delocalization, this red-shift is even more pronounced.⁵⁰ The coordination indeed causes a stabilization of the lowest excited state of the ILCT transition, resulting thus in a lower energy; this provides an enhancement of the second-order NLO response, respect that of the free pyridyl ligand.

Recalling the statement of the Oudar “two-level” model,⁶ β is larger when the energy gap between the transition energy levels is smaller; as a consequence the NLO properties of these complexes increase after complexation. The UV-Visible spectra result more complex for related complexes whose ligands bear weakly donor or strongly acceptor substituents in the *para*-position. Both pyridine and carbonyl ligands might indeed contribute with further MLCT transitions, resulting in one more CT absorption band to take in account.⁵⁰

The EFISH technique can be employed to evaluate the quadratic hyperpolarizability for these compounds, since the CT axis is set along the dipole direction and other contributions can be neglected. The R substituent strongly affects β_{EFISH} : if R is a strongly donating group, β is positive, while if R is a strongly acceptor group, then β takes negative values.⁵¹ The second case can be better understood by considering that the dipole moment after excitation will be reduced and that with strong electron-withdrawing groups the predominant MLCT transition will have an opposite vectorial direction with respect to the dipole moment.

The coordination effect becomes modest by extending the π -conjugated bridge, for instance on going from pyridine to stilbazole. Moreover, by derivatization of the styryl unit, the overall NLO response undergoes no sensitive variations, oppositely to what evidenced for purely organic compounds, especially if it carries electron-withdrawing groups.⁵² This can be made clear by noticing that, when the substituents are electron-donor, β is mostly characterized by ILCT transitions from the donor towards the metal-carbonyl moiety and it has positive values since the transition occurs in the same direction of the ground state dipole moment. Oppositely when the substituents are electron-acceptor, the aromatic unit near the metal centre (the pyridine in this case) acts as primary acceptor of the electron density, instead the acceptor group itself; this is particularly implemented if the electron-withdrawing groups are weak.

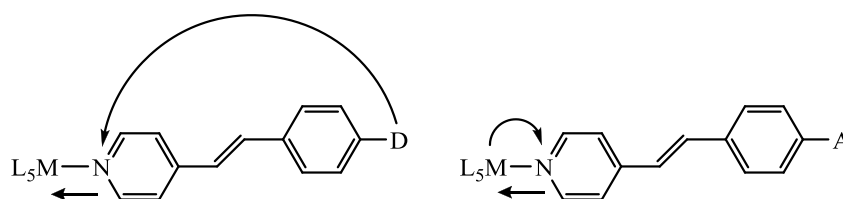


Figure 9. CT transitions for those complexes with stilbazole ligands.

To tune the metal electronic nature it is also important to take in account the ancillary ligands effects. In fact, when strongly electron-withdrawing groups as co-ligands are adopted, the metal accepting nature results emphasized and high values of β can be achieved by using the appropriate metal.⁵³

It was also shown that for ruthenium amine complexes bearing pyridyl ligands by substitution of the neutral counterparts with *trans*-[2-(4-pyridyl)vinyl]pyridinium⁵⁴ or N-methyl-4,4'-bipyridinium⁵⁵ as ligands results in an enhancement of their second-order NLO properties. Moreover, it is also possible to increase β_0 by using ligands able to enrich the metal centre electron density⁵⁶ or by N-arylation of the pyridinium acceptor groups.⁵⁷ However, extending the π -bridge by adding more double bonds in the *trans*-[2-(4-pyridyl)vinyl]pyridinium ligand, does not result in a NLO-response increase, because of the competitive presence of ILCT and MLCT transitions.⁵⁸ The same was observed for V-shaped ruthenium complexes with two or more 4-styrylpyridyl ligands.⁵⁹

Different metal complexes with a 4-4'-styryl-2,2'-bipyridyl ligand were reported.⁶⁰ Again β resulted to be related to the nature of the metal, the ligand and the ancillary ligands; in particular it was observed an enhancement of the NLO response with stronger electron-donor substituents on the bipyridyl ligands and with the increase of metal centre Lewis acidity (e.g. a Zn complex has higher β than a complex with Hg).

The NLO response is also enhanced by using stronger electron-withdrawing ancillary ligands (e.g. Cl>OAc or OTf>Br).⁶¹ The chelation effect also must be pointed out: complexes with two 4-styrylpyridines show lower $\mu\beta$, when compared with complexes bearing a 4,4'-styryl-2,2'-bipyridyl ligand, since the latter ones provide a better co-planarity and π -conjugation (Table 5).^{60a}

62

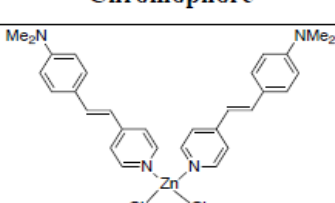
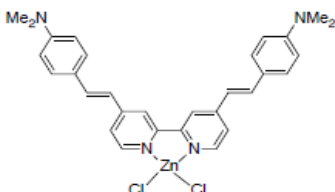
Chromophore	$\mu\beta_{1,34}$ (10^{-48} esu)
	706
	1420

Table 5. Effect of chelation on $\mu\beta$ values determined in chloroform through EFISH technique of two similar Zn complexes; on the top the Zn centre bears two styrylpyridines, while on the bottom it is bound to a 4,4'-styryl-2,2'-bipyridyl ligand.

For comparison, the same family of chelating ligand has been used to synthesize complexes of Ag(I) and Cu(I), whose NLO response has been determined via HRS technique.⁶³ The nature of the metal affects the β_0 magnitude. If the geometry is the same, the more the Lewis acidity of the metal ion increases, the more ILCT transitions, which are dominant in the NLO response, will decrease, thus resulting in an improvement of NLO activity. For Zn(II) complex β_0 is higher than Ag(I) and Cu(I) ones, in agreement to what stated above.

The Zn(II) ion results very versatile, thanks to its electronic configuration (d^{10}) and lack of ligand field effects, which made possible the synthesis of the octahedral D_3 complex where the Zn ion bounds three 4,4'-styryl-2,2'-bipyridines.⁶⁴ Of this complex were synthesized analogues using Ni(II), Cu(II), Ru(II) and Fe(II) with the same ligands.⁶⁵ Regarding ligands, β is more affected by the length of the π -conjugated fragment than by the terminal donor group; moreover by increasing the number of the ligands the NLO response increases. The octahedral Cu(II) and Ni(II) complexes show smaller β values than the analogous Zn(II) complex, due to a distortion from the ideal octahedral disposition. However, Ru(II) and Fe(II) spectra also display a MLCT band in the Vis region, which concurs to their NLO response. The MLCT and ILCT bands are approximately parallel but oppositely directed; this should lower the value of the quadratic hyperpolarizability. This is true for the iron complex, but not in the case of ruthenium. The reason of this is still uncertain.

Some studies have been also performed on the NLO activity of complexes where the metal (Zn(II), Ru(III) or Ir(III)) bears a donor ligand (i.e. a terpyridyl one) and an acceptor co-ligand.⁶⁶

According to what asserted above, if compared to that of the free terpyridyl ligand, the quadratic hyperpolarizability is increased by complexation to an acidic metal, mostly thanks to a stabilization of the terpyridine π^* orbital, given by the coordination. Further, β is negative for the Ru(III) and Ir(III) complexes, while it is positive for the Zn(II) one, showing for the first time the metal influence on both the absolute value and the sign of β in this particular case. It is possible to explain this by considering the dominant contribution of ILCT transition for the Zn(II) complex, differently to the Ru(III) and the Ir(III) complexes, where an important contribution is also given by LMCT and MLCT transitions, respectively. Lately, it was reported that the metal centre in a Ru(III)bis-terpyridyl complex can work as a polarizable linker between the donor and the acceptor fragments.⁶⁷

The second-order NLO properties of macrocyclic ligands, such as phthalocyanines and porphyrins, were also investigated.⁶⁸ Usually porphyrins act like spacers within *push-pull* systems; one of the first applications was performed by Le Cours and co-workers.⁶⁹ The quadratic hyperpolarizability values of this family of complexes are acceptable, but a particular attention might be paid on the

incident radiation wavelength: first studies on these complexes have indeed overestimated β because of resonance enhancement.⁷⁰ Also the solvent can affect the value of β : overestimated β values were reported for metal porphyrinates in non-polar solvents, due to their aggregation.⁷¹ It is worth to notice that the second-order NLO properties for these complexes can be further increased if two metal-polypyridyl fragments are linked, through an ethylene bridge, to the porphyrinato-Zn core, in order to have *push-pull* systems strongly polarized.⁷²

One last example, even if there are many others, could be that of divalent Co, Fe, Cu, Ni and Zn complexes with Schiff-bases, which give place to non-centrosymmetric frameworks. In these complexes the metal center can play both the role of donor, involving MLCT transitions, or polarizable bridge if a strong electron-withdrawing and a strong donating substituent are present on the chelating ligand.⁷³

From now on, will be discussed more in details the NLO properties of Platinum and Iridium complexes, which are one of the main object of this thesis.

1.6.2. Second-order NLO properties of Pt complexes

This section will be dedicated to Pt(II) complexes, from an overview of the state-of-art and moving then to the real purpose of this thesis.

Cyclometallated platinum complexes represent an interesting class in second-order non linear optics. Some examples of this family, in specific neutral Pt(II)(ppy)(acac) complexes (where ppy is phenylpyridine, acac is acetylacetonate) have been already explored by our group (Figure 10).⁷⁴

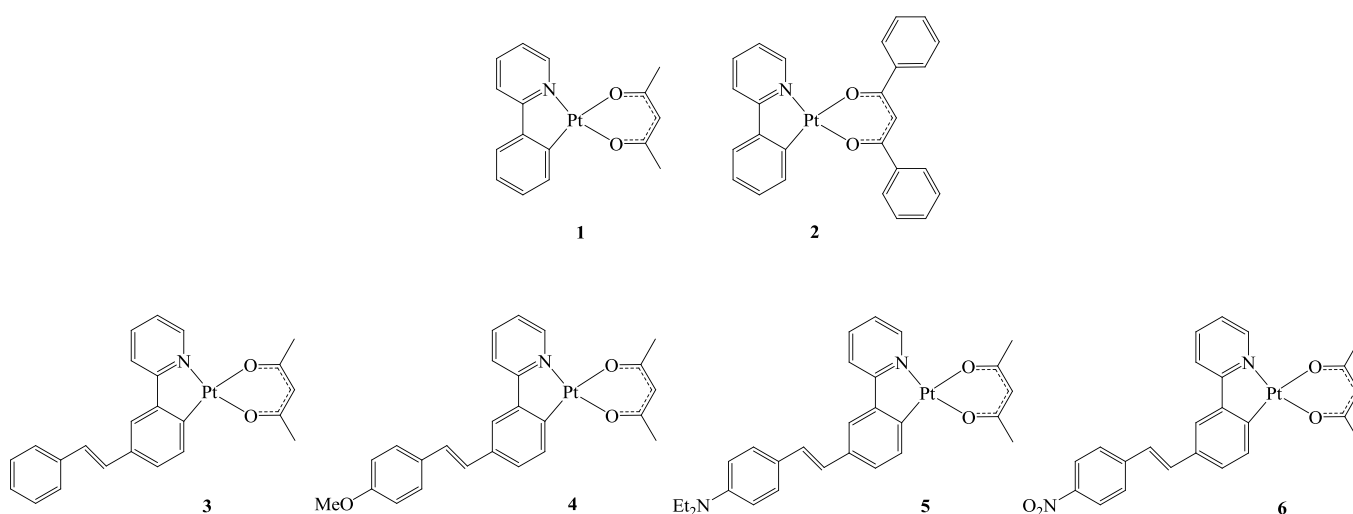


Figure 10. Studied Pt(II)(ppy)(acac) complexes for second-order non linear optics.

Complexes **1** and **2** do not show absorption at long wavelengths; the LUMO is focused on the pyridine fragment, while the HOMO major contribution comes from the Pt centre and the phenyl fragment of the phenylpyridine. The dipole moment lies along the axis which connects the two aromatic rings of the phenylpyridine. The NLO response is hence characterized by a mixture of MLCT and ILCT (from phenyl to pyridine) transitions: $\mu\beta_{\text{EFISH}}$ values for these compounds is modestly high (ca $-535 \cdot 10^{-48}$ esu for **1** and ca $-770 \cdot 10^{-48}$ esu for **2**), but lower than the analogous complex with Iridium as metal centre (ca $-910 \cdot 10^{-48}$ esu for the analogous of **1** and ca $-1340 \cdot 10^{-48}$ esu for the analogous of **2**).

For those complexes where the pyridyl ring bears a styryl fragment, the enhancement of the π -delocalization leads to an increase of the NLO response and a sign inversion of the $\mu\beta_{\text{EFISH}}$ values. This can be attributed to the dipole moment direction, which lies along the styryl fragment, whose ILCT transitions characterize for the most the $\mu\beta_{\text{EFISH}}$ value. This is not true for the complex **6**, which carries an electron-withdrawing group and whose calculated dipole moment is quasi-orthogonal to the styryl fragment; its NLO response can be attributed to MLCT transitions. The more the electron-donating ability of the 4-styryl-2-phenylpyridine ligand increases, the higher will be the corresponding $\mu\beta_{\text{EFISH}}$ value: this comes mainly from an enhancement of the ground state dipole moment.

It is also worth to note that the complex **4** is characterized by a $\mu\beta_{\text{EFISH}}$ value that is four times higher than the corresponding free 4-styryl-2-phenylpyridine ligand ($\mu\beta_{\text{EFISH, ligand}} = 370 \cdot 10^{-48}$ esu; $\mu\beta_{\text{EFISH, complex}} = 1330 \cdot 10^{-48}$ esu), proving that for this compound cyclometallation with a Pt(II) metal confers a huge enhancement of the second-order NLO properties.

Also N[^]C[^]N Pt(II) complexes have lately aroused interest for what concerns second-order non linear optics. Such compounds are already known to possess remarkable emission abilities, but they also have a great potential for application as NLO-phores. Following the early studies of Asselberghs et al.⁷⁵, few years ago in our group a series of Pt(II) 1,3-di(2-pyridyl)benzene complexes with chlorine or phenylacetylde as ancillary ligands have been examined (Figure 11).⁷⁶

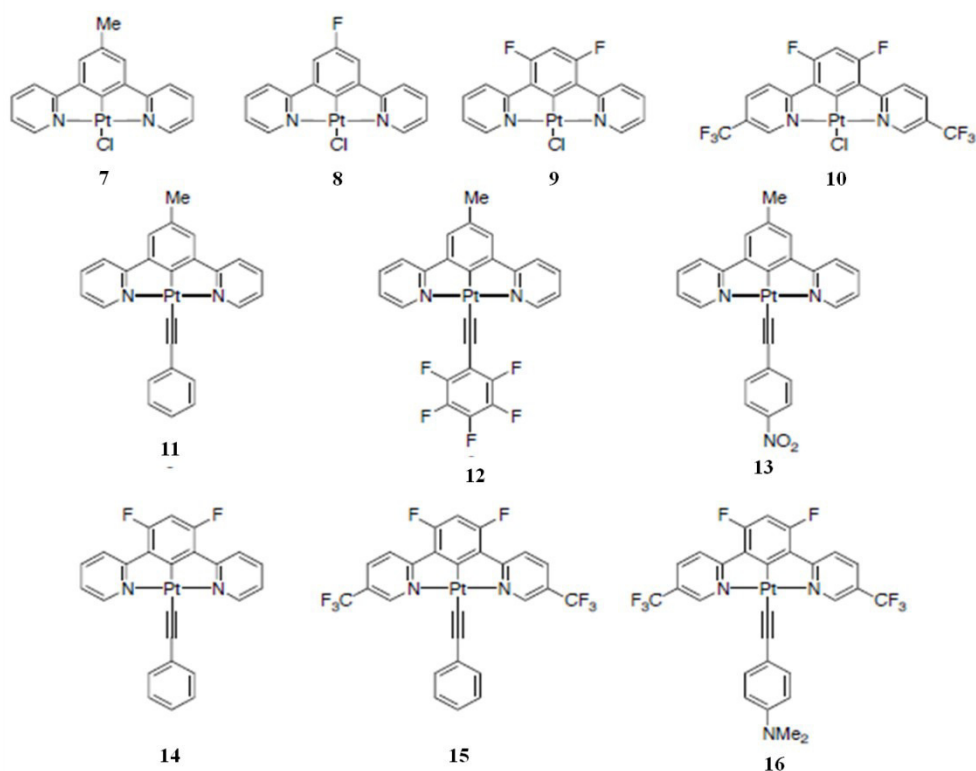


Figure 11. Pt(II) N^CN complexes studied in our group.

The complexes with a chlorine as ancillary ligand (complexes **7** to **10**) have an absorbance spectra displaying mixed LC/CT bands between 350 and 450 nm, while absorption spectra of those bearing a phenylacetylide as co-ligand present a series of less resolved LLCT bands in the same interval. The LUMO is dispersed on the pyridyl ligand, while the HOMO is principally localized on the phenyl ring of the N^CN ligand, on the metal and on the respective ancillary ligand (i.e. chlorine or phenylacetylide). Complexes **14**, **15** and **16**, with electron-withdrawing units on the dipyriddy benzene, the HOMO is mostly on the ancillary ligand, while the LUMO is on the two pyridines and slightly on the central phenyl ring as well.

$\mu\beta_{\text{EFISH}}$ values have been determined through the EFISH technique using DMF as solvent: these values have a negative sign, due to a dipole moment decrease upon irradiation, and are mostly attributed to the MLCT transition from the metal to the N^CN ligand.

Complex **4** was characterized by the largest $\mu\beta_{\text{EFISH}}$ value (i.e. $-2470 \cdot 10^{-48}$ esu), thanks to the remarkable dipole moment, while the highest β_{EFISH} value was obtained with complex **16** (i.e. $-470 \cdot 10^{-48}$ esu, $\mu\beta_{\text{EFISH}} = -2020 \cdot 10^{-48}$ esu).

Discussing about Pt(II)-N^CN complexes, it is worth to mention also the studies made by Guerchais, Dragonetti and co-workers, who explored the second-order non-linear optics of

complexes consisting in a Pt(II) bound to symmetric 1,3-bis(benzoxazolyl)benzene or asymmetric 2-[4-fluoro-3-(1-methyl-1*H*-benzimidazol-2-yl)phenyl]benzothiazole or 2-[3-(benzothiazol-2-yl)phenyl]benzo[*d*]oxazole ligands (Figure 12).⁷⁷

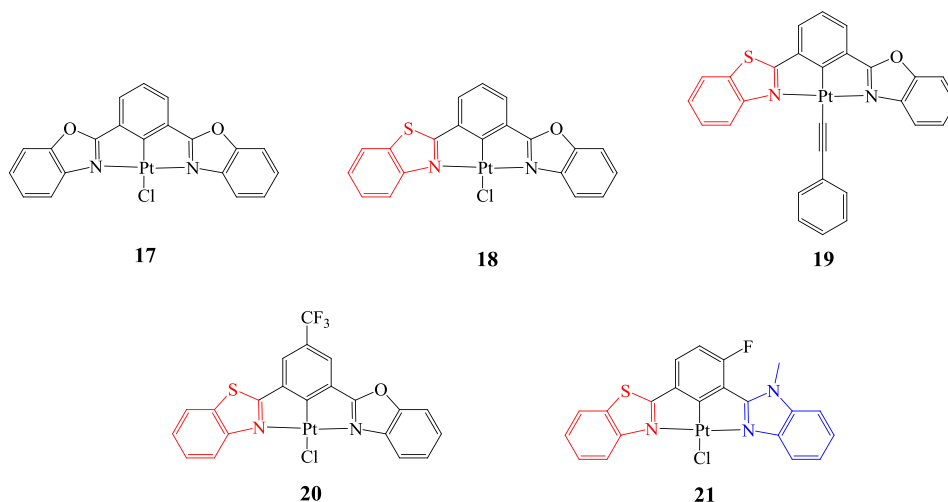


Figure 12. Pt(II) complexes with a N^CN terdentate ligands series.

The absorbance spectra of compounds in Figure 12 display bands typically assigned to $\pi \rightarrow \pi^*$ transitions in the UV region and MLCT transitions at lower frequencies (or longer wavelengths). While the HOMO is mainly delocalized on the chlorine atom and on the central phenyl ring of the terdentate ligand, the LUMO is delocalized on the whole terdentate ligand but principally on electron-withdrawing fragment (i.e. the benzylthiazole unit, in red).

$\mu\beta_{\text{EFISH}}$ values are modest, but interestingly complex **17** has a slightly larger NLO response than the related compound made with a 1,3-dipyridylbenzene ligand. In all the derivatives there is a $\mu\beta_{\text{EFISH}}$ enhancement; the reasons are different. On going from **17** to **18**, $\mu\beta_{\text{EFISH}}$ increases by substitution of a benzoxazole with a benzothiazole, whose LUMO is lower in energy, while an exchange with a benzimidazole (complex **21**) causes a higher dipole moment. Both the introduction of the electron-withdrawing CF_3 group (**20**), and the substitution of the chlorine atom with a phenylacetylide (**19**) also affect positively the NLO response.

In summary, regarding Pt(II) complexes with N^CN ligands, and particularly those with 1,3-dipyridyl benzene ligands, it has been demonstrated how they can provide a satisfying NLO response, which can be modulated by promoting the CT transitions between the metal centre and the ligands.

As discussed previously, metal σ -acetylides have been widely studied as NLO-phores and mainly improved by Humphrey et al.⁷⁸ In these systems the metal plays the role of donor unit of a donor-

acceptor framework, connected by a π -delocalized bridge. Pt(II)-alkynyl complexes have been investigated as optimal candidates for optical power limiting,⁷⁹ TPA (two-photon absorption),⁸⁰ solar cells,⁸¹ or reverse saturable absorption.⁸²

These compounds exploit the quasi-linear M-C \equiv C-R structure, which gives a suitable interaction between the metal d orbitals and the π^* of the σ -acetylide providing an important second-order NLO response determined by MLCT excitations at low energy.

The earliest Pt- σ -acetylide complex for second-order non-linear optics applications was published by Marder and co-workers.⁸³

The presence of the carbon-carbon triple bond confers a reduction of the molecular CT character, making possible to achieve final materials characterized by better optical transparency. However, it is important not to forget that an improved transparency is accompanied by a decrease of the quadratic hyperpolarizability.

To valorize the second-order NLO properties even keeping satisfying optical transparency, the π -conjugation was extended with a diphosphine-Pt moiety as core element, which links the acceptor with the phenylethynyl donor fragment.

Since it was observed that binding Pt to σ -acetylide allows to achieve good $\mu\beta$ values, it is worth to consider platinum as an effective component in NLO materials.

Few years later, our group published a *push-pull* binuclear complex, where two donor Pt σ -acetylide fragments are bound to a 2,1,3-benzothiadiazole, which works as acceptor (Figure 13).⁸⁴

In this compound the HOMO main contributions come from Pt orbitals and the π orbitals of thiophene and benzothiadiazole, while the LUMO is entirely located on the benzothiadiazole fragment and no contribution comes from the metals.

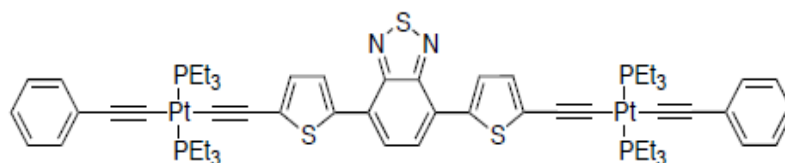


Figure 13. Bi-metallic σ -acetylide complex reported by our group.

$\mu\beta_{\text{EFISH}}$ value for this complex is $-520 \cdot 10^{-48}$ esu: it is good even if related dinuclear compounds with Ruthenium display a slightly better response.⁸⁵

1.7. Novel Fullerene Platinum Alkynyl complexes⁸⁶

The fact that Platinum alkynyls moiety have electron-donor abilities gave the idea of designing an hybrid with a C₆₀-fullerene, since fullerenes are electron-poor molecules with remarkably strong aromaticity.⁸⁶ In fact, it was shown by our group how, thanks to its strong acceptor capacities and its broad polarizability, C₆₀-fullerene is a suitable building block for NLO materials.⁸⁷ Some publications about photoinduced electron transfer in both Pt(II)-bis(N-(4-ethynylphenyl)carbazole)bipyridine-fullerene⁸⁸ and Pt(II)-bis(N-(4-ethynylphenyl)phenothiazine)bipyridine-fullerene⁸⁹ already came out, in particular regarding the fabrication of organometallic photovoltaic cells;⁹⁰ despite this, to the best of my knowledge, no combined metal σ -acetylide fullerene systems have been investigated for what concerns second-order non-linear optics properties. These observations incited me to synthesize systems as the following ones (Figure 14) during my PhD thesis: C₆₀ fullerene is linked to an ethynyl-thienyl fragment, which acts as π -delocalized bridge between the fullerene and the metal centre, via a cyclopropane ring, which provides a smooth electronic communication through the so-called *periconjugation*,⁹¹ an intramolecular electronic interaction already observed by Prato et al.^{91a}

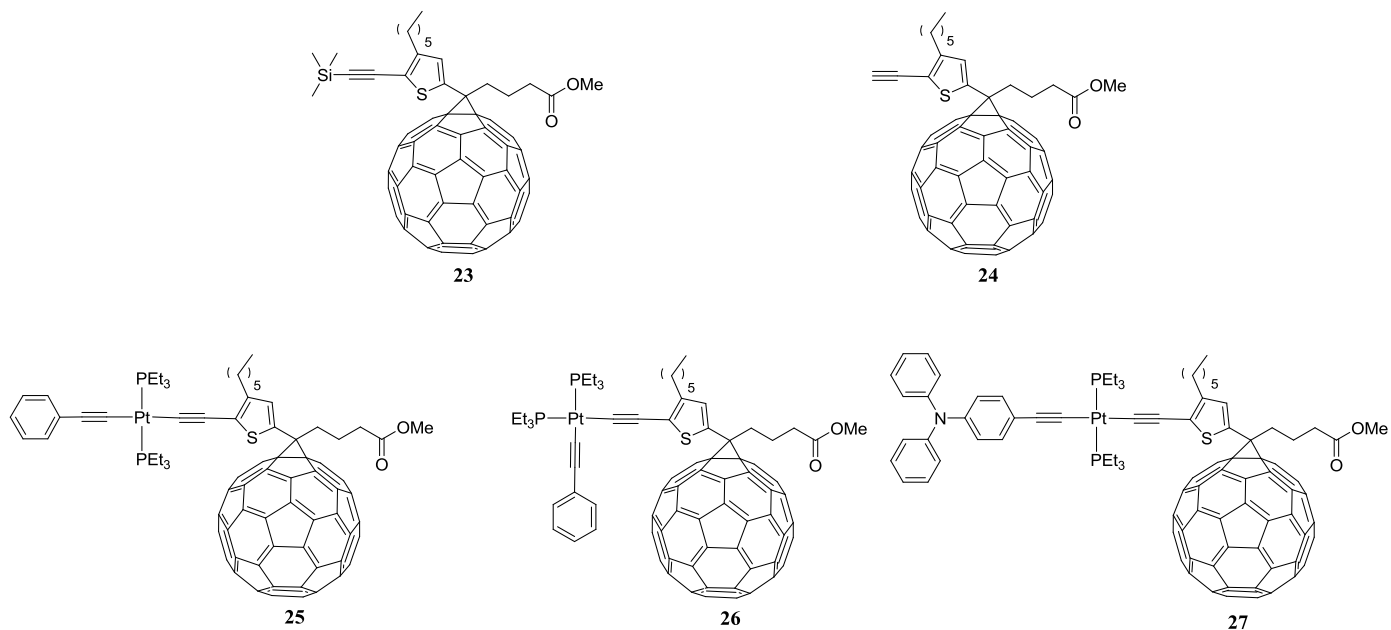


Figure 14. Hybrid C₆₀ fullerene- σ acetylide compounds synthesized during my PhD.

First, compounds **23** and **24** have been synthesized. Then, in order to study the effect on the second-order NLO response upon Pt(II) introduction, related metal complexes **25**, **26** and **27** have been prepared. Furthermore, since it is known, and it has already been discussed in the previous paragraphs, that an extension of the π -delocalized fragment can carry out an increase of the

second-order NLO response and that terthiophene is a worthy π -conjugated electron-releasing unit,⁹² the consequence of the introduction of a terthiophene instead of the thienyl fragment have been investigated, by synthesis of compounds **28** and **29** (Figure 15).

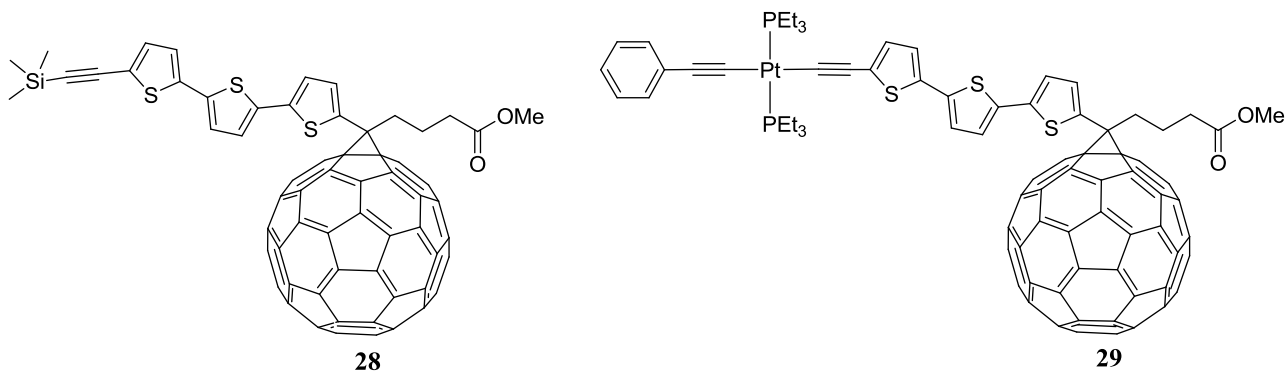
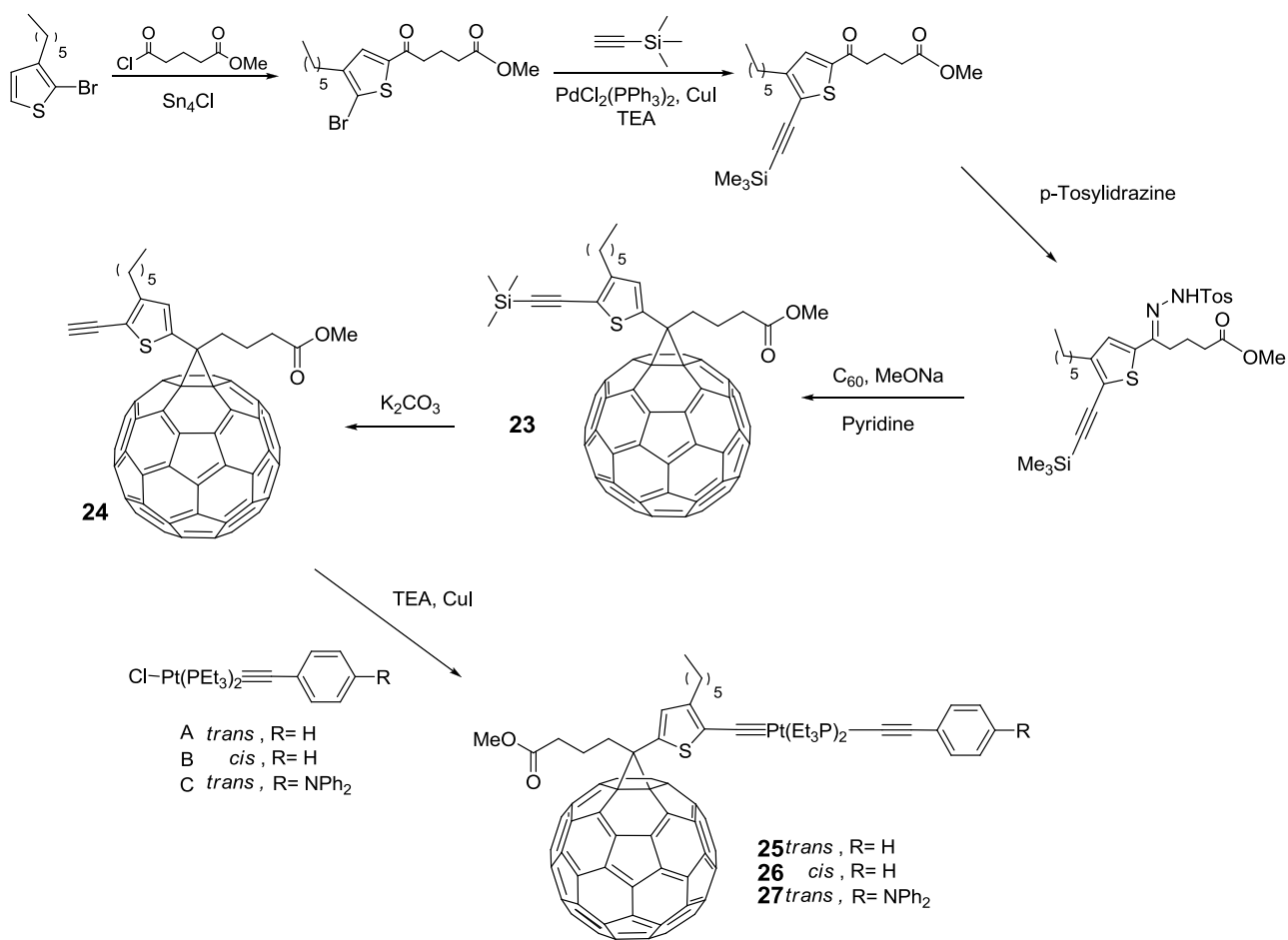


Figure 15. Synthesized compounds bearing a terthiophene instead of a thiophene as π -delocalized bridge.

1.7.1. Synthesis of the compounds **23-29**

The synthetic steps will be described in detail in the Experimental section (Chapter 3), while the general Scheme 1 is reported below.

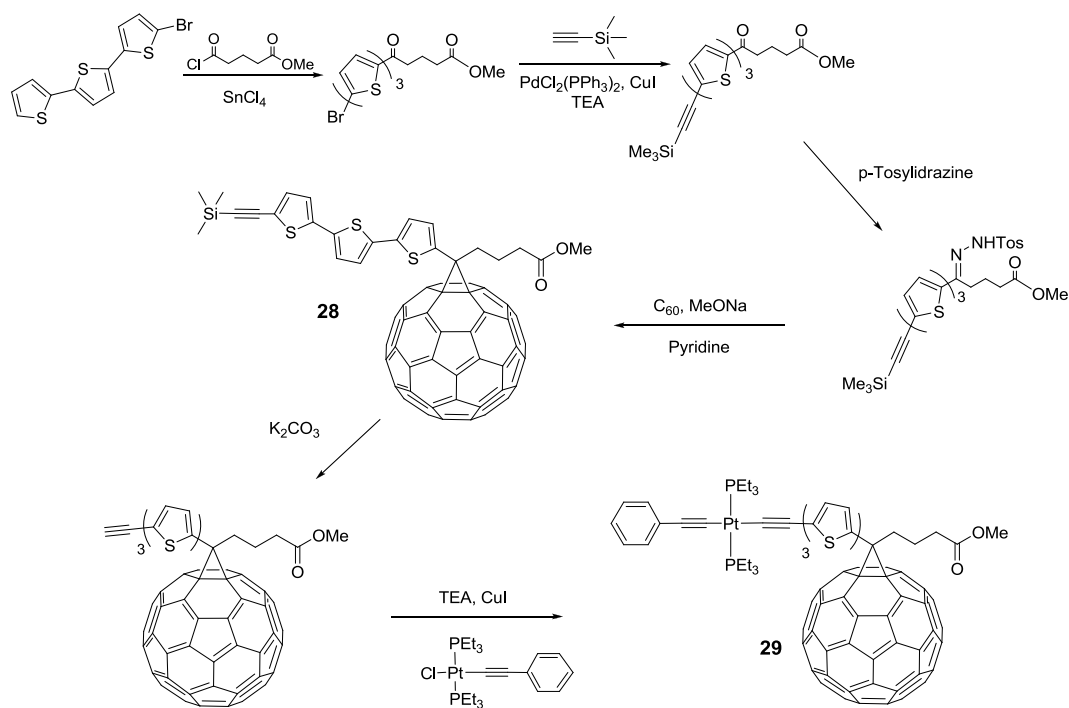


Scheme 1. General synthetic strategy for compounds 23-27.

The novel thiophene-substituted methanofullerenes **23** and **24** were prepared as described in literature for other methanofullerenes;⁹⁴⁻⁹⁶ the Pt complexes **25**, **26** and **27** were synthesized as in the previous Scheme 1.

The first step is a Friedel-Crafts acylation, followed by a Sonogashira's coupling; by reacting with the proper *para*-tosyl hydrazine with the C₆₀ fullerene in presence of sodium methoxide allows the formation of the related methanofullerene. The Platinum derivatives were prepared by deprotecting compound **23** and making it react with the suitable Platinum σ -acetylide complex, previously synthesized, in the presence of copper(I) iodide and triethylamine (TEA).

Complex **29** was prepared starting from the commercially available terthiophene in a similar manner from the new methanofullerene, **28** (Scheme 2).



Scheme 2. General procedure for compounds **28** and **29**.

2.7.2. Photophysics and second-order NLO measurements of compounds **23**–**29**.

Absorption data of the synthesized compounds are reported in the following chart. All compounds display bands in the range between 255 and 332 nm, as one would expect from thienyl-fullerene derivatives.⁹³ The platinum complexes show an additional band at higher wavelengths (355–482 nm), which can be assigned to the alkynyl-platinum fragment, as already reported.⁹⁷ Compound **28** also have a band at 375 nm, which is typical of the terthiophene group.⁹⁸

Compound	Absorption ^a λ_{\max} / nm (ϵ / $M^{-1} \text{ cm}^{-1}$)	$\mu\beta_{\text{EFISH}}$ ($\times 10^{-48} \text{ esu}$) ^b	μ ($\times 10^{-18} \text{ esu}$) ^c	β_{EFISH} ($\times 10^{-30} \text{ esu}$) ^d
23	259 (95515), 329 (33683)	-350	4.2	-83
24	260 (94597) 327 (35867)	570	4.3	133
25	259 (74672), 332 (34045), 356 (33794)	-3100	5.8	-534

26	259 (72220),	-3200	13.33	-241
	331 (33320),			
	355 (30600)			
27	259 (73100),	-2700	5.9	-458
	327 (30114),			
	482 (1530)			
28	260 (89900),	-1400	3.6	-389
	330 (35462),			
	375 (23215)			
29	255 (87500),	-3200	5.1	-627
	276 (74432),			
	296 (65910),			
	301 (64839),			
	402 (1557)			

Table 6. (a) In CH₂Cl₂. (b) In DMF with an incident light of 1.907 μm; estimated uncertainty in EFISH measurements is ± 10%. (c) Computed dipole moments in DMF using B3LYP//6-311g/LANL2DZ//C-PCM level of theory (see chapter 3). (d) The zero-frequency static quadratic hyperpolarizabilities β₀ are -71, 114, -459, -205, -391, -331 and -547 (·10⁻³⁰ esu) for 23-29, respectively, calculated using the previously reported Eq. 7 (see section 2.1).**

Here below in Figure 16 are shown the computed HOMOs (Highest Occupied Molecular Orbitals) and LUMOs (Lowest Unoccupied Molecular Orbitals) of the synthesized compounds by means of *Density Functional Theory* (DFT), made by Dott. S. Fantacci (CNR-ISTM, Perugia) in order to investigate the effect of different substituents.

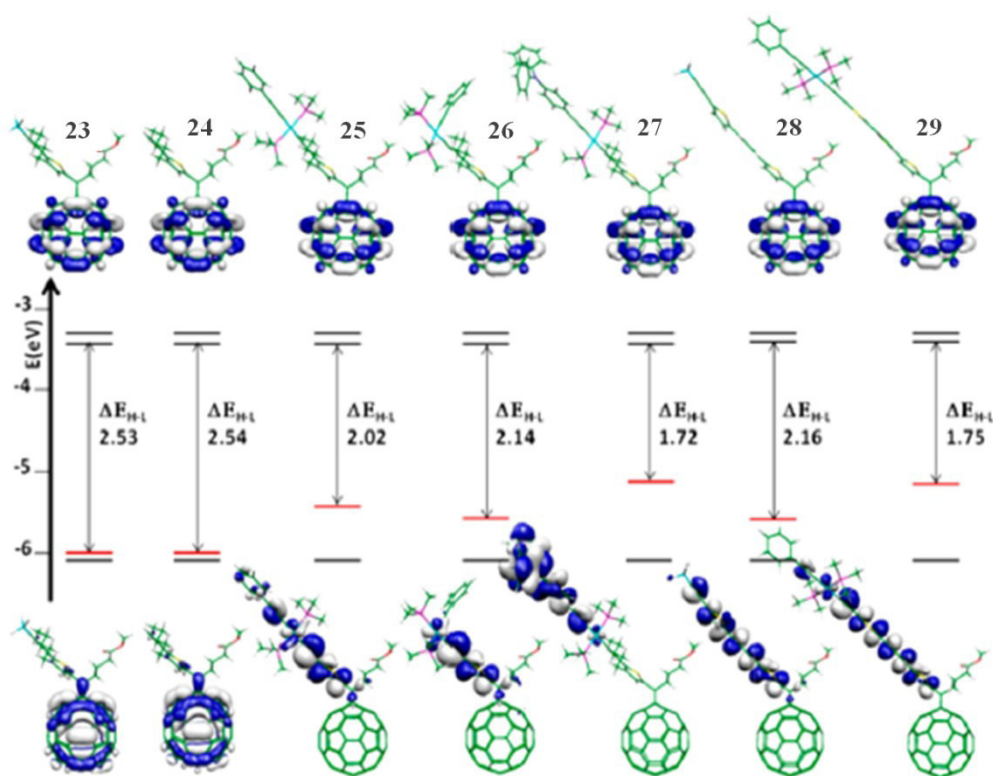


Figure 16. Frontier molecular orbitals of synthesized compounds. HOMO and LUMO isodensity plots are displayed (isodensity contour plot 0.02). The levels with chromophore contribute are red coloured, while those focused on C₆₀ fullerene are in black.

In this Figure are shown the LUMO, LUMO+1, HOMO and the highest occupied orbital centered on the fullerene. Compounds **23** and **24** have the HOMO which is delocalized on the fullerene, with a contribution from the cyclopropane ring. Differently, in compounds **25** – **29** the HOMO and HOMO-1 are totally delocalized on the Pt-alkynyl-thienyl or terthiophene fragments. The orbitals based on the fullerene are at the same energy value for all the compounds (i.e. 6.11 – 6.13 eV) and are due to the bonding π combination of the p orbitals of the sp² hybridized carbons. For compounds **23** and **24** the fullerene orbitals are the HOMO-1/HOMO-2 couple, for complexes **25** – **27** and **29** they are the HOMO-4/HOMO-5 couple, while for compound **28** are the couple HOMO-2/HOMO-3. As it is possible to understand from the Figure 16, for all the compounds the LUMO and LUMO+1 are fullerene-centered and compose the two antibonding π combinations of the p orbitals of the carbon. LUMO orbitals have basically the same energy in all compounds in the range between 3.42 – 3.44 eV; an analogous situation occurs for the LUMO+1 (3.36 – 3.38 eV). The energy of both HOMOs and LUMOs centered on fullerene does not depend on the different substituents. Relying on the electronic states in Figure 16, while for **23** and **24**, both the states are localized on the fullerene, for **25** – **29** have been observed charge transfer excited states between the alkynyl-thienyl or terthiophene moieties and the fullerene. This

difference strongly affects the second-order NLO response and explains also the higher $\mu\beta$ and β values found for **3** – **7** compared to **23** and **24** (see Table 6).

For **23** and **24** very similar values of dipole moments have been calculated (4.2 and 4.3 D, respectively), hence the removal of the trimethylsilyl protective group does not affect the electronic charge distribution. Complexes **25** and **26** have a different isomerism; in **25** (*trans*) the large dipole contribution oriented along the alkynyl axis is compensated by the fullerene dipole component, while for **26** (*cis*) the large dipole moment component is orthogonal, so it is not balanced. Charge distribution of complex **27** is similar to **25** and by substitution of the phenyl with the triphenylamine unit does not change the overall dipole moment. In a same way the introduction of the terthiophene fragment instead of the exylthiophene does not have strong effects on the μ value, which is just poorly reduced, as calculated on going from **23** to **28** and from **25** to **29**.

The EFISH technique¹³ have been applied to evaluate the NLO response in solution of all compounds. This method can achieve direct information about the intrinsic NLO properties of the molecules, through the Equation 10 (see the section 2.1):

$$\chi_{EFISH} = \frac{\mu\beta_{EFISH}(-2\omega; \omega, \omega)}{5kT} + \gamma(-2\omega; \omega, \omega, 0)$$

Where $\mu\beta_{EFISH}/5kT$ is the dipolar orientation contribution to the non linearity of the molecule and $\gamma(-2\omega; \omega, \omega, 0)$, the third order polarizability, which can be usually neglected in studies of second-order NLO properties of dipolar systems. β_{EFISH} is the projection along the dipole moment axis of the vectorial component of the quadratic hyperpolarizability tensor; in order to obtain β_{EFISH} , it is necessary to know μ . In this study theoretical dipole moments have been computed in DMF by Dott. S. Fantacci (CNR, Perugia); the procedure is better described in the experimental section (Chapter 3).

It has been found that compound **1**, which bears a weak inductive donor group consisting in the trimethylsilyl fragment,⁹⁹ hence it is characterized by a moderate $\mu\beta_{EFISH}$ value (i.e. $-350 \cdot 10^{-48}$ esu; see Table 6). The negative sign suggests a decrease of the dipole moment excited state with respect the ground state.^{52a} By formation of complexes **25** and **26**, the NLO response increases by a factor of almost 9 ($-3100 \cdot 10^{-48}$ esu and $-3200 \cdot 10^{-48}$ esu, respectively), due to an enhancement of both the dipole moment and the quadratic hyperpolarizability (Table 6). Moreover, the dipole moment of complex **3** is ca. half that of complex **26**, this means that a larger value of β_{EFISH} ($-534 \cdot 10^{-48}$ esu) is achieved in the *trans* isomer, hence when the two alkynyl groups are in *trans*

position, as expected for a more efficient *push-pull* system. The response slightly decreases in complex **27**, upon substitution of the phenyl ring with a diphenyl aniline, suggesting that the obtained total NLO response is determined by positive and negative contributions, caused by different NLO-active CT transitions, as previously found by our group for other Pt(II) complexes.⁷⁶ Surprisingly, with a trimethylsilyl group, the substitution of the hexylthiophene with a terthiophene brings to an enhancement of the $\mu\beta_{\text{EFISH}}$ value by a factor of 4 (compare **1** and **28** in Table 6), while a less important increase is registered with the *trans*-bis-(triethylphosphine)(phenylacetylide)platinum moiety (compare **25** to **29**).

This impressive $\mu\beta_{\text{EFISH}}$ values found with these fullerene platinum alkynyl derivatives are outstanding for neutral metal complexes; complex **25**, indeed, to the best of my knowledge, seems to have the largest absolute value of $\mu\beta_{\text{EFISH}}$ ever recorded for a Pt-alkynyl complex. Such a large value has been achieved only by a compound, i.e. a fullerene-ruthenium compound, *cis*-Cl-*trans*-PPh₃-[Ru(9-fulleridene-4,5-diazafluorene)-(PPh₃)₂Cl₂].^{88b}

All the trials in order to prepare second-order NLO-active polymer films with this latter Ru complex were useless. Hence, as new attempt, it has been decided to prepare composite films of **25** and **27** in both polystyrene and poly(methyl-methacrylate) in order to investigate the second harmonic generation (SHG) signal of the resulting poled host-guest systems. The films preparation procedure will be described in the experimental section (Chapter 3).

The corona wire poling (65°C and 9.5 kV) of a film containing 3-6% of complex **25** in a PMMA matrix (Figure 17a) leads to a modest SHG signal, upon the orientation of the dipolar NLO-phores; unfortunately, the SHG signal drops rapidly after the removal of the electric field. By using complex **27** instead of **25** (Figure 17b) the SHG signal increases by a factor of 2; moreover for complex **27** when the PMMA is replaced by the polystyrene as matrix a further double enhancement of the SHG signal is obtained, which again rapidly decreases by a factor of 6 when the electric field is removed, providing a final $\chi_{33}^{(2)}$ value of about 0.5 pm/V (Figure 17c).

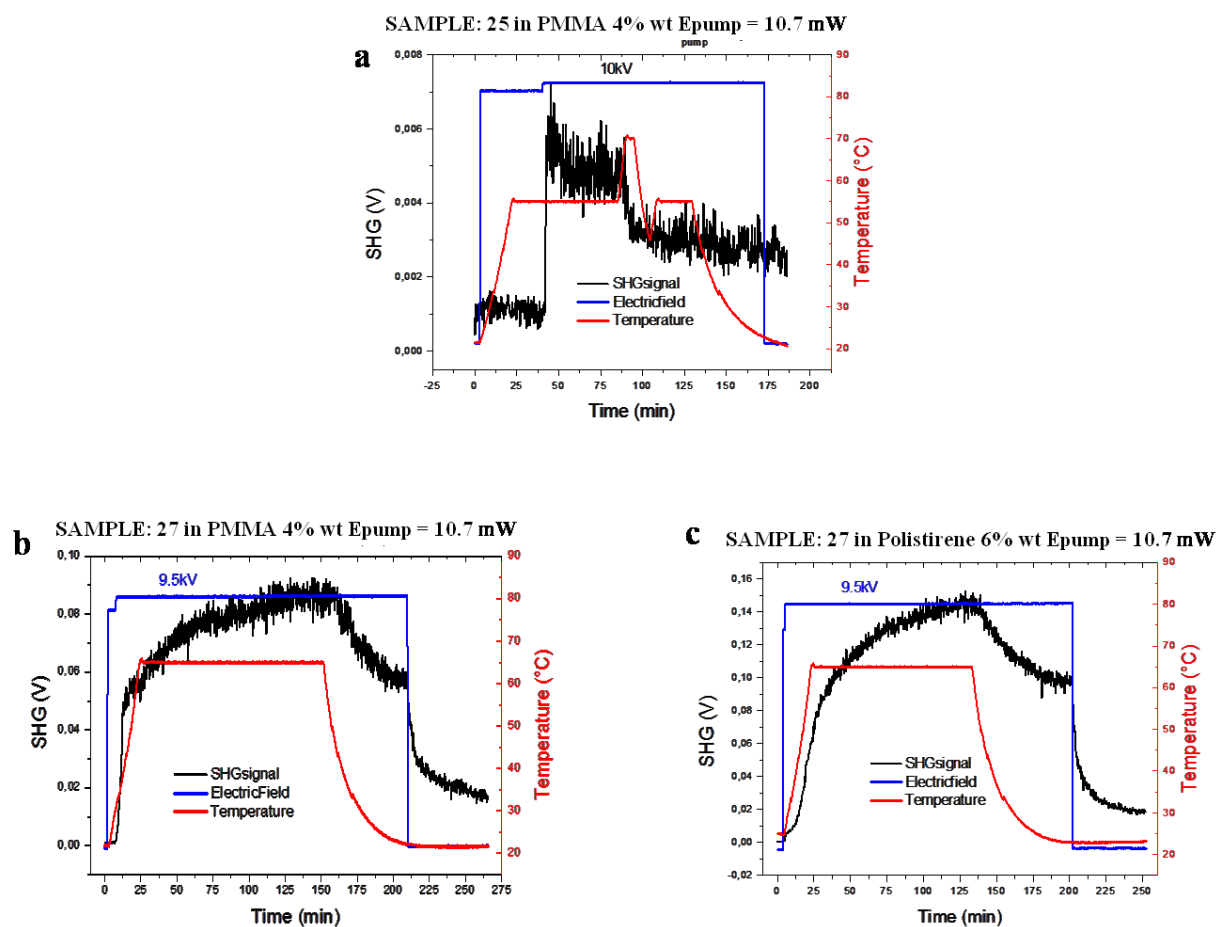


Figure 17. SHG plots of thin films containing (a) 4% (wt) of complex 3 in a PMMA matrix; (b) 4% (wt) of complex 5 in a PMMA matrix; (c) 6% (wt) of complex 5 in a polistirene matrix.

1.7.3. Conclusions

In summary, this part of my project confirmed the large fullerene potential as an acceptor group in conceiving second-order NLO-phores; its combination with a Pt-alkynyl moiety, indeed, provides a remarkable enhancement of the second-order NLO activity, as seen for instance on going from compound **24** to complex **25** or **27** and from compound **28** to **29**. Moreover the synthesized novel fullerene platinum alkynyl complexes, in particular **27**, are very promising as components for building up efficient second-order NLO devices, since their dispersion and orientation in polymer films, such as PMMA or polystyrene matrix is quite easy.

These data also confirmed the crucial role of the matrix, whose functional groups can lead to host-guest and host-host interactions, thus affecting the final stability of the organized molecules.^{38,74b} To increase this stability and thus improve the overall NLO response, as next step the NLO-phores could be covalently anchored to the matrix, in order to decrease their freedom of movement and as a consequence also their loss of orientation after the removal of the electric field.

Indeed, the progressive weakening with time of the SHG signal, due to the loss of the molecules orientation within the polymeric film is a well known problem of NLO-active material that still needs to be fixed.

1.8. Second-order non linear optics in Iridium complexes

Some Ir(III) complexes both neutral and cationic are characterized by good second-order NLO properties, which have been extensively investigated by our group. Although the NLO activity of some iridium complexes with monodentate pyridyl ligands¹⁰⁰ or terpyridyl ligands¹⁰¹ showed good results, most of the research interest was focused on cyclometallated Ir(III) complexes.

Among them, a promising class of cationic Ir(III) NLO-phores are those bearing a 1,10-phenanthroline,¹⁰² (Figure 18) since they possess a high second-order NLO response and don't absorb strongly at long wavelengths; as a consequence, the SHG can be achieved with no important cost in transparency towards the intensity of its emission.

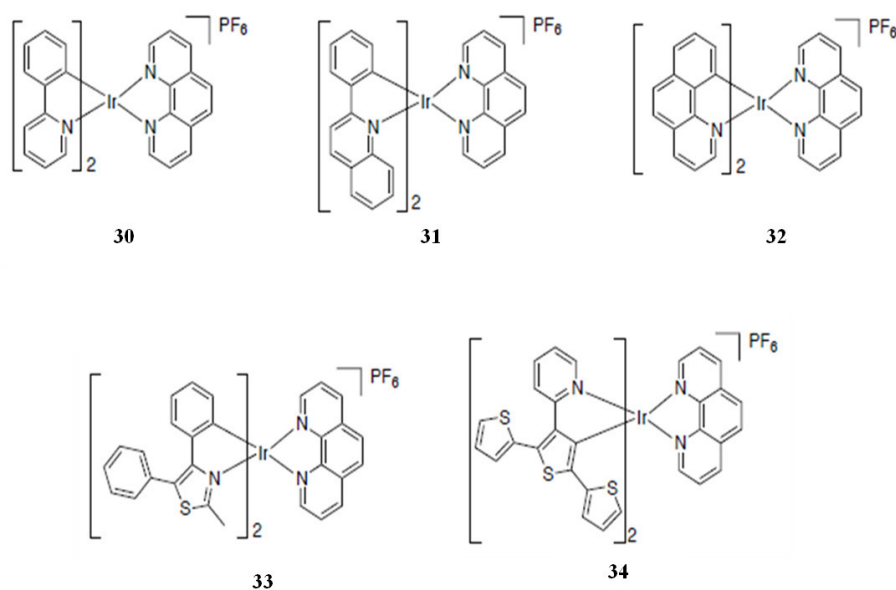


Figure 18. Ir(III) complexes studied by our group.

Complex **30** has been further functionalized on the phenanthroline moiety.¹⁰³ Among these latter, the best $\mu\beta_{\text{EFISH}}$ value has been obtained with the complex bearing a 1,10 phenanthroline with a $-\text{NO}_2$ group on the position 5 ($\mu\beta_{\text{EFISH}} = -2230 \cdot 10^{-48}$ esu), larger than those obtained for the analogous complexes with $-\text{NMe}_2$, $-\text{CH}_3$ or $-\text{H}$ in the same position 5.

To better understand this, frontier orbitals have to be considered. For this family of complexes, indeed, the HOMO is mostly composed by an antibonding combination of the t_{2g} of the metal and the π orbitals of the cyclometalated ligand, while the LUMO is constituted by the phenanthroline π^* orbital. The $-$ nitro antibonding orbital more effectively mixes with the π^* orbital on the phenanthroline: as a consequence it is stabilized, so the HOMO-LUMO gap is reduced. The resulting $\mu\beta$ value is due to a negative cooperating MLCT transitions. Differently, when the substituent is the dimethyl-amino group, a highly positive ILCT contribute has to be taken in account, resulting in a decrease of the absolute value of $\mu\beta_{\text{EFISH}}$.

If π -conjugated groups, phenyls for instance, are attached to phenanthroline positions 4 and 7, the resulting extended π -conjugated system provides an enhanced NLO response.

Interestingly, no remarkable increase was registered by our group upon substitution on the cyclometallated ligand.¹⁰⁴ Indeed, by replacing the 2,2'-phenylpyridine with a more π -conjugated system, such as benzo[h]quinoline, **31**, or 2-phenylquinoline, **32**, the NLO activity is not affected in a significant way. The response slightly decreases with the cyclometallated ligand 4,5-diphenyl-2-methyl-thiazole, **33**, and 3'-(2-pyridyl)-2,2':5',2''-tethiophene, **34**.

In summary for these complexes the NLO activity is not importantly affected by the cyclometallated fragment, but it can be modulated by the nature of the substituent on the phenanthroline ligand. Also the ion pairing can affect the $\mu\beta_{\text{EFISH}}$ absolute value: if the ion pair is not too tight, i.e. for PF_6^- , the absolute value can grow after dilution, due to a parallel decrease of the ion pairing extent. This can be assigned to a reduction of the electronic perturbation, brought by the counterion on the LUMO of the cyclometallated Ir(III) complex.

Ir(III) compounds, analogous to the $\text{Pt}(\text{ppy})(\text{acac})$ complexes observed in the paragraph 1.6.2, were also investigated by our group (Figure 19).^{74a}

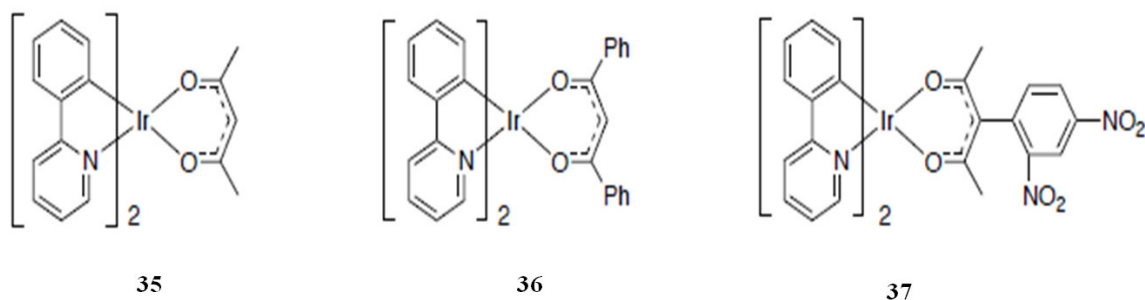


Figure 19. Investigated $\text{Ir}(\text{ppy})_2(\text{acac})$ related complexes.

Compound **36** has the largest $\mu\beta_{\text{EFISH}}$ value ($-1340 \cdot 10^{-48}$ esu), because of the two phenyl rings, which improve the π -delocalization. On the contrary, the electron-withdrawing 2,4-dinitrophenyl

group of complex **37**, leads to a much lower response ($-975 \cdot 10^{-48}$ esu). In fact, for these complexes the HOMO orbital results in an antibonding combination of d_{xy} Ir orbital and π ppy orbital, while the LUMO main contribution is given by the π^* orbitals of both the ppy and the acac ligands. The major positive contributions to the quadratic hyperpolarization comes from MLCT character transitions, while the largest negative contributions arise from higher energy transitions involving mostly ppy-ILCT transitions and a slight metal character. Hence, transitions involving just the acac ligand are less important and their contribution to β_{EFISH} is not so remarkable. Lately the second-order NLO properties of similar compounds bearing two 4-styryl-2-phenylpyridines have been examined (Figure 20).¹⁰⁵

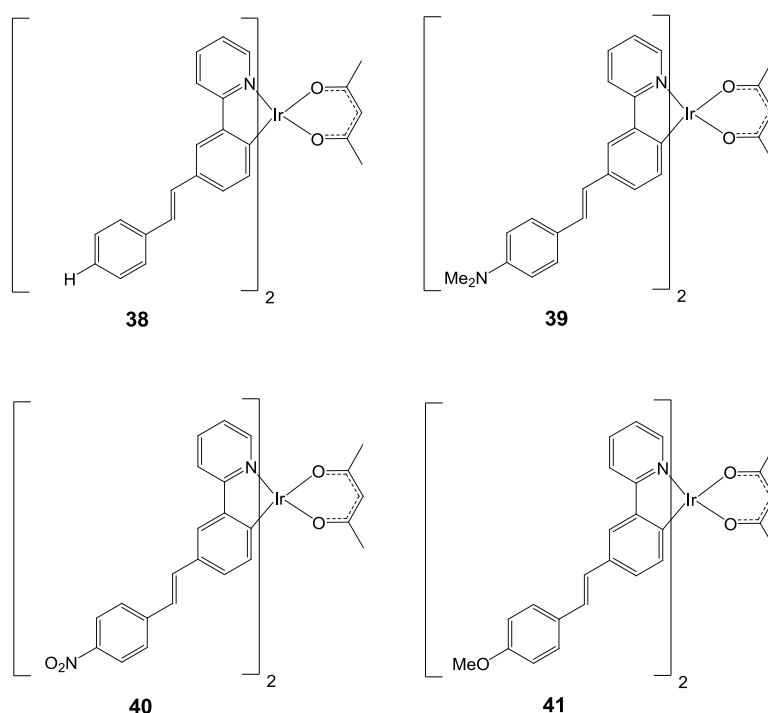


Figure 20. Other Ir(ppy)₂acac complexes studied by our group.

The β_{EFISH} values for these complexes were measured using a wavelength of 1.907 μm . Complexes **38,39,41** have second-order hyperpolarizability absolute values quite similar, but lower than **40**, whose β_{EFISH} is comparable to that of the already mentioned Ir(ppy)₂acac.

In these latter complexes the overall response is generated by the contribution of different positive and negative CT transitions, similarly to the previous Ir(III) compounds.

The second-order NLO response of cationic $[\text{Ir}(\text{ppy})_2(4,5\text{-diazafuorene})]^+$ and $[\text{Ir}(\text{ppy})_2(9\text{-fulleriden-4,5-diazafuorene})]^+$ with $\text{C}_{12}\text{H}_{25}\text{SO}_3^-$ or PF_6^- as counterions, and the neutral $[\text{Ir}(\text{ppy})_2(9\text{-fulleriden-4-monoazafluorene})]$ have also been investigated by our group.¹⁰⁶ The

$\mu\beta_{\text{EFISH}}$ values are quite high and dominated by Intra Ligand CT focused on the 2,2'-phenylpyridyl fragment. The fullerene weakens the interaction between the LUMO of the complex and the counterion, increasing the NLO activity. $\mu\beta_{\text{EFISH}}$ value for the neutral complex is comparable to other Ir(III) bis-phenylpyridine complexes, as expected for the absence of the ionic couple.

Besides, Ir(ppy)₃ complexes also resulted to be active NLO-phores.¹⁰⁷ In this context, some of us studied a series of these compounds bearing differently substituted 2,2'-phenylpyridines, in order to highlight how the NLO response would have been affected (Figure 21).

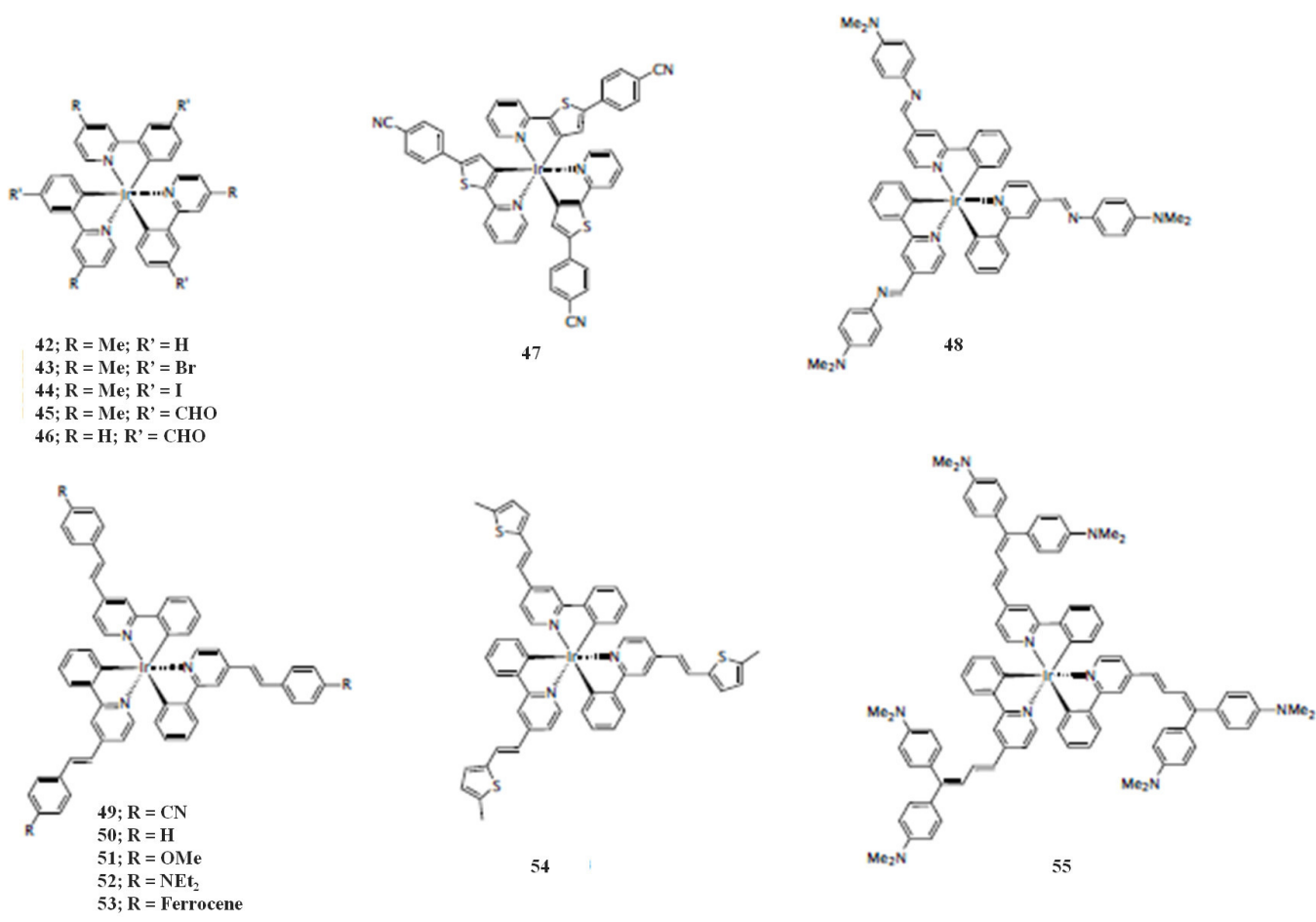


Figure 21. The Ir(ppy)₃ complexes studied for second-order NLO.

The HOMO orbital is focused both on the metal *t*_{2g} orbitals and the *p* orbitals of the phenyl (or thienyl) fragments. For complex 48 the iridium contribution to the HOMO is smaller. On the other hand, the LUMO is totally centered on the phenylpyridine ligands.

Complexes 43, 44, 45, 46, 50, 51 and 53, bearing electron-withdrawing or weakly electron-donating substituents, provide a positive value of $\mu\beta_{\text{EFISH}}$, dominated by MLCT transitions from

the iridium to the phenylpyridine. The $\mu\beta_{\text{EFISH}}$ absolute value results smaller for complexes with ligands bearing electron-acceptors, due to the contribution of ILCT transitions.

Complexes with strong electron-donors show a higher NLO response; for instance $\mu\beta_{\text{EFISH}}$ of complex **48** is equal to $1430 \cdot 10^{-48}$ esu.

For complexes **50** to **55** the second-order NLO response was also studied through the HLS technique, in order to investigate both the dipolar and octupolar components. It came out that β_{HLS} values are larger than β_{EFISH} ones, suggesting for this class of compounds a much important octupolar contribution to the overall quadratic hyperpolarizability. β_{HLS} increases with the electro-donating strength of the phenylpyridine moiety, reaching a maximum value for **55**, whose β_{HLS} was estimated to be *ca.* $-460 \cdot 10^{-48}$ esu.

1.9. Novel neutral homo- and heteroleptics Ir(III) NLO-phores.

During my PhD I've investigated also the novel Ir(III) complexes shown in Figure 22, whose second-order NLO properties have been examined. Some of them possess also from modest to remarkable luminescent and bio-medical properties, which will be better deepened in Chapter 2. The synthesis of the complexes will be discussed in the experimental section (see Chapter 3).

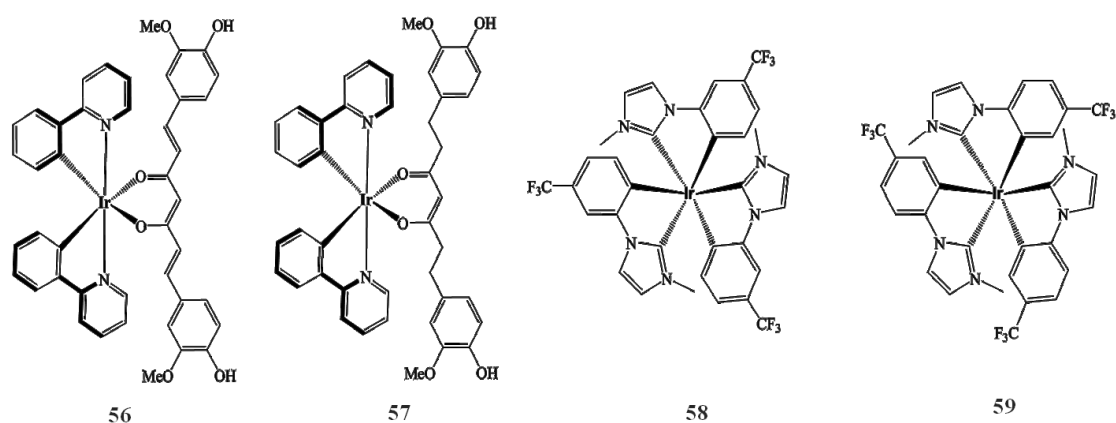


Figure 22. Novel Ir(III) complexes, object of my thesis.

For all complexes the NLO response in solution was measured in chloroform at a concentration of 10^{-3} M. It resulted that complexes **58** and **59** in solution are characterized by fair values of $\mu\beta_{\text{EFISH}}$ ($-690 \cdot 10^{-48}$ esu and $-288 \cdot 10^{-48}$ esu, respectively), whereas **57** and **56** are characterized by a modest negative value of $\mu\beta_{\text{EFISH}}$ (i.e. $-930 \cdot 10^{-48}$ esu and $-1050 \cdot 10^{-48}$ esu, respectively). This absolute value

in comparable with that of the already reported complex **35**, which has a response of $-910 \cdot 10^{-48}$ esu.

For complex **56**, which is characterized by the highest $\mu\beta_{\text{EFISH}}$ in solution, also the NLO response in the solid state was evaluated. In order to investigate the second harmonic generation (SHG) response of the resulting poled host-guest system, a composite film of the complex **56** was prepared; the preparation procedure will be described in the experimental section (Chapter 3).

The corona wire poling (65°C and 9.5 kV) of a film containing 5% of complex **56** in a PMMA matrix (Figure 23) leads to a fair SHG signal, upon the orientation of the dipolar NLO-phores, which decreases by the half when the electric field is removed, providing a final $\chi_{33}^{(2)}$ value of 2.82 pm/V .

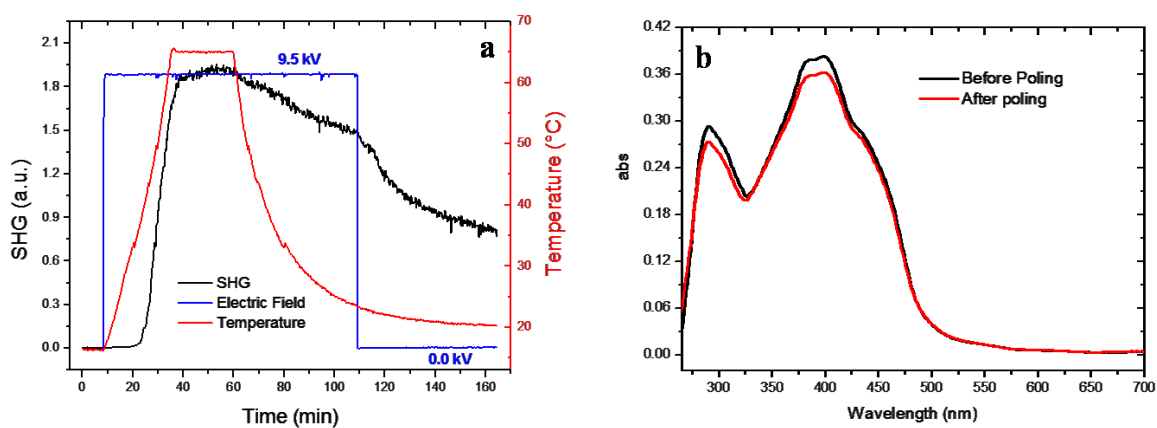


Figure 23. (a) SHG plot of thin films containing 5% (wt) of complex **56** in a PMMA matrix. (b) Absorbance spectrum before (black line) and after (blue line) poling.

This $\chi_{33}^{(2)}$ value is remarkable for such a simple complex. In fact, it was reported that for composite films of the related complex $[\text{Ir}(\text{ppy})_2(\text{acac})]$ (**35**) in PMMA matrix, the second harmonic signal, already low at the beginning in arbitrary units, rapidly (about 2 h) fell down upon turning off the electric field.¹⁰⁵ Clearly the curcumin ligand is able to stabilize the orientation of the NLO-active Ir(III) complex in the polymeric PMMA matrix, allowing a good and stable SHG response.

1.9.1. Conclusions.

Some novel neutral iridium(III) complexes have been prepared and well characterized. They show a fair to good NLO response. The most active is a bis(cyclometallated phenylpyridine)iridium(III) complex bearing a curcumin ligand. Its second-order NLO activity in solution is similar to that of the related complex with acetylacetonate instead of curcumin. However it is much more efficient

to prepare composite films with a stable SHG response, showing that curcumin plays a key role in stabilizing the orientation of the NLO-active chromophores inside the PMMA matrix.

1.10. Anionic Ir(III) NLO-phores.

To my knowledge, no anionic iridium complex has been investigated for its NLO properties. Therefore, I've synthesised different anionic Ir(III) complexes using different types of pyridines, a quinoline and a thiazole as chelating ligands with cyanide, cyanate and thiocyanate as ancillary ligands.

The synthesized compounds are reported below (Figure 21):

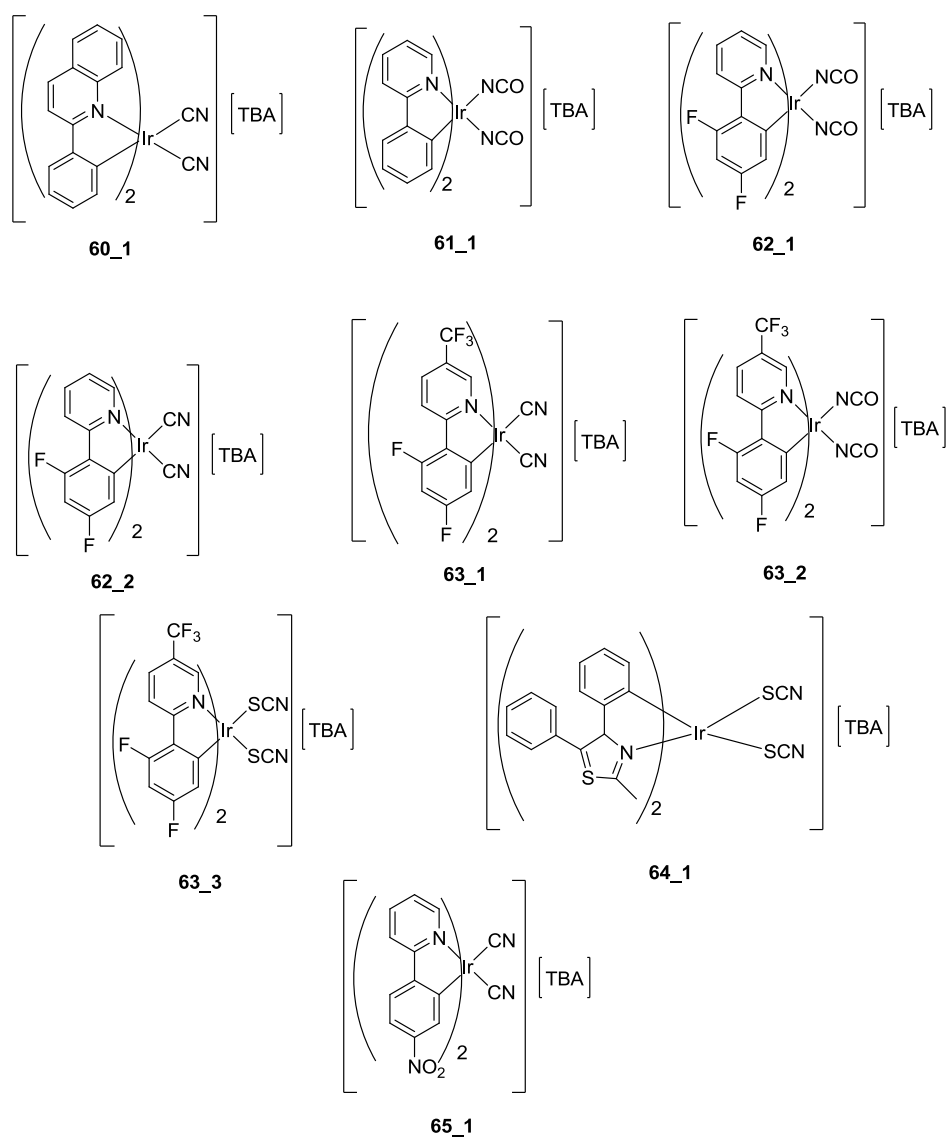


Figure 24. Synthesized Ir(III) anionic complexes.

1.10.1. Synthesis and characterization

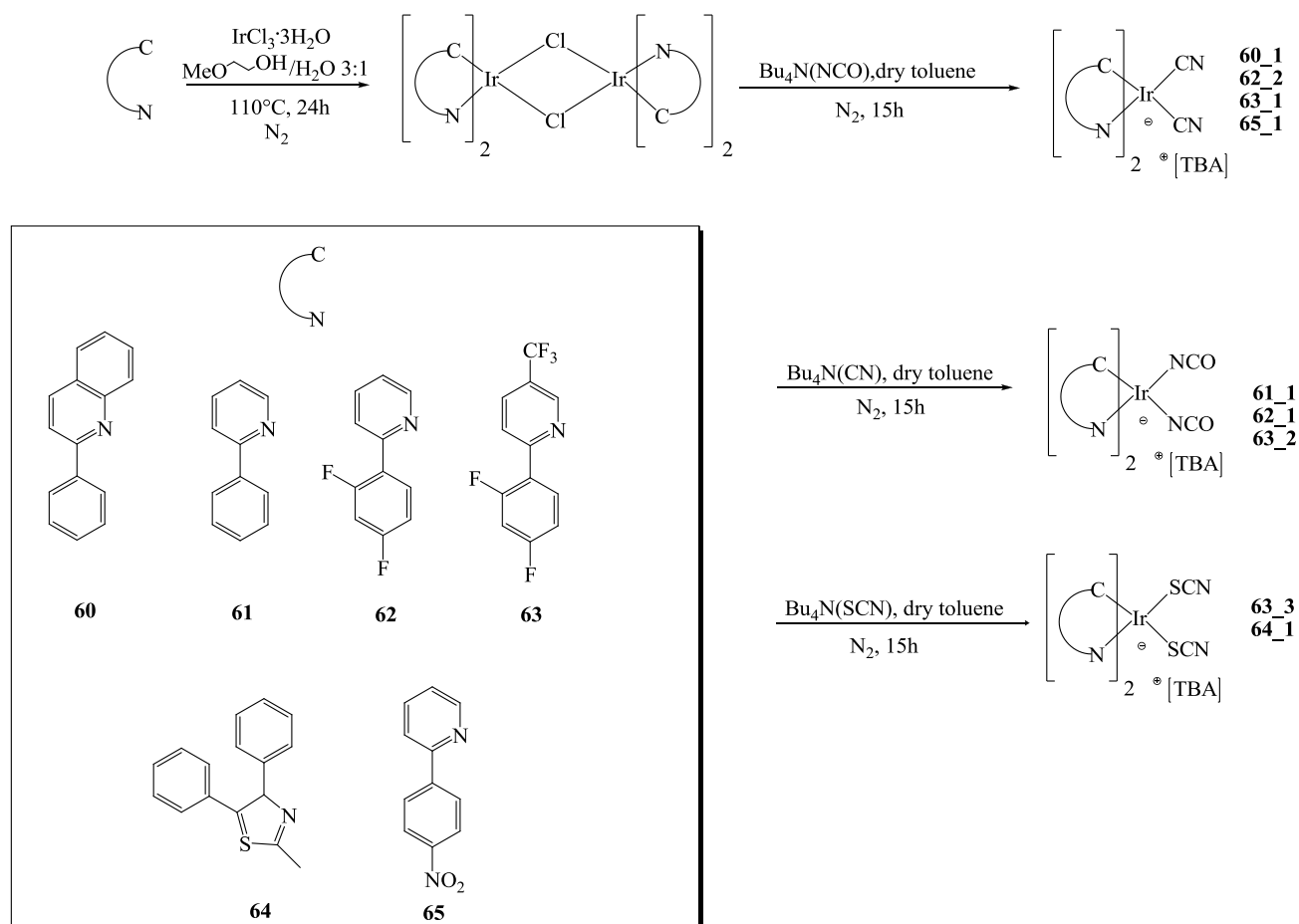
1.10.1.1. Synthesis of the anionic Iridium (III) complexes.

All the starting dimers of the related iridium complexes shown above were synthesized following the same general procedure (better discussed in Chapter 3): under N₂ atmosphere, commercial Iridium trichloride, IrCl₃·3H₂O was dissolved in a 1:1 mixture of methoxyethanol, MeOEtOH and water, and refluxed with the stoichiometric quantity of pyridine (or quinoline, or thiazole,). After 24 hours the corresponding dimer (oil or solid) was obtained.

All pyridines were commercial, except the one used for the dimer **63**, which was prepared by a Suzuki reaction between 2,4-difluorophenylboronic acid and 2-Br-5(trifluoromethyl)pyridine in the presence of [PdCl₂(PPh₃)₂] as catalyst.

All the iridium (III) anionic complexes were prepared from the related dimer, by using the same procedure: under a N₂ atmosphere, the iridium dimer was dissolved in dry CH₂Cl₂ and the respective ancillary ligand source (i.e. tetrabutylammonium cyanate, tetrabutylammonium cyanide and tetrabutylammonium thiocyanate) was added in stoichiometric amount.

The general reaction scheme is reported below (the detailed procedure will be presented in Chapter 3):



Scheme 3. General procedure for the anionic Ir(III) complexes.

1.10.1.2. Characterization of Iridium derivatives.

All compounds were characterized by UV-visible spectroscopy; the instrument specifics are reported in the Experimental section (Chapter 3). The spectra were measured in CH_2Cl_2 solution at 298 K in the range of wavelengths from 230 to 800 nm.

The absorption data in CH_2Cl_2 solution are reported in the following Table 7:

Compound	Absorption $\lambda_{\text{max}}/\text{nm}$ ($\epsilon/\text{M}^{-1}\text{cm}^{-1}$)
60_1	264(76800), 282(76500), 332(36500), 437(9400)
61_1	275(64400), 348(12600), 463(4580)
62_1	268(62100), 317(13500), 393(6120)
62_2	252(28800), 360(4630)
63_1	269(7295)

63_2	276(13394)
63_3	259(36129)
64_1	231(31100), 269(13400), 385(2610)
65_1	225(31400), 264(37100), 289(35300)

Table 7. The absorption spectra of this complexes display bands in the UV and the visible region due to intraligand ($\pi-\pi^*$) and MLCT (metal-to-ligand-charge-transfer) transitions, respectively^[108]. Hay in his recent paper has analyzed the spectral properties of iridium(III) complexes using density functional theory (DFT), in which the low-lying transitions are categorized as metal-to-ligand-charge-transfer transitions and the high energy bands at above 280 nm are assigned to intraligand ($\pi-\pi^*$) transitions^[109,110].

1.10.2. EFISH measurements.

To evaluate the second order non-linear hyperpolarizability of these complexes, the already described EFISH technique was used. The measured data are reported in the following Table 8:

Sample	Solvent	Concentration/M	$\mu\beta/x10^{-48}$ esu
61_1	CHCl ₃	10 ⁻³	-580
62_1	CHCl ₃	10 ⁻³	-400
62_2	CHCl ₃	10 ⁻³	-577

Table 8. $\mu\beta_{\text{EFISH}}$ measurement for the related complexes, measured in a CHCl₃ solution at a 10⁻³ M concentration.

These data are preliminary and EFISH measurements were not performed on all the synthesized complexes. Up to now, all the investigated complexes show good negative values; **61_1**, which bears no substituents on the phenylpyridine ring, has the highest absolute value; a similar value is obtained with complex **62_2**. In this kind of complexes the NLO response can be modulated by the nature of both the phenylpyridine substituents and the ancillary ligands.

1.10.3. Conclusions.

Various novel anionic iridium(III) complexes have been prepared and well characterized. They are characterized by good second-order NLO properties, a remarkable observation because the NLO

response of anionic iridium complexes have never been studied up to now. In the near future, the luminescent properties of these complexes will be investigated.

1.11. References:

1. *McGraw-Hill Encyclopedia of Science and Technology* (5th ed.). McGraw-Hill. 1993.
2. P. A. Franke, A. E. Hill, C. W. Peters, G. Weinreich, *Phys. Rev. Lett.* **1961**, 7, 118.
3. N. Bloembergen, *Nonlinear Optics*, **1965**, Benjamin, New York.
4. S. Di Bella, C. Dragonetti, M. Pizzotti, D. Roberto, F. Tessore, R. Ugo, *Top. Organomet. Chem.* **2010**, 28, 1-55.
5. Design and Construction of Molecular Assemblies with Large Second-Order Optical Nonlinearities. Quantum Chemical Aspects. Kanis D. R., Ratner M. A., Marks T. J., *Chem. Rev.* **1994**, 94, 195.
6. a) J. L. Oudar, D. S. Chemla, *J. Chem. Phys.* **1977**, 66, 2664; b) J. L. Oudar, *J. Chem. Phys.* **1977**, 67, 446.
7. a) O. Riant, G. Bluet, S. Brasselet, N. Druze, I. Ledoux, F. Lefloch, A. Skibniewski, J. Zyss, *Mol. Cryst. Liq. Cryst.* **1998**, 322, 35; b) J. Zyss, I. Ledoux, *Chem. Rev.* **1994**, 94, 77; c) H. Le Bozec, T. Le Bouder, O. Maury, I. Ledoux, J. Zyss, *J. Opt. A: Pure Appl. Opt.* **2002**, 4, S189.
8. A. Ashkin, G. D. Boyd, J. M. Dziedzic, *IEEE J. Quantum Electron.* **1966**, 2, 109.
9. M. Bass, P. A. Franken, J. F. Ward, G. Weinreich, *Phys. Rev. Lett.* **1962**, 9, 446.
10. R. W. Boyd, *Nonlinear Optics 3rd edition*, **2008**, Academic Press.
11. J. F. Nye, *Physical Properties of Crystals* (Clarendon, Oxford, 1985), Chap. 13.
12. Kerr, John (1875). "A new relation between electricity and light: Dielectric media birefringent". *Philosophical Magazine*. **4.50**, 332, 337.
13. a) I. Ledoux, J. Zyss, *J. Chem. Phys.* **1982**, 73, 203; b) G. R. Meredith, *Rev. Sci. Instrum.* **1982**, 53, 48; c) K. D. Singer, A. F. Garito, *J. Chem. Phys.* **1981**, 75, 3572; d) C. G. Bethea, *Appl. Opt.* **1975**, 14, 1447.

14. E. A. Guggenheim, *Trans. Faraday Soc.*, **1951**, 47, 573.
15. D. J. Williams, *Angew. Chem. Int. Ed. Engl.* **1984**, 23, 690.
16. P.D. Maker, *Phys Rev A* **1970**, 1, 923.
17. K. Clays, A. Persoons, *Phys. Rev. Lett.* **1991**, 66, 2980.
18. W. M. Laidlaw, R. G. Denning, T. Verbiest, E. Chauchard, A. Persoons, *Proc. SPIE Int. Soc. Opt. Eng.* **1994**, 2143, 14.
19. S. Bruni, E. Cariati, F. Cariati, F. A. Porta, S. Quici, D. Roberto, *Spectrochimica Acta Part A* **2001**, 57, 1417.
20. C. H. Wang, J. N. Woodford, A. K.-Y. Jen, *Chem. Phys.* **2000**, 262, 475.
21. D. R. Kanis, M. A. Ratners, T. J. Marks, *Chem. Rev.* **1994**, 94, 195.
22. L.-T. Cheng, W. Tam, S. H. Stevenson, G. R. Meredith, G. Rikken, S. R. Marder, *J. Phys. Chem.* **1991**, 95, 10631.
23. L.-T. Cheng, W. Tam, S. R. Marder, A. E. Stiegman, G. Rikken, C. W. Spangler, *J. Phys. Chem.* **1991**, 95, 10643.
24. a) S. R. Marder, D. N. Beratan, L.-T. Cheng, *Science* **1991**, 252, 103; b) F. Meyers, S. R. Marder, B. M. Pierce, J. L. Bredas, *J. Am. Chem. Soc.* **1994**, 116, 10703; c) C. B. Gorman, S. R. Marder, *Proc. Natl. Acad. Sci. USA* **1993**, 90, 11297.
25. S. R. Marder, B. Kippelen, A. K.-Y. Jen, N. Peyghambarian, *Science*, **1997**, 388, 845.
26. a) I. D. L. Albert, T. J. Marks, M. A. Ratner, *J. Am. Chem. Soc.* **1997**, 119, 6575-6582; b) C.-F. Shu, Y.-K. Wong, *J. Mater. Chem.* **1998**, 8, 833.
27. P. R. Varanasi, A. K.-Y. Jen, J. Chandrasekhar, I. N. N. Namboothiri, A. Rathna, *J. Am. Chem. Soc.* **1996**, 118, 12443.

28. a) V. P. Rao, K. Y. Wong, A. K.-Y. Jen, K. J. Drost, *Chem. Mater.* **1994**, *6*, 2210; b) E. M. Breitung, C.-F. Shu, R. J. McMahon, *J. Am. Chem. Soc.* **2000**, *122*, 1154.
29. a) A. K.-Y. Jen, V. P. Rao, K. Y. Wong, K. J. Drost, *J. Chem. Soc. Chem. Commun.* **1993**, 90; b) V. P. Rao, A. K.-Y. Jen, K. Y. Wong, K. J. Drost, *Tetrahedron Lett.* **1993**, *34*, 1747.
30. Y. K. Wang, C.-F. Shu, E. M. Breitung, R. J. McMahon, *J. Mater. Chem.* **1999**, *9*, 449.
31. A. K.-Y. Jen, Y. Cai, P. W. Bedworth, S. R. Marder, *Adv. Mater.* **1997**, *9*, 132.
32. K. D. Singer, J. E. Sohn, L. A. King, H. M. Gordon, *J. Opt. Soc. Am. B* **1989**, *6*, 1339.
33. S. J. Benight, D. H. Bale, B. C. Olbricht, L. R. Dalton, *J. Mater. Chem.* **2009**, *19*, 7466.
34. S. K. Kurtz, T. T. Perry, *J. Appl. Phys.* **1968**, *39*, 3798.
35. D. Espa, L. Pilia, L. Marchiò, F. Artizzu, G. Di Carlo, D. Marinotto, A. Serpe, F. Tessore, P. Deplano, *Dalton Trans.* **2016**, *45*, 17431.
36. P. D. Maker, R. W. Terhune, M. Nisenoff, C. M. Savage, *Phys. Rev. Lett.* **1962**, *8*, 21.
37. a) J. Jerphagnon, S. K. Kurtz, *Phys. Rev. B: Solid State* **1970**, *1*, 1739-1744; b) W. N. Herman, L. M. Hayden, *J. Opt. Soc. Am. B* **1995**, *12*, 416.
38. D. Marinotto, R. Castagna, S. Righetto, C. Dragonetti, A. Colombo, C. Bertarelli, M. Garbugli, G. Lanzani, *J. Phys. Chem. C* **2011**, *115*, 20425.
39. a) E. Cariati, M. Pizzotti, D. Roberto, F. Tessore, R. Ugo, *Coord. Chem. Rev.* **2006**, *250*, 1210; b) O. Maury, H. Le Bozec, *Metal-Based Quadratic Nonlinear Optical Materials*, **2010**, John Wiley & Sons, Ltd, Chichester, UK; c) N. J. Long, *Angew. Chem. Int. Ed. Engl.* **1995**, *34*, 21.
40. M. L. H. Green, S. R. Marder, M. E. Thompson, J. A. Bandy, D. Bloor, P. V. Kolinsky, R. J. Jones, *Nature* **1987**, *330*, 360.

41. S. Barlow, S. R. Marder, *Chem. Commun.* **2000**, 1555.
42. J. C. Calabrese, L.-T. Cheng, J. C. Green, S. R. Marder, W. Tam, *J. Am. Chem. Soc.* **1991**, *113*, 7227.
43. J. A. Mata, E. Peris, I. Asselberghs, R. Van Boxel, A. Persoons, *New J. Chem.* **2001**, 299.
44. T. Farrell, A. R. Manning, T. C. Murphy, T. Meyer-Friedrichsen, J. Heck, I. Asselberghs, A. Persoons, *Eur. J. Inorg. Chem.* **2001**, 2365.
45. V. Alain, M. Blanchard-Desce, C.-T. Chen, S. R. Marder, A. Fort, M. Barzoukas, *Synth. Met.* **1996**, 133.
46. S.-J. Wang, Y.-F. Wang, C. Cai, *J. Phys. Chem. C* **2015**, *119*, 16256.
47. a) C. E. Powell, M. G. Humphrey, *Coord. Chem. Rev.* **2004**, *248*, 725; b) M. P. Cifuentes, M. G. Humphrey, *J. Organomet. Chem.* **2004**, 689, 3968.
48. F. Nisic, A. Colombo, C. Dragonetti, E. Garoni, D. Marinotto, S. Righetto, F. De Angelis, M. G. Lobello, P. Salvatori, P. Biagini, F. Melchiorre, *Organometallics* **2015**, *34*, 94.
49. L.-T. Cheng, W. Tam, G. R. Meredith, S. R. Marder, *Mol. Cryst. Liq. Cryst.* **1990**, *189*, 137.
50. D. Roberto, R. Ugo, S. Bruni, E. Cariati, F. Cariati, P. C. Fantucci, I. Invernizzi, *Organometallics* **2000**, *19*, 1775.
51. L.-T. Cheng, W. Tam, D. F. Eaton, *Organometallics* **1990**, *9*, 2856.
52. a) D. R. Kanis, P. G. Lacroix, M. A. Ratner, T. J. Marks, *J. Am. Chem. Soc.* **1994**, *116*, 10089; b) D. W. Bruce, A. Thornton, *Mol. Cryst. Liq. Cryst.* **1993**, *231*, 253.
53. a) F. Tessore, D. Roberto, R. Ugo, P. Mussini, S. Quici, I. Ledoux-Rak, J. Zyss, *Angew. Chem. Int. Ed.* **2003**, *42*, 456; b) F. Tessore, D. Locatelli, S. Righetto, D. Roberto, R. Ugo, *Inorg. Chem.* **2005**, *44*, 2437.

54. B. J. Coe, J. P. Essex-Lopresti, J. A. Harris, S. Houbrechts, A. Persoons, *Chem. Commun.* **1997**, 1645.
55. B. J. Coe, M. C. Chamberlain, J. P. Essex-Lopresti, S. Gaines, J. C. Jeffery, S. Houbrechts, A. Persoons, *Inorg. Chem.* **1997**, *36*, 3284.
56. B. J. Coe, L. A. Jones, J. A. Harris, E. E. Sanderson, B. S. Brunshwig, I. Asselberghs, K. Clays, A. Persoons, *Dalton Trans.* **2003**, 2335.
57. B. J. Coe, J. A. Harris, L. J. Harrington, J. C. Jeffery, L. H. Rees, S. Houbrechts, A. Persoons, *Inorg. Chem.* **1998**, *37*, 3391.
58. B. J. Coe, L. A. Jones, J. A. Harris, B. S. Brunshwig, I. Asselberghs, K. Clays, A. Persoons, J. Garin, J. Orduna, *J. Am. Chem. Soc.* **2004**, *126*, 3880.
59. a) B. J. Coe, J. A. Harris, B. S. Brunshwig, *Dalton Trans.* **2003**, 2384; b) B. J. Coe, S. P. Foxon, E. C. Harper, M. Helliwell, J. Raftery, C. A. Swanson, B. S. Brunshwig, K. Clays, E. Franz, J. Garin, J. Orduna, P. N. Horton, M. B. Hursthouse, *J. Am. Chem. Soc.* **2010**, *132*, 1706; c) B. J. Coe, *Acc. Chem. Res.* **2006**, *39*, 383.
60. a) M. Bourgault, C. Mountassir, H. Le Bozec, I. Ledoux, G. Pucetti, J. Zyss, *J. Am. Chem. Soc. Chem. Commun.* **1993**, 1623; b) A. Hilton, T. Renouard, O. Maury, H. Le Bozec, I. Ledoux, J. Zyss, *Chem. Commun.* **1999**, 2521.
61. M. Bourgault, K. Baum, H. Le Bozec, G. Pucetti, I. Ledoux, J. Zyss, *New J. Chem.* **1998**, 517.
62. D. Roberto, R. Ugo, F. Tessore, E. Lucenti, S. Quici, S. Vezza, S. Bruni, I. Ledoux-Rak, J. Zyss, *Organometallics* **2002**, *21*, 161.
63. T. Renouard, H. Le Bozec, I. Ledoux, J. Zyss, *Chem. Commun.* **1999**, 871.
64. K. Sénéchal, O. Maury, H. Le Bozec, I. Ledoux, J. Zyss, *J. Am. Chem. Soc.* **2002**, *124*, 4561.

65. a) O. Maury, L. Viau, K. Sénéchal, B. Corre, J.-P. Guégan, T. Renouard, I. Ledoux, J. Zyss, H. Le Bozec, *Chem. Eur. J.* **2004**, *10*, 4454; b) C. Feuvrie, O. Maury, H. Le Bozec, I. Ledoux, J. P. Morral, G. T. Dalton, M. Samoc, M. G. Humphrey, *J. Phys. Chem. A* **2007**, *111*, 8980.
66. a) D. Roberto, F. Tessore, R. Ugo, S. Bruni, A. Manfredi, S. Quici, *Chem. Commun.* **2002**, 846; b) S. De Angelis, S. Fantacci, A. Sgamellotti, F. Cariati, D. Roberto, F. Tessore, R. Ugo, *Dalton Trans.* **2006**, 6707.
67. A. Colombo, D. Locatelli, D. Roberto, F. Tessore, R. Ugo, M. Cavazzini, S. Quici, F. De Angelis, S. Fantacci, I. Ledoux-Rak, N. Tancrez, J. Zyss, *Dalton Trans.* **2012**, *41*, 6707.
68. M. O. Senge, M. Fazekas, E. G. A. Notaras, W. J. Blau, M. Zawadzka, O. B. Locos, E. M. NiMhuircheartaigh, *Adv. Mater.* **2007**, *19*, 2737.
69. a) S. M. Le Cours, H.-W. Guan, S. G. Di Magno, C. H. Wang, M. J. Therien, *J. Am. Chem. Soc.* **1996**, *118*, 1497; b) L. Karki, F. W. Vance, J. T. Hupp, S. M. Le Cours, M. J. Therien, *J. Am. Chem. Soc.* **1998**, *120*, 2606.
70. M. Pizzotti, E. Annoni, R. Ugo, S. Bruni, S. Quici, P. C. Fantucci, M. Bruschi, G. Zerbi, M. Del Zoppo, *J. Porph. Phthal.* **2004**, *8*, 1311.
71. M. Pizzotti, F. Tessore, A. Orbelli Biroli, R. Ugo, F. De Angelis, S. Fantacci, A. Sgamellotti, D. Zuccaccia, A. Macchioni, *J. Phys. Chem. C* **2009**, *113*, 11131.
72. A. Nayak, J. Park, K. De Mey, X. Hu, T. V. Duncan, D. N. Beratan, K. Clays, M. J. Therien, *ACS Cent. Sci.* **2016**, *2*, 954.
73. a) P. G. Lacroix *Eur. J. Inorg. Chem.* **2001**, 339; b) S. Di Bella, I. Fragalà, I. Ledoux, M. A. Diaz-Garcia, T. J. Marks, *J. Am. Chem. Soc.* **1997**, *119*, 9550.
74. a) A. Valore, A. Colombo, C. Dragonetti, S. Righetto, D. Roberto, R. Ugo, F. De Angelis, S. Fantacci, *Chem. Commun.* **2010**, *46*, 2414; b) A. Colombo, C. Dragonetti, D. Marinotto, S. Righetto, D. Roberto, S. Tavazzi, M. Escadeillas, V. Guerschais, H. Le Bozec, A. Boucekkine, C. Latouche, *Organometallics* **2013**, *32*, 3890.

75. A. Scarpaci, C. Monnereau, N. Hergué, E. Blart, S. Legoupy, F. Odobel, A. Gorfo, J. Pérez-Moreno, K. Clays, I. Asselberghs, *Dalton Trans.* **2009**, 4538.
76. E. Rossi, A. Colombo, C. Dragonetti, S. Righetto, D. Roberto, R. Ugo, A. Valore, J. A. G. Williams, M. G. Lobello, F. De Angelis, S. Fantacci, I. Ledoux-Rak, A. Singh, J. Zyss, *Chem. Eur. J.* **2013**, *19*, 9875.
77. T. T. Dang, J.-F. Soulé, H. Doucet, M. A. Benmensour, A. Boucekkine, A. Colombo, C. Dragonetti, S. Righetto, D. Jacquemin, J. Boixel, V. Guerschais, *Eur. J. Inorg. Chem.* **2016**, 4774.
78. a) K. A. Green, M. P. Cifuentes, M. Samoc, M. G. Humphrey, *Coord. Chem. Rev.* **2011**, 255, 2025; b) K. A. Green, M. P. Cifuentes, M. Samoc, M. G. Humphrey, *Coord. Chem. Rev.* **2011**, 255, 2530; c) G. Grelaud, M. P. Cifuentes, F. Paul, M. G. Humphrey, *J. Organomet. Chem.* **2014**, 751, 181; d) E. Kulasekera, S. Petrie, R. Stranger, M. G. Humphrey, *Organometallics*, **2014**, *33*, 2434.
79. a) G.-J. Zhou, W.-Y. Wong, *Chem. Soc. Rev.* **2011**, *40*, 2541; b) G.-J. Zhou, W.-Y. Wong, Z. Lin, C. Ye, *Angew. Chem. Int. Ed.* **2006**, *45*, 6189.
80. G. G. Dubinina, R. S. Price, K. A. Abboud, G. Wicks, P. Wnuk, Y. Stepanenko, M. Drobizhev, A. Rebane, K. S. Schanze, *J. Am. Chem. Soc.* **2012**, *134*, 19346.
81. a) W.-Y. Wong, C.-L. Ho, *Acc. Chem. Res.* **2010**, *43*, 1246; b) F.-R. Dai, H.-M. Zhan, Q. Liu, Y.-Y. Fu, J.-H. Li, Q.-W. Wang, Z. Xie, L. Wang, F. Yan, W.-Y. Wong, *Chem. Eur. J.* **2012**, *18*, 1502; c) Q. Wang, W.-Y. Wong, *Polym. Chem.* **2011**, *2*, 432; d) F.-R. Dai, Y.-C. Chen, L.-F. Lai, W.-J. Wu, C.-H. Cui, G.-P. Tan, X.-Z. Wang, J.-T. Lin, H. Tian, W.-Y. Wong, *Chem. Asian J.* **2012**, *7*, 1426.
82. R. Liu, N. Dandu, C. McCleese, Y. Li, T. Lu, H. Li, D. Yost, C. Wang, S. Kilina, C. Burda, W. Sun, *Eur. J. Inorg. Chem.* **2015**, 5241.
83. P. Nguyen, G. Lesley, T. B. Marder, *Chem. Mater.* **1997**, *9*, 406.
84. A. Colombo, F. Nisic, C. Dragonetti, D. Marinotto, I. P. Oliveri, S. Righetto, M. G. Lobello, F. De Angelis, *Chem. Commun.* **2014**, *50*, 7986.

85. R. Durand, S. Gauthier, S. Achelle, S. Kahlal, J.-Y. Saillard, A. Barsella, L. Wojcik, N. Le Poul, F. Robin-Le Guen, *Dalton Trans.* **2017**, 46, 3059.
86. **Novel fullerene platinum alkynyl complexes with high second-order nonlinear optical properties as a springboard for NLO-active polymer films.** C. Dragonetti, A. Colombo, M. Fontani, D. Marinotto, F. Nisic, S. Righetto, D. Roberto, F. Tintori, S. Fantacci. *Organometallics*, **2016**, 7, 1015.
87. a) M. Prato, *J. Mater. Chem.* **1997**, 7, 1097; b) D. M. Guldi, *Chem. Commun.* **2000**, 321; c) Nakamura, Y.; Minami, S.; Iizuka, K.; Nishimura, J. *Angew. Chem., Int. Ed.* **2003**, 42, 3158.
88. a) N. Tsuboya, R. Hamasaki, M. Ito, M. Mitsuishi,; T. Miyashita, Y. Yamamoto, *J. Mater. Chem.* **2003**, 13, 511; b) A. Valore, M. Balordi, A. Colombo, C. Dragonetti, S. Righetto, D. Roberto, R. Ugo, T. Benincori, G. Rampinini, F. Sannicolò, *Dalton Trans.* **2010**, 39, 10314; c) C. Dragonetti, A. Valore, A. Colombo, S. Righetto, G. Rampinini, F. Colombo, L. Rocchigiani, A. Macchioni, *Inorg. Chim. Acta*, **2012**, 382, 72; d) W.-Y. Wang, L. Wang, N.-N. Ma, C.-L. Zhu, Y.-Q. Qiu, *Dalton Trans.* **2015**, 44, 10078.
89. S. H. Lee, C. T. L. Chan, K. M. C. Wong, W. H. Lam, W. M. Kwok, V. W. W. Yam, *Dalton Trans.* **2014**, 43, 7624.
90. S. H. Lee, C. T. L. Chan, K. M. C. Wong, W. H. Lam, W. M. Kwok, V. W. W. Yam, *J. Am. Chem. Soc.* **2014**, 136, 10041.
91. F. Guo, K. Ogawa, Y. G. Kim, E. O. Danilov, F. N. Castellano, J. R. Reynolds, K. S. Schanze, *Phys. Chem.* **2007**, 9, 2724.
92. a) F. Wudl, T. Suzuki, M. Prato, *Synth. Met.* **1993**, 59, 297. b) T. Benincori, E. Brenna, F. Sannicolò, L. Trimarco, G. Zotti, P. Sozzani, *Angew. Chem., Int. Ed. Engl.* **1996**, 35, 648.
93. F. Nisic, A. Colombo, C. Dragonetti, A. Cominetti, A. Pellegrino, N. Perin, R. Po, A. Tacca, *Int. J. Photoenergy*, **2014**, 1.
94. H. Zhao, X. Guo, H. Tian, C. Li, Z. Xie, Y. Geng, F. Wang, *J. Mater. Chem.* **2010**, 20, 3092.

95. H. J. Choi, K. Son, T. Kim, K. Kim, K. Ohkubo, S. Fukuzumi, *J. Mater. Chem.* **2010**, *20*, 475.
96. H. J. Choi, T. Honda, S. Seki, S. Fukuzumi, *Chem. Commun.* **2011**, *47*, 11213.
97. a) A. Colombo, F. Nisic, C. Dragonetti, D. Marinotto, I. P. Oliveri, S. Righetto, M. G. Lobello, F. De Angelis, *Chem. Commun.* **2014**, *50*, 7986; b) F. Nisic, A. Colombo, C. Dragonetti, E. Garoni, D. Marinotto, S. Righetto, F. De Angelis, M. G. Lobello, P. Salvatori, P. Biagini, F. Melchiorre, *Organometallics*, **2015**, *34*, 94.
98. C. Saravanan, C.-L. Liu, Y.-M. Chang, J.-D. Lu, Y.-J. Hsieh, S.-P. Rwei, L. Wang, *ACS Appl. Mater. Interfaces*, **2012**, *4*, 6133.
99. P. G. Gassman, P. A. Deck, C. H. Winter, D. A. Dobbs, D. H. Cao, *Organometallics*, **1992**, *11*, 959.
100. V. Calabrese, S. Quici, E. Rossi, E. Cariati, C. Dragonetti, D. Roberto, E. Tordin, F. De Angelis, S. Fantacci, *Chem. Commun.* **2010**, 8374.
101. a) D. Roberto, F. Tessore, R. Ugo, S. Bruni, A. Manfredi, S. Quici, *Chem. Commun.* **2002**, 846; b) F. Tessore, D. Roberto, R. Ugo, M. Pizzotti, S. Quici, M. Cavazzini, S. Bruni, F. De Angelis, *Inorg. Chem.* **2005**, *44*, 8967.
102. a) A. Valore, E. Cariati, C. Dragonetti, S. Righetto, D. Roberto, R. Ugo, F. De Angelis, S. Fantacci, A. Sgamellotti, A. Macchioni, D. Zuccaccia, *Chem. Eur. J.* **2010**, *16*, 4814; b) I. González, D. Cortés-Arriagada, P. Dreyse, L. Sanhueza-Vega, I. Ledoux-Rak, D. Andrade, I. Brito, A. Toro-Labbé, M. Soto-Arriaza, S. Caramori, B. Loeb, *Eur. J. Inorg. Chem.* **2015**, 4946.
103. C. Dragonetti, S. Righetto, D. Roberto, R. Ugo, A. Valore, S. Fantacci, A. Sgamellotti, F. De Angelis, *Chem. Commun.* **2007**, 4116.
104. a) C. Dragonetti, S. Righetto, D. Roberto, A. Valore, *Phys. Status Solidi C*. **2009**, *S1*, S50; b) C. Dragonetti, S. Righetto, D. Roberto, A. Valore, T. Benincori, F. Sannicolò, F. De Angelis, S. Fantacci, *J. Mater. Sci.: Mater. Electron.* **2009**, *20*, S460; c) C. Dragonetti, S. Righetto, D.

- Roberto, R. Ugo, A. Valore, F. Demartin, F. De Angelis, A. Sgamellotti, S. Fantacci, *Inorganica Chim. Acta.* **2008**, 361,4070.
105. C. Dragonetti, A. Colombo, D. Marinotto, S. Righetto, D. Roberto, A. Valore, M. Escadeillas, V. Guerchais, H. Le Bozec, A. Boucekkine, C. Latouche, *J. Organomet. Chem.* **2014**, 751, 568.
106. C. Dragonetti, A. Valore, A. Colombo, D. Roberto, S. Righetto, G. Rampinini, F. Colombo, L. Rocchigiani, A. Macchioni, *Inorganica Chim. Acta.* **2012**, 382, 72.
107. M. Zaarour, V. Guerchais, H. Le Bozec, C. Dragonetti, S. Righetto, D. Roberto, F. De Angelis, S. Fantacci, M. G. Lobello, *Dalton Trans.* **2013**, 42, 155.
108. Miyaura, N.; Suzuki, A. *Chem. Commun.* **1979**, 866.
109. Schmid, B.; Garces, F. O.; Watts, R. J. *Inorg. Chem.* **1994**, 33, 9.
110. Hay, P. J. *J. Phys. Chem. A* **2002**, 106, 1634.
111. Nazeeruddin, Md. K.; Humpry-Baker, R.; Berner, D.; Rivvier, S.; Zuppiroli, L.; Graetzel, M. *JACS*, **2003**, 125, 8790.

II. LUMINESCENCE IN Pt(II) AND Ir(III) COMPLEXES

2.1. Introduction to luminescence

Luminescence is a photophysical phenomenon occurring when an electronically excited species releases its excess energy by emission of light after a decay process. Depending on the nature of excitation different type of luminescence can be observed: electroluminescence for example is due to electrical excitation, whereas chemiluminescence can take place after a chemical or a biochemical reaction; in the latter case one can also speak of bioluminescence. In this thesis we will deeply study photoluminescence, which occurs when a molecule or a material emits light after the absorption of photons from an incident radiation.

When an electromagnetic radiation interacts with matter, absorption from the electronic state a to the electronic state b can be observed only if a dipole moment is generated after such interaction. The dipole arises from a different charge distribution between the two energetic levels. This transition dipole defines the strength of the absorption band associated with the excitation. The absorption strength or the intensity is proportional to the square of the transition dipole magnitude, μ_{ba} and it's called dipole strength (D_{ba})¹:

$$D_{ba} = |\mu_{ba}|^2 = |\langle \psi_b | \tilde{\mu} | \psi_a \rangle|^2$$

where ψ_b and ψ_a are the wave functions of the transition, while $\tilde{\mu}$ is the operator related to the dipole.

In accordance with the Born-Oppenheimer approximation, the nuclei, being much larger and heavier than the electrons, can be considered fixed; as a consequence, in describing the wave function of a molecule it is possible to separate electronic and nuclear contributions and ignore the latter.

Since we're observing a transition between two different quantic states, there is no way to define precisely the contribution of each state; to get an expression for the extent of the oscillating electric dipole moment when a system is described by a mixture of two states, we can use the mixed state probability density². Thus it comes out that the amplitude of the oscillating electric dipole moment, μ_{ba} can be described as:

$$\mu_{ba} = \left| \int \psi_b^* e r \psi_a d\tau \right|$$

where e is the charge of the electron, and r is the position vector from the nucleus.

Further it is also possible to distinguish between electronic, vibrational and rotational wave functions, when the transition moment integral has to be calculated.

$$\Psi = \Psi_{\text{electronic}} \Psi_{\text{vibrational}} \Psi_{\text{rotational}}$$

In order to occur, a transition needs to satisfy the selection rules, which can be obtained from the previous equation:

1. Transitions between states with different spin multiplicity cannot take place; further there must be a variation of symmetry in the molecule and the states characterizing the electric dipole transitions must have opposite parity (only $g \rightarrow u$ and $u \rightarrow g$ transitions are permitted “Laporte rule”).
2. Sometimes, in particular conditions, selection rules can be bypassed:
 1. Spin-orbit interactions. States with different multiplicity (e.g. singlet and triplet states) can be mixed by inter- and intra-molecular perturbations, which depend on the nuclei magnetic field, hence on the mass of the molecule (heavy atom effect). According to this, second and third row transition metals are able to make transitions between singlet and triplet states happen.
 2. Vibronic coupling. If two states are separated by a thin energy gap, a simple molecular vibration can be able to mix such states and therefore cause a symmetry forbidden transition, which anyway takes place at low intensities.

One additional important rule resulting from the Born-Oppenheimer approximation is the Franck-Condon principle,³ according to which the most probable transitions between two electronic states can happen when the respective vibrational state wave functions resemble. The most probable transition which can be observed is the so called *vertical transition* (Figure 25)

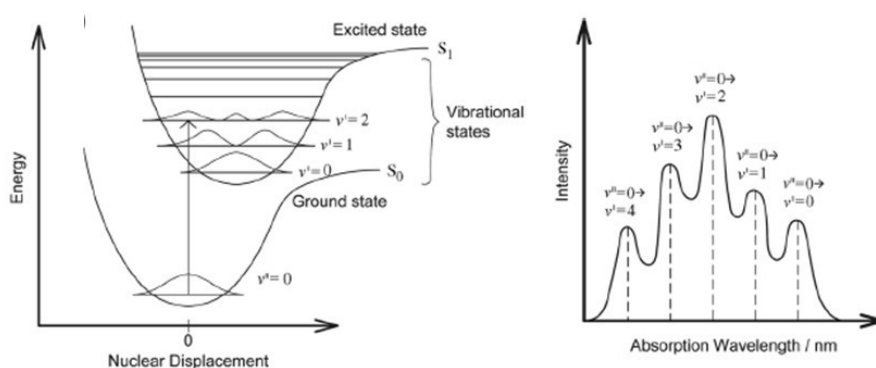


Figure 25. Left: potential curves of a generic transition $S_0 \rightarrow S_1$. Because the nuclei are heavier than the electrons, they are considered at fixed equilibrium position during an electronic transition, hence the transitions are said to be vertical. In this figure, the most likely vibronic transition is that from to the vibrational state $v'=2$ of the electronic excited state S_1 . Right: the

respective schematic absorption spectra of the electronic transition is shown. The most probable transition is characterized by a higher intensity.

The magnitude of the transition is related to the square of the overlap integral of the two involved states; from this it's possible to gain information about the absorption and emission spectra of the compounds.

The most common way to represent the electronic states of molecules is the Jablonsky diagram (Figure 26),⁴ in which are shown all the pathways (radiative and non-radiative) adopted by a molecule in releasing excess energy.

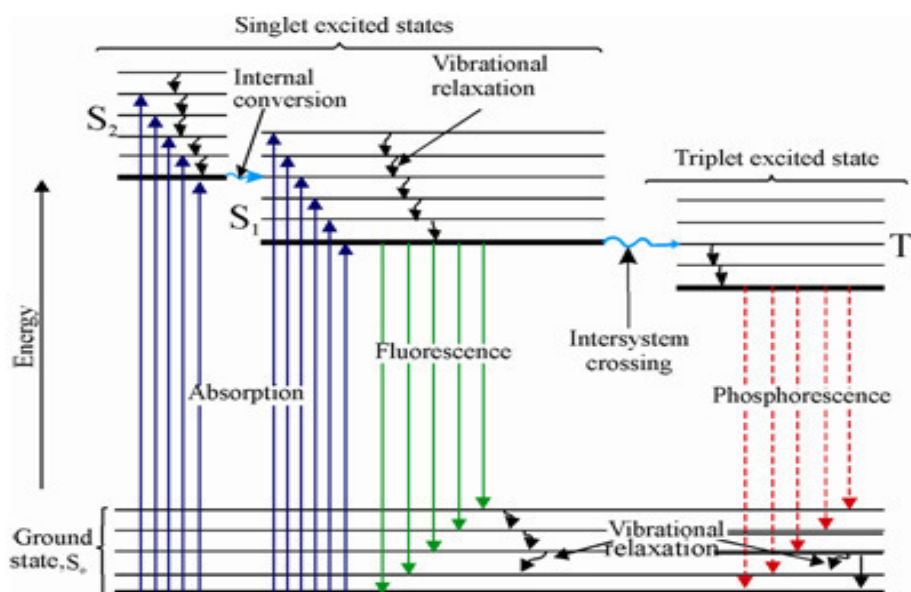


Figure 256. Jablonski diagram representing the electronic energy levels of molecules and the possible occurring transitions between fundamental and excited states. After the absorption different competitive radiative or non-radiative processes can occur.

Upon electronic excitation, the absorbed energy can be released via different competitive processes, such as light emission or different deactivation pathways, which might compete each other, when occurring in comparable time scale. The emissive decay of excited states electrons can be observed only in two pathways, i.e. fluorescence and phosphorescence. While internal conversion (IC) and vibrational relaxation are extremely fast ($10^{-12} - 10^{-10}$ seconds), intersystem crossing (ISC) is slightly slower and is more common when the molecule contains heavy atoms. These non-radiative pathways are faster and can compete with radiative transitions such as fluorescence ($10^{-10} - 10^{-6}$ seconds, if the electronic states have the same multiplicity) and phosphorescence ($10^{-4} - 10^4$ s, if the electronic states have different multiplicity). However, according to the energy gap law, the non-radiative transitions rate is inversely dependent to the energy gap between the two 0-0 electronic levels of the two involved states. Hence the emission

will occur always from the lowest vibrational level of the lowest electronic excited state (Kasha's rule).⁵

Fluorescence comes from an allowed spin electronic transition (hence, $\Delta S = 0$), for instance from the first excited state, S_1 , to the ground state, S_0 . Phosphorescence arises from a forbidden energy releasing to the ground state from an excited state characterized by a different spin symmetry (hence, $\Delta S \neq 0$), e.g. from the first triplet excited state, T_1 , to the singlet ground state, S_0 .

Phosphorescence is rarely observed at room temperature in organic compounds solutions, in these conditions, indeed, this process is slower (lifetimes of the magnitude order of 1s), compared to faster non-radiative decay processes, which thus predominate. Oppositely, these latter processes are inhibited by cooling the system at very low temperature (e.g. 77 K); under these conditions the molecules are more rigid, the vibrations weaker, and the phosphorescent light is observable.

In the case of photoluminescence, the amount of formed triplet and singlet is related to the relative magnitude of the singlet state radiative constant, k_r^S , and the rate constant for a non-radiative pathway from S_1 to T_1 , named *inter-system crossing*, k_{ISC} . Independently from the triplet yield, the triplet state radiative rate constant, k_r^T , once formed, is usually slow. However, as already mentioned above, if a heavy atom, for instance a third row transition metal, is embedded in the molecule framework, k_r^T , can be remarkably enhanced, thanks to the large spin-orbit coupling associated with the heavier atom (*heavy atom effect*). If this happens, radiative emission becomes competitive with deactivating processes and the phosphorescence can be observed even at room temperature.

2.2. Application of luminescent materials in solid state lighting

Nowadays, one of the most important challenges is to satisfy the increasing energy demand. In fact, with the exponential growth of world population, the demand is still increasing more and more. The energy production is primarily limited on fossil fuels (a not-renewable energy source) and nuclear power, although renewable energies have been introduced.

In 2007 the European Union (EU) proposed remarkable aims to get in the near future (i.e. by 2020):

1. to reduce the greenhouse gas emission by 20%;
2. to reduce the European energy consumption by 20%;
3. to supply at least the 20% of the energy with low-carbon, renewable energy-based sources;
4. to improve the energy efficiency by 20%.⁶⁻⁸

these aims are quite ambitious considering the amount of energy currently employed by transport, industries and common houses. One of the major energy requirements comes from the lighting; the demand of new advanced materials in this field (such as displays and illumination) has generated significant activity in the past years. In 2014, for instance, lighting used about the 19% of the world electricity; of this 19%, 14% was employed in the EU.⁹

We must say that most of the present technologies used in lighting can be definitely improved, conceiving a huge potential for energy savings.

Just few years ago, for instance, luminescent materials could find applications in a wide range of daily routine, such as projection televisions (PTVs), cathode ray tubes (CRTs), fluorescent tubes, X-ray detectors, et al.¹⁰

One of the most efficient and eco-friendly state-of-the-art in energy technology is the already mentioned solid state lighting (SSL), which is rapidly evolving, reaching remarkable efficiency levels higher than 276 lm/W, if compared to 40-100 lm/W obtained for fluorescent lamps.⁹

When compared to traditional lighting technologies, SSL are known to reduce the production of heat and other collateral emission in the non-visible spectrum.^{11,12}

Within SSL technologies it is possible to include light-emitting diodes (LEDs) and organic light-emitting diodes (OLEDs).

A LED is a device based on a semiconductor, which generates light using electric current. The architecture of such device coincides to a p-n junction diode, where the “n” side contains an excess of electrons (negative), while the “p” side contains an excess of holes (positive). When the electricity is switched on, the electrons can recombine with the holes, generating energy in form of photons. The semiconductor energy band gap, defines the wavelength of the emitted light, hence its color. LEDs are usually made by materials based on inorganic semiconductor. For instance, blue LEDs are composed by InGaN (indium gallium nitride) and GaN (gallium nitride).¹³ LEDs have demonstrated to be suitable candidates to replace traditional lighting devices thanks to their simple architecture, high efficiency and facile color tunability.^{14,15}

However some challenges are still present. One of the main difficulties, which has limited the potential of this technology, for what involves the industrial large scale production, is the trade-off between the power density and the surface area.¹⁶ Further a remarkable drawback is that the employed materials are not eco-friendly; therefore, there is the wish to head towards greener materials.¹⁴

This target has been reached by replacing LEDs inorganic semiconductors with organic ones to obtain the new devices, called organic light-emitting diodes (OLEDs). These devices offer several advantages with respect to traditional lighting technologies: OLEDs are thin and light, thus they

can be employed in lightweight panels and in foldable or curved screens. Further advantages are the fast switching time, the durability, the better color quality and the improved contrast scale.¹⁷ The general performance and the efficiency of light emitting devices is assessed by the external quantum efficiency (EQE, i.e. the number of emitted photons divided by the number of injected electrons), the power efficiency (emitted flux per electric input - in lumens - per electrical watt) and the current efficiency (output light per electric flux - in candela - per Ampere).¹⁸

The device stability is evaluated in terms of lifetime ($t_{1/2}$, time to reach half of the maximum luminance, in h) and total output energy (E_{tot} , in J, integral of the radiant flux versus time from $t=0$ – application of the bias – to $t = t_{1/2}$),¹⁹

In the following paragraph the OLEDs architecture will be discussed.

2.2.1. OLED (Organic light-emitting diode) devices

OLEDs are a screen technology based on photoactive organic molecules, which are receiving a lot of interest and are replacing conventional screen technologies.²⁰ As already mentioned, OLEDs offer many attractive advantages such as self-luminescence, which allows to eliminate the backlighting in the device and to obtain displays which are lighter, thinner and more efficient than the traditional ones. Furthermore, in OLEDs only the required pixels (and not the whole panel) emit light, thus lowering the power requirement by 20-80% respect to the LCDs screen.²¹ Moreover OLED displays are able to provide colors closer to reality, wider viewing angles and higher contrast.

Despite electroluminescent organic compounds were already observed by Pope et al. in the 1963,²² because of the high voltage required and of the low efficiencies, the development of devices exploiting this phenomenon was rather slow.

Later, in 1987, Tang and Van Slyke of Eastman Kodak Co. showed what is considered the first OLED device.²³ It was built by vapor deposition of a diamine and tris(8-hydroxyquinolate)aluminum (Figure 27) in a double layer architecture.

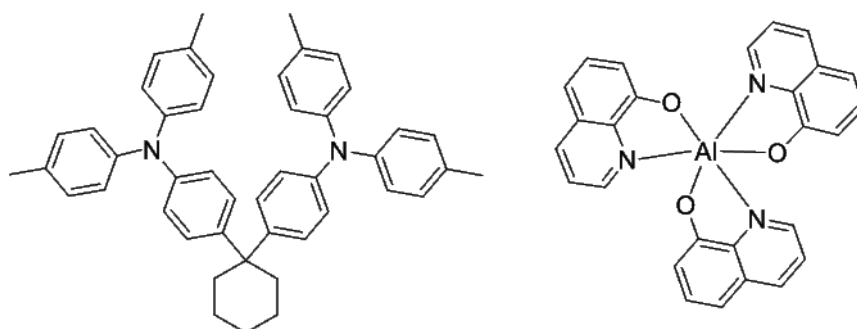


Figure 27. Schematic structure of 1,1-bis(4-di-p-tolylaminophenyl) cyclohexane on the left, and tris(8-hydroxyquinolate)aluminum (Alq3), on the right.

Three years later, Friend and co-workers at Cambridge University developed a polymer-based device (PLED), whose efficiency reached 0.05%.²⁴ Recently phosphorescent luminophores, which allow to fabricate highly efficient organic electroluminescent devices, are used.²⁵

Briefly, OLEDs are composed by a thin layer of an emissive material between two electrodes; the overall thickness is generally of a few hundreds of nm. The cathode is made typically by metallic Li-Al or Mg-Ag alloys, while the anode is usually composed by a transparent blend, such as Indium Tin Oxide (ITO). The following Figure 28 represents a typical OLED architecture.

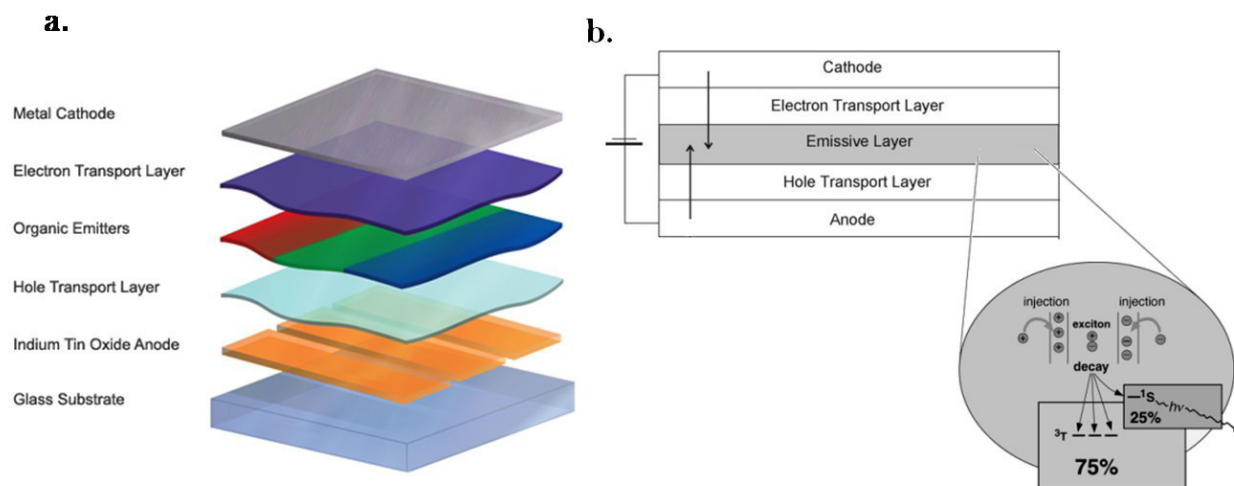


Figure 28. (a) a representation of a typical OLED architecture. (b) Schematic diagram of an electroluminescent device. Bottom: magnified illustration of the key process of its light generation.

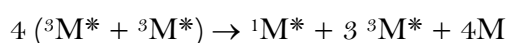
In such devices, electrons and holes are injected from the electrodes towards opposite layers of the multilayer organic film. Under the action of the applied electric field, holes and electrons move through the thin film to a central interface, where they recombine to generate neutral excited states, or excitons, whose relaxation to the fundamental state provides the emission of colored radiation. These organic layers include an electron transporting layer (ETL), which carries electrons from the cathode to the central emitting layer, and a hole transporting layer (HTL), which instead transports holes. In the state-of-art devices, also an exciton blocking layer, such as 2,9-dimethyl-4,7-diphenyl-1,10-phenanthroline (BCP), is incorporated in order to confine the excitons in the central organic emitting layer, thus enhancing the electroluminescence quantum efficiency.²⁶

The emitter can be directly deposited between the conductive layers or, more commonly, doped into the ETL, usually Alq₃ (Figure 28).

In those devices where the emitter is doped in a host polymeric layer, excitons generation occurs in such layer and the excitation energy must be transferred to dopant molecules excited states,

which next relax radiatively to the fundamental state. The crucial point in OLEDs technology is to make sure that the number of holes and electrons, which meet in the central layer, is equal.

Differently from photoluminescence, in electroluminescence both singlet and triplet excited states, excitons for instance, are directly formed and their relative amount is determined mostly by spin statistic of charge carrier recombination, which brings to a theoretical 1:3 (singlet:triplet) ratio.²⁷ This means that the internal quantum efficiency for OLEDs based entirely on organic emitting layer is restricted to 25%, since the excitons would be restricted by spin conservation. The left input energy goes wasted into device overheating. Thus, since the integration of a heavy metal ion in the emitter framework increases triplet generation, if an OLED is fabricated using such metals, it can exploit all the electro-generated singlet and tripled excitons, trending towards 100% of internal efficiency.²⁸ Unfortunately a device is rarely able to reach this ideal maximum; this is partly due to the long triplet excited state life-time, resulting in serious triplet-triplet annihilation principally at high electric currents and high concentrations of doping agents:



where M indicates the molecular dopant.

Practically, to prevail over fluorescence emitters, phosphorescence quantum yield (i.e. the ratio between emitted and absorbed photons) should be at least 25% at 298 K, with a lifetime window between 5 and 50 μs .^{20a}

Another keypoint is given by the emission wavelength. For fully colored screens, indeed, an efficient OLED emission must cover three colors: blue ($\sim 450 - 470$ nm) green ($\sim 500 - 550$ nm) and red ($\sim 650 - 700$ nm). Crucial parameters to stabilize the screen color quality are the chromaticity coordinates, defined by the *Commission Internationale d'Eclairage* (CIE). From these coordinates, showed by the diagram in Figure 29, it is possible to extract not only the color itself but even the color saturation. This latter is very important in screen application, where the primary colors need to be saturated as much as possible, that is CIE must be positioned close to the edge of the triangle.

While green and red emitters for OLEDs have been widely identified, blue ones remain more challenging so far, because of the large energy gap between the triplet excited state and the ground state.

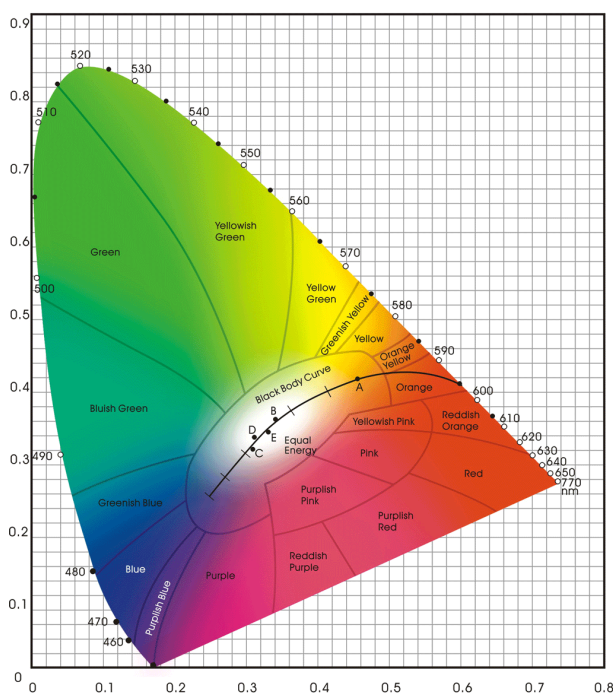


Figure 29. CIE diagram.

2.3. Organometallic complexes for luminescence

The demand for novel luminescent materials able to be suitable for the manufacturing process and show the wanted photophysical properties has generated a prominent activity in the last few years.

Currently, the research is active in exploring organometallic complexes with a potential application in optoelectronics thanks to their long emission life time, wide Stokes shifts, capacity of harvesting triplet states and tuneability of excited states.²⁹

Some possible application for these compounds can be found as emitters in electroluminescent devices,³⁰⁻³³ such as OLEDs or LEECs, as chromophores in NLO,³⁴⁻³⁶ as dyes in DSSCs,^{37,38} as solar fuels,³⁹ as photoredox catalysts,^{40,41} and in bio-imaging.^{42,43}

Concerning photoluminescent devices, dopants containing 2nd and 3rd row transition metals organometallic systems complexes are of particular interest with respect to purely organic emitting layers; Their high spin-orbit coupling constant provides a remarkable mixing of d_{metal} and π_{ligand} orbitals, thus removing the spin-forbidden nature of the triple state radiative relaxation and providing, hence, an easier formation of triplet excited states through *inter-system crossing*. This leads to high phosphorescence efficiencies.

Also, organometallic compounds, being comparatively smaller, are in general more easily sublimable than high molecular weight polymers, leading to a facilitation in devices fabrication.

Furthermore the presence of a metal centre leads to the generation of new bands as a consequence of the mixing of the metal orbitals and those of the ligands.

This means that, by an appropriate ligands selection, it is possible to design a series of organometallic compounds where the identity of the emitting state is predetermined.⁴⁴

Four types of electronic states or transitions are expected for transition metal complexes (Figure 30):

1. $d-d$ transitions (metal-centred, MC): upon ligand coordination, metal d orbitals are splitted. Excited $d-d$ transitions stem from the promotion of a d electron in the same d orbitals, which are essentially confined to the metal.
2. $d-\pi^*$ transitions (metal-to-ligand-charge-transfer, MLCT): involve the excitation of a metal centred electron to a π^* anti-bonding orbital of the ligand framework.
3. π,π^* or n,π^* transitions (intra-ligand transition, IL): concern the promotion of an electron from a π -bonding or non-bonding (n) orbital to a higher in energy anti-bonding orbital.
4. $\pi-d$ transitions (ligand-to-metal-charge-transfer, LMCT): these states arise from an electronic charge transfer from the ligand π -system to a metal-centred orbital.

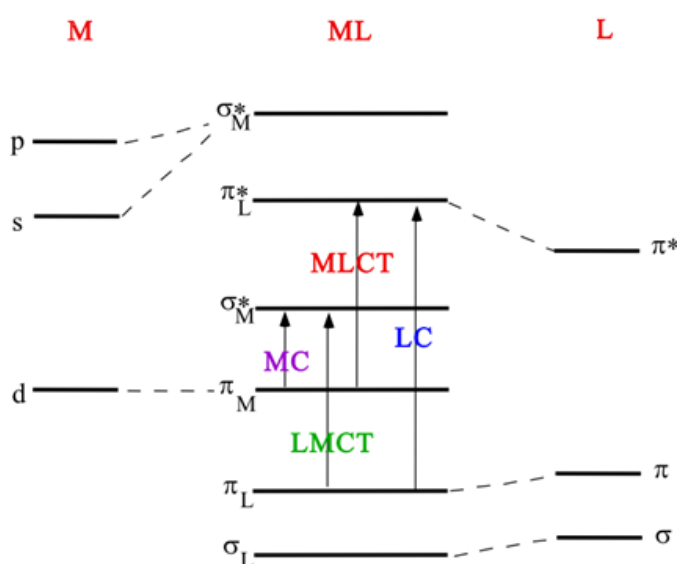


Figure 30. Example of electronic transitions in transition metal complexes (details in the text). M (left) and L (right) are, respectively, metal and ligand molecular orbital while ML (center) are those of the complex.

It is worth to mention that, transition metal complexes offer a remarkable range of opportunities since, depending on the metal and the ligands, it is possible to obtain a huge variety of coordination geometries, binding strength and the presence of distinct redox centers on metal and ligands.

In this context, I've dedicated part of my work to synthesize Ir(III) complexes, which are known to possess high photoluminescent quantum efficiency, great emission and an easy color tunability. The fact that Ir(III) complexes often show a strong luminescent emission from triplet states has made these compounds promising candidates for solid state lighting (SSL).^{30,45-47}

2.3.1. Ir(III) complexes for luminescence.

Iridium complexes have been extensively investigated thanks to their highly efficient luminescence and possibility to widely tune it.⁴⁸⁻⁵¹ Indeed, the broad range of ligand families already synthetically affordable makes sure that the emission color of Ir(III) complexes can be easily modulated over the whole visible spectrum.⁵²

The emissive materials used in state-of-the-art OLEDs rely on phosphorescent complexes as red and green emitters. Some examples are reported in the Figure 31.⁵³

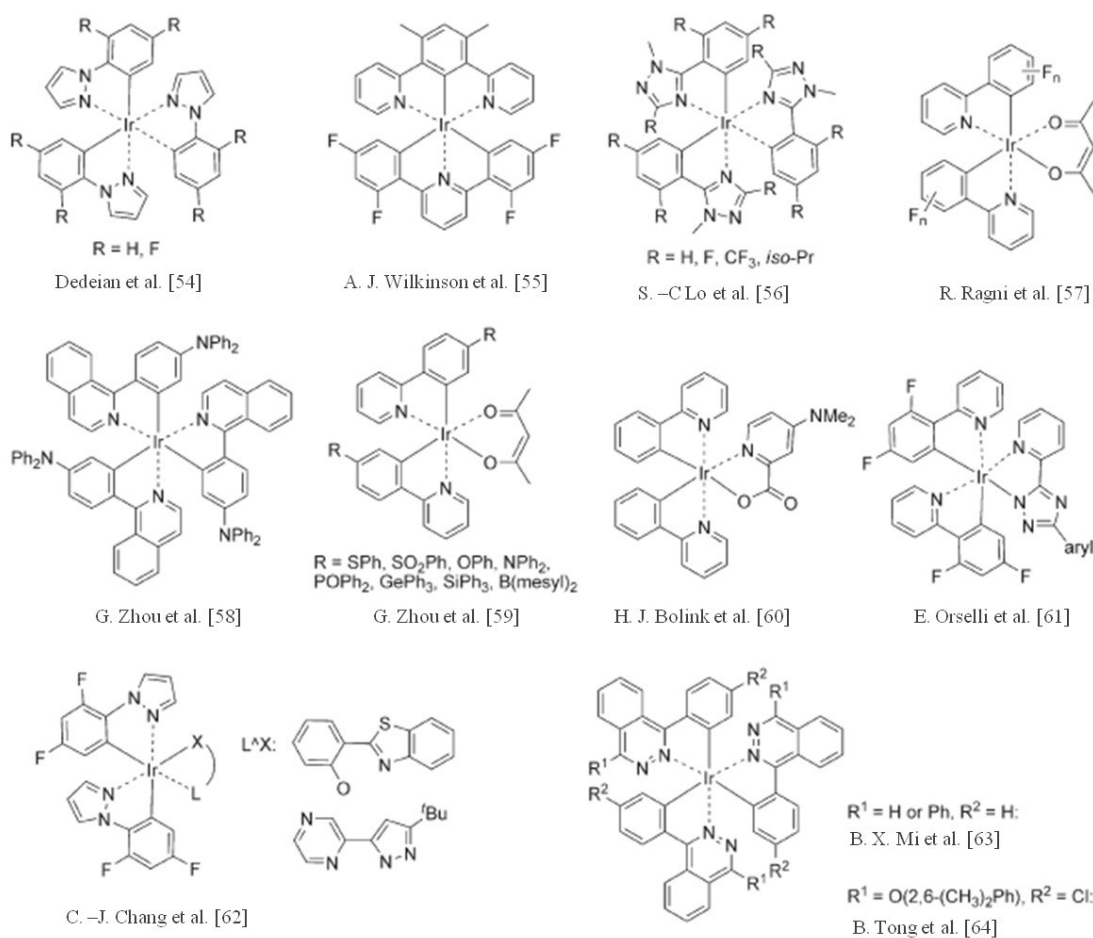


Figure 31. State-of-art Ir(III)-based green and red emitters.

However, despite in the last decades many phosphorescent red and green emitters have been reported, the design of high-performance blue-emitting materials is still a challenge.⁶⁵

For blue emitters indeed only fluorescent compounds are used at present,⁶⁶⁻⁶⁸ thus there is still a lack of phosphorescent complexes able to satisfy the following criteria for deep blue emitters:

1. own the appropriate chromaticity standards defined by the European Broadcasting Union (EBU) and National Television System Committee (NTSC) with CIE (Commission Internationale de l'Éclairage) coordinates of (0.15, 0.06) and (0.14, 0.08), respectively;
2. are characterized by high photoluminescence quantum yields (Φ_{PL}) that means OLEDs with high external quantum efficiencies, in particular at useful brightnesses (at least 100 cd m⁻² for displays and 1000 cd m⁻² for lighting);
3. exhibit device stabilities comparable to fluorescent complexes.⁶⁹

Among the examined phosphorescent complexes, iridium(III) compounds have attracted most interest as emitters in electroluminescent devices due to their high Φ_{PL} , phosphorescence

lifetimes (τ_{PL}) and easy color tunability based on the choice of ligands around the metal centre, as already explained above.

To modulate the emission towards the blue, usually electron-withdrawing substituents are embedded on the cyclometalating ligands framework of the iridium complexes. By employing this strategy three issues come out. The first is that the electrochemical stability of fluorinated substituents, such as in the largely studied FIrpic [iridium(III)bis(4,6-difluopyridinato-N,C^{2'})picolinate] sky-blue emitter (Figure 32),⁷⁰ is poor, translating to dramatically reduced device stability;⁷¹

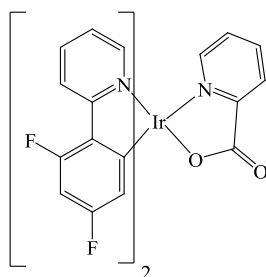


Figure 32. [iridium(III)bis(4,6-difluopyridinato-N,C^{2'})picolinate].

while the use of different more strongly electron-withdrawing substituents do not necessarily translate into bluer-emitting complexes, despite lowering the HOMO of the compound.⁷² The second is that with the increasing of the emissive triplet state energy, a non-radiative recombination given by thermally-accessible metal-centred excited states becomes more problematic, causing a degradation of the complex.⁷³ Lastly, most iridium(III) complexes do not match the deep blue chromaticity requirements, but possess CIE_y ordinates larger than 0.1 as their triplet energies are not high enough (at least 2.8 eV);^{74,75} those that do match the chromaticity requirements possess relatively low maximal external quantum efficiency (EQE_{max}) values (<10%).⁷⁶

Another adopted strategy to modulate the emission of both charged and neutral iridium(III) complexes towards blue is to substitute the typically adopted coordinating pyridine rings with more sigma-donating heterocycles that help to destabilize the LUMO of the complexes, such as imidazoles⁷⁷ and N-heterocyclic carbene (NHC) ligands.^{76b,77b,78} Despite Ir(III) complexes incorporating arylimidazole ligands with remarkable efficiencies have been reported, these emitters are not sufficiently blue,⁷⁹ while most NHC-containing iridium complexes, although deep blue emitting,⁸⁰ possess very low Φ_{PL} , as well exemplified by complexes **66** ($\Phi_{\text{PL}} = 0.2\%$ in 2-MeTHF) and **67** ($\Phi_{\text{PL}} = 5\%$ in 2-MeTHF) in Figure 33.^{80a} With a suitable design of the

substituents of the cyclometalating NHC ligand, several researchers have reported OLEDs with higher efficiencies, but at the expense of the deep blue nature of the emission.⁸¹ Thompson and Forrest investigated the complex *mer/fac*-Ir(pmp)₃ (pmp = [tris(*N*-phenyl,*N*-methylpyridoimidazol-2-yl)iridium(III)], **68**, proving that it was possible to obtain complexes with emission at 418 and 465 nm in 2-MeTHF and with remarkable Φ_{PL} of ca. 77%;^{76b} the *mer*-**68**-based OLED, where **68** was employed as the emitter, showed CIE of (0.16, 0.15) and External Quantum Efficiency (EQE₁₀₀₀) at 1000 cd m⁻² of 13.3%, while the one with *fac*-**68** as the emitter showed CIE of (0.16, 0.09) and an EQE₁₀₀₀ of 9.0%. The enhancement in **68** photoluminescence quantum yield (PLQY) can be in part attributed to a stabilization of the emissive triplet state and a concomitant enlargement in the energy gap to the non-emissive metal-centred state due to the presence of the nitrogen atom in the pyridoimidazol-2-yl moiety, which regulates the LUMO energy.

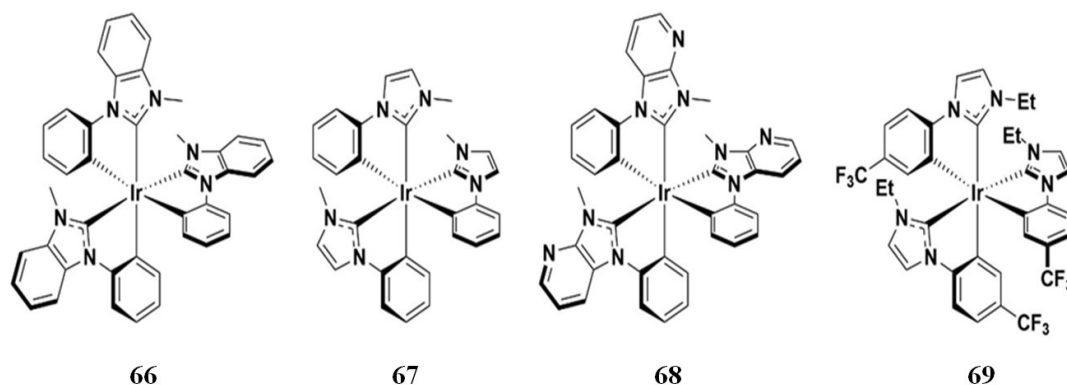


Figure 33. State-of-art homoleptic Iridium-carbene complexes.

In the following I will present my thesis work involving the luminescent properties of various iridium complexes. First I will show the results obtained with a homoleptic neutral Ir(III)-NHC complex, which was prepared and deeply studied thanks to a collaboration with Prof. Eli Zysman-Colman of the University of St. Andrews (Scotland, UK). For this activity I've been guested in his laboratory and I shared the work with Dr. Amlan Kumar Pal, one of the group researchers. We found that high Φ_{PL} can be obtained in NHC ligand-based iridium complexes *via* stabilization of the HOMO energy, and thus the emissive triplet state, to tone down thermal population of the non-emissive metal-centred states.

Then, I will present the luminescent properties of the already introduced Ir-THC complex bearing two cyclometalated phenylpyridines and tetrahydrocurcumin (see Chapter 1). In order to investigate the effect of the introduction of electron-withdrawing elements, I also synthesized and

studied the related fluorinated complex with two Fluorine atoms on the cyclometalated phenylpyridines. The variation of the emission of the respective OLED devices was investigated. The luminescent properties in solution were studied in collaboration with Prof. J. A. Gareth Williams of the University of Durham (UK) whereas the OLED devices were made thanks to a collaboration with Dr. Massimo Cocchi (Bologna CNR). The complex **57** also found application as photosensitizer in photodynamic therapy. This study was carried out in collaboration with Prof. Simona Polo of the Istitute Firc of molecular oncology (IFOM) in Milan.

2.4. Two novel luminescent homoleptic Ir(III)-NHC complexes

During my stay in the laboratory of Prof. Zysman-Colman, we investigated two novel homoleptic charge-neutral meridional (*mer*-) complexes, **58** and **59** (Figure 34a), introduced in the Chapter 1, comprising 3-methyl-1-(3/4-(trifluoromethyl)phenyl)-1*H*-3 λ^4 -imidazole as the pre-carbenic ligands;⁸² a similar complex, **69** (Figure 33),⁸³ was recently reported as an electron blocking layer (EBL) material for deep blue OLEDs. This work is also object of a publication, indeed it has been accepted in the journal *Advanced Materials*,⁸² complex **58** was synthesized by Dr. A. K. Pal, who did also the preliminary calculations and some photophysics studies, while complex **59** was prepared by me. Dr. C. F. R. Mackenzie performed also some photophysics analysis, Dr. S. Krotkus and Prof. I. D. W. Samuel fabricated the OLED devices and made all the related solid state studies, while Dr. D. B. Cordes and Prof. A. M. Slawin did the XRD studies. The whole work was supervised by Prof Eli Zysman-Colman and Prof. Ifor David William Samuel of the University of St. Andrews.

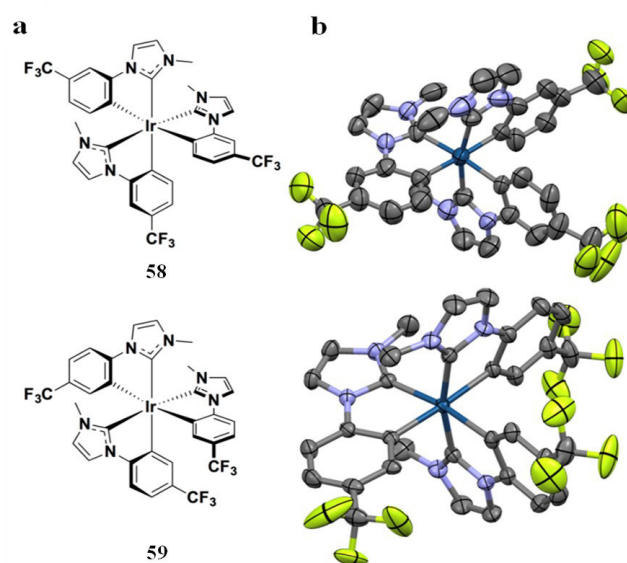


Figure 34. (a) Chemical structures and (b) thermal ellipsoid plots of **58** and **59**. Hydrogen and solvent atoms have been omitted for clarity and ellipsoids drawn at 50 % probability.

Iridium complexes **58** and **59**, Figure 34a, were synthesized by reaction of NHC ligands **L58** and **L59** with $[\text{Ir}(\text{COD})(\mu\text{-Cl})_2]$ (where COD = 1,5-cyclooctadiene) via a one-pot transmetalation route using Ag_2O and triethylamine in degassed refluxing chlorobenzene (see the *experimental section* for details on the synthesis).⁸³ A mixture of *fac*- and *mer*-homoleptic complexes were obtained and the kinetically favourable *mer*-isomer, which is the major product, was purified by silica gel column chromatography followed by recrystallization. Both complexes are air- and moisture-stable, off-white to colourless crystalline solids, and soluble in several organic solvents such as ethyl acetate, acetonitrile and dichloromethane. Complexes **58** and **59**, as well as related ligands **L58** and **L59**, were characterized by ^1H , ^{13}C and ^{19}F NMR spectroscopy, HRMS, melting point determination and elemental analyses. Besides, the structures and meridional configuration of both complexes were unequivocally established by single crystal X-ray diffraction analysis (Figure 34b).

2.4.1. Electrochemical studies and DFT calculations.

In order to clear up the energies of the frontier molecular orbitals, the electrochemistry of both complexes **1** and **2** was studied by cyclic voltammetry (CV) in degassed CH_3CN . The first redox potentials, reported with respect to SCE ($\text{Fc}/\text{Fc}^+ = 0.38 \text{ V}$ in MeCN),⁸⁴ are compiled in the following Table 9, whereas the CV plots are shown in the Figure 35.

Compounds	Experimental				Calculated			
	$E_{1/2}^{\text{Ox}} / \text{V}$	$E_{1/2}^{\text{Red}} / \text{V}$	$\Delta E_{\text{redox}}^a / \text{V}$	$E_{\text{HOMO}} / \text{eV}^b$	$E_{\text{HOMO}} / \text{eV}^c$	$E_{\text{LUMO}} / \text{eV}^c$	$\Delta E_{ \text{LUMO-HOMO} } / \text{eV}$	
66^d	0.76	-2.75	3.51	----	----	----	----	
67^d	0.59	----	----	----	----	----	----	
68^e	0.68	-2.35	3.03	----	-5.14	-1.23	3.91	
69^f	0.74	----	3.37	-5.20	----	----	----	
58	0.88 (71)	----	3.70	-5.34	-5.27	-0.56	4.71	
59	0.80 (90)	----	3.52	-5.27	-5.23	-0.71	4.52	

Table 9. Redox potentials of **58** and **59** and reference complexes **66**, **67**, **68** and **69**. Potentials are in volts (V) vs. SCE in CH_3CN with 0.1 M in $[\text{n-Bu}_4\text{N}]\text{PF}_6$, recorded at 298 K at a scan rate of 100 mV/s using a glassy carbon electrode as a working electrode, a silver and a platinum wire as reference and counter electrodes, respectively. The difference between the cathodic, E_{pc} , and

anodic, E_{pa} , peak potentials, ΔE_p , (millivolts) is given in parentheses. ^a $\Delta E_{redox} = |E_{ox} - E_{red}|$. Where no reduction wave is observed, E^{red} is deduced from $E_{pa}^{ox} + E_{opt}$, where E_{opt} is taken as the energy corresponding to 10% of the intensity of the lowest energy absorption band.^[86] ^b Orbital energies are calculated from the onset of oxidation, $E_{HOMO} = -(E_{ox}^{onset} + 4.8)$ where E_{ox}^{onset} is reported vs. the Fc/Fc^+ couple. ^c DFT calculated orbital energies. ^d Redox potentials are from Ref^[80a] in DMF, where a correction factor of 0.45 V has been introduced to reference the data vs. SCE in MeCN.^[87] ^e Redox potentials are from Ref^[76b] in DMF, where a correction factor of 0.45 V has been introduced to reference the data vs. SCE in MeCN.^[87] ^f Redox potentials are from Ref^[83] in DCM, where a correction factor of 0.46 V has been introduced to reference the data vs. SCE.^[87]

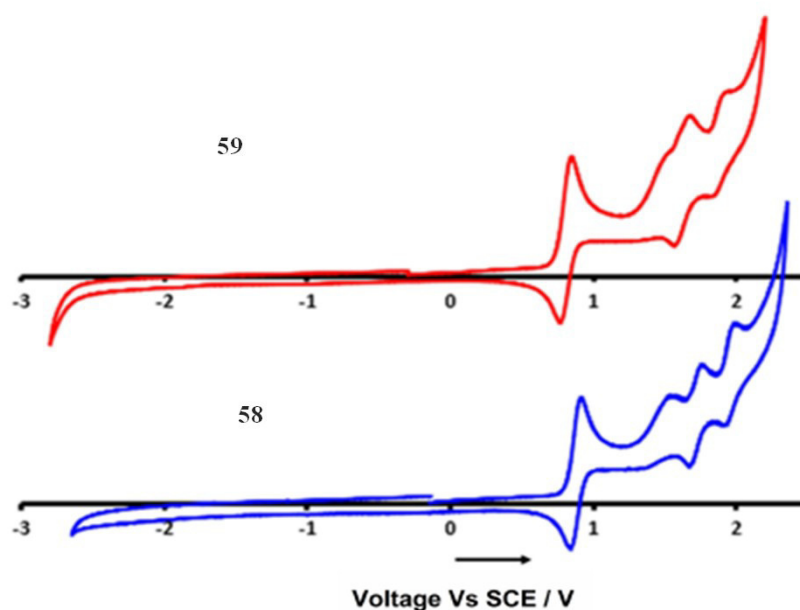


Figure 35. Cyclic voltammogram of complexes **58** (blue) and **59** (red) in degassed MeCN at r.t. at a scan rate of 100 mV/s.

Both complexes undergo some oxidation events, where the first are quasi-reversible. No reduction of **58** and **59** within the accessible solvent window have been observed. The oxidation potentials of **1** and **2** are anodically shifted compared to **66**, **67** and **68**; this can be attributed to the presence of the electron-withdrawing $-CF_3$ groups on the cyclometalating aryl ring. The cathodically shifted oxidation wave of **59** compared to **58** is in agreement with the calculated HOMO of **59** ($E_{HOMO} = -5.23$ eV) vs. **58** ($E_{HOMO} = -5.27$ eV), though DFT calculation predict a somewhat shallower HOMO for **68** ($E_{HOMO} = -5.14$ eV) than what was experimentally observed.^{76b} Furthermore, the $-CF_3$ group in **58** (*para* to Ir- C_{aryl} bond, $\sigma_p = 0.54$; σ_p = Hammett parameter for *para*- substituent)⁸⁵ is more strongly electron-withdrawing if compared to the $-CF_3$ group in **59** (*meta* to Ir- C_{aryl} bond, $\sigma_m = 0.43$; σ_m = Hammett parameter for *meta*- substituent); this causes an anodic shift of 80 mV of the first oxidation potential of complex **58** with respect that of complex **59**. DFT calculations show that the HOMOs of these complexes are formed mostly of a combination between the metal *d*-orbitals and the π -orbitals of the cyclometalating aryl groups on the C[^]C ligands (Figure 36). Due to the lack of any observable reduction waves for **58** and **59**, the redox gaps, ΔE_{redox} , of these

complexes were deduced by using the optical gaps. Complex **59** has a ΔE_{redox} similar to that of **66** whereas that of **1** is wider by 180 mV. The calculated LUMO orbitals for **58** and **59** are mostly localized on the CF_3 -aryl moiety and partially on the NHC moieties, while for **68** the LUMO is centered on the pyridyl-imidazolyl (Py-Im) moiety. The trend calculated in HOMO-LUMO energy gaps ($\Delta E_1 > \Delta E_2 > \Delta E_{R_3}$) meets very well that observed for the ΔE_{redox} of these complexes.

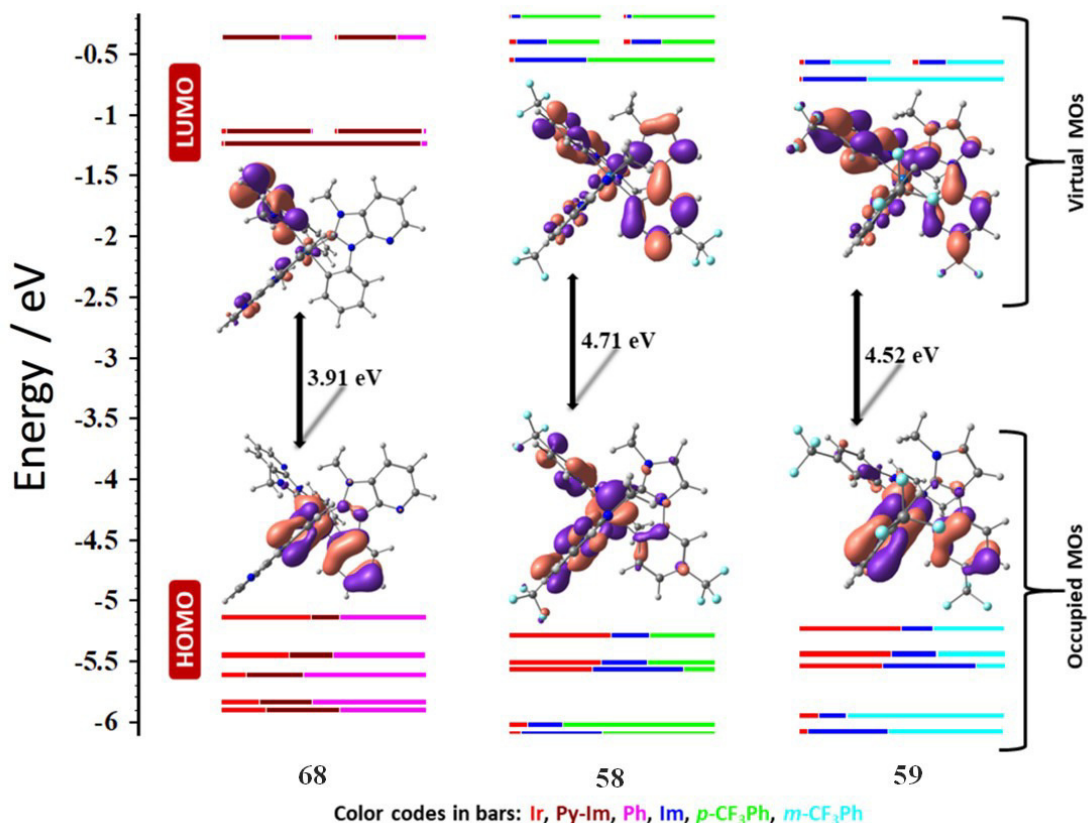


Figure 36. Calculated frontier MO energies of **68**, **58** and **59**, obtained from DFT [(B3LYP/SBKJC-VDZ for Ir(III)) and (6-31g** for C,H,N,(F))] with CPCM(CH_2Cl_2) and 0.5 eV threshold of degeneracy (orbitals are isocontoured at 0.03).

2.4.2. Photophysics.

In Figure 37 are displayed the experimental UV-Vis absorption spectra of **58** and **59** overlaid with the related TD-DFT predicted transitions; the related data are reported in Tables 10, 11 and 12.

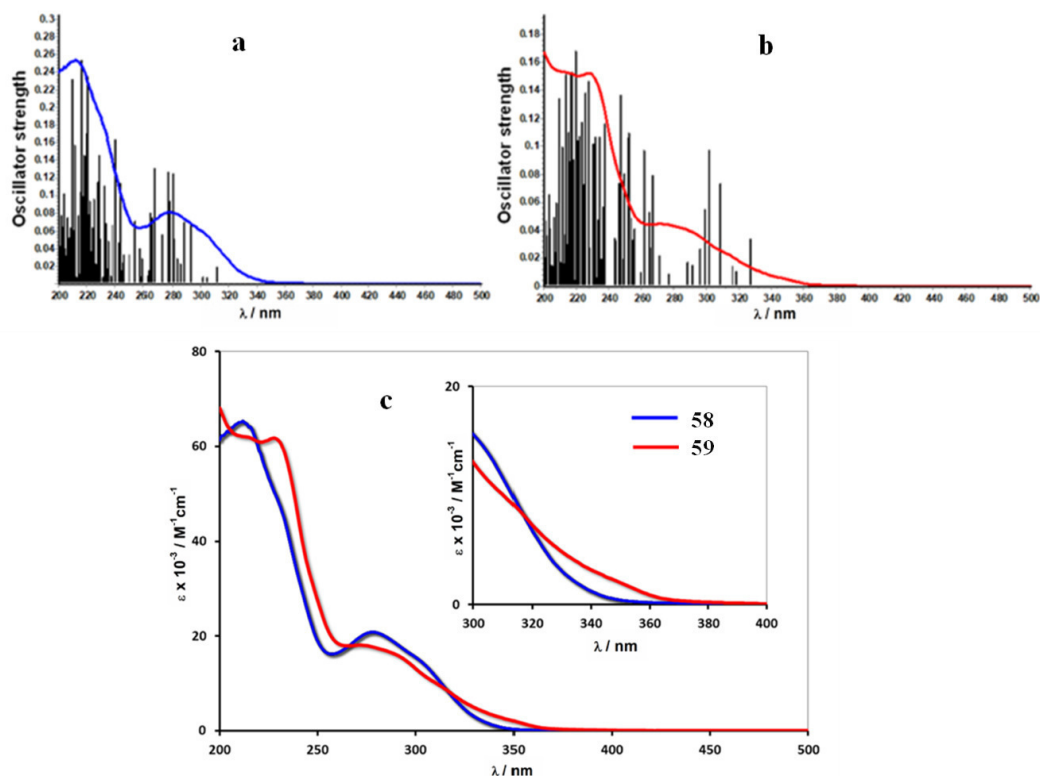


Figure 37. Overlay of experimental UV-vis absorption spectra (curved lines) of complexes 58 (a) and 59 (b) with their predicted transitions (vertical bars) calculated by singlet TD-DFT at room temperature in CH_2Cl_2 . (c) Overlapping of UV-vis absorption spectra of complexes 58 and 59.

Compound	$\lambda_{\text{abs}} / \text{nm}$ ($\epsilon \cdot 10^{-4} / \text{M}^{-1}\text{cm}^{-1}$)
58	211 (6.51), 230 sh (4.81), 278 (2.08), 301 sh (1.54)
59	214 (6.21), 228 (6.19), 272 (1.81), 290 sh (1.61), 311 sh (1.01)
66 ^a	242 (5.1), 304 (2.9)
67 ^a	230 (4.1), 289 (1.4), 340 sh (0.28)
68 ^b	231 (9.9), \approx 316 (6.5)
69 ^c	222 (5.5), 277 (1.7)

Table 10. UV-Vis absorption data of complexes 58 and 59 (in CH_2Cl_2 at room temperature) and benchmark compounds 66, 67, 68 and 69. (a) From reference 83 in CH_2Cl_2 . (b) From reference 95 CH_2Cl_2 . (c) From reference 96.

The assignment of the nature of key absorption bands is given in Tables 11 and 12.

state	$\lambda_{\text{abs}}/\text{nm}$ (TD-DFT)	$\lambda_{\text{abs}}/\text{nm}$ ($\epsilon \cdot 10^{-4} \text{ M}^{-1} \text{ cm}^{-1}$) [experimental]	f(TD-DFT)	Major transition(s)	Character ^a
54	216	211 (6.51)	0.2540	H-8 \rightarrow L (14%) H-6 \rightarrow L+4 (22%)	CF ₃ -Ph(π) to CF ₃ -Ph(π^*) (major) + CF ₃ -Ph(π) to Im(π^*) (minor)
48	220	230 (4.81)	0.2352	H-9 \rightarrow L+1 (19%) H-7 \rightarrow L (18%) H-7 \rightarrow L+1(10%) H-5 \rightarrow L+4 (10%)	CF ₃ -Ph(π) to CF ₃ -Ph(π^*) (major) + CF ₃ -Ph(π) to Im(π^*) (minor)
11	277	278 (2.08)	0.1265	H-2 \rightarrow L+2 (41%) H \rightarrow L+5 (40%)	Ir(d π) to CF ₃ -Ph(π^*) (major) + Im(π) to CF ₃ - Ph(π^*) (minor)
1	312	301 (1.54)	0.0189	H \rightarrow L (95%)	Ir(d π) to CF ₃ -Ph(π^*) (major) + Ir(d π) to Im(π^*) (minor) + CF ₃ -Ph(π) to CF ₃ -Ph(π^*) (minor)

Table 11. Selected transitions (from TD-DFT) calculations of complex **58** in the singlet ground state (B3LYP/SBKJC-VDZ[Ir]6-31G** [C,H,N,F], CPCM (dichloromethane)). ^a CF₃-Ph stands for the trifluoromethylphenyl group, whereas Im for the imidazole moiety of **L58**.

state	$\lambda_{\text{abs}}/\text{nm}$ (TD-DFT)	$\lambda_{\text{abs}}/\text{nm}$ ($\epsilon \cdot 10^{-4} \text{ M}^{-1} \text{ cm}^{-1}$) [experimental]	f(TD-DFT)	Major transition(s)	Character ^a
54	217	214 (6.21)	0.1532	H-4 \rightarrow L+3 (20%) H-6 \rightarrow L+5 (18%) H-2 \rightarrow L+8 (14%)	CF ₃ -Ph(π) to CF ₃ -Ph(π^*) (major) + Im(π) to Im(π^*) (minor)
50	220	228 (6.19)	0.1678	H-2 \rightarrow L+7 (63%) H-2 \rightarrow L+6(17%)	Im(π) to Im(π^*) (major) + Ir(d π) to CF ₃ -Ph(π^*) (minor)
15	262	272 (1.81)	0.0973	H \rightarrow L+5 (65%) H-3 \rightarrow L+2 (12%)	CF ₃ -Ph(π) to CF ₃ -Ph(π^*) (major) +Ir(d π) to CF ₃ - Ph(π^*) (minor)

5	302	290 (1.61)	0.0972	H-2→L (86%)	Im(π) to CF ₃ -Ph(π^*) (major) + Ir(d π) to CF ₃ -Ph(π^*) (minor)
1	328	311 (1.01)	0.0341	H→L (97%)	Im(π) to CF ₃ -Ph(π^*) (major) + Ir(d π) to Im(π^*) (minor) + CF ₃ -Ph(π) to CF ₃ -Ph(π^*) (minor)

Table 12. Selected transitions (from TD-DFT) calculations of complex **59** in the singlet ground state (B3LYP/SBKJC-VDZ[Ir]6-31G** [C,H,N,F], CPCM (dichloromethane)). ^a CF₃-Ph stands for the trifluoromethylphenyl group, whereas Im for the imidazole moiety of **L59**.

The absorption spectra of **58** and **59** display similar profiles. Absorption bands at high energy ($\lambda < 270$ nm, $\epsilon > 2.5 \times 10^4$ M⁻¹ cm⁻¹) are attributed primarily to ligand centred (¹LC) $\pi \rightarrow \pi^*$ transitions which involve both the aryl and the imidazole moieties. For complex **59**, the band at 228 nm also consists of a Ir(d π) \rightarrow Imidazole(π^*) singlet mixed metal-to-ligand charge transfer (¹MLCT) and intra-ligand charge transfer (¹ILCT) transition. Bands within 270-290 nm are mixed LC and MLCT in character. The low intensity ($\epsilon \sim 1-1.5 \times 10^4$ M⁻¹cm⁻¹) absorption maxima at 301 nm and 311 nm, respectively, for **58** and **59** are assigned principally to a mixed ¹MLCT/¹ILCT transition, according to literature.^{80a, 81} The observed redshift of the absorption onset at ~ 350 nm for **59** respect to that of **58** (Figure 37c) arises from its smaller energy gap compared to **58** in agreement with DFT calculations. The absorption profiles of **58** and **59** are comparable to those of **67** and **69**; the absorption spectra of **58**, **59** and **69** are blue-shifted compared to **67**, as expected.

Complexes **58** and **59** show deep blue emission in degassed CH₂Cl₂ (Figure 38); emission spectrum of **58** is modestly blue-shifted respect to **59** at 77 K in 2-MeTHF (Figure 38).

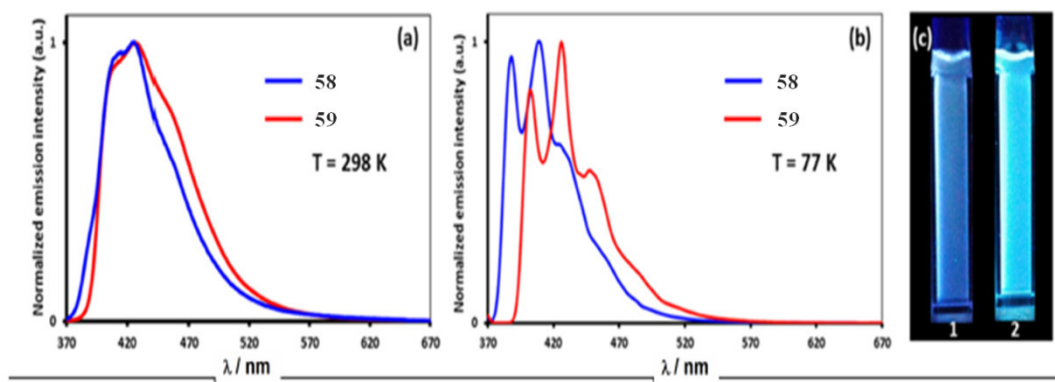


Figure 38. Luminescence spectra of complexes **58** and **59** ($\lambda_{exc} = 330$ nm) (a) at 298 K in dichloromethane solutions and (b) at 77 K in frozen 2-MeTHF; (c) Emission colors of complexes **58** and **59** at 298 K in dry dichloromethane solutions.

The emission profiles shown above coupled with the calculated spin density distributions of **58** and **59** (Figure 39) hint that the emission of these complexes arises from an admixture of triplet ligand-centred (3LC) and metal-to-ligand charge transfer (3MLCT) states. The energies of the triplet states of **58** and **59**, as calculated from the E_{0-0} peaks at 77 K meet well with their related DFT predicted triplet state energies (**58**: $E_T = 3.19$ eV (77 K) and 3.42 eV (DFT); **59**: $E_T = 3.08$ eV (77 K) and 3.31 eV (DFT)).

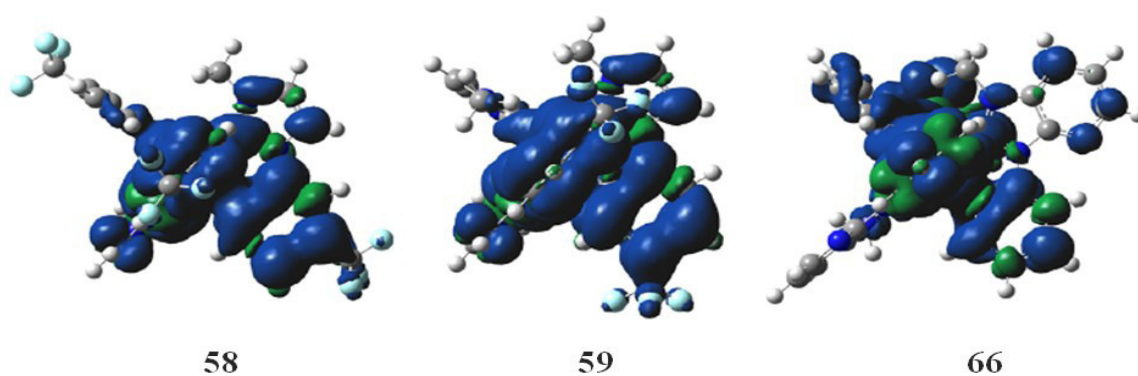


Figure 39. Triplet spin density distributions of complexes **58** and **59** and reference complex **66**, obtained from DFT [(UB3LYP/SBKJC-VDZ for Ir(III)) and (6-31g** for C,H,N,F)] with CPCM(dichloromethane). Contours are isovalued at 0.004.

Complex **58** is characterized by a fair Φ_{PL} of 25% in solution, oppositely to complex **59** which is a remarkably bright emitter ($\Phi_{PL} = 72\%$), comparable to **68** ($\Phi_{PL} = 78\%$) and to the structurally related complex *fac*-Ir(cnpmic)₃ ([iridium(III)tris(1-cyanophenyl-3-methylimidazolin-2-ylidene-C,C^{2'})]; $\Phi_{PL} = 78\%$),^{80b} see the following Table 13.

	In solution				
	298 K ^a			77 K ^b	
	$\lambda_{\text{PL}} / \text{nm}^c$	$\Phi_{\text{PL}} / \%^{c,d}$	τ / ns^c	$\lambda_{\text{PL}} / \text{nm}^c$	τ / ns^c
58	414, 424, 453 (sh)	25	280 (65%), 1816 (35%)	388, 408, 425, 455 (sh)	1111 (79%), 2603 (21%)
59	412, 427, 454 (sh)	72	698 (48%), 1820 (52%)	402, 426, 447, 483 (sh)	1422 (73%), 3550 (27%)
66^e	394	0.2	15	383, 405	2400
67^e	~ 395 ^f	5	620	384, 404, 424	2400
68^g	465	78	800	414	1000
69^h	422	32.5 ⁱ	----	408 (sh), 422	4520

Table 13. Photophysical data of **58**, **59** and **66-69**. ^a In deaerated CH₂Cl₂ solution; ^b In aerated 2-MeTHF solution; ^c $\lambda_{\text{exc}} = 330 \text{ nm}$; ^d Using quinine sulfate in 0.5 M H₂SO₄, $\Phi_{\text{PL}} = 54.6\%$; ^[88] ^e From Ref ^[80a] in 2-MeTHF; ^f This value is not reported beyond “similar to R1” in Ref ^[80a]; ^g From Ref ^[76b] in 2-MeTHF; ^h From Ref ^[83] in THF; ⁱ Referenced with *fac*-Ir(ppy)₃ ($\Phi_{\text{PL}} = 100\%$).

Both complexes possess bi-exponential τ_{PL} , with longer τ_{PL} values at 77 K in deaerated 2-MeTHF if compared with those at 298 K in degassed dichloromethane. In comparison to complex **68**, the greatest intensity emission maxima of **58** and **59** are significantly blue shifted (*ca.* 2079 cm⁻¹ and 1914 cm⁻¹ for **58** and **59**, respectively), which is in agreement to their ΔE_{redox} gaps. Compared to **69**, complex **59** exhibits a remarkably higher Φ_{PL} , probably due to a decrease in non-radiative decay through the shorter alkyl chain.

Complex **58** shows a blue-shifted emission when doped in PMMA films [PMMA = poly(methyl methacrylate)] compared to that in solution (compare Figure 38a with Figure 40a and Table 13 with Table 14) while the emission maxima do not change for complex **59** as a function of medium (see the related data in Table 14).

Compound	10 wt% doped PMMA film (298K)		
	$\lambda_{\text{PL}} / \text{nm}^a$	$\Phi_{\text{PL}} / \%^{a,b}$	τ / ns^a
58	393, 409, 430 (sh)	13.7 (N ₂)	2167
		13.5 (air)	

Table 14. Photophysical data of complex **58** and **59**. ^a $\lambda_{\text{exc}} = 300$ nm, thin film lifetime measurements performed *in vacuo*, weighting refers to the normalised pre-exponential factors evaluated from the multi-exponential decay fit; ^b using an integrating sphere.

However, at 77 K we observe a blue-shift for **59**, which is an indication of a greater MLCT contribution to the emissive triplet state.^{80a}

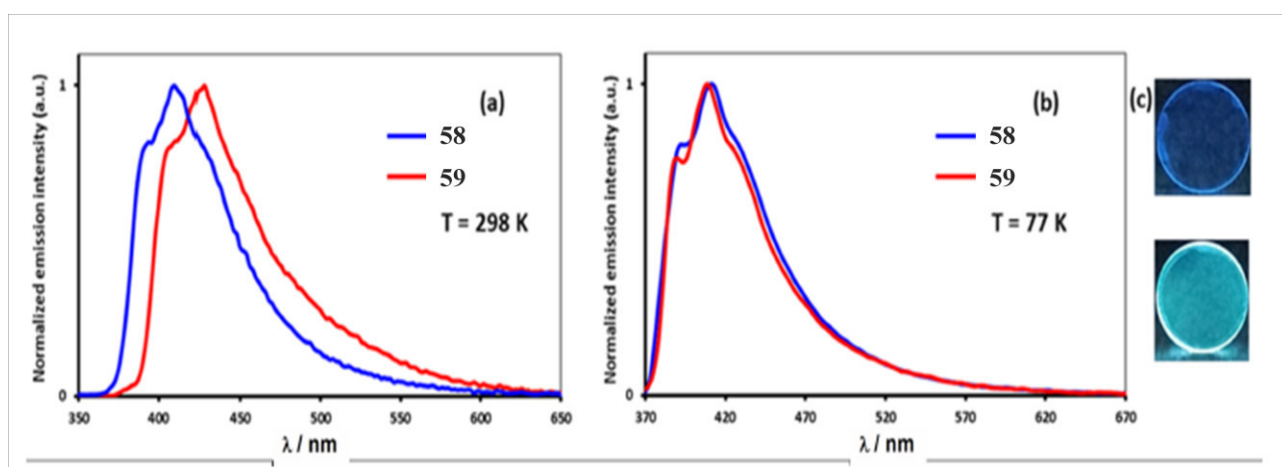


Figure 40. (a) Luminescence spectra of complexes **58** and **59** at 298 K as 10 wt% doped PMMA films ($\lambda_{\text{exc}} = 300$ nm) (PMMA = poly(methyl methacrylate)); (b) Luminescence spectra of complexes **58** and **59** at 77 K as 10 wt% doped PMMA films ($\lambda_{\text{exc}} = 300$ nm); (c) Emission colors of complexes **58** and **59** at 298 K as 10 wt% doped PMMA films.

More importantly, the trend in relative Φ_{PL} values in solution translates in a way similar to those found in the doped films where the Φ_{PL} for **59** is 46.6% compared to 13.7% for **58**.

2.4.3. Device fabrications.

By considering the attractive optoelectronic features of complexes **58** and **59**, OLED devices were fabricated, adopting **59** as the emitter and **58** as an electron blocking layer (EBL). Figure 41 displays the device structures comprising **58**, **59** and various hole transport layers (HTLs).

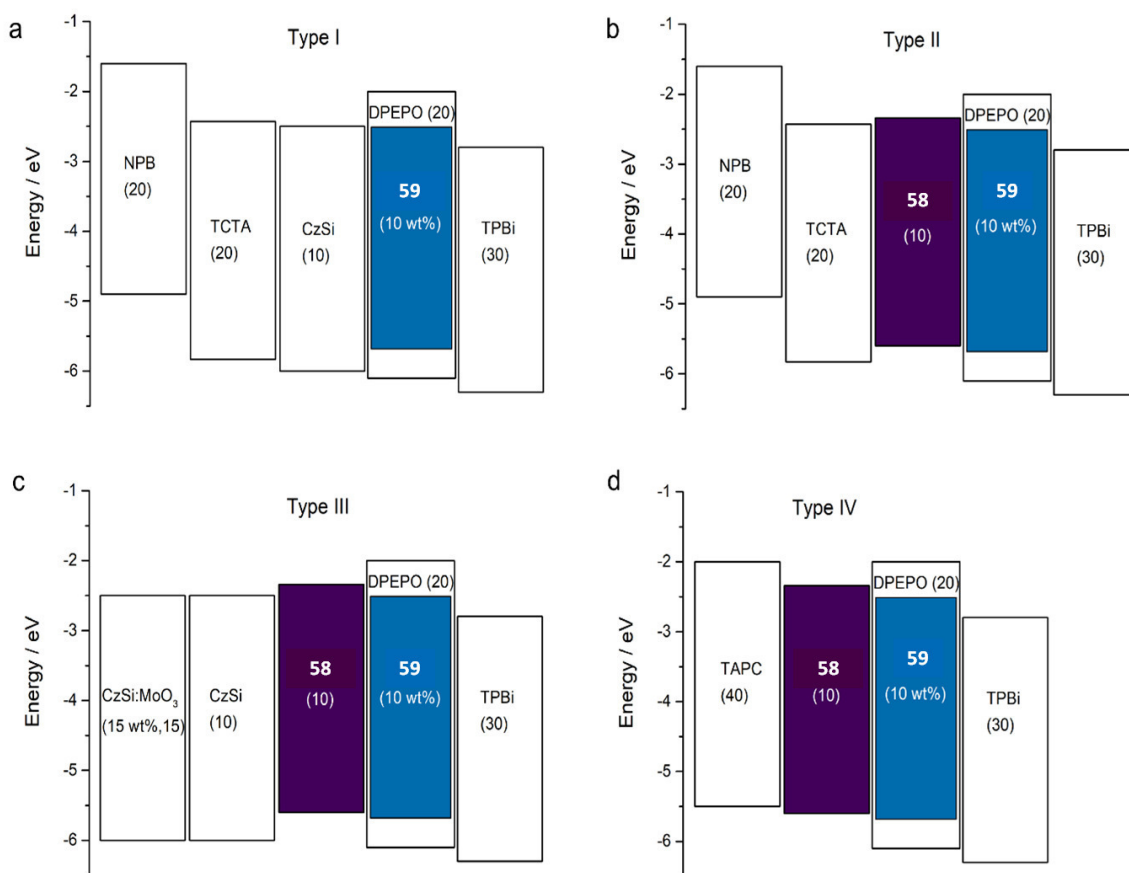


Figure 41. Device architectures with different hole transport (HTL) and electron blocking layers (EBL). (a) Type I device comprising NPB (*N,N'*-Di(1-naphthyl)-*N,N'*-diphenyl-(1,1'-biphenyl)-4,4'-diamine) and TCTA (Tris(4-carbazoyl-9-ylphenyl)amine) as HTL. CzSi is used as a high triplet energy exciton blocker. (b) Type II device with similar structure to Type I, but with 58 employed as an EBL. (c), (d), Type III and Type IV devices, consisting of CzSi (9-(4-*tert*-butylphenyl)-3,6-bis(triphenylsilyl)-9*H*-carbazole) and TAPC (4,4'-Cyclohexylidenebis[*N,N*-bis(4-methylphenyl)benzenamine]) HTLs, respectively. 58 is used as an EBL and exciton blocking layer in both of these devices.

The high emission energy of **59** limits the choice of the host material. The emitting layer (EML) in all the devices is made by a DPEPO matrix (DPEPO = bis[2-(diphenylphosphino)phenyl]ether oxide) doped with 10 wt% of **59**. DPEPO was chosen thanks to its wide band gap and high triplet energy, which is higher than the triplet energy of **59** ($E_T = 2.99\text{-}3.30\text{ eV}$).⁸⁹ This means that the device excited state is confined onto the emitter and cannot freely be back-transferred to the host DPEPO molecules. The Φ_{PL} in the DPEPO film was 41 %.

The emission lifetime of **59** embedded in the DPEPO film is 4.88 μs at room temperature (Figure 42); it is consistent with a fast ISC rate and a ligand-centred emission originating from the lowest excited triplet state.⁹⁰ The emission lifetime increases to 5.56 μs at 77 K (Figure 42). The decrease in the emission lifetime upon heating is consistent with the thermal population of the non-radiative state model (Figure 42).⁹¹

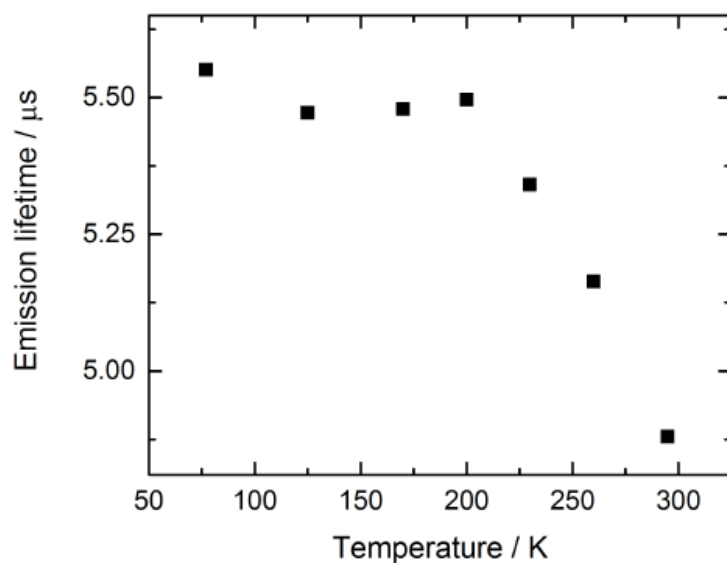


Figure 42. Emission lifetime dependence on temperature of DPEPO:2 film.

The majority of the electrons injected into the EML are carried through the host matrix before being captured by the emitter dopant; subsequently they recombine with the holes trapped on the emitter molecule to form excitons. High triplet energy exciton blockers are thus essential at the HTL/EML interface to prevent non-radiative exciton recombination. The 10 nm interlayer of the high triplet energy CzSi ($E_T = 3.02$ eV) was thus inserted (Type I device, Figure 41a).⁹² Despite **58** shows moderate Φ_{PL} in thin film, its high triplet energy and high electronic band gap were exploited for **58** to act as both exciton blocking and electron blocking layer in Devices II-IV, which adopt different hole injection/transport layer materials and architectures (Figure 41b-d).

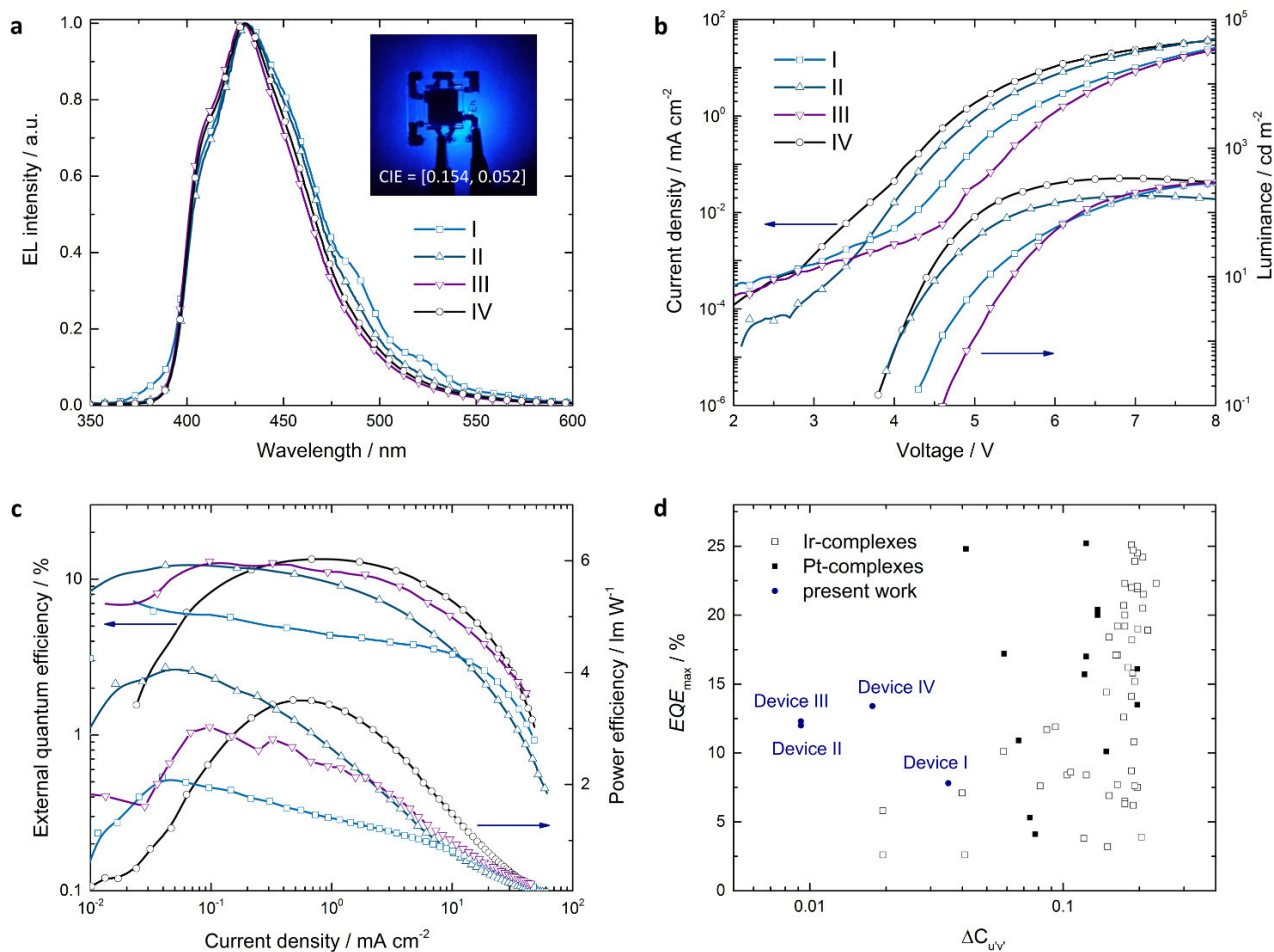


Figure 43. Performance of deep blue phosphorescent OLEDs. (a) Normalized electroluminescence (EL) spectra of four different OLED architectures. Inset shows the photograph of the PhOLED emission with the corresponding CIE colour coordinates of the optimized Device IV. (b) Current density-voltage-luminance characteristics of devices I-IV. (c) External quantum efficiency and power efficiency of PhOLEDs at different current densities. (d) Selected peak external quantum efficiency data versus difference in CIE 1976 UCS color coordinates between OLED emission and EBU blue standard (0.15, 0.06). Data based on available literature for deep-blue OLEDs employing iridium(III) complexes (open black squares) and platinum(III) complexes (solid black squares). Solid blue circles represent OLED devices of the present work.

Figure 43 shows the performances of all the devices, while Table 15 reports their main parameters. For all the devices a deep-blue electroluminescence was recorded with a peak emission of $\lambda_{EL} \approx 430$ nm (Figure 43a). The role of **58** to prevent lost of electrons from the EMLs is emphasized by the lower turn-on voltage (4.05 V against 4.55 V) and an order of magnitude lower leakage current of Device II compared to Device I (Figure 43b). Besides, the LUMO level of CzSi provides no barrier for the electrons to leave the EML. In addition, the shallow LUMO of **58** avoids electron leakage from the dopant molecule and transports holes to the EML, which

supports high charge balance within the EML, thus enhancing the probability of radiative exciton recombination in the DPEPO:**59** film.

The difference between the triplet energy of the emitter and CzSi results to be not sufficiently high to avoid the exciton quenching at the EML/EBL interface due to thermal population of the non-radiative triplet states of the CzSi. These features lead to a high maximum external quantum efficiency (EQE_{max}) of 12.1% for Device II, which corresponds to a remarkable improvement if compared to the moderate EQE_{max} of 7.2% of Device I (Figure 43c). While the concept of using a wide gap phosphorescent emitter as the EBL has been already investigated,^{76b} the use of **58** is unique because it combines very high triplet energy with a shallow LUMO, which are both fundamental for achieving efficient deep blue electro-phosphorescence.

The choice of the HTL sequence resulted to be essential to further boost the device performance. Complex **58** was used in both Device III and Device IV. The selection of HTLs further shifts the great EQE values to the display-relevant brightness of 100 cd m^{-2} . The improvement in the OLED performance is correlated with the improved charge balance at higher current densities and the lower number of the organic interfaces.⁹³

Optimized Device IV shows CIE coordinates of (0.154, 0.052), an EQE_{max} of 13.4% and an EQE of 12.5 % at 100 cd m^{-2} ; it represents to our knowledge the best performing deep-blue OLED ever reported so far, with color coordinates matching the display requirements for blue by the EBU.

Figure 43d compares the Devices I-IV, object of this thesis, with reported blue phosphorescent OLEDs. The devices are compared based on the color coordinate difference in CIE1978 UCS color space between the OLED emission and the EBU standard blue colour of (0.15, 0.06). CIE1978 UCS represent the uniform chromaticity space, and thus the differences in the color coordinates represent the perceived colour difference. The device performance comparison with the selected best deep blue OLEDs is given in Table 15.

Device	V_{on} / V	$\lambda_{\text{EL}} / \text{nm}$	FWHM / nm	(CIE _x , CIE _y)	EQE / %		PE / lmW ⁻¹	
					Max	@ 100 cd m^{-2}	Max	100 cd m^{-2}
I	4.50	431	68.0	(0.154, 0.077)	7.2	3.8	2.81	1.04
II	4.05	431	65.4	(0.151, 0.059)	12.1	6.4	3.95	1.50
III	4.95	430	62.0	(0.156, 0.056)	12.3	10.0	3.00	2.00
IV	4.05	430	63.1	(0.154, 0.052)	13.4	12.5	3.50	2.98

				0.052)				
Ref ^[76a] , Ir emitter	-	395	-	(0.17, 0.06)	5.8	-	1.7	-
Ref ^[76b] , Ir emitter	7.00	430	-	(0.16, 0.09)	10.1	-	-	-
Ref ^[94] , Pt emitter		451	29	(0.148, 0.079)	24.8	22.7		
Ref ^[95] , TADF emitter	4.00	428	65	(0.16, 0.06)	10.3	5.4	3.50	-

Table 15. Device metrics and comparison to selected literature device data with similar CIE coordinates.

2.4.4. Conclusions.

In summary, during my stay in the University of St. Andrews, two deep blue-emitting homoleptic *mer*-Ir(III) NHC complexes **58** and **59** were synthesized and well characterized. Complex **58** was used as an electron and exciton blocking layer due to its high triplet energy and shallow LUMO level while complex **59** was employed within the emitting layer in vacuum-deposited OLEDs (Devices **II**, **III** and **IV**) and the results compared with the device where CzSi was used as the EBL (Device **I**). A consistent improvement in EQE_{max} (7.2% to 13.4% from Device **I** to **IV**) and color purity and chromaticity ($\text{CIE}_y = 0.077$ to 0.052 from Device **I** to **IV**) were observed with the involvement of **58** as the electron and/or exciton blocker. The efficiency remains as high as 12.5% at the display relevant brightness of 100 cd m⁻². To the best of our knowledge, Device **IV** represents the bluest and best-performing iridium-based OLED reported so far, and the only device that meets the display requirements defined by the European Broadcasting Union.

2.5. Two novel luminescent tetrahydrocurcumin bis(cyclometalated phenylpyridine) Ir(III) complexes.

Besides the above Ir(III) homoleptic complexes and respective devices, complexes **57** and its fluorinated analogous with the introduction of two fluorine atoms on the phenylpyridine

fragment, complex **70** (Figure 44) were also evaluated as possible emitters, hence the two OLED devices, containing complexes **57** and **70**, respectively, were also fabricated.

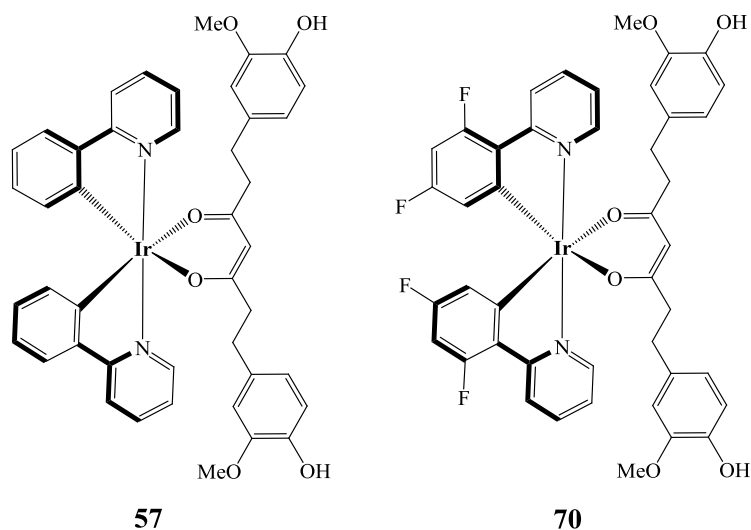
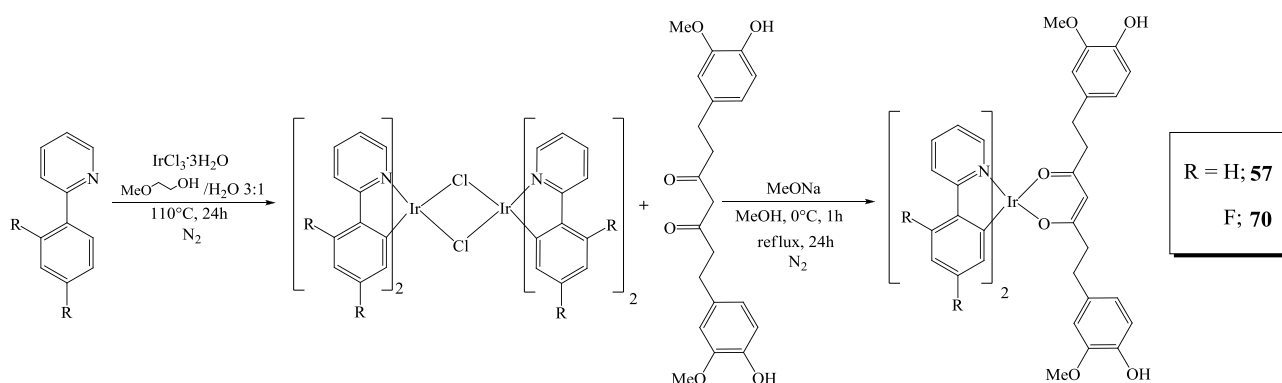


Figure 44. Novel luminescent heteroleptic Ir(III) complexes.

2.5.1. Synthesis and characterization.

2.5.1.1. Synthesis of the neutral heteroleptic iridium (III) complexes.

Both the complexes were synthesized as shown below (Scheme 4)



Scheme 4. General synthetic route for complexes **57** and **70**.

All the starting dimers of the related iridium complexes shown above were synthesized following the same general procedure (better discussed in Chapter 3): under N_2 atmosphere, commercial

Iridium trichloride, $\text{IrCl}_3 \cdot 3\text{H}_2\text{O}$ was dissolved in a 1:1 mixture of methoxyethanol, MeOEtOH and water, and refluxed with the stoichiometric quantity of the related commercial pyridine. After 24 hours the corresponding dimer powder was obtained.

The final iridium (III) complexes were prepared from the related dimer. Under N_2 atmosphere the tetrahydrocurcumin ligand is dissolved in methanol; the temperature is cooled down at 0°C , MeONa is slowly added and the solution is stirred for 1h. The temperature is let to raise up at room temperature and the dimer is added. After 3 vacuum-nitrogen cycles, the solution is refluxed for 24h.

2.5.1.2. Characterization.

In the Figure 45 Uv-Vis spectra of both complexes **57** and **70** are shown and compared with that of the already mentioned complex **35** (see Chapter 1, paragraph 1.8). For both complex **57** and **70** also emission studies have been carried out, thanks to the collaboration of Prof. J. A. G. Williams of the University of Durham.

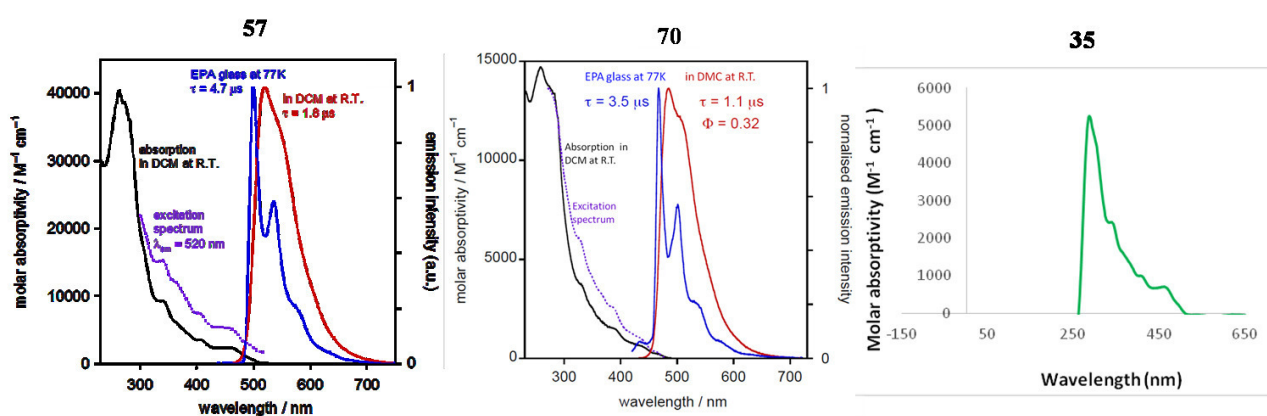


Figure 45. Absorption spectra for complexes **57** (left), **70** (centre) and **35** as reference (right). For complex **57** and complex **70** also emission spectra in solution are provided.

The UV-vis spectra of all complexes show moderately intense absorption bands stretching into the visible region due to charge-transfer transitions, along with $\pi-\pi^*$ bands in the UV region.

Complex **57** resulted to be an extraordinarily bright green emitter at room temperature ($\lambda_{\text{max}} = 520 \text{ nm}$; Figure 45, left panel, red line). The luminescence lifetime is $1.8 \mu\text{s}$ in deoxygenated CH_2Cl_2 solution, whilst its photoluminescence quantum yield of 0.90 makes it one of the most brightly emitting Ir(III) complexes reported, comparable to that of the archetypal complex *fac*-

Ir(ppy)₃.⁹⁶ Complex **70**, on the other hand, showed an extremely lower photoluminescence quantum yield of 0.32, with a luminescence lifetime of 1.1 μs in deoxygenated CH₂Cl₂ solution.

2.5.2. Device fabrications.

By considering the extraordinary luminescent properties of complex **57** and in order to study the resulting effect by introduction of electron-withdrawing elements in complex **70**, the variation in the respective OLEDs emission was investigated; the fabricated devices were also compared with a complex **35**-based OLED (Figure 46).

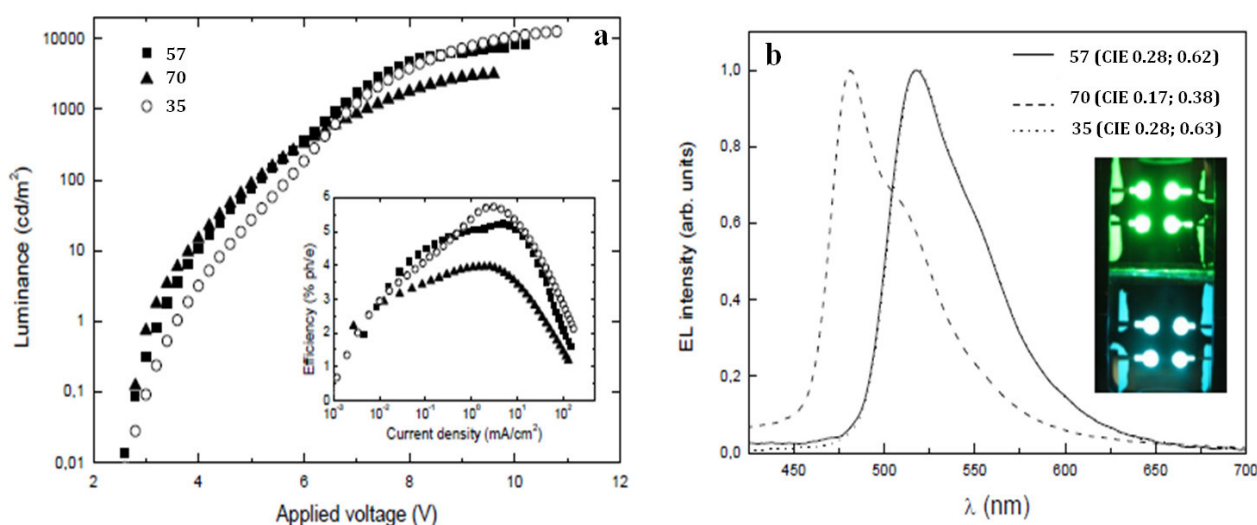


Figure 46. Performance of the fabricated OLEDs. (a) Luminance-Voltage plot of complexes **57**, **70** and **35**. The small panel display the efficiency for all the devices. (b) Normalized electroluminescence spectra of the OLEDs, represented in the photographs.

All the devices have similar performances (Figure 46a) providing a EQE_{\max} of 6%, 5% and 4% for **35**, **57** and **70**, respectively. Interestingly at an applied voltage lower than 6V, the OLEDs based on either **57** or **70** afforded a higher luminance than the complex **35**-based device. Complex **70** and complex **35** are green emitter, as shown in Figure 46b; their EL plots are overlying and provide a EL intensity max at 525 nm with almost equal CIE coordinates of (0.28; 0.62) for **57** and (0.28; 0.63) for **35**, which match the green region of the CIE diagram (Figure 29). As expected, the introduction of two fluorine atoms in the phenylpyridine moiety (complex **70**) induces a blue-shift of the emission of the respective OLED, which has a EL intensity max at 480 nm and CIE coordinates of (0.17; 0.38).

2.5.3. Conclusions.

In conclusion, two novel neutral iridium (III) heteroleptic complexes **57** and **70** have been reported and their respective OLED devices have been fabricated. Both the novel complexes-based devices have a performance similar to that of the OLED based on the known complex **35**. The slightly better response at lower voltage is an aspect that will be further investigated. The blue-shifted emission induced by the introduction of electro-withdrawing groups in the molecular framework was also confirmed, by the introduction of two fluorine atoms on going from complex **57** to complex **70**.

Interestingly, complex **57** thanks to its remarkably luminescent properties and its molecular structure resulted to be also very promising as photosensitizer in the photodynamic therapy. In the following these properties will be deepened.

2.6. Promising applicability of the novel luminescent tetrahydrocurcumin bis(cyclometalated phenylpyridine) Ir(III) complex in photodynamic therapy (PTD).

2.6.1. Photodynamic therapy: introduction and state of art of antitumoral coordination compounds.

One of the most important challenges of the health industry is the fight against cancer. In this field in the last few years, *photodynamic therapy* (PDT) is becoming of increasing interest for the treatment of several type of tumor, such as those of the skyn, esophagus, bladder, lungs and brain.^{97,98} The most important feature of this therapy is that it is not invasive and it is able to destroy the tumoral cells in the presence of a photosensitizer, light and tissue oxygen.

When the photosensitizer is irradiated with a visible light at appropriate wavelength, it becomes electronically excited, going from the ground singlet state (S_0) to the excited one (S_1). This latter is able to populate the triplet excited state (T_1) through a *intersystem-crossing* (ISC) mechanism. As we have already seen in the chapter II, concerning the introduction to luminescence, the ISC mechanism is promoted by *spin-orbit* coupling effects.

The photosensitizer triplet state can generate cytotoxic species through two mechanisms (Figure 47):

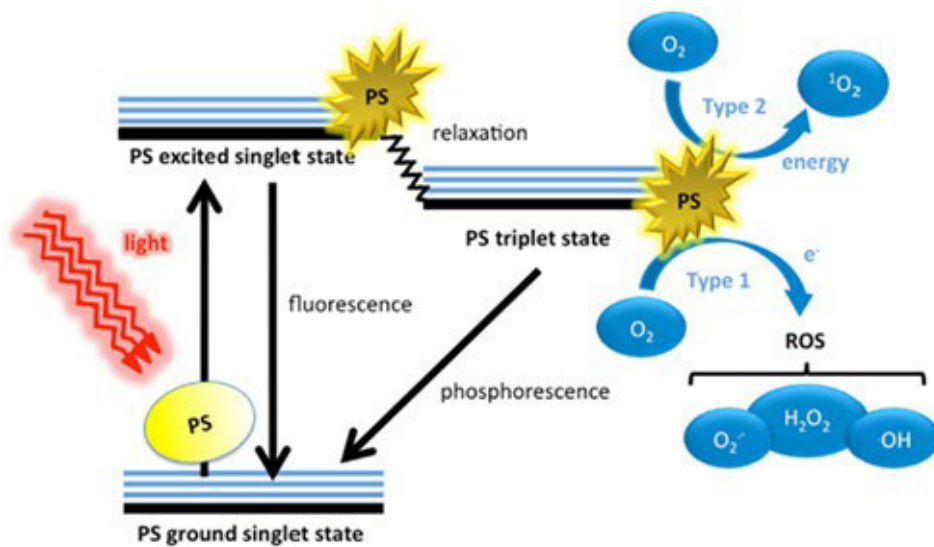


Figure 47. General mechanism of Photodynamic therapy.

- i. In the first one it interacts with biological molecules, thus producing radicalic species, which react with molecular oxygen; highly reactive oxidant species (**ROS**).
- ii. In the second mechanism the excess energy is directly transferred from the photosensitizer T₁ state to the molecular oxygen, to form the singlet oxygen ¹O₂, which causes the formation of radicalic species, through cascade reactions, destroying the irradiated tissue.^{97,98}

The tumoral cells can die by apoptosis and/or necrosis.⁹⁷ The apoptosis (Figure 48), or programmed cellular death, involves the activation of proteolytic enzymes, which leave the plasmatic membrane intact, but induce the death of the cells, which fragment themselves in vesicles, surrounded by membrane. These membrane casings are phagocytized by macrophages, before the membrane breaking and thus, before the inflammatory response can be transmitted.

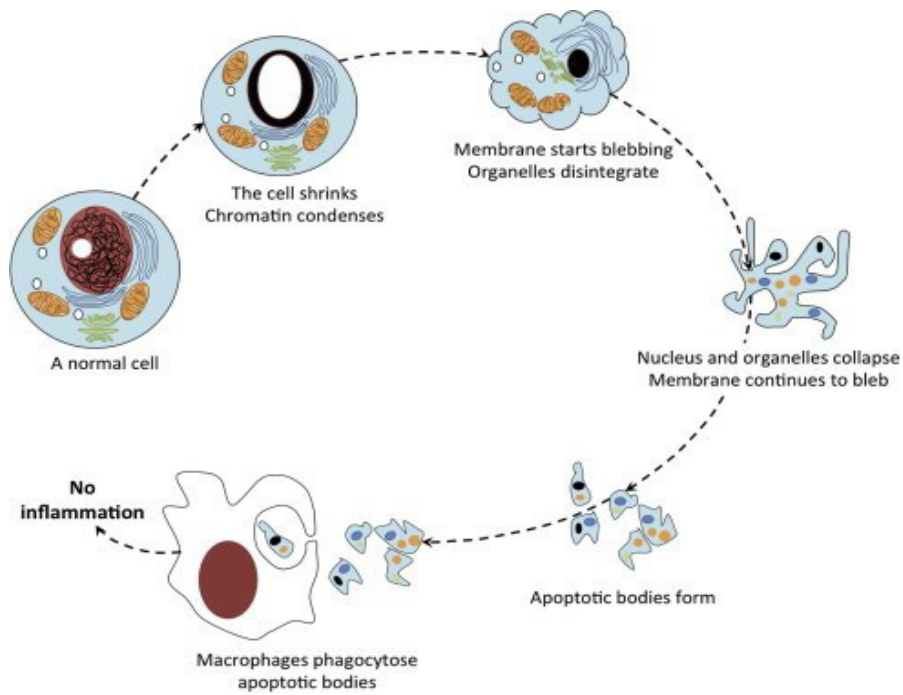


Figure 48. Apoptosis mechanism.

In the necrosis mechanism (Figure 49), instead, the cell swells; the plasmatic membrane breaks and the intracellular material is released, with consequent inflammation.

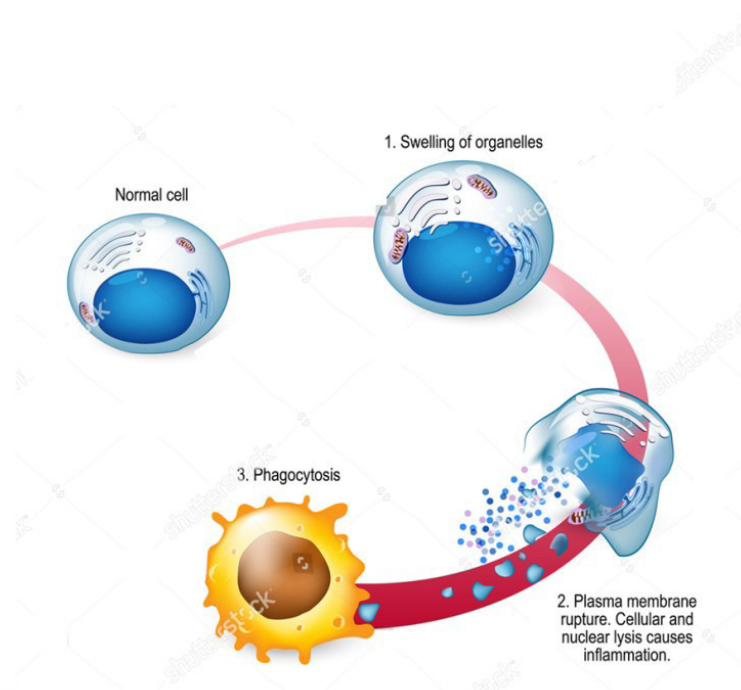


Figure 49. Necrosis mechanism.

By the purpose of therapeutic benefits, the first one looks like the preferable cellular death mechanism. It's interesting to point out that the type of cellular death depends on the photosensitizer accumulation spots. For instance, its localization in the mitochondria or in the endoplasmic reticulum, often induces the apoptosis, while an accumulation in the membranes or lysosomes, provokes necrosis.

An important aspect is that the singlet oxygen has a half-life lower than 320 ns, hence it cannot diffuse more than 10-55 nm, confining the oxidative damages only to those tumoral cells target of the therapy.⁹⁷

Beside the tumoral cells, also the cancer tissue blood vessels are an aim in the tumoral therapies; in fact, after a vessel damage, the ill tissue is deprived by oxygen and nutrients. Further, the photodynamic therapy can stimulate the immune response, facilitating the tumor disappearing.⁹⁷

A photodynamic therapy treatment consists in several steps (Figure 50):

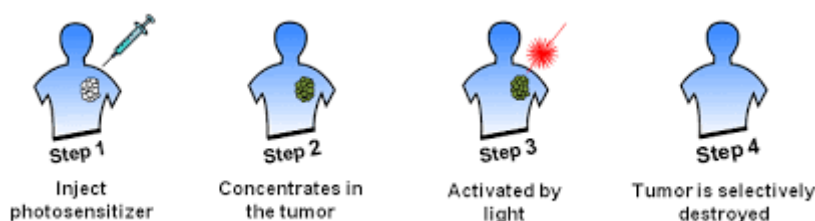


Figure 50. General steps in photodynamic therapy.

1. Photosensitizer subministration;
2. Its accumulation in the tumoral tissue;
3. Photosensitizer irradiation with consequent generation of cytotoxic species;
4. Cellular death.

The photodynamic therapy aim is to prevent the damage of the healthy tissues, which is common in the usual anticancer therapies. Respect with the traditional therapies such as chirurgic operations, radiotherapies or chemotherapies, the photodynamic therapy has the remarkable advantage of being less invasive, because it can be directed toward the tumoral tissue and the light used to excite the photosensitizer can be accurately focused, for instance by using optical fibres.

The photosensitizer excitation induced by the absorption of two photons (TPA: Two-Photon Absorption) is a promising approach to increase the photons penetration ability in tissues.^{98,99} In fact, if the photosensitizers are able to simultaneously absorb two photons at lower energy, it becomes possible using NIR (Near Infra-Red) wavelengths to induce the photosensitizer excitation. This represents a huge benefit, because it allows to excite the photosensitizer by the employment of very low frequencies, whit a higher radiation power of tissue penetration, thus

limiting its undesired absorption from the overlying tissues. The therapeutic window which can be employed in the photodynamic therapy, indeed, covers wavelengths from 650 to 850 nm. Under 650 nm there are strong absorptions from several biomolecules, such as emoglobine, which limit *in vivo* light penetration in tissues, while above 850 nm there is the absorption of the water molecules present in tissues.⁹⁸

An ideal photosensitizer should have the following features:⁹⁸

- It must absorb in the wavelength window mentioned above (with one- or two-photon processes) and have a high molar extinction coefficient (ϵ);
- It must have a triplet state with an energy (higher than 94 kJ/mol) sufficient to promote the singlet oxygen formation and with a lifetime long enough to efficiently produce cytotoxic species;
- It must be photostable;
- It must be non-toxic in light absence to prevent any side effect;
- It must be able to be selectively transported to the active site;
- It must be easily eliminated by the organism.

A large number of organic photosensitizers is used in the photodynamic therapy, in particular phtalocyanines, chlorines, fullerenic or porphirinic derivatives.^{97, 98} For instance, the Verteporfin (Figure 51a) has been proved to be useful for anticancer, dermatologic and oftalmic treatments. Foscan (Figure 51b), a chlorine derivative, also, has been approved in advanced carcinoma treatments for head and neck cells.

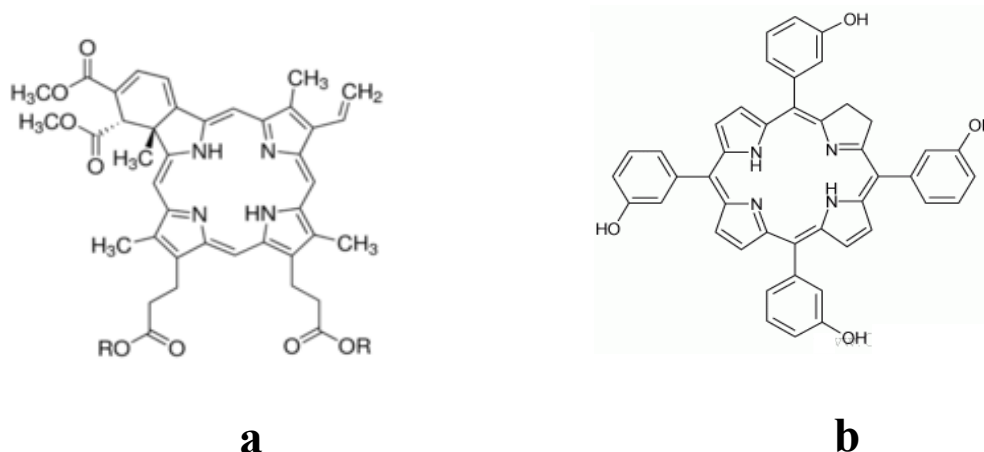


Figure 51. Structure of Verteporfin (a) and Foscan (b).

These derivatives though show side effects.¹⁰⁰

Outside the photodynamic therapy, several coordination compounds, in particular platinum complexes, such as *cis*-platin (Figure 52), have been demonstrated to be effective in the cancer

treatments.¹⁰¹⁻¹⁰³ However they have serious collateral effects, such as neuro, epato, and nephrotoxicity; further it has been observed an arising resistance towards these platin-based drugs.

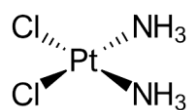


Figure 52. *cis*-platin structure.

Surprisingly, the study of coordination compounds as photosensitizers is still very limited,⁹⁸ although are becoming of increasing interest metal complexes with the following features:

- i. Easy formation of the triplet state, characterized by a life time with the appropriate timing and energy;
- ii. Easy formation of ¹O₂;
- iii. Efficient absorption of two photon.

Among the more promising compounds, Ir(III) and Pt(II) complexes stand out.

Despite their great potential, confirmed by *in vitro* studies, to the best of my knowledge, there are not yet *in vivo* application of coordination compounds as photosensitizer for photodynamic therapy of tumoral cells. This is probably due to the lack of selectivity towards ill tissues.

It is known that, once injected *in vivo*, an anticancer drug must cross the endothelial barrier, determined by the wall structure (endothelium) of the blood vessels. The smaller molecules (2-10 nm) are caught via pinocytosis (Figure 53) by the endothelial cells, while the bigger particles can travel in the blood to tissues through capillary windows.

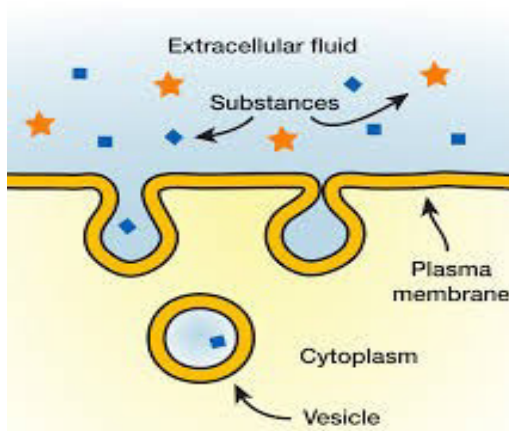


Figure 53. General scheme of pinocytosis, a type of endocytosis by which small substances in the extracellular fluids are brought within the cells via a cell membrane invagination, which incapsulates these particles in vesicle inside the cell.

The tumoral tissues endothelium is different from that of the healthy ones, both for the wall cellular composition and for the windows dimensions; taking advantage of these differences, it is possible to direct the drug, by using the so called *EPR effect* (Enhanced Permeability and Retention).¹⁰⁴ Two directing strategies exist, the active and the passive one.

This latter exploits the EPR effect and involves the accumulation of a carrier with the appropriate dimensions to suit to the cancer cells specific windows. To this aim, are interesting particle carriers such as microspheres, nanoparticles, nanogels and polymeric micellae, which bear the drug.

The active targeting, instead, needs a directional pendant, such as monoclonal antibodies, specific for antigens tumor-associated, peptidic sequences, carbohydrates or small molecules. This pendant works like darts, intercepted just by the target cells.

2.6.2. Curcuminoids and their complexes.

As already mentioned in the previous section, Ir(III) complexes became one of the most promising family of compounds for anticancer applications.

Further it is also known that curcumin (Figure 54) has analogues chemopreventive properties against a variety of tumours.

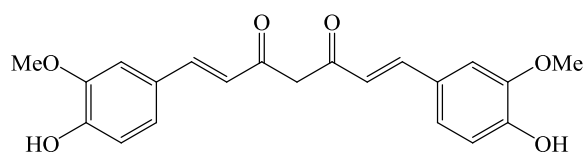


Figure 54. Chemical structure of curcumin.

Curcumin, 1,7-bis(4-hydroxy-3-methoxyphenyl)-1,6-heptadiene-3,5-dione (CUR), is a polyphenolic natural product isolated from the root of *Curcuma longa*, a rhizomatous herbaceous plant. CUR has been used as a well-recognized dietary spice for centuries and its pharmacological activities have been explored in various clinical studies including anti-inflammatory, anti-oxidant, anti-dementia, and anti-diabetic properties.¹⁰⁵ In particular, it appears to have chemopreventive properties against a various number of human malignancies and is nowadays in clinical trials as an anticancer agent.¹⁰⁶ In clinical trials Phase I, it was observed that humans can tolerate a CUR dose as high as 8 g/day with no side effects.¹⁰⁷ However, CUR shows poor oral bioavailability: its concentration, in human plasma and other tissues, indeed, is extremely low even after a high oral dose. This is due to its instability with respect to hydrolysis of the β -diketone unit under physiological conditions, rapidly leading to species such as ferulic acid and vanillin (Figure 55).¹⁰⁸

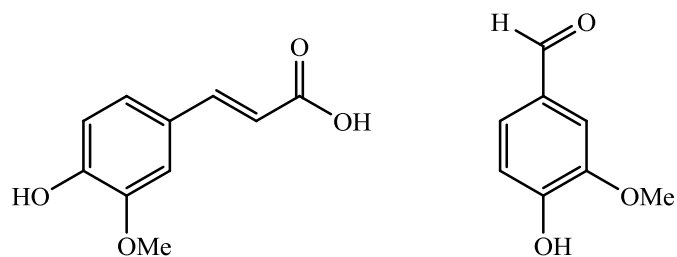


Figure 55. Chemical structures of ferulic acid (left) and vanillin (right).

Interestingly, binding this β -diketone moiety in the deprotonated anionic form to a metal centre increases remarkably its hydrolytic resistance, with respect to free curcumin, and the resulting complexes can show cytotoxic activity.^{108, 110} In fact, a bioreductively-activated cobalt(III) carrier system for curcumin delivery with enhanced drug stability and efficacy against colon cancer cells was recently reported (Figure 56).^{108b}

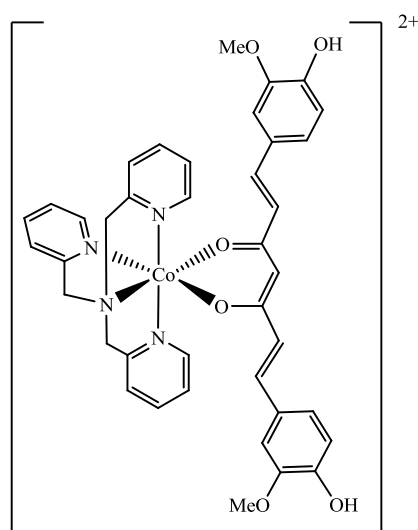


Figure 56. Co-curcumin ionic complex reported by Huang et al.

The high instability of CUR suggests that they might be its metabolism products to be responsible for its pharmacological *in vivo* effects.¹¹¹ In particular, tetrahydrocurcumin (THC) is one of CUR active metabolites (Figure 57) and might play a crucial role in CUR-induced biological effects.

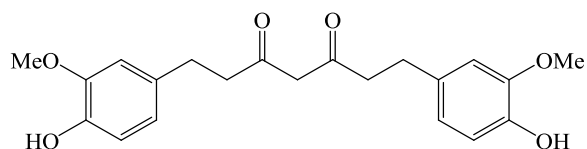


Figure 57. Chemical structure of THC.

Its easy absorption via the gastrointestinal tract suggests that THC might be even a better candidate than CUR for anticancer agents design.¹¹² According to this observation, THC exhibits

important cell growth inhibition by inducing human breast cancer MCF-7 cells to undergo mitochondrial apoptosis and G2/M arrest.¹¹²

The photobiological activity of curcumin is related to its ability to generate reactive oxygen species (ROS) which lead to cancer cell death by apoptosis *via* mitochondrial pathways,¹⁰⁸ as anticipated in the previous section.

Curcumin's photochemical properties are hence significant in this context.¹¹³ It shows a strong absorption band around 410–430 nm and fluorescence in the region 460–560 nm in solution at room temperature, with a quantum yield in the range 0.02–0.08 according to the solvent. While the singlet excited state (S_1) decays by a non-radiative process, its triplet state (T_1) reacts with ground-state 3O_2 to generate singlet oxygen 1O_2 efficiently. CUR is thus of great interest for photodynamic therapy (PDT).

However, although curcumin could have potential as a PDT agent, its low bioavailability would severely limit its efficacy. The higher stability of metal complexes of CUR, coupled with longer-wavelength absorption, could render them suitable for such phototherapeutic applications.¹⁰⁸ Surprisingly, despite growing interest in the use of Ir complexes as PDT agents,¹¹⁴ no iridium complex bearing curcumin as a ligand has been reported up to now.

Cyclometallated Ir(III) complexes could have great potential in PDT since they may efficiently generate 1O_2 due to the presence of the heavy atom, which promotes a fast intersystem crossing to triplet states with microsecond lifetimes.¹¹⁵ Moreover, as already shown by our group, they are often luminescent,^{116–118} offering potential for cellular imaging, and for what is known as *theranostics*, the combination of therapy and imaging.¹¹⁷

2.6.3. Two novel curcuminoid bis(cyclometalated phenylpyridine) Ir(III) complexes.

On the basis of the above observations, I decided to prepare and study an Ir(III) complex bearing two cyclometallated phenylpyridine (ppy) ligands and curcumin, **56** and its analogous with tetrahydrocurcumin, **57**, whose metal complexes have never been reported. Both of them have been already introduced previously in this thesis (Figure 58).

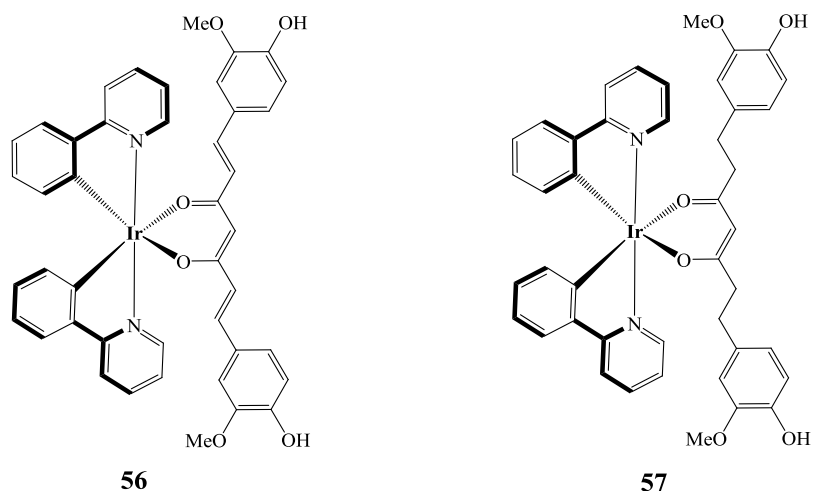


Figure 58. Ir(III) synthesized complexes.

As already introduced, they were synthesized by reaction of $[\text{Ir}(\text{N}^{\wedge}\text{C}\text{-ppy})_2(\mu\text{-Cl})_2]$ with the commercial curcumin or tetrahydro-curcumin pro-ligand in methanol in the presence of sodium methoxide to deprotonate the β -diketone. The desired products were purified by recrystallization from a mixture of dichloromethane and diethylether. The identities and purities of the products were confirmed by ^1H and ^{13}C NMR spectroscopy and by elemental analysis (details about synthesis and NMR spectra are provided in the Chapter 3).

2.6.3.1. Photophysics studies.

The UV-vis spectra of the two complexes show moderately intense absorption bands stretching into the visible region due to charge-transfer transitions, along with $\pi\text{-}\pi^*$ bands in the UV region (Figure 59).

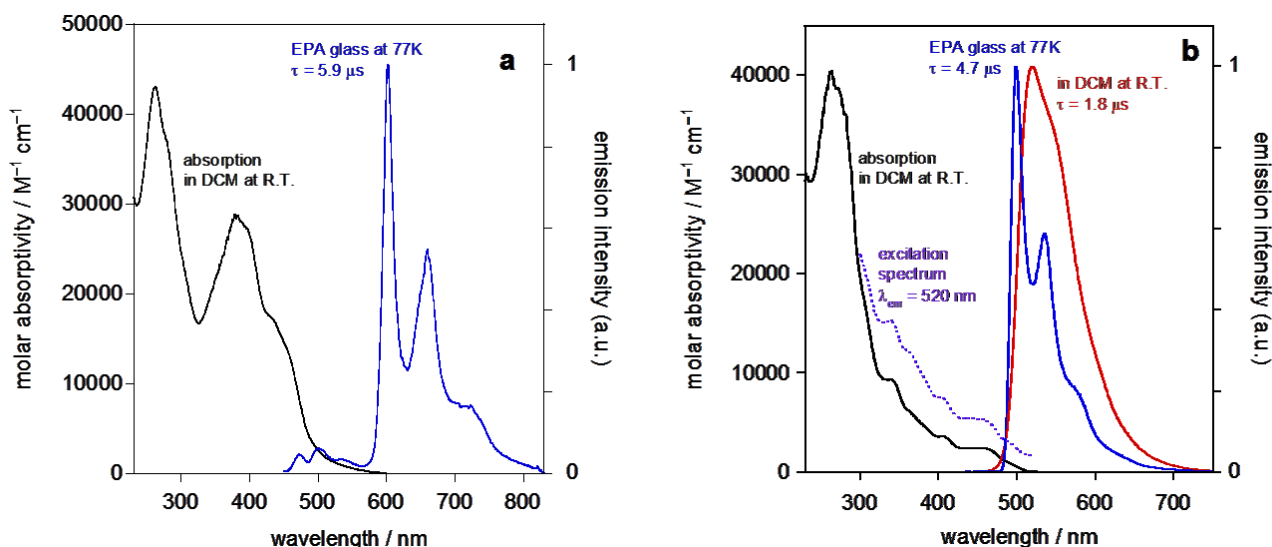


Figure 59. (a) Absorption spectrum (black line) of **56** in CH_2Cl_2 at 295 ± 1 K and emission spectrum in EPA glass at 77 K (blue line). (b) Absorption spectrum (black), emission spectrum (red) and excitation spectrum (dotted purple line) of **57** in CH_2Cl_2 at 295 ± 3 K, together with the emission spectrum in EPA at 77 K. (blue).

At room temperature (black line, spectrum **a**), complex **56** shows no detectable luminescence in deoxygenated CH_2Cl_2 solution. The absence of luminescence could be explained with a *trans-cis* isomerization of the olefinic double bond, which acts as a deactivation pathway, as previously suggested by our group in Ir(III) complexes incorporating C=C-appended ligands.^{119, 120} It could be also due to the CUR ligand having low-energy π^* orbitals associated with it, such that the lowest-energy triplet excited state (T_1) becomes fully localised on this ligand, oppositely to it having the usual $d_{\text{Ir}} / \pi_{\text{ppy}} \rightarrow \pi^*_{\text{ppy}}$ charge-transfer character, that would typically provide efficient phosphorescence. Such an effect is well-established for Ir(III) complexes with $O^{\wedge}O$ ligands featuring more extended conjugation, such as dibenzoylmethane, which have low-energy ligand-based triplet-states.¹²¹ A similar effect has been observed for related platinum(II) complexes with $O^{\wedge}O$ ligands featuring low-energy triplet states.¹²² At low temperature (77 K; blue line, spectrum **a**), the deactivating pathway is inhibited: hence, the complex emits in the red region of the spectrum, displaying a highly structured profile, $\lambda_{(0,0)} = 602$ nm, and a lifetime of 5.9 μs .

Oppositely, as already shown previously, complex **57**, lacking olefinic bonds in the $O^{\wedge}O$ ligand, is an extraordinarily bright green emitter at room temperature ($\lambda_{\text{max}} = 520$ nm; red line, spectrum **b**). **57** luminescence lifetime is 1.8 μs in deoxygenated CH_2Cl_2 solution while its photoluminescence quantum yield of 0.90 renders it one of the most brightly emitting Ir(III) complexes reported so far. This contrasts strikingly with tetrahydrocurcumin itself, which is only very weakly emissive in ethanol solution at room temperature ($\Phi = 0.007$).¹²³

The strong green phosphorescence of **57** in deoxygenated solution is strongly quenched by oxygen. The emission lifetime drops to 70 ns in air-equilibrated solution, from which a rough estimate of the bimolecular rate constant for quenching by O₂ can be calculated to be $6.2 \times 10^9 \text{ M}^{-1} \text{ s}^{-1}$. Such quenching of transition metal complexes is often accompanied by formation of the excited ¹Δ_g state of oxygen, commonly referred to as singlet oxygen or ¹O₂. In the present instance, the emission of the ¹O₂ thereby generated could be readily detected in the near infrared (NIR) region (1274 nm; see Figure 60). Using a known procedure¹²⁴ with perinaphthenone (also known as phenalenone) as the standard ($\Phi = 0.95$), the quantum yield of ¹O₂ generation was estimated to be 0.42 in CH₂Cl₂.

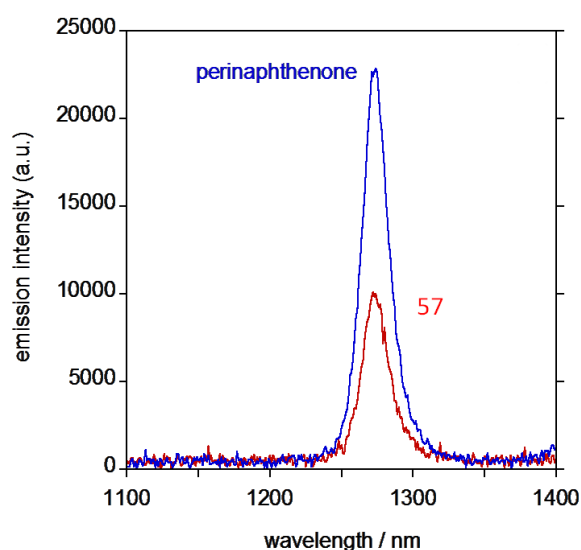


Figure 60. Singlet oxygen emission spectra from isoabsorbant solutions of Ir-THC (red) and perinaphthenone (blue) in air-equilibrated CH₂Cl₂ at 295 ± 1 K.

2.6.3.2. Internalization studies.

The cellular uptake of these new Ir(III) complexes was probed by emission microscopy. Both complexes are characterized by high cell permeability and fast internalization kinetics in A549 – a human alveolar basal epithelial cancer cell line – and in cervical cancer HeLa cells (Figure 61a and Figure 62).

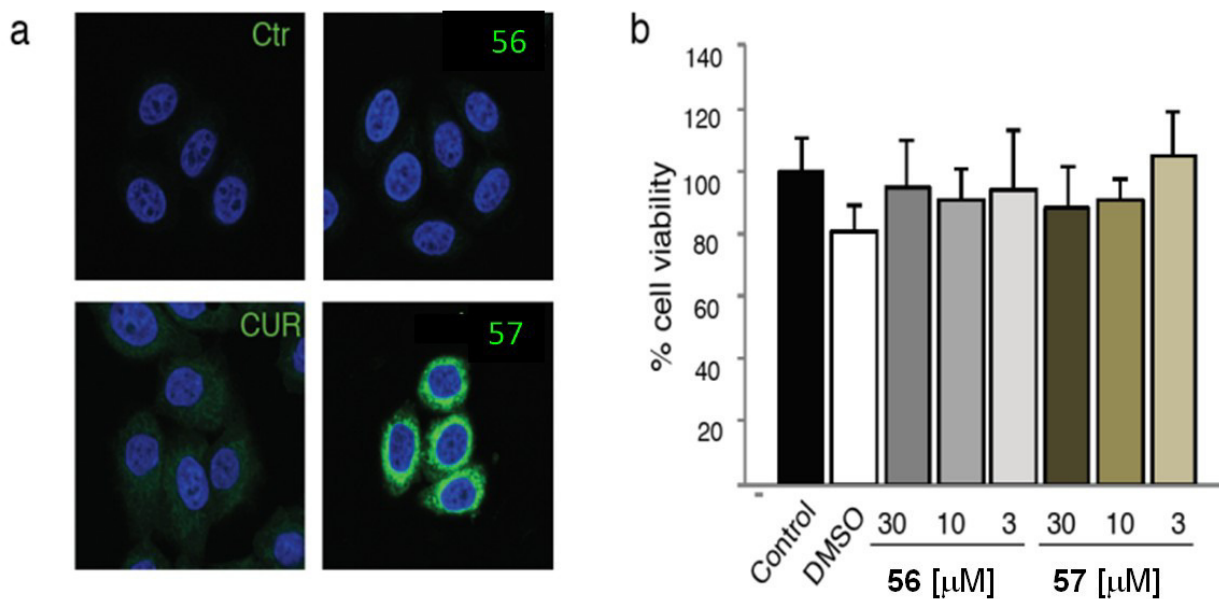


Figure 61. (a) Immunofluorescence analysis of HeLa cells incubated for 2 h with the indicated compounds at 30 μM concentration and co-stained with the nucleus-specific dye DAPI. Images were taken by confocal microscopy with an excitation wavelength of 495 nm. Emission from the complexes is green; DAPI is blue and localised to the nuclei. (b) MTT assay of A549 cells continuously treated for 2 days with the indicated concentrations of compounds 56 and 57 without irradiation.

While **56** is barely detectable (as is the case also for controls treated with CUR or THC), the emission from the cells treated with the complex **57** is extremely bright (Figure 61a). It is visible even after incubation at a dose of 0.3 μM and is localized inside the cells at the mitochondria, as confirmed by co-staining experiments with MitoTracker[®] dyes (Figure 62).

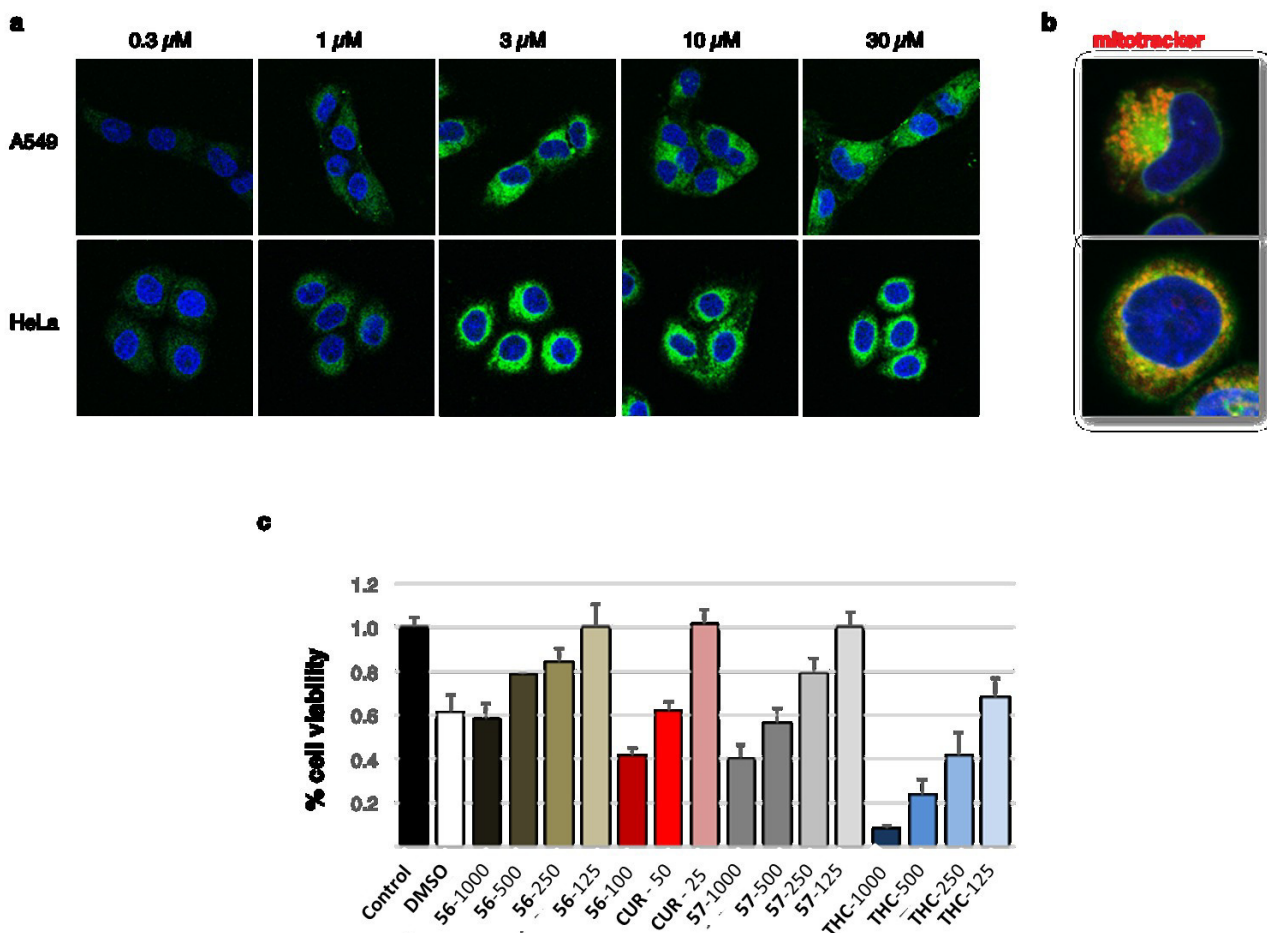


Figure 62. 57 rapidly internalizes and shows a mitochondrial staining. (a) Internalization of the 57 compound in A549 (upper panel) and HeLa (lower panel) cells at the indicated concentrations. After 2 h incubation, images of the compound (green) were captured by confocal microscopy upon 499-550 nm excitation. Blue, DAPI staining of the nuclei. Similar results were obtained after 30 min incubation. (b) Co-localization of 57 with mitotracker. Cells were treated for 2 h with 30 μ M 57, then cells were incubated with MitoTrackerRed CMXRos (ThermoFisher) at 100 nM for 45 min. Cells were then washed twice and fixed. Images were captured by confocal microscopy (detection at 499-530 nm for the compound and 650-700 nm for the MitoTracker). Blue = DAPI staining of the nuclei. (c) CCK assay of A549 cells continuously treated without irradiation for 24h with the different concentrations (μ M) of the indicated compounds (in bold). DMSO was added at the maximum concentration used for the compounds (2%). Curcumin were tested lower concentrations as it appears to be toxic already at 50 μ M.

It is notable that the cells appear to be unaffected by the presence of the two complexes. This observation was further confirmed by an MTT assay performed at various concentrations of the complexes: no reduction in cell viability was evident, even after 48 h of continuous treatment at concentration of 30 μ M under normal cell culture conditions (Figure 61b). These results were further confirmed by a CCK (cell counting kit) assay (Figure 62c). The photocytotoxicity of the Ir-THC complex was assessed through irradiation at different wavelengths coupled with time-lapse microscopy to view the effect of light on the cells. The cells were irradiated with a xenon lamp through three different excitation filters (360-370 nm, 465-495 nm and 530-560 nm) and for different lengths of time (0.5 s, 1 s and 2 s) and were subsequently monitored over a period of 48 h.

As can be seen in Figure 63, A549 cells treated with 30 μM of **57** for 2 h in the incubator, and irradiated in the wavelength range 465-495 nm for 2 s (at a power of 5.6 mW mm^{-2}), underwent apoptosis within less than 2 h. The use of light in the 530-560 nm region has an intermediate effect in initiating apoptosis, consistent with the limited absorption of the complexes at such long wavelengths. Based on the previous observations, we hypothesize that $^1\text{O}_2$ or related reactive oxygen species generated upon excitation of the compound are responsible for the observed phototoxicity. The contrast between the light-induced cytotoxicity and the lack of toxicity in the absence of light is of crucial importance for the design of PDT agents.

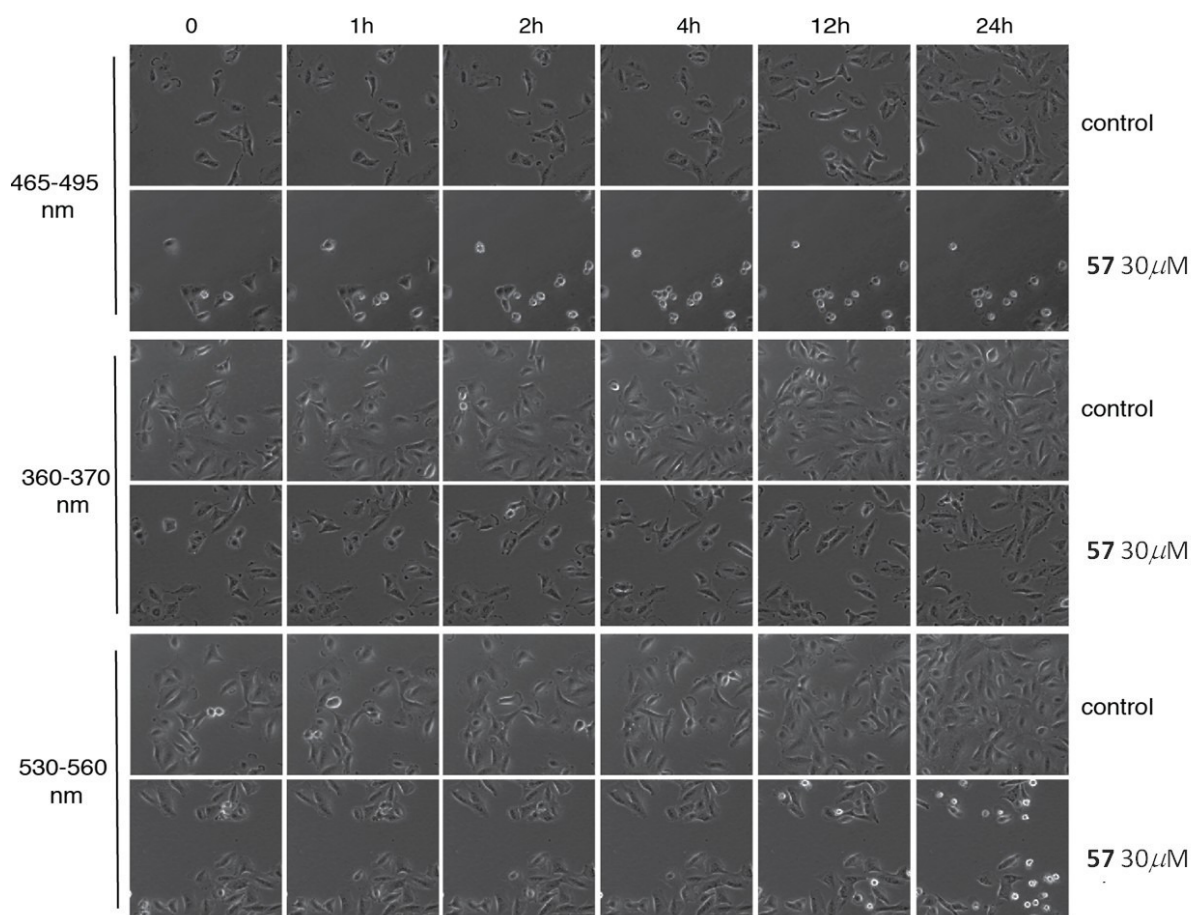


Figure 63. Optimal phototoxicity for **57 occurs with 465-495 nm excitation. Sample images of time-lapse experiments performed on A549 cells treated with 30 μM **57** for 2 h and irradiated with different excitation filters (360-370 nm, 465-495 nm and 530-560 nm) and time (0.5 s, 1 s and 2s). Frames are selected according with the time indicated.**

To compare **56** and **57** and confirm the specificity of the cytotoxicity, several experiments have been performed in which A549 cells were treated with the two complexes and the free pro-ligands CUR and THC at a concentration of 30 μM in each case (Figure 64).

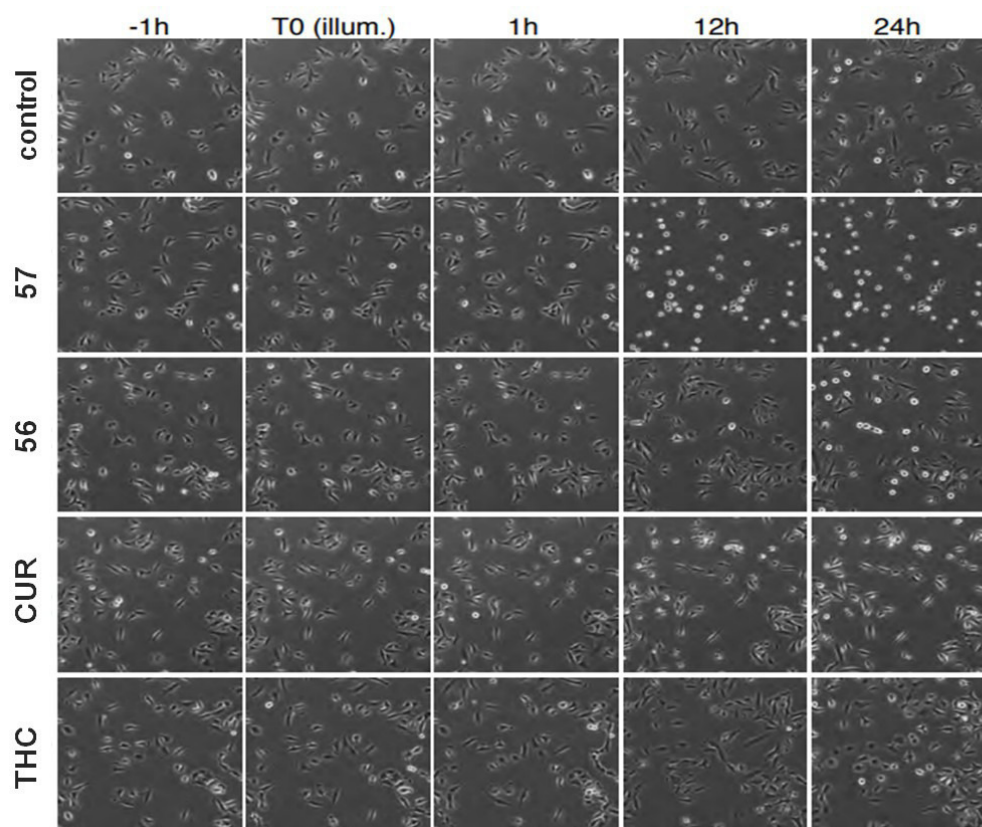


Figure 64. Sample images of the time-lapse experiment performed on A549 cells treated for 2 h with the indicated compounds at 30 μM concentration before irradiation and recording. Cells were irradiated for 2s in the wavelength range 465-495 nm (5.6 mW mm^{-2}) and this time point is considered T0.

Complex **56** upon irradiation showed much reduced activity compared to **57**, an observation that is consistent with the earlier conclusion of rapid deactivation of the excited state. It is remarkable to note that, for cells treated with the Ir complexes, neighbouring cells in the culture plates that were *not* subject to irradiation were perfectly viable. Free CUR showed limited phototoxicity while free THC did not show any such activity at all, demonstrating the fundamental role played by the coordination to the iridium(III) center for the phototoxicity.

Subsequent experiments were conducted with **57** at a range of lower concentrations. Results indicated that a dose of 10 μM is sufficient to kill all the treated cells when irradiated for 2s (Figure 65a). In order to assess the broader applicability to other cell lines, analogous phototoxicity experiments have been carried out on HeLa cells and human brain glioblastoma T89G cells, treated with 4 and 8 μM of **57**. No evident differences are visible among the various cell lines, though A549 cells appear to be more resistant at 4 μM concentration (Figure 65b).

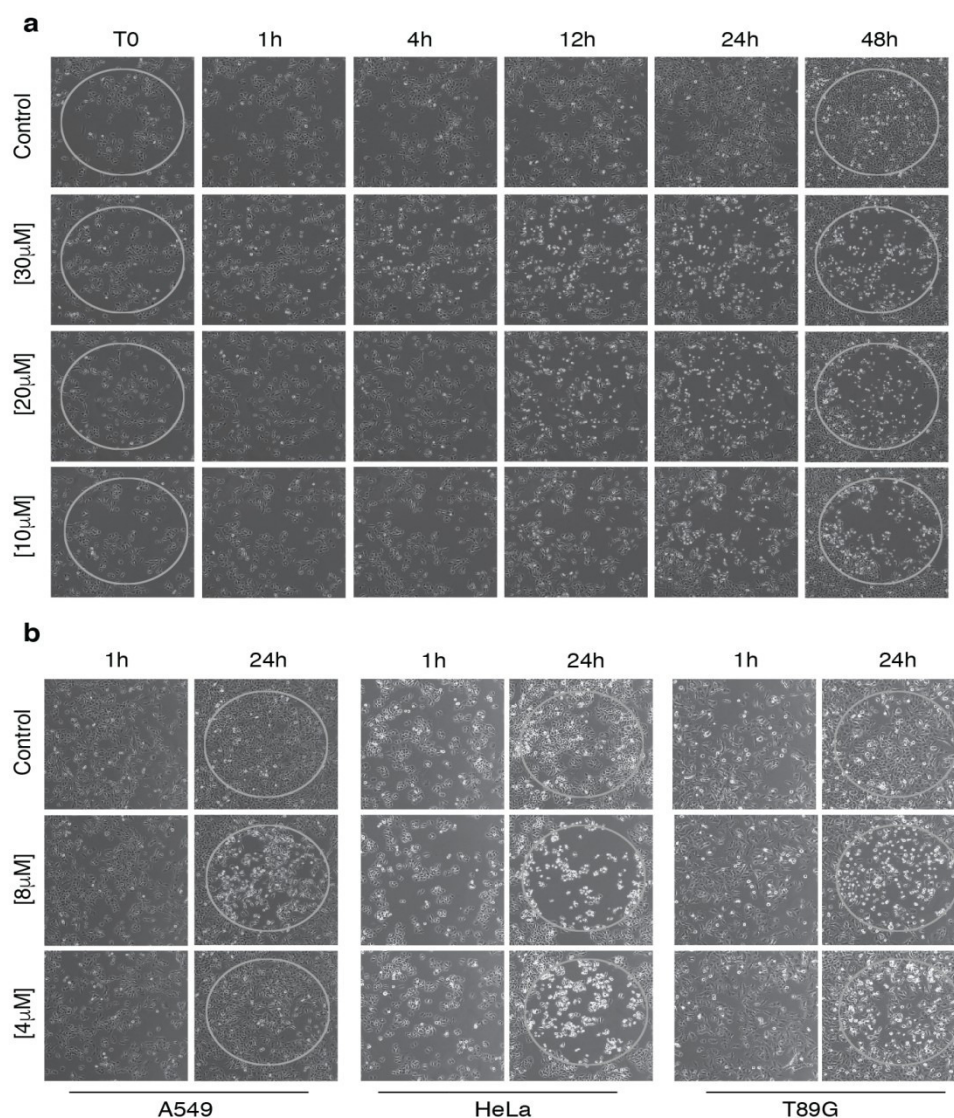


Figure 65. (a) Sample images of the time-lapse experiment performed on A549 cells treated with Ir-THC at the concentrations indicated. Circles underline the irradiated region of the wells. **(b)** Comparison of images obtained at 1 and 24 h treatment of A549, HeLa and T89G cells at 4 and 8 μM . Cells were irradiated for 2 s in the wavelength range 465-495 nm (5.6 mW mm^{-2}).

The LD_{50} (half lethal dose concentration) of complex **57** was calculated with the set parameters (2h pre-incubation, 465-495 nm, 2s irradiation) using the CCK assay in HeLa and A549. **57** gave LD_{50} values of 5-7 μM (see the Experimental Section; Chapter 3). We also tested the effect of longer irradiation of cells treated with a lower concentration of complex. Strikingly, phototoxicity is visible even with 1 μM of **57**, when cells are irradiated for 20s (Figure 66). These results are exceptionally promising for photodynamic therapy, since the phototoxicity index (PI) of the complexes is remarkably high (>200) and the time of light exposure are very low.

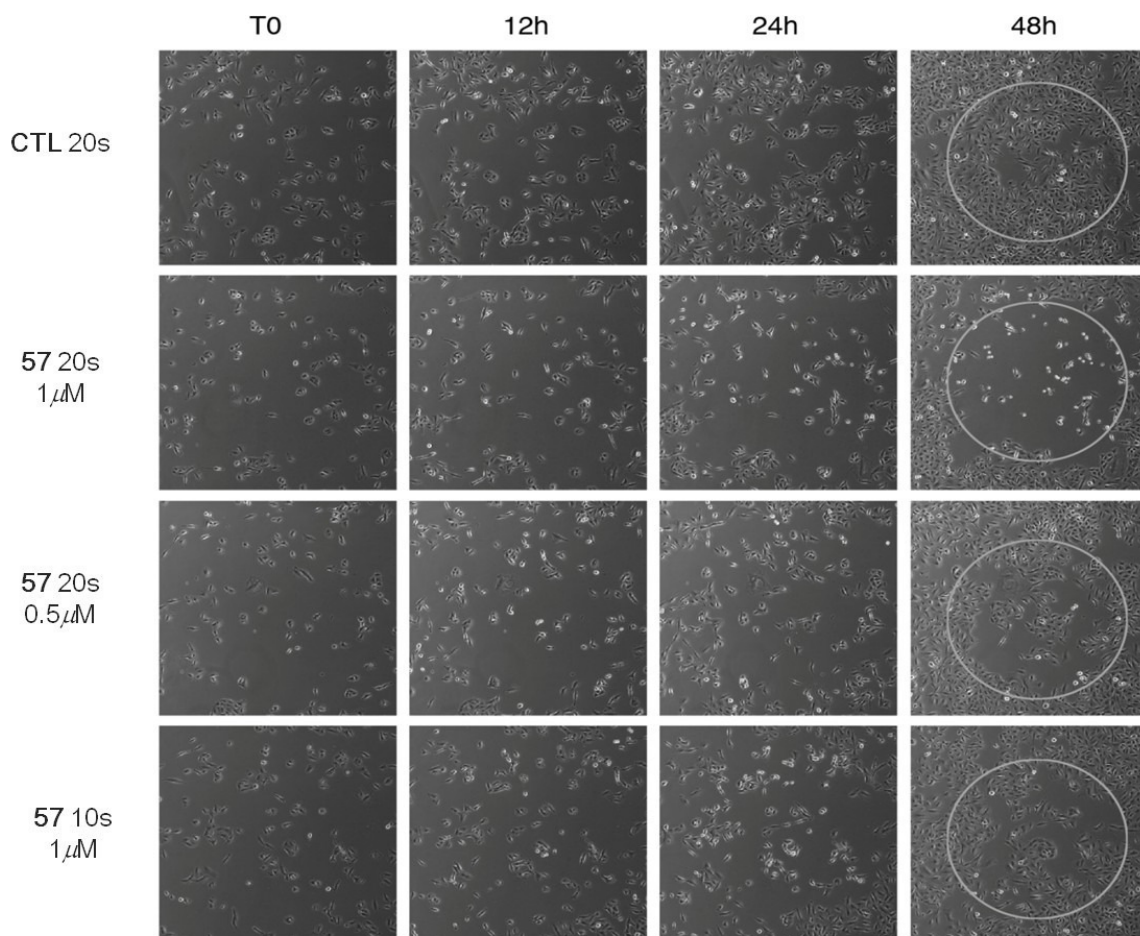


Figure 66. Cells undergo apoptosis even at 1 μ M **57** if irradiated for 20s. Sample images taken at the indicated time of a time-lapse experiment. A549 were treated with 1 or 0.5 μ M **57** for 2h and irradiated with 465-495 nm excitation filter for 10s or 20s, as indicated. Circles underline the irradiated region of the wells.

2.6.3.3. Conclusions.

In conclusion, the new cyclometallated Ir(III) complex with a tetrahydrocurcumin ligand, **57**, appears to be a very promising tool for combined photodynamic therapy and cellular imaging. It has several desirable properties for the purpose:

- i. it is highly phosphorescent and soluble;
- ii. it easily enters into cells where it is concentrated in mitochondria, even at limited concentration;
- iii. it is highly phototoxic upon irradiation with suitable light, but not cytotoxic in the dark.

These results highlight how photoactive metal complexes of curcuminoids may offer interesting future potential for phototherapeutic applications in combination with emission imaging microscopy.

This work is object of a paper written in collaboration with Prof. J. A. G. Williams of the University of Durham and Prof. S. Polo of the Istitute Firc of molecular oncology (IFOM) in Milan.¹²⁵

2.7. References

1. William W. Parson (auth.) - *Modern Optical Spectroscopy_ With Exercises and Examples from Biophysics and Biochemistry* - Springer-Verlag Berlin Heidelberg (2007).
2. Robert Eisberg, Robert Resnick (auth.) – *Quantum physics of atoms, molecules, solids, nuclei and particles* - 2nd Edition (1985).
3. G. B. Porter, *J. Chem. Educ.*, **1983**, 60, 785.
4. A. Jablonski, *Nature*, **1933**, 131, 839.
5. B. Y. M. Kasha, *Discuss. Faraday Soc.*, **1950**, 9, 14.
6. Europäische Kommission, *Dimens. Contemp. Ger. Arts Lett.*, **2010**, 1.
7. J. H. Kamlage, P. Nanz, *Glob. Soc.*, **2017**, 31, 65.
8. S. Bouzarovski, S. Tirado Herrero, *Eur. Urban Reg. Stud.*, **2017**, 24, 69.
9. A. De Almeida, B. Santos, B. Paolo, M. Quicheron, *Renew. Sustain. Energy Rev.*, **2014**, 34, 30.
10. T. Jüstel, H. Nikol, C. Ronda, *Angew. Chem. Int. Ed*, **1998**, 37, 3084.
11. J. Y. Tsao, in *LEDs for General Illumination Update 2002 – Full Edition*, **2002**.
12. R. Haitz, J. Y. Tsao, *Optik and Photonic*, **2011**, 6, 26.
13. G. Zorpette, *IEEE Spectr.*, **2002**, 39, 70.
14. C. J. Humphreys, *MRS Bull.*, **2008**, 33, 459.
15. Z. Xia, Q. Liu, *Prog. Mater. Sci.*, **2016**, 84, 59.
16. J. Y. Tsao, *IEEE Circuit. Dev.*, **2004**, 20, 28.
17. B. Geffroy, P. le Roy, C. Prat, *Polym. Int.*, **2006**, 55, 572.
18. R. D. Costa, E. Ortí and H. J. Bolink, *Pure Appl. Chem.*, **2011**, 83, 2115.
19. G. Kalyuzhny, M. Buda, J. Mcneill, P. Barbara and A. J. Bard, *J. Am. Chem. Soc*, **2003**, 125, 6272.

20. for example see: a) R.C. Evans, P. Douglas, C. J. Winscom, *Coord. Chem. Rev.*, **2006**, 250, 2093.
b) G. Malliaras, R. Friend, *Phys. Today*, **2005**, 14, 53. c) A. Bergh, G. Craford, A. Duggal, R. Haitz, *Phys. Today*, **2001**, 54, 42. d) E. Holder, B. M. W. Langeveld, U. S. Schubert, *Adv. Mater.*, **2005**, 17, 1109. e) Y. R. Sun, N. C. Giebink, H. Kanno, B. W. Ma, M. E. Thompson, S. R. Forrest, *Nature*, **2006**, 440, 908. f) J. Slinker, D. Bernardis, P. L. Houston, H. D. Abruña, S. Bernhard, G. G. Malliaras, *Chem. Commun.*, **2003**, 2392.
21. J. K. Borchardt, *Mater. Today*, **2004**, 7, 42.
22. M. Pope, H. P. Kallmann, P. J. Magnate, *Chem. Phys.* **1963**, 38, 2042.
23. C. W. Tang, S. A. Van Slyke, *Appl. Phys. Lett.* **1987**, 51, 913.
24. J. H. Burroughes, D. D. C. Bradley, A. R. Brown, R. N. Marks, K. Mackay, R. H. Friend, P. L. Burn, A. B. Holmes, *Nature* **1990**, 347, 539.
25. a) M. A. Baldo, D. F. O'Brien, Y. You, A. Shoustikov, S. Sibley, M. E. Thompson, S. R. Forrest, *Nature* **1998**, 395, 151; b) S. Lamansky, P. Djurovich, D. Murphy, F. Abdel-Razzaq, H.-E. Lee, C. Adachi, P. E. Burrows, S. R. Forrest, M. E. Thompson, *J. Am. Chem. Soc.* **2001**, 123, 4304.
26. a) R. C. Kwong, M. R. Nugent, L. Michalski, T. Ngo, K. Rajan, Y.-J. Tung, M.S. Weaver, T. X. Zhou, M. Hack, M. E. Thompson, S. R. Forrest, J. J. Brown, *Appl. Phys. Lett.* **2002**, 81, 162; b) M. Ikai, S. Tokito, Y. Sakamoto, T. Suzuki, Y. Taga, *Appl. Phys. Lett.* **2001**, 79, 156 ; c) C. Adachi, M. A. Baldo, M. E. Thompson, S. R. Forrest, *J. Appl. Phys.* **2001**, 90, 5048; d) F. Li, M. Zhang, G. Cheng, J. Feng, Y. Zhao, Y. G. Ma, S. Y. Lui, J. C. Shen, *Appl. Phys. Lett.* **2004**, 84, 148.
27. M. A Baldo, D. F. O'Brien, M. E. Thompson, S. R. Forrest, *Phys. Rev. B* **1999**, 60, 14422.
28. a) M. A. Baldo, S. Lamansky, P. E. Burrows, M. E. Thompson, S. R. Forrest, *Appl. Phys. Lett.* **1999**, 75, 4 ; b) C. Adachi, M. A. Baldo, S. R. Forrest, M. E. Thompson, *Appl. Phys. Lett.* **2000**, 77, 904.
29. M. Pope, H. P. Kallmann, P. J. Magnate, *Chem. Phys.* **1963**, 38, 2042.
30. Y. Chi and P.-T. Chou, *Chem. Soc. Rev.*, **2010**, 39, 638.
31. R. D. Costa, E. Ortí, H. J. Bolink, F. Monti, G. Accorsi and N. Armaroli, *Angew. Chem. Int. Ed.*, **2012**, 51, 8178.

32. G. Zhou, W. Y. Wong and X. Yang, *Chem. Asian J.*, **2011**, 6, 1706.
33. I. Omae, *Coord. Chem. Rev.*, **2016**, 310, 154.
34. C. Dragonetti, S. Righetto, D. Roberto, R. Ugo, A. Valore, S. Fantacci, A. Sgamellotti and F. De Angelis, *Chem. Commun.*, **2007**, 2, 4116.
35. V. Aubert, L. Ordronneau, M. Escadeillas, J. A. G. Williams, A. Boucekkine, E. Coulaud, C. Dragonetti, S. Righetto, D. Roberto, R. Ugo, A. Valore, A. Singh, J. Zyss, I. Ledoux-Rak, H. Le Bozec and V. Guerschais, *Inorg. Chem.*, **2011**, 50, 5027.
36. C. Dragonetti, A. Colombo, D. Marinotto, S. Righetto, D. Roberto, A. Valore, M. Escadeillas, V. Guerschais, H. Le Bozec, A. Boucekkine and C. Latouche, *J. Organomet. Chem.*, **2014**, 751, 568.
37. A. Sinopoli, C. J. Wood, E. A. Gibson and P. I. P. Elliott, *Inorg. Chim. Acta*, **2017**, 457, 81.
38. A. F. Henwood, Y. Hu, M. T. Sajjad, G. K. V. V. Thalluri, S. S. Ghosh, D. B. Cordes, A. M. Z. Slawin, I. D. W. Samuel, N. Robertson and E. Zysman-Colman, *Chem. Eur. J.*, **2015**, 21, 19128.
39. N. D. McDaniel, S. Bernhard, *Dalton Trans.*, **2010**, 39, 10021.
40. K. Teegardin, J. I. Day, J. Chan, J. Weaver, *Org. Process Res. Dev.*, **2016**, 20, 1156.
41. C. K. Prier, D. A. Rankic and D. W. C. MacMillan, *Chem. Rev.*, **2013**, 113, 5322.
42. K. K. W. Lo, *Acc. Chem. Res.*, **2015**, 48, 2985.
43. K. K.-W. Lo, K. Y. Zhang, *RSC Adv.*, **2012**, 2, 12069.
44. G.A. Crosby, *Acc. Chem. Res.*, **1975**, 8, 231.
45. A. Barbieri, G. Accorsi, N. Armaroli, *Chem. Commun.*, **2008**, 2185.
46. W. C. H. Choy, W. K. Chan and Y. Yuan, *Adv. Mater.*, **2014**, 26, 5368.
47. A. F. Henwood, E. Zysman-Colman, *Top. Curr. Chem.*, **2016**, 374, 1.
48. J. A. G. Williams, A. J. Wilkinson, V. L. Whittle, *Dalton Trans.*, **2008**, 2081.
49. C.-H. Yang, M. Mauro, F. Polo, S. Watanabe, I. Muenster, R. Fröhlich, L. De Cola, *Chem. Mater.*, **2012**, 24, 3684.

50. M. Mydlak, C. Bizzarri, D. Hartmann, W. Sarfert, G. Schmid and L. De Cola, *Adv. Funct. Mater.*, **2010**, 20, 1812.
51. P. Brulatti, R. J. Gildea, J. A. K. Howard, V. Fattori, M. Cocchi, J. A. G. Williams, *Inorg. Chem.*, **2012**, 51, 3813.
52. a) Y. You, S. Y. Park, *Dalton Trans.*, **2009**, 1267; b) M. S. Lowry, S. Bernhard, *Chem. – Eur. J.*, **2006**, 12, 7970; c) S. Lamansky, P. Djurovich, D. Murphy, F. Abdel-Razzaq, H.-E. Lee, C. Adachi, P. E. Burrows, S. R. Forrest, M. E. Thompson, *J. Am. Chem. Soc.*, **2001**, 123, 4304; d) S. Lamansky, P. Djurovich, D. Murphy, F. Abdel-Razzaq, R. Kwong, I. Tsyba, M. Bortz, B. Mui, R. Bau, M. E. Thompson, *Inorg. Chem.*, **2001**, 40, 1704.
53. C. Ulbricht, B. Beyer, C. Friebe, A. Winter, U. S. Schubert, *Adv. Mater.*, **2009**, 21, 4418.
54. K. Dedeian, J. Shi, N. Shepherd, E. Forsythe, D. C. Morton, *Inorg. Chem.* **2005**, 44, 4445.
55. A. J. Wilkinson, H. Puschmann, J. A. K. Howard, C. E. Foster, J. A. G. Williams, *Inorg. Chem.* **2006**, 43, 8685.
56. S. C. Lo, C. P. Shipley, R. N. Bera, E. Harding, A. R. Cowley, P. L. Burn, I. D. W. Samuel, *Chem. Mater.* **2006**, 18, 5119.
57. R. Ragni, E. A. Plummer, K. Brunner, J. W. Hofstraat, F. Babudri, G. F. Farinola, F. Naso, L. De Cola, *J. Mater. Chem.* **2006**, 16, 1161.
58. G. Zhou, W.-Y. Wong, B. Yao, Z. Xie, L. Wang, *Angew. Chem. Int. Ed.* **2007**, 46, 1149.
59. G. Zhou, C.-L. Ho, W.-Y. Wong, Q. Wang, D. Ma, X. Jing, F. Wang, Z. Lin, T. B. Marder, A. Beeby, *Adv. Funct. Mater.* **2008**, 18, 499.
60. H. J. Bolink, E. Coronado, S. G. Santamaria, M. Sessolo, N. Evans, C. Klein, E. Baranoff, K. Kalyanasundaram, M. Graätzel, M. K. Nazeeruddin, *Chem. Commun.* **2007**, 3276.
61. E. Orselli, G. S. Kottas, A. E. Konradsson, P. Coppo, R. Frohlich, L. De Cola, A. van Dijken, M. Büchel, H. Bönner, *Inorg. Chem.* **2007**, 46, 11082.
62. C.-J. Chang, C.-H. Yang, K. Chen, Y. Chi, C.-F. Shu, M.-L. Ho, Y.-S. Yeh, P.-T. Chou, *Dalton Trans.* **2007**, 1881.
63. B. X. Mi, P. F. Wang, Z. Q. Gao, C. S. Lee, S. T. Lee, H. L. Hong, X. M. Chen, M. S. Wong, P. F. Xia, K. W. Cheah, C. H. Chen, W. Hunag, *Adv. Mater.* **2009**, 21, 339.

64. B. Tong, Q. Mei, S. Wang, Y. Fang, Y. Meng, B. Wang, *J. Mater. Chem.* **2008**, 18, 1636.
- 65 a) J.-S. Lu, H.-F. Chen, J.-C. Kuo, R. Sun, C.-Y. Cheng, Y.-S. Yeh, H.-C. Su, K.-T. Wong, *J. Mater. Chem. C*, **2015**, 3, 2802; b) J. Qiao, L. Duan, L. Tang, L. He, L. Wang, Y. Qiu, *J. Mater. Chem.*, **2009**, 19, 6573.
66. a) A. F. Henwood, S. Evariste, A. M. Z. Slawin and E. Zysman-Colman, *Faraday Discuss.*, **2014**, 174, 165; b) S.-J. Yun, H.-J. Seo, M. Song, S.-H. Jin and Y. I. Kim, *Bull. Korean Chem. Soc.*, **2012**, 33, 3645.
- 67 S. B. Meier, W. Sarfert, J. M. Junquera-Hernández, M. Delgado, D. Tordera, E. Ortí, H. J. Bolink, F. Kessler, R. Scopelliti, M. Grätzel, M. K. Nazeeruddin, E. Baranoff, *J. Mater. Chem. C*, **2013**, 1, 58.
68. a) E. Orselli, G. S. Kottas, A. E. Konradsson, P. Coppo, R. Fröhlich, L. De Cola, A. van Dijken, M. Büchel, H. Börner, *Inorg. Chem.*, **2007**, 46, 11082; b) J. M. Fernandez-Hernandez, S. Ladouceur, Y. Shen, A. Iordache, X. Wang, L. Donato, S. Gallagher-Duval, M. de Anda Villa, J. D. Slinker, L. De Cola, E. Zysman-Colman, *J. Mater. Chem. C*, **2013**, 1, 7440.
69. X. Yang, X. Xu, G. Zhou, *J. Mater. Chem. C* **2015**, 3, 913.
- 70 E. Baranoff, B. F. E. Curchod, *Dalton Trans.* **2015**, 44, 8318.
- 71 V. Sivasubramaniam, F. Brodkorb, S. Hanning, H. P. Loeb, V. van Elsbergen, H. Boerner, U. Scherf, M. Kreyenschmidt, *J. Fluorine Chem.* **2009**, 130, 640.
72. A. K. Pal, A. F. Henwood, D. B. Cordes, A. M. Z. Slawin, I. D. W. Samuel, E. Zysman-Colman, *Inorg Chem*, **2017**, 56, 7533.
73. a) P.-T. Chou, Y. Chi, M.-W. Chung, C.-C. Lin, *Coord. Chem. Rev.* **2011**, 255, 2653; b) H. Fu, Y.-M. Cheng, P.-T. Chou, Y. Chi, *Mater. Today* **2011**, 14, 472; c) Y. You, W. Nam, *Chem. Soc. Rev.* **2012**, 41, 7061; d) D. Jacquemin, D. Escudero, *Chem Sci* **2017**, 8, 7844.
74. Y. Im, S. Y. Byun, J. H. Kim, D. R. Lee, C. S. Oh, K. S. Yook, J. Y. Lee, *Adv. Funct. Mater.* **2017**, 27.
75. H. H. Kuo, Y. T. Chen, L. R. Devereux, C. C. Wu, M. A. Fox, C. Y. Kuei, Y. Chi, G. H. Lee, *Adv Mater* **2017**, 29.
76. a) R. J. Holmes, S. R. Forrest, T. Sajoto, A. Tamayo, P. I. Djurovich, M. E. Thompson, J. Brooks, Y.-J. Tung, B. W. D'Andrade, M. S. Weaver, R. C. Kwong, J. J. Brown, *Appl. Phys.*

- Lett.* **2005**, 87, 243507; b) J. Lee, H.-F. Chen, T. Batagoda, C. Coburn, P. I. Djurovich, M. E. Thompson, S. R. Forrest, *Nat Mater* **2016**, 15, 92.
77. a) U. Kazuo, S. Hisahiro, C. Cao, K. Junji, *Advanced Materials* **2014**, 26, 5062; b) C. H. Hsieh, F. I. Wu, C. H. Fan, M. J. Huang, K. Y. Lu, P. Y. Chou, Y. H. Yang, S. H. Wu, I. C. Chen, S. H. Chou, K. T. Wong, C. H. Cheng, *Chemistry* **2011**, 17, 9180; c) J. Zhuang, W. Li, W. Wu, M. Song, W. Su, M. Zhou, Z. Cui, *New J. Chem.* **2015**, 39, 246; d) U. Kazuo, S. Hisahiro, I. Fumiaki, K. Junji, *Advanced Optical Materials* **2016**, 4, 86.
78. M. Elie, J. L. Renaud, S. Gaillard, *Polyhedron* **2018**, 140, 158.
79. J. Zhuang, W. Li, W. Su, Y. Liu, Q. Shen, L. Liao, M. Zhou, *Organic Electronics* **2013**, 14, 2596.
80. a) T. Sajoto, P. I. Djurovich, A. Tamayo, M. Yousufuddin, R. Bau, M. E. Thompson, R. J. Holmes, S. R. Forrest, *Inorganic Chemistry* **2005**, 44, 7992; b) H. Stephan, D. C. Enrico, F. Jochen, L. J. M., L. Christian, E. Peter, F. Evelyn, M. Oliver, M. Ingo, S. Christian, W. Gerhard, *Adv. Mater.* **2008**, 20, 3325.
81. a) H. Sasabe, J. Takamatsu, T. Motoyama, S. Watanabe, G. Wagenblast, N. Langer, O. Molt, E. Fuchs, C. Lennartz, J. Kido, *Adv Mater.* **2010**, 22, 5003; b) Y. Cheng-Han, C. Yi-Ming, C. Yun, H. Chia-Jung, F. Fu-Chuan, W. Ken-Tsung, C. Pi-Tai, C. Chih-Hao, T. Ming-Han, W. Chung-Chih, *Angew. Chem. Int. Ed.* **2007**, 46, 2418; c) K. Y. Lu, H. H. Chou, C. H. Hsieh, Y. H. Yang, H. R. Tsai, H. Y. Tsai, L. C. Hsu, C. Y. Chen, I. C. Chen, C. H. Cheng, *Adv Mater*, **2011**, 23, 4933.
82. **High Efficiency Deep Blue-Emitting Organic Light Emitting Diodes based on Iridium(III) Carbene Complexes.** A. K. Pal, S. Krotkus, M. Fontani, C. F. R. Mackenzie, D. B. Cordes, A. M. Slawin, I. D. W. Samuel, E. Zysman-Colman, *Adv. Mater*, **2018**, 1804231, DOI: 10.1002/adma.201804231.
83. Z. Chen, L. Wang, S. Su, X. Zheng, N. Zhu, C. L. Ho, S. Chen, W. Y. Wong, *ACS Appl Mater Interfaces*, **2017**, 9, 40497.
84. V. V. Pavlishchuk, A. W. Addison, *Inorg. Chim. Acta*, **2000**, 298, 97.
85. S. Admassie, O. Inganäs, W. Mammo, E. Perzon, M. R. Andersson, *Synthetic Metals*, **2006**, 156, 614.

86. N. G. Connelly, W. E. Geiger, *Chemical Reviews* **1996**, 96, 877.
87. C. Hansch, A. Leo, R. W. Taft, *Chem. Rev.* **1991**, 91, 165.
88. W. H. Melhuish, *J. Phys. Chem.* **1961**, 65, 229.
89. a) C. Han, Y. Zhao, H. Xu, J. Chen, Z. Deng, D. Ma, Q. Li, P. Yan, *Chem. Eur. J.* **2011**, 17, 5800; b) Q. Zhang, B. Li, S. Huang, H. Nomura, H. Tanaka, C. Adachi, *Nature Photonics*, **2014**, 8, 326.
90. G. J. Hedley, A. Ruseckas, I. D. W. Samuel, *Chem. Phys. Lett.* **2008**, 450, 292.
91. T. Sajoto, P. I. Djurovich, A. B. Tamayo, J. Oxgaard, W. A. Goddard, M. E. Thompson, *Journal of the American Chemical Society*, **2009**, 131, 9813.
92. a) M.-H. Tsai, T.-H. Ke, H.-W. Lin, C.-C. Wu, S.-F. Chiu, F.-C. Fang, Y.-L. Liao, K.-T. Wong, Y.-H. Chen, C.-I. Wu, *ACS Applied Materials & Interfaces* **2009**, 1, 567; b) M. H. Tsai, H. W. Lin, H. C. Su, T. H. Ke, C. c. Wu, F. C. Fang, Y. L. Liao, K. T. Wong, C. I. Wu, *Adv. Mater.* **2006**, 18, 1216.
93. Hossein Zamani Siboni, Y. Luo, H. Aziz, *J. Appl. Phys.* **2011**, 109, 044501.
94. F. Tyler, L. Guijie, W. Lele, L. Jian, *Adv. Mater.* **2014**, 26, 7116.
95. C.-Y. Chan, L.-S. Cui, J. U. Kim, H. Nakanotani, C. Adachi, *Adv. Funct. Mater.* **2018**, 28, 1706023.
96. T. Sajoto, P.I. Djurovich, A.B. Tamayo, J. Oxgaard, W.A. Goddard, M.E. Thompson, *J. Am. Chem. Soc.*, **2009**, 131, 9812.
97. P. Agostinis, et al. *CA: A Cancer J. Clin.* **2011**, 61, 250.
98. S.J.A. Pope, et al *RSC Adv* **2013**, 3, 25550.
99. H.L. Anderson, et al. *Angew. Chem. Int. Ed* **2009**, 48, 3244.
100. G. Gasser, et al, *Chem. Sci.* **2015**, 6, 2660.

101. S.J. Lippard, et al. *J. Inorg. Biochem.* **2012**, *110*, 58.
102. N.J. Wheate, et al. *Dalton Trans.* **2010**, *39*, 8113.
103. M.B. Baile, et al. *Int. J. Pharm. R.R.* **2015**, *4*, 59.
104. X. Wang, et al. *Acc. Chem. Res.* **2015**, *48*, 2622.
105. a) B.B. Aggarwal, B. Sung, *Trends Pharmacol. Sci.* **2009**, *30*, 85–94. b) P. Rinwa, B. Kaur, A.S. Jaggi, N. Singh, *Naunyn Schmiedeberg's Arch. Pharmacol.* **2010**, *381*, 529–539. c) R.A. Sharma, A.J. Gescher, W.P. Steward, *Eur. J. Cancer* **2005**, *41*, 1955.
106. a) A. Goel, A.B. Kunnumakkara, B.B. Aggarwal, *Biochem. Pharmacol.* **2008**, *75*, 787–809. b) H. Zhou, C.S. Beevers, S. Huang, *Curr. Drug Targets* **2011**, *12*, 332.
107. A.L. Cheng, C.H. Hsu, J.K. Lin, M.M. Hsu, Y.F. Ho, T.S. Shen, J.Y. Ko, J.T. Lin, B.R. Lin, W. Ming-Shiang, H.S. Yu, S.H. Jee, G.S. Chen, T.M. Chen, C.A. Chen, M.K. Lai, Y.S. Pu, M.H. Pan, Y.J. Wang, C.C. Tsai, C.Y. Hsieh, *Anticancer Res.* **2001**, *21*, 2895.
108. a) S. Banerjee, A.R. Chakravarty, *Acc. Chem. Res.* **2015**, *48*, 2075 and references therein; b) A.K. Renfrew, N.S. Bryce, T.W. Hambley, *Chem. Sci.* **2013**, *4*, 3731.
109. a) R.A. Sharma, W.P. Steward, A.J. Gescher, *Adv. Exp. Med. Biol.* **2007**, *595*, 453; b) P. Anand, A.B. Kunnumakkara, R.A. Newman, B.B. Aggarwal, *Mol. Pharmaceutics*, **2007**, *4*, 807.
110. F. Kuhlwein, K. Polborn, W. Beck, *Anorg. Allg. Chem.* **1997**, *623*, 1211.
111. a) C. Ireson, S. Orr, D.J. Jones, R. Verschoyle, C.K. Lim, J.L. Luo, L. Howells, S. Plummer, R. Jukes, M. Williams, W.P. Steward, A. Gescher, *Cancer Res.* **2001**, *61*, 1058. b) M.H. Pan, T.M. Huang, J.K. Lin, *Drug Metab. Dispos.* **1999**, *27*, 486.
112. N. Kang, M.-M. Wang, Y.-H. Wang, Z.-N. Zhang, H.-R. Cao, Y.-H. Lv, Y. Yang, P.-H. Fan, F. Qiu, X.-M. Gao, *Food Chem Toxicol.* **2014**, *67*, 193.
113. K. I. Priyadarsini, *J. Photochem. Photobiol. C: Photochem. Rev.* **2009**, *10*, 81.
114. a) L. K. McKenzie, I. V. Sazanovich, E. Baggaley, M. Bonneau, V. Guerchais, J. A. G. Williams, J. A. Weinstein, H. E. Bryant, *Chem. Eur. J.* **2017**, *23*, 234; b) L. K. McKenzie, H. E. Bryant, J. A. Weinstein, *Coord. Chem. Rev.* **2018**, DOI: 10.1016/j.ccr.2018.03.020

115. I. P. Djurovich, D. Murphy, M. E. Thompson, B. Hernandez, R. Gao, P. L. Hunt, M. Selke, *Dalton Trans.* **2007**, 3763.
116. a) C. Dragonetti, L. Falciola, P. Mussini, S. Righetto, D. Roberto, R. Ugo, A. Valore, F. De Angelis, S. Fantacci, A. Sgamellotti, M. Ramon, M. Muccini, *Inorg. Chem.* **2007**, *46*, 8533; b) C. Dragonetti, S. Righetto, D. Roberto, R. Ugo, A. Valore, F. Demartin, F. De Angelis, A. Sgamellotti, S. Fantacci, *Inorg. Chim. Acta* **2008**, *361*, 4070; c) E. Margapoti, V. Shukla, A. Valore, A. Sharma, C. Dragonetti, C.C. Kitts, D. Roberto, M. Murgia, R. Ugo, M. Muccini, *J. Phys. Chem. C* **2009**, *113*, 12517; d) E. Margapoti, M. Muccini, A. Sharma, A. Colombo, C. Dragonetti, D. Roberto, A. Valore, *Dalton Trans.* **2012**, *41*, 9227; e) A. Colombo, F. Fiorini, D. Septiadi, C. Dragonetti, F. Nisic, A. Valore, D. Roberto, M. Mauro, L. De Cola, *Dalton Trans.* **2015**, *44*, 8478.
117. T. Huang, Q. Yu, S. Liu, W. Huang, Q. Zhao, *Dalton Trans.* **2018**, *47*, 7628.
118. S. Lamansky, P. Djurovich, D. Murphy, F. Abdel-Razzaq, R. Kwong, I. Tsyba, M. Bortz, B. Mui, R. Bau, M.E. Thompson, *Inorg. Chem.* **2001**, *40*, 1704.
119. A. Colombo, C. Dragonetti, D. Roberto, A. Valore, C. Ferrante, I. Fortunati, A. L. Picone, F. Todescato, J.A.G. Williams, *Dalton Trans.* **2015**, *44*, 15712.
120. V. Aubert, L. Ordronneau, M. Escadeillas, J.A.G. Williams, A. Boucekkine, E. Coulaud, C. Dragonetti, S. Righetto, D. Roberto, R. Ugo, A. Valore, A. Singh, J. Zyss, I. Ledoux-Rak, H. Le Bozec, V. Guerschais, *Inorg. Chem.*, **2011**, *50*, 5027.
121. a) S. Lamansky, P. Djurovich, D. Murphy, F. Abdel-Razzaq, H.E. Lee, C. Adachi, P.E. Burrows, S.R. Forrest, M.E. Thompson, *J. Am. Chem. Soc.*, **2001**, *123*, 4304; b) Q. Zhao, L. Fi, F. Li, M. Yu, Z. Liu, T. Yi, C. Huang, *Chem. Commun.* **2008**, 685.
122. M. Spencer, A. Santoro, G.R. Freeman, A. Díez, P.R. Murray, J. Torroba, A.C. Whitwood, L.J. Yellowlees, J.A.G. Williams, D. W. Bruce, *Dalton Trans.*, **2012**, *41*, 14244.
123. A. Castellan, R. Ruggiero, L.G. da Silva, E. Portes, S. Grelier, C. Gardrat, *J. PhotoChem. PhotoBiol. A* **2007**, *190*, 110.
124. D. L. Rochester, S. Develay, S. Zális, J. A. G. Williams, *Dalton Trans.*, **2009**, 1728.

125. **A highly luminescent tetrahydrocurcumin Ir(III) complex with remarkable photoactivated anticancer activity.** A. Colombo, M. Fontani, C. Dragonetti, D. Roberto, J. A. G. Williams, R. Scotto di Perrotolo, F. Casagrande, S. Barozzi, S. Polo, Submitted to *Chem. Eur. J.*

III. EXPERIMENTAL SECTION.

All complexes, except **58** and **59**, synthesized in St. Andrews, were prepared in Milan.

3.1. General comments.

Solvents and Reagents

- *Compounds synthesized in Milan*

All the reagents and solvents have been bought from the Sigma-Aldrich company. All reactions were carried out using standard Schlenk techniques under an inert (N₂ or Ar) atmosphere. Purification and handling of all compounds were carried out under air. Column chromatography was performed using silica gel (Silica-P from Silicycle, 60 Å, 40-63 μm).

- *Compounds synthesized in St. Andrews*

Commercial chemicals were used as supplied. All reactions were carried out using standard Schlenk techniques under an inert (N₂) atmosphere. Purification and handling of all compounds were carried out under air. All products were stored in the dark. Anhydrous toluene was obtained from a Pure Solv™ solvent purification system (Innovative Technologies). Chromatography was performed on columns with an i.d. of 25–30 mm on silica gel (Geduran® Silicagel 60, 40–63 μm; Merck). The progress of reactions and the elution of products were followed by TLC (silica gel on aluminum sheets, SiliaPlate™ TLC Plates, Silicycle, 250 μm with indicator F-254).

Nuclear Magnetic Resonance

- *Compounds synthesized in Milan*

¹H-NMR spectra have been recorded using Bruker Avance DRX instruments at the frequencies 300 MHz, 400 MHz or 600 MHz; ¹³C-NMR spectra have been recorded with the same instruments at the frequencies 75.468 MHz, 100.613 MHz or 150.903 MHz. Chemical shifts are given in ppm (part per million) and relative to the residual solvent peaks (CHCl₃ or CH₂Cl₂) for ¹H- and ¹³C-NMR.

- *Compounds synthesized in St. Andrews*

¹H-, ¹³C- and ¹⁹F- NMR spectra were recorded with Bruker AVANCE II spectrometer (500 MHz for ¹H; 125 MHz for ¹³C; 470 MHz for ¹⁹F).

Melting points

Melting points (Mp) were recorded using open-end capillaries on an Electrothermal melting point apparatus IA9200 and are uncorrected. The heating rate was 0.5 or 1.0 °C/min.

Elemental analysis and mass spectroscopy

- *Compounds synthesized in Milan*

Mass spectra were obtained with a FT-ICR Mass Spectrometer APEX II & Xmass software (Cruker Daltonics) - 4.7 Magnet and Autospec Fission Spectrometer (Fast Atom Bombardment - FAB - ionisation).

- *Compounds synthesized in St. Andrews*

High resolution mass spectra were recorded by EPSRC National Mass Spectrometry Service Centre, Swansea University. Elemental analyses were performed by Mr. Stephen Boyer, London Metropolitan University.

UV-Vis Absorption

- *Compounds synthesized in Milan*

UV-Vis absorption spectra were recorded in pure CH₂Cl₂ with JASCO V530 spectrometer at room temperature, using quartz cuvettes with an optical path of 1 cm., against a reference of pure CH₂Cl₂ contained within a matched cuvette. Molar absorptivity determination was verified by linear leastsquares fit of values obtained from independent solutions at varying concentrations ranging from 10⁻⁴ to 10⁻⁵ M.

- *Compounds synthesized in St. Andrews*

All samples were prepared in HPLC grade solvent with varying concentrations on the order of μM. Absorption spectra were recorded at RT using a Shimadzu UV-1800 double beam spectrophotometer. Molar absorptivity determination was verified by linear leastsquares fit of values obtained from at least five independent solutions at varying concentrations with absorbance ranging from 6.88 × 10⁻¹ to 3.19 × 10² μM.

Photophysical measurements

- *Compounds synthesized in Milan*

Luminescence spectra in solution were recorded using a FluoroMax-2 spectrofluorimeter equipped with an R928 photomultiplier tube. Quantum yields were determined using as standard a solution of quinine sulfate in 1M H₂SO₄ (aq) ($\Phi = 0.548$). The luminescence lifetimes were measured by time-correlated single-photon counting, following excitation with a pulsed laser diode at 374 nm. The emitted light was detected at 90° using a Peltier-cooled R928 photomultiplier tube after passage through a monochromator.

- *Compounds synthesized in St. Andrews*

The sample solutions for the room temperature emission measurements were prepared in HPLC grade dichloromethane and degassed using three freeze-pump-thaw cycles using an in-house designed quartz cuvette. Steady-state and time-resolved emission spectra were recorded at room temperature using a Gilden fluoroSENS fluorimeter. The samples were excited at the absorption maxima of the dominant low-energy mixed CT band as indicated in Table 3 (see par. 2.4.2. Chapter 2). Excited state lifetimes were measured by time correlated single photon counting (TCSPC) using an Edinburgh Instruments FLS980 fluorimeter using a pulsed diode laser (exciting at 378 nm) and PL emission was detected at the corresponding steadystate emission maximum for each complex. The PL decays were fitted to a single exponential decay function. In the case of multi-exponential fit the normalized pre-exponential factors are quoted. Emission quantum yields were determined using the optically dilute method.¹ The equation $\Phi_s = \Phi_r(A_r/A_s)(I_s/I_r)(n_s/n_r)^2$ was used to calculate the relative quantum yield, where Φ_r is the absolute quantum yield of the reference, n is the refractive index of the solvent, A is the absorbance at the excitation wavelength, and I is the integrated area under the corrected emission curve. The subscripts s and r refer to the sample and reference, respectively. An aerated solution of quinine sulfate in 0.5M H₂SO₄ ($\Phi_r = 0.546$) was used as the external reference.² Thin film PLQY measurements were performed using an integrating sphere in a Hamamatsu C9920-02 system.³ Samples were excited by a xenon lamp coupled to a monochromator, which enabled selectivity of the excitation wavelength, chosen here to be 330 nm. The output was then fed into the integrating sphere via a fiber, exciting the sample. PL was collected with a multimode fibre and detected with a back-thinned CCD. The thin film PLQY were then measured in N₂ filled sphere. Time-resolved PL measurements related to device fabrication were carried out using the time-correlated single-photon counting technique. The samples

were excited at 390 nm by a pulsed laser diode (Picoquant, model PLS 370) giving 10 pJ per pulse at a repetition rate of 20 kHz and were kept in a vacuum of $< 8 \times 10^{-4}$ mbar.

Electrochemistry measurements

Cyclic voltammetry (CV) measurements were carried out at room temperature with an electrochemical analyzer potentiostat model 620E from CH Instruments at a sweep rate of 100 mV/s. Differential pulse voltammetry (DPV) was conducted with an increment potential of 0.004 V and a pulse amplitude, width, and period of 50 mV, 0.05, and 0.5 s, respectively. Solutions for CV and DPV were prepared in MeCN and degassed with MeCN-saturated N₂ bubbling for about 10 min prior to scanning. Tetra(*n*-butyl)ammonium hexafluorophosphate (TBAPF₆; *ca.* 0.1 M in MeCN) was used as the supporting electrolyte. A silver wire was used as the pseudoreference electrode; a glassy-carbon electrode was used for the working electrode and a Pt wire was used as the counter S-4 electrode. The redox potentials are reported relative to a standard calomel electrode (SCE) electrode with a ferrocenium/ferrocene (Fc⁺/Fc) redox couple as an internal reference (0.38 V vs SCE).⁴ Experimental uncertainties are as follows: absorption maxima, ± 2 nm; molar absorption coefficient, 10%; redox potentials, ± 10 mV; emission maxima, ± 3 nm; emission lifetimes, $\pm 10\%$; luminescence quantum yields, $\pm 10\%$.

EFISH measurements

EFISH measurements⁵ were carried out at the Dipartimento di Chimica of the Università degli Studi di Milano in DMF solutions at a concentration of 10^{-4} M or 10^{-3} M, with a non-resonant incident wavelength of 1.907 μm , obtained by Raman-shifting the fundamental 1.064 μm wavelength produced by a Q-switched, mode-locked Nd³⁺:YAG laser manufactured by Atalaser. The apparatus used for EFISH measurements is a prototype made by SOPRA (France). The $\mu\beta_{\text{EFISH}}$ values reported are the mean values of 16 measurements performed on the same sample. The sign of $\mu\beta$ is determined by comparison with the solvent (DMF).

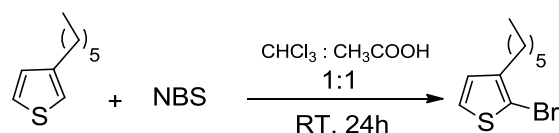
Thin films of the complexes (**25**, **27**, **56**, **58** or **59**) dispersed in polymethylmethacrylate (PMMA) or polystyrene were prepared by spin coating a few drops of a dichloromethane solution (complex/PMMA or polystyrene = 4-6 wt %, while PMMA or polystyrene = 10 wt % with respect to the solvent) on a glass substrate (thickness 1 mm) previously cleaned with water/acetone. Parameters of spinning (RPM = revolutions per minute): RPM 1 = 700; Ramp 1 = 1 s, Time 1 = 5 s; RPM 2 = 1000; Ramp 2 = 5 s, Time 2 = 10 s; RPM 3 = 1000; Ramp 3 = 1 s, Time 3 = 10 s.

Second Harmonic Generation (SHG) experiments were performed using a Q-switched Nd:YAG (Quanta System Giant G790-20) laser at 1.064 nm wavelength with a pulse of 7 ns and 20 Hz repetition rate. For poling measurements, the fundamental beam (0.55 mJ for pulse) was polarized in the plane of incidence (p-polarized) and focused with a lens ($f = 600$ mm) on the sample with an angle of about 55° in order to optimize the SHG signal. The sample was placed over the hot stage whose temperature was controlled by a GEFran 800, while the coronawire voltage was applied by a TREK610E high-voltage-supply. Rejection of the fundamental beam was performed by an interference filter and a glass cut-off filter, and the p-polarized SHG signal at 532 nm was detected with a UV-Vis Hamamatsu C3830 photomultiplier tube. The corona poling process was carried out at 9.5 kV while increasing the temperature at a rate of $2.3^\circ\text{C min}^{-1}$ up to 65°C inside a specially built dry box, in N_2 atmosphere. The temperature was maintained at 65°C for 2 h and then decreased to room temperature. The setup for Maker fringe measurements was similar to the previous except that the fundamental beam was attenuated to 1 mJ for pulse and the sample was placed over a rotation stage.

3.2. Synthesis of complexes

3.2.2. Synthesis of compounds 23 and 24.

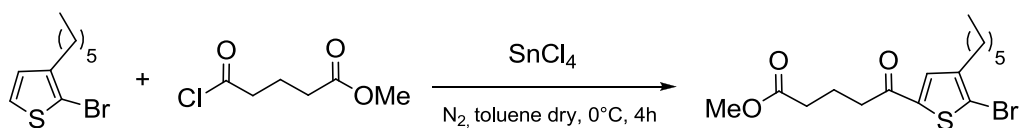
➤ *Synthesis of the 2-bromo-3-ethylthiophene intermediate*



At room temperature the 3-hexylthiophene (300 mg, 1.78 mmol) is solubilized in a solution 1:1 of chloroform and acetic acid (5.4 mL). The reaction is placed in dark and *N*-bromosuccinimide (317 mg, 1.78 mmol) is added in portions. The reaction is left under stirring for 24h. A saturated solution of NaHCO_3 is added until neutral pH and an extraction with DCM is performed. The organic phase is washed with water, dried with Na_2SO_4 and solvent is removed under reduced pressure. The yield is quantitative (94 %).

$^1\text{H NMR}$ (400 MHz, CDCl_3): δ (ppm) 7.22 (d, $J = 5.5$ Hz, 1H), 6.84 (d, $J = 5.5$ Hz, 1H), 2.63 (m, 2H), 1.65 (bs, 2H), 1.39 (s, 6H), 0.96 (m, 3H).

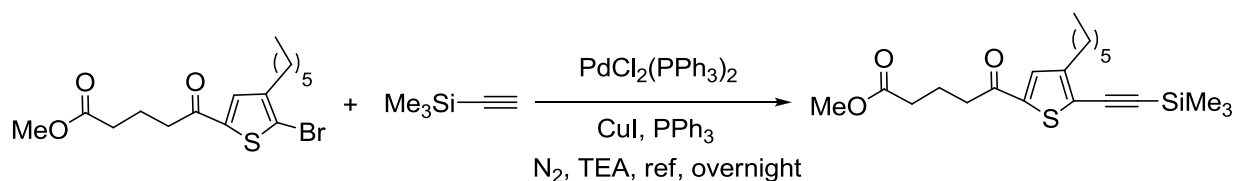
➤ *Synthesis of the methyl 5-(5-bromo-4-hexylthiophen-2-yl)-5-oxopentanoate intermediate*



This intermediate was synthesized via Friedel-Craft acylation. At room temperature and under N₂ atmosphere the 2-bromo-3-hexylthiophene (524 mg, 2.12 mmol) is solubilized in dry toluene (3.6 mL). The solution is cooled down at 0°C and, slowly, glutaric acid monomethyl ester chloride (293 μL, 2.12 mmol) and SnCl₄ (248 μL, 2.12 mmol) are added. The reaction is left under stirring at 0°C for 4h. The solution is diluted with EtOAc and washed with water. The organic layer is dried over Na₂SO₄ and the solvent is removed under reduced pressure. The crude product is purified by flash chromatography on silica gel, using hexane/EtOAc 8/2 as eluent, to give the desired product. Yield 88%.

¹H NMR (400 MHz, CDCl₃): δ (ppm) 7.32 (s, 1H), 3.56 (s, 3H), 2.80 (t, *J* = 8.1 Hz, 2H), 2.45 (t, *J* = 8.1 Hz, 2H), 2.31 (t, *J* = 8.1 Hz, 2H), 1.92 (t, *J* = 8.9 Hz, 2H), 1.48 (t, *J* = 8.9 Hz, 2H), 1.21 (s, 6H), 0.78 (s, 3H).

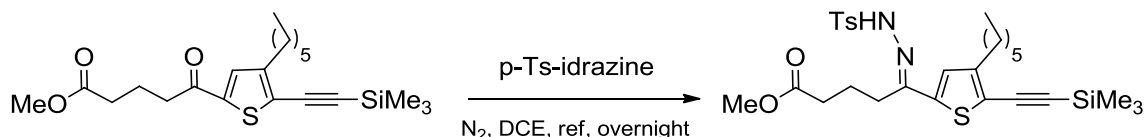
➤ *Synthesis of the methyl 5-(4-ethyl-5-((trimethylsilyl)ethynyl)thiophen-2-yl)-5-oxopentanoate intermediate*



This intermediate was synthesized via Sonogashira's coupling.⁷ Under N₂ atmosphere is prepared a solution of the previous intermediate (232.5 mg, 0.57 mmol), the ethynyltrimethylsilane (121.5 μL, 0.86 mmol), the PdCl₂(PPh₃)₂ (24 mg, 0.03 mmol), the CuI (3.3 mg, 0.02 mmol) and the PPh₃ (4.5 mg, 0.02 mmol) in TEA (6 mL). Then the mixture is refluxed overnight (70°C). After cooling to room temperature, the solvent is evaporated at reduced pressure, the residue is diluted with DCM and washed with water. The organic layer is dried over Na₂SO₄ and the solvent is removed under reduced pressure. The crude product is purified by flash chromatography on silica gel, using hexane/EtOAc 9/1 as eluent, to give the desired product. Yield 81 %.

¹H NMR (400 MHz, CDCl₃): δ (ppm) 7.45 (s, 1H), 3.69 (s, 3H), 2.94 (t, *J* = 8.3 Hz, 2H), 2.67 (t, *J* = 8.3 Hz, 2H), 2.44 (t, *J* = 8.3 Hz, 2H), 2.06 (t, *J* = 8.3 Hz, 2H), 1.63 (t, *J* = 8.4 Hz, 2H), 1.32 (s, 6H), 0.92 (s, 3H), 0.28 (s, 9H).

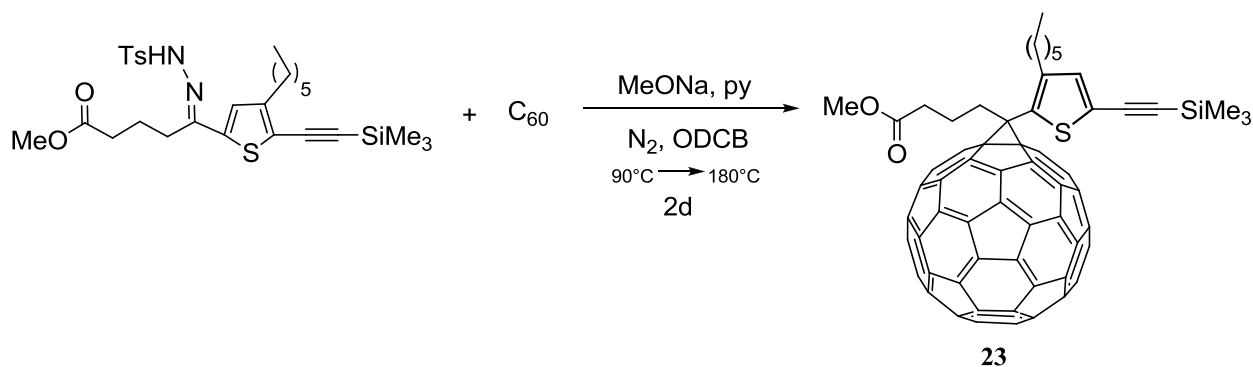
➤ *Synthesis of the methyl 5-(4-hexyl-5-((trimethylsilyl)ethynyl)thiophen-2-yl)-5-(2-tosylhydrazono)pentanoate intermediate*



Under N_2 atmosphere is prepared a solution of the previous intermediate (100 mg, 0.25 mmol) and *p*-Ts-hydrazine (57 mg, 0.31 mmol) in DCE. The mixture is refluxed overnight (83°C). After cooling to room temperature, the solvent is evaporated at reduced pressure, the residue is diluted with EtOAc and washed with water. The organic layer is dried over Na_2SO_4 and the solvent is removed under reduced pressure. The crude product is purified by flash chromatography on silica gel, using hexane/EtOAc 7/3 as eluent, to give the desired product. Yield 76 %.

^1H NMR (400 MHz, CDCl_3): δ (ppm) 9.06 (s, 1H), 7.90 (d, $J = 8.2$ Hz, 2H), 7.32 (d, $J = 8.2$ Hz, 2H), 6.90 (s, 1H), 3.79 (s, 3H), 2.59 (m, 2H), 2.42 (m, 2H), 2.32 (d, $J = 4.5$ Hz, 2H), 1.73 (t, $J = 5.7$ Hz, 2H), 1.59 (t, $J = 7.2$ Hz, 2H), 1.30 (s, 6H), 0.90 (m, 6H), 0.27 (s, 9H).

➤ *Synthesis of compound 23*

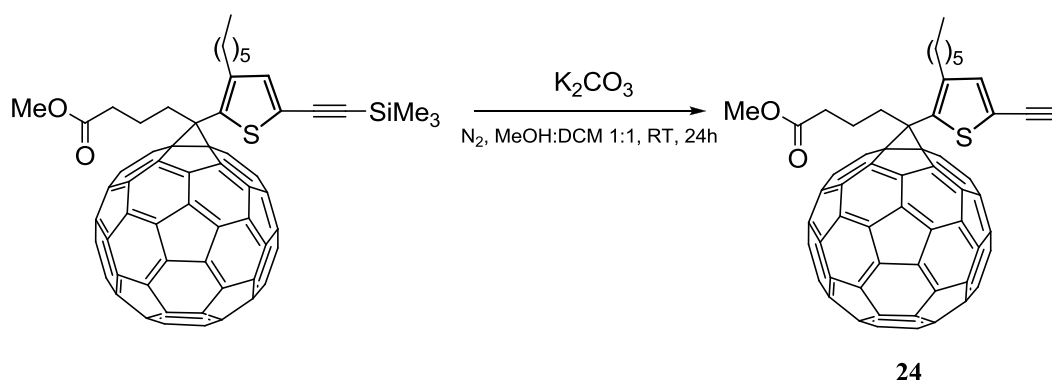


Under N_2 atmosphere is prepared a solution of the tosylhydrazone derivative (376.6 mg, 0.67 mmol), MeONa (36.2 mg, 0.67 mmol), and dry pyridine (6.7 mL). The mixture is left under stirring at room temperature for 30 min. Then a solution of C_{60} -fullerene (396 mg, 0.55 mmol) in *o*-dichlorobenzene (39 mL) is added, and the homogeneous reaction mixture is stirred at 80°C under N_2 atmosphere overnight. Then the mixture is refluxed for 24 h (180°C), after cooling to

room temperature the solvent is evaporated at reduced pressure, and the residue is purified by flash chromatography on silica gel with toluene/hexane 1/1 as eluent, to give the desired product. Yield 50%.

$^1\text{H-NMR}$ (400 MHz, CDCl_3): δ (ppm) 7.23 (s, 1H), 3.71 (s, 3H), 2.94 (t, $J = 7.7$ Hz, 2H), 2.79 (t, $J = 7.4$ Hz, 2H), 2.59 (t, $J = 7.4$ Hz, 2H), 2.25 (m, 2H), 1.70 (t, $J = 7.0$ Hz, 2H), 1.34 (bm, 6H), 0.90 (d, $J = 7.0$ Hz, 3H), 0.30 (s, 9H).

➤ *Synthesis of compound 24*



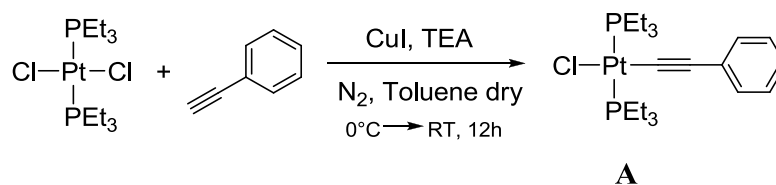
Under N_2 atmosphere a solution of the fullerenic substrate (282.6 mg, 0.26 mmol) in dry MeOH/ dry DCM 1/1 is prepared. Then K_2CO_3 is added (142.7 mg, 1.03 mmol); the mixture is left under stirring at room temperature for 24h. The solvent is evaporated at reduced pressure, the residue is diluted with DCM and washed with water. The organic layer is dried over Na_2SO_4 and the solvent is removed under reduced pressure. The crude product is purified by flash chromatography on silica gel, using hexane/toluene 1/1 as eluent, to give the desired product. Yield 59%.

$^1\text{H-NMR}$ (400 MHz, CDCl_3): δ (ppm) 7.25 (s, 1H), 3.72 (s, 3H), 3.69 (s, 1H), 2.95 (t, $J = 7.7$ Hz, 2H), 2.81 (t, $J = 7.4$ Hz, 2H), 2.60 (t, $J = 7.4$ Hz, 2H), 2.28 (m, 2H), 1.71 (t, $J = 6.7$ Hz, 2H), 1.33 (bm, 6H), 0.89 (bm, 3H).

3.2.3. Synthesis of complexes 25, 26 and 27.

3.2.3.1. Synthesis of complex 25.

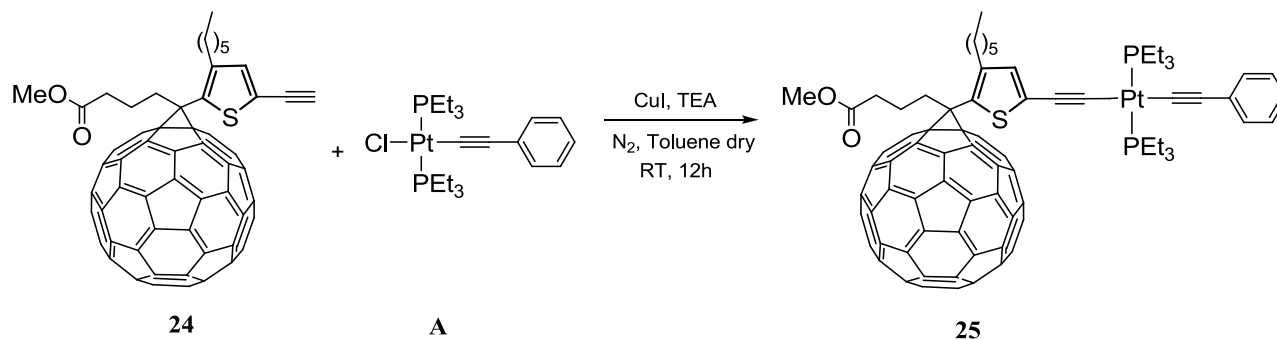
➤ *Synthesis of the Pt complex A*



Under N_2 atmosphere a solution of *trans*-Pt-dichloro-bis(triethylphosphine) complex (150 mg, 0.3mmol) in dry toluene is prepared. Then CuI (7.4 mg, 0.04 mmol) and TEA (10.9 mL). The temperature is cooled down to 0°C and the phenylacetylene is added (33 μL). The mixture is left under stirring at room temperature for 12h. Then the mixture is filtered and the solvent is removed at reduced pressure. The residue is diluted with DCM and washed first with a solution of NH_4Cl 5% and after with water. The organic layer is dried over Na_2SO_4 and the solvent is removed under reduced pressure. The crude product is purified by recrystallization in DCM/hexane. Yield 94%.

$^1\text{H-NMR}$ (400 MHz, CDCl_3): δ (ppm) 7.55 (m, 2H), 7.23 (m, 3H), 1.47 (m, 12H), 0.98 (m, 18H).

➤ *Synthesis of complex 25*

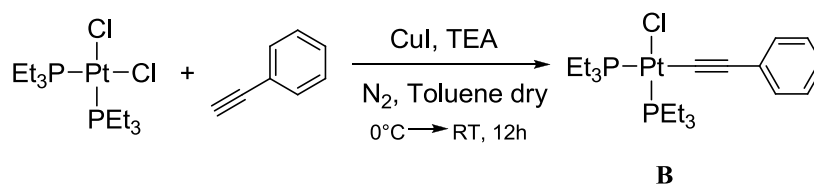


Under N_2 atmosphere a mixture of complex **A** (17 mg, 0.03 mmol), CuI (1 mg, 0.004 mmol) and TEA (1.1 mL) dry toluene is prepared. The mixture is cooled down to 0°C ; then the compound **24** (30 mg, 0.03 mmol) solubilized in dry toluene is added. The mixture is left under stirring for 12h. Then the mixture is filtered and the solvent is removed at reduced pressure. The residue is diluted with DCM and washed first with a solution of NH_4Cl 5% and after with water. The organic layer is dried over Na_2SO_4 and the solvent is removed under reduced pressure. The crude product is purified by flash chromatography on silica gel, using hexane/DCM 1/1 as eluent, to give the desired product. Yield 60%.

$^1\text{H-NMR}$ (400 MHz, CDCl_3): δ (ppm) 7.40 (d, $J = 8.2$ Hz, 2H), 7.30-7.25 (m, 2H), 7.22 (s, 1H) 7.00 (m, 1H), 3.55 (s, 3H), 2.95 (t, $J = 9.5$ Hz, 2H), 2.75 (t, $J = 7.4$ Hz, 2H), 2.60 (t, $J = 7.4$ Hz, 2H), 2.37-2.35 (m, 2H), 2.25-2.20 (m, 12H), 2.09-2.08 (m, 18H) 1.70 (t, $J = 7.1$ Hz, 2H), 1.34-1.29 (m, 6H), 1.1-0.9 (m, 3H).

3.2.3.2. Synthesis of complex 26.

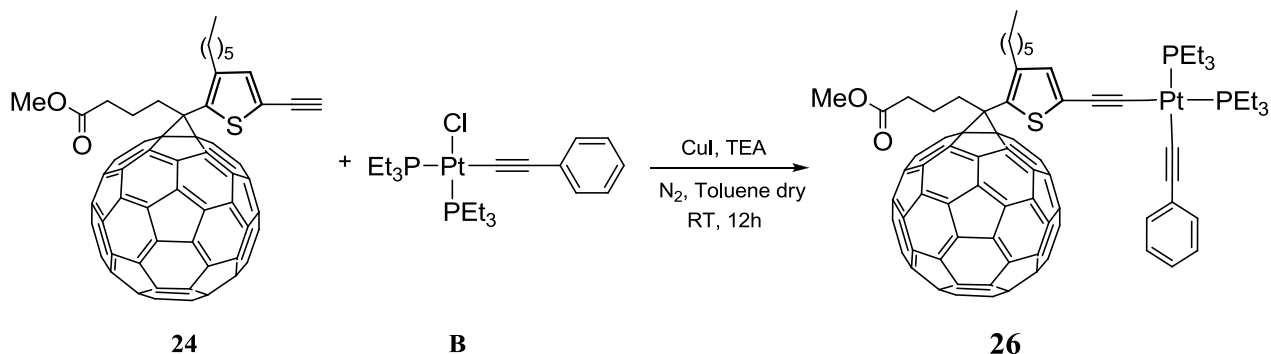
➤ *Synthesis of the Pt complex B*



Under N_2 atmosphere is prepared a solution of *cis*-Pt-dichloro-bis(triethylphosphine) complex (150 mg, 0.3mmol) in dry toluene. Then CuI (7.4 mg, 0.04 mmol) and TEA (10.9 mL). The temperature is cooled down to 0°C and the phenylacetylene is added (33 μL). The mixture is left under stirring at room temperature for 12h. Then the mixture is filtered and the solvent is removed at reduced pressure. The residue is diluted with DCM and washed first with a solution of NH_4Cl 5% and after with water. The organic layer is dried over Na_2SO_4 and the solvent is removed under reduced pressure. The crude product is purified by recrystallization in DCM/hexane. Yield 90%.

$^1\text{H-NMR}$ (400 MHz, CDCl_3): δ (ppm) 7.55 (m, 2H), 7.23 (m, 3H), 1.47 (m, 12H), 0.98 (m, 18H).

➤ *Synthesis of complex 26*



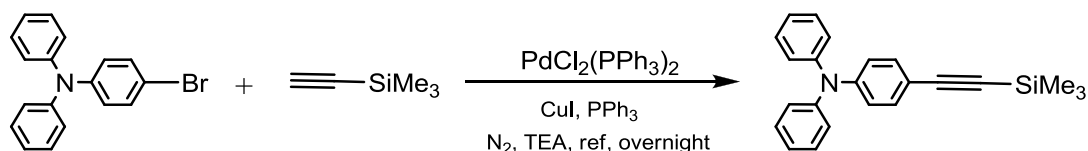
Under N₂ atmosphere a mixture of complex **B** (17 mg, 0.03 mmol), CuI (1 mg, 0.004 mmol) and TEA (1.1 mL) dry toluene is prepared. The mixture is cooled down to 0°C; then compound **24** (30 mg, 0.03 mmol), solubilized in dry toluene, is added. The mixture is left under stirring for 12h. Then the mixture is filtered and the solvent is removed at reduced pressure. The residue is diluted with DCM and washed first with a solution of NH₄Cl 5% and after with water. The organic layer is dried over Na₂SO₄ and the solvent is removed under reduced pressure. The crude product is purified by flash chromatography on silica gel, using hexane/DCM 1/1 as eluent, to give the desired product. Yield 30%.

¹H-NMR (400 MHz, CDCl₃): δ (ppm) 7.38 (d, *J* = 8.2 Hz, 2H), 7.27-7.22 (m, 2H), 7.18 (s, 1H) 7.00 (m, 1H), 3.55 (s, 3H), 2.95 (t, *J* = 9.5 Hz, 2H), 2.75 (t, *J* = 7.4 Hz, 2H), 2.60 (t, *J* = 7.4 Hz, 2H), 2.37-2.35 (m, 2H), 2.20-2.18 (m, 12H), 2.05-2.03 (m, 18H) 1.70 (t, *J* = 7.1 Hz, 2H), 1.34-1.29 (m, 6H), 1.1-0.9 (m, 3H).

3.2.3.3. Synthesis of complex **27**.

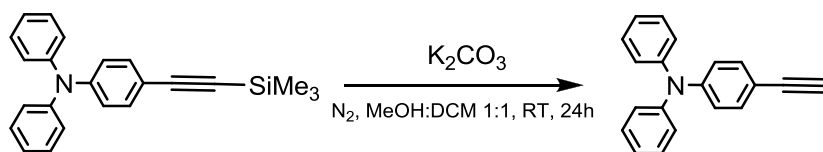
➤ *Synthesis of the Pt complex C*

- *Synthesis of the ligand 4-ethynyl-N,N-diphenylaniline*



Under N₂ atmosphere is prepared a solution of 4-Br-N,N-diphenylaniline (85 mg, 0.26 mmol), ethynyltrimethylsilane (56 μL, 0.39 mmol), PdCl₂(PPh₃)₂ (11 mg, 0.02 mmol), CuI (1.5 mg, 0.008 mmol) and PPh₃ (2 mg, 0.008 mmol) in TEA (4 mL). Then the mixture is refluxed (70°C) for 24h. After cooling to room temperature, the solvent is evaporated at reduced pressure, the residue is diluted with DCM and washed with water. The organic layer is dried over Na₂SO₄ and the solvent is removed under reduced pressure. The crude product is purified by flash chromatography on silica gel, using hexane/EtOAc 8/2 as eluent, to give the desired product. Yield 75%.

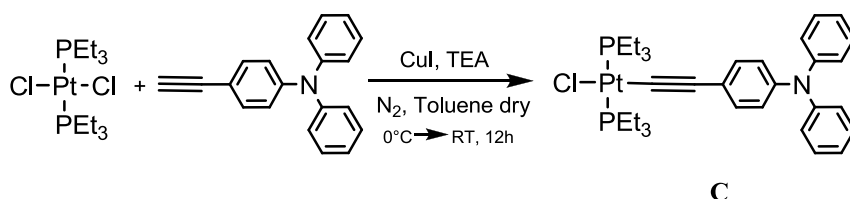
¹H-NMR (400 MHz, CDCl₃): δ (ppm) 7.37 (d, *J* = 6.8 Hz, 2H), 7.31 (m, 4H), 7.14 (m, 4H), 7.09 (m, 2H), 7.01 (d, *J* = 6.8 Hz, 2H), 0.30 (s, 9H).



Under N_2 atmosphere is prepared a solution of *N,N*-diphenyl-4-((trimethylsilyl)ethynyl)aniline (57.4 mg, 0.17 mmol) in dry MeOH/ dry DCM 1/1 (15 mL). Then K_2CO_3 is added (92.9 mg, 0.67 mmol). The mixture is left under stirring at room temperature for 24h. The solvent is evaporated at reduced pressure, the residue is diluted with DCM and washed with water. The organic layer is dried over Na_2SO_4 and the solvent is removed under reduced pressure. The crude product is purified by flash chromatography on silica gel, using hexane/toluene 1/1 as eluent, to give the desired product. Yield 71%.

1H -NMR (400 MHz, $CDCl_3$): δ (ppm) 7.37 (d, $J = 6.8$ Hz, 2H), 7.31 (m, 4H), 7.14 (m, 4H), 7.09 (m, 2H), 7.01 (d, $J = 6.8$ Hz, 2H), 4.05 (s, 1H).

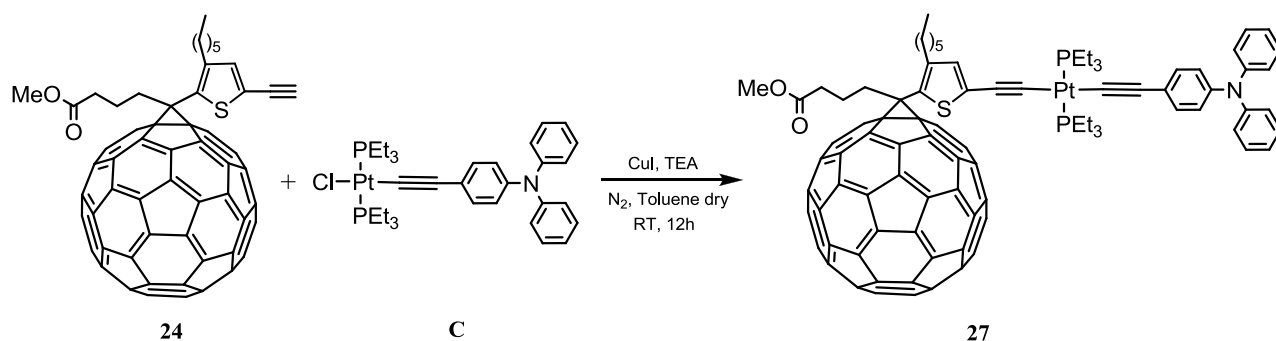
- *Synthesis of the Pt complex C*



Under N_2 atmosphere is prepared a solution of *trans*-Pt-dichloro-bis(triethylphosphine) complex (140 mg, 0.3mmol) in dry toluene. Then CuI (7.4 mg, 0.04 mmol) and TEA (10.9 mL). The temperature is cooled down to $0^\circ C$ and the 4-ethynyl-*N,N*-diphenylaniline is added (75 mg, 0.28 mmol). The mixture is left under stirring at room temperature for 12h. Then the mixture is filtered and the solvent is removed at reduced pressure. The residue is diluted with DCM and washed first with a solution of NH_4Cl 5% and after with water. The organic layer is dried over Na_2SO_4 and the solvent is removed under reduced pressure. The crude product is purified by recrystallization in DCM/hexane. Yield 63%.

1H -NMR (400 MHz, $CDCl_3$): δ (ppm) 7.34-7.22 (m, 8H), 7.14 (d, $J = 8.2$ Hz, 2H), 7.10-7.08 (d, $J = 8.2$ Hz, 2H), 6.93 (d, $J = 8.2$ Hz, 2H), 2.30-2.20 (m, 12H), 2.05-2.00 (m, 18H).

➤ *Synthesis of complex 27*



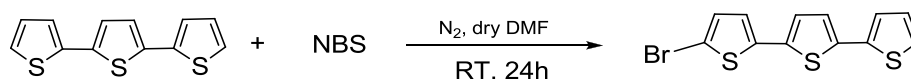
Under N₂ atmosphere a mixture of complex **C** (56.4 mg, 0.017 mmol), CuI (1.85 mg, 0.01 mmol) and TEA (0.5 mL) in dry toluene (4.5 mL) is prepared. The mixture is cooled down to 0°C; then compound **24** (77 mg, 0.017 mmol), solubilized in dry toluene (1 mL), is added. The mixture is left under stirring for 12h. Then the mixture is filtered and the solvent is removed at reduced pressure. The residue is diluted with DCM and washed first with a solution of NH₄Cl 5% and after with water. The organic layer is dried over Na₂SO₄ and the solvent is removed under reduced pressure. The crude product is purified by flash chromatography on silica gel, using hexane/DCM 2/3 as eluent, to give the desired product. Yield 50%.

¹H-NMR (400 MHz, CDCl₃): δ (ppm) 7.31-7.24 (m, 8H), 7.15 (d, *J* = 8.2 Hz, 2H), 7.12 (s, 1H), 7.10-7.08 (m, 2H), 6.93 (d, *J* = 8.2 Hz, 2H) 3.55 (s, 3H), 2.95 (t, *J* = 7.4 Hz, 2H), 2.75 (t, *J* = 7.4 Hz, 2H), 2.60 (t, *J* = 7.1 Hz, 2H), 2.30-2.20 (m, 12H), 2.05-2.00 (m, 18H), 1.73 (t, *J* = 7.1 Hz, 2H), 1.33-1.29 (m, 6H), 1.1-0.9 (m, 3H).

3.2.4. Synthesis of compound **28** and complex **29**.

3.2.4.1. Synthesis of compound **28**.

➤ *Synthesis of the 1-Br-terthiophene intermediate*

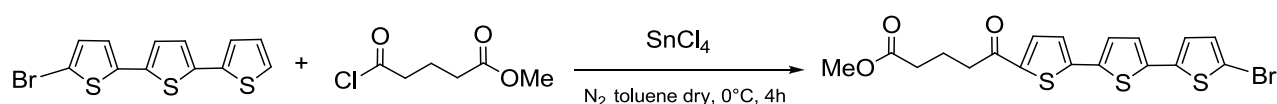


At room temperature the terthiophene (200 mg, 0.81 mmol) is solubilized in dry DMF (11.5 mL). The system is placed in dark and N-bromosuccinimide (151 mg, 0.81 mmol) is added in portions. The reaction is left under stirring for 24h. A saturated solution of NaHCO₃ is added until neutral

pH and an extraction with DCM is performed. The organic phase is washed with water, dried with Na_2SO_4 and the solvent is removed under reduced pressure. The yield is quantitative (94 %).

^1H NMR (400 MHz, CDCl_3): δ (ppm) 7.25 (d, $J = 3.8$ Hz, 1H), 7.19 (d, $J = 3.5$ Hz, 1H), 7.08 (d, $J = 3.8$ Hz, 1H), 7.04 (m, 2H), 7.00 (d, $J = 3.8$ Hz, 1H), 6.92 (d, $J = 3.8$ Hz, 1H).

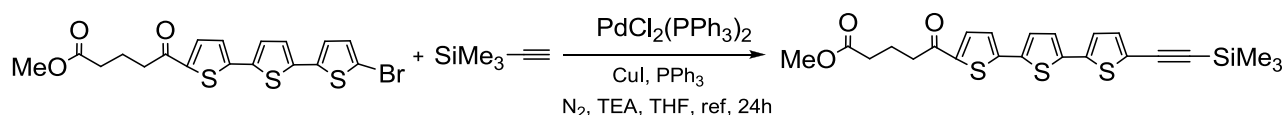
➤ *Synthesis of the glutaric-methylester derivative*



At room temperature and under N_2 atmosphere the intermediate (100 mg, 0.30 mmol) is solubilized in dry toluene (2 mL). The solution is cooled down at 0°C and slowly methyl glutaric acid monomethyl ester chloride (42 μL , 0.30 mmol) and SnCl_4 (35.7 μL , 0.30 mmol) are added. The reaction is left under stirring at 0°C for 4h. The solution is diluted with EtOAc and washed with water. The organic layer is dried over Na_2SO_4 and the solvent is removed under reduced pressure. The crude product is purified by flash chromatography on silica gel, using hexane/EtOAc 8/2 as eluent, to give the desired product. Yield 91%.

^1H NMR (400 MHz, CDCl_3): δ (ppm) 7.64 (d, $J = 4$ Hz, 1H), 7.22 (d, $J = 4$ Hz, 1H), 7.17 (d, $J = 4$ Hz, 1H), 7.06 (d, $J = 4$ Hz, 1H), 7.01 (d, $J = 4$ Hz, 1H), 6.93 (d, $J = 4$ Hz, 1H), 3.71 (s, 3H), 2.98 (t, $J = 7.2$ Hz, 2H), 2.47 (t, $J = 7.2$ Hz, 2H), 2.10 (m, 2H).

➤ *Synthesis of the alkyne derivative*

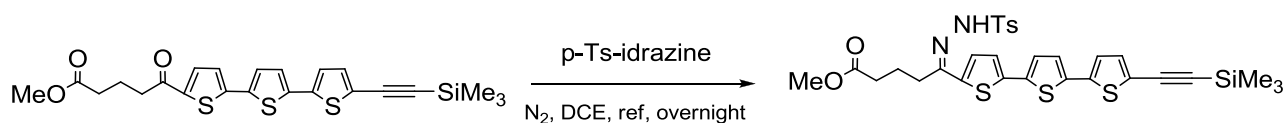


Under N_2 atmosphere is prepared a solution of the previous intermediate (33.5 mg, 0.07 mmol), ethynyltrimethylsilane (15 μL , 0.1 mmol), $\text{PdCl}_2(\text{PPh}_3)_2$ (3 mg, 0.004 mmol), CuI (0.5 mg, 0.002 mmol) and PPh_3 (0.5 mg, 0.002 mmol) in TEA (1 mL) and dry THF (2 mL). Then the mixture is refluxed (70°C) for 24h. After cooling to room temperature, the solvent is evaporated at reduced pressure, the residue is diluted with DCM and washed with water. The organic layer is dried over Na_2SO_4 and the solvent is removed under reduced pressure. The crude product is purified by flash

chromatography on silica gel, using hexane/EtOAc 8/2 as eluent, to give the desired product. Yield 84%.

$^1\text{H NMR}$ (400 MHz, CDCl_3): δ (ppm) 7.65 (d, $J = 4$ Hz, 1H), 7.24 (d, $J = 4$ Hz, 1H), 7.18 (d, $J = 4$ Hz, 1H), 7.15 (d, $J = 4$ Hz, 1H), 7.11 (d, $J = 4$ Hz, 1H), 7.07 (d, $J = 4$ Hz, 1H), 3.71 (s, 3H), 2.99 (t, $J = 7.2$ Hz, 2H), 2.47 (t, $J = 7.2$ Hz, 2H), 2.11 (m, 2H), 0.28 (s, 9H).

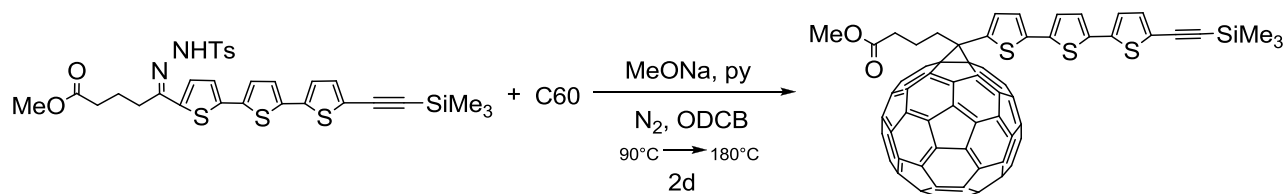
➤ *Synthesis of the *p*-tosylhydrazone derivative*



Under N_2 atmosphere is prepared a solution of the previous intermediate (42 mg, 0.1 mmol) and *p*-Ts-hydrazine (23 mg, 0.12 mmol) in DCE. The mixture is refluxed overnight (83 °C). After cooling to room temperature, the solvent is evaporated at reduced pressure, the residue is diluted with EtOAc and washed with water. The organic layer is dried over Na_2SO_4 and the solvent is removed under reduced pressure. The crude product is purified by flash chromatography on silica gel, using hexane/EtOAc 7/3 as eluent, to give the desired product. Yield 61 %.

$^1\text{H NMR}$ (400 MHz, CDCl_3): δ (ppm) 9.08 (s, 1H), 7.93 (d, $J = 7.7$ Hz, 1H), 7.83 (d, $J = 7.7$ Hz, 1H), 7.33 (d, $J = 7.6$ Hz, 1H), 7.15 (s, 1H), 7.09 (m, 1H), 7.04 (s, 1H), 3.81 (s, 3H), 2.60 (t, $J = 7.4$ Hz, 2H), 2.45 (m, 2H), 2.06 (bm, 2H), 0.26 (s, 9H).

➤ *Synthesis of compound 2d*



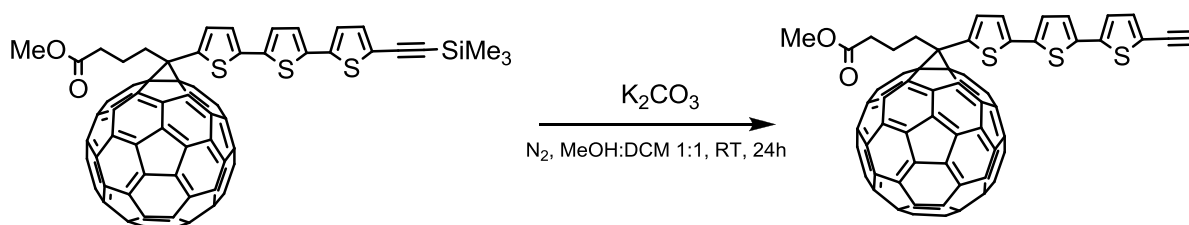
Under N_2 atmosphere is prepared a solution of the previous intermediate (63.8 mg, 0.11 mmol), MeONa (6.0 mg, 0.11 mmol), and dry pyridine (1.1 mL). The mixture is left under stirring at room temperature for 30 min. Then a solution of C_{60} -fullerene (66 mg, 0.09 mmol) in *o*-dichlorobenzene (6.4 mL) is added, and the homogeneous reaction mixture is stirred at 80°C under N_2 atmosphere overnight. Then the mixture is refluxed for 24 h (180°C), after cooling to

room temperature the solvent is evaporated at reduced pressure, and the residue is purified flash chromatography on silica gel with toluene/hexane 1/1 as eluent, to give the desired product. Yield 40%.

$^1\text{H-NMR}$ (400 MHz, CDCl_3): δ (ppm) 7.43 (d, $J = 3.6$ Hz, 1H), 7.26 (d, $J = 3.6$ Hz, 1H), 7.20-7.16 (m, 3H), 7.06 (d, $J = 3.6$ Hz, 1H), 3.71 (s, 3H) 2.99 (t, $J = 7.7$ Hz, 2H), 2.47 (t, $J = 7.7$ Hz, 2H), 2.11 (m, 2H), 0.26 (s, 9H).

3.2.4.2. Synthesis of complex **29**.

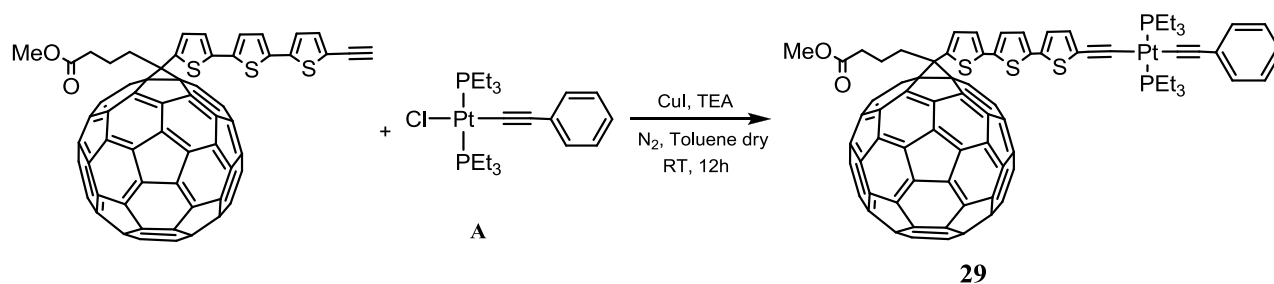
➤ *Synthesis of the σ -acetylide ligand*



Under N_2 atmosphere is prepared a solution of the compound **28** (40 mg, 0.03 mmol) in dry MeOH/ dry DCM 1/1 (10 mL). Then K_2CO_3 is added (16 mg, 0.12 mmol). the mixture is left under stirring at room temperature for 24h. The solvent is evaporated at reduced pressure, the residue is diluted with DCM and washed with water. The organic layer is dried over Na_2SO_4 and the solvent is removed under reduced pressure. The crude product is purified by flash chromatography on silica gel, using hexane/toluene 1/1 as eluent, to give the desired product. Yield 71%.

$^1\text{H-NMR}$ (400 MHz, CDCl_3): δ (ppm) 7.45 (d, $J = 3.7$ Hz, 1H), 7.28 (d, $J = 3.7$ Hz, 1H), 7.21-7.17 (m, 3H), 7.06 (d, $J = 3.6$ Hz, 1H), 3.71 (s, 3H), 3.69 (s, 1H), 2.99 (t, $J = 7.7$ Hz, 2H), 2.47 (t, $J = 7.7$ Hz, 2H), 2.11 (m, 2H).

➤ *Synthesis of complex 29*

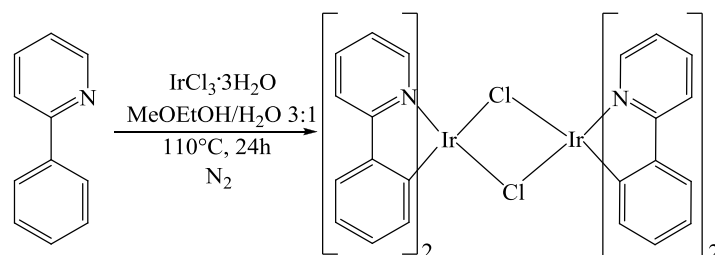


Under N_2 atmosphere a mixture of complex **A** (9.6 mg, 0.017 mmol), CuI (2 mg, 0.01mmol) and TEA (0.5 mL) in dry toluene (4.5 mL) is prepared. The mixture is cooled down to 0°C ; then the σ -acetylide ligand (20 mg 0.017 mmol), solubilized in dry toluene (1 mL), is added. The mixture is left under stirring for 12h. Then the mixture is filtered and the solvent is removed at reduced pressure. The residue is diluted with DCM and washed first with a solution of NH_4Cl 5% and after with water. The organic layer is dried over Na_2SO_4 and the solvent is removed under reduced pressure. The crude product is purified by flash chromatography on silica gel, using hexane/DCM 2/3 as eluent, to give the desired product. Yield 52%.

$^1\text{H-NMR}$ (400 MHz, CDCl_3): δ (ppm) 7.42 (d, $J = 3.6$ Hz, 1H), 7.40 (d, $J = 8.2$ Hz, 2H), 7.35 (m, 3H), 7.24 (d, $J = 3.6$ Hz, 1H), 7.20-7.16 (m, 3H), 7.06 (d, $J = 3.6$ Hz, 1H), 3.70 (s, 3H), 2.95 (t, $J = 9.5$ Hz, 2H), 2.75 (t, $J = 7.4$ Hz, 2H), 2.60 (t, $J = 7.4$ Hz, 2H), 2.25-2.20 (m, 12H), 2.09-2.08 (m, 18H).

3.2.5. Synthesis of the neutral heteroleptic Ir(III) complexes **56** and **57**.

➤ *Synthesis of the dimer $[\text{Ir}(\text{ppy})_2(\mu\text{-Cl})_2]$*

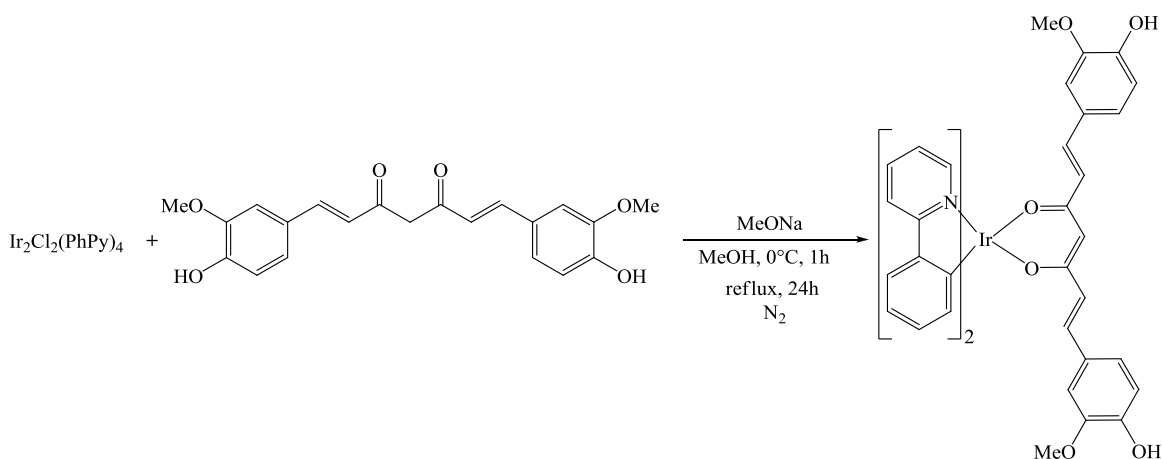


At room temperature, iridium trichloride tri-hydrate (360 mg, 1.01 mmol) was dissolved in a mixture of 2-methoxyethanol (60 mL) and water (20 mL). 2-phenylpyridine (506 μL , 3.03 mmol)

was added and the reaction mixture was refluxed for 24 h under nitrogen atmosphere. The solution was cooled to room temperature and the yellow precipitate was collected on a glass filter. The solid was washed with methanol and diethyl ether and then dissolved in dichloromethane and precipitated with pentane. The desired product was obtained in 71% yield.

$^1\text{H-NMR}$ (400 MHz, DMSO): δ (ppm) 9.81 (d, $J= 8.1$ Hz, 2H), 9.55 (d, , $J= 8.1$ Hz, 2H), 8.26 (d, $J= 8.1$ Hz, 2H), 8.18 (d, $J= 8.0$ Hz, 2H), 8.12 (t, $J= 8.0$ Hz, 2H), 8.01(t, $J= 8.1$ Hz, 2H), 7.79 (d, $J= 8.0$ Hz, 2H), 7.73 (d, $J= 8.0$ Hz, 2H), 7.57 (t, $J= 8.0$ Hz, 2H), 7.45 (t, $J= 8.0$ Hz, 2H), 6.90 (t, $J= 8.0$ Hz, 2H), 6.86 (t, $J= 8.0$ Hz, 2H), 6.77 (t, $J= 8.0$ Hz, 2H), 6.69 (t, $J= 8.0$ Hz, 2H), 6.27 (d, $J= 8.1$ Hz, 2H), 5.67 (d, $J= 8.1$ Hz, 2H).

3.2.5.1. Synthesis of complex 56



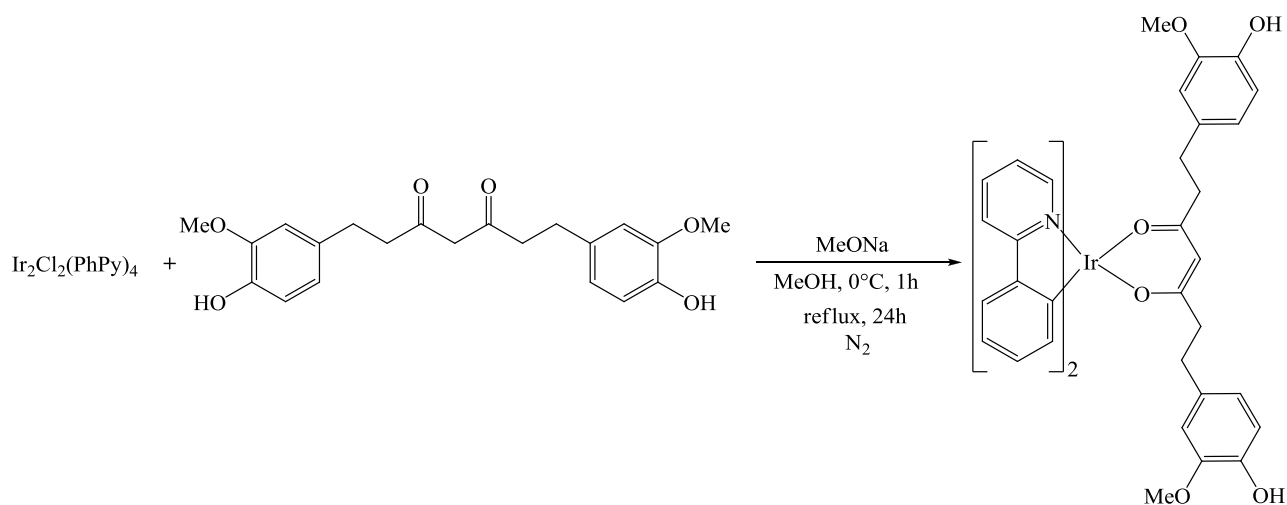
Curcumin (200 mg, 0.54 mmol) was dissolved in methanol (11 mL) and NaOMe (29 mg, 0.54 mmol) was added. The mixture was stirred for 1 h at 0°C and then $[\text{Ir}(\text{ppy})_2(\mu\text{-Cl})]_2$ (291 mg, 0.27 mmol) was added. The resulting orange solution was stirred at reflux for 24 h. The orange-red precipitate was filtered and then was dissolved in the minimum amount of dichloromethane and precipitated with diethylether. The pure product was obtained as an orange precipitate in 57 % yield.

$^1\text{H-NMR}$ (600 MHz, CD_3CN): δ (ppm) 8.85 (d, $J= 5.6$ Hz, 2H), 8.02 (d, $J= 8.2$ Hz, 2H), 7.86 (t, $J= 7.5$ Hz, 2H), 7.68 (d, $J= 7.7$ Hz, 2H), 7.27 (d, $J= 6.1$ Hz, 2H), 7.17 (d, $J= 15.7$ Hz, 2H), 7.12 (d, $J= 1.6\text{Hz}$, 2H), 6.99 (dd, $^1J= 8.2$ Hz, $^2J= 1.6$ Hz 2H), 6.86 (t, $J= 7.3$ Hz, 2H), 6.78 (d, $J= 8.2$ Hz, 2H), 6.72 (t, $J= 7.3$ Hz, 2H), 6.61 (d, $J= 15.7$ Hz, 2H), 6.25 (d, $J= 7.5$ Hz, 2H), 5.75 (s, 1H), 3.87 (s, 6H).

$^{13}\text{C-NMR}$ (150 MHz, CD_3CN): δ (ppm) 176.8, 168.2, 148.1, 147.8, 147.6, 147.6, 145.4, 137.8, 136.1, 133.0, 128.7, 128.4, 128.0, 123.9, 122.2, 121.7, 120.8, 118.7, 115.0, 110.0, 103.1, 55.7.

Anal. Calcd.(%) for $C_{44}H_{39}IrN_2O_6$: C, 59.78; H, 4.45, N, 3.17 . Found: C 59.81; H 4.47, N 3.15.

3.2.5.2. Synthesis of complex 57.



Tetrahydrocurcumin was dissolved (146 mg, 0.39 mmol) in methanol (10 mL) and $NaOMe$ (21.2 mg, 0.39 mmol) was added. The mixture was stirred at $0^\circ C$ for 1 h and then $[Ir(ppy)_2(\mu-Cl)]_2$ (210 mg, 0.2 mmol) was added. The resulting yellow solution was stirred at reflux for 24 h. The precipitate was filtered and recrystallized from dichloromethane/diethylether. The pure product was obtained as dark yellow solid in 54 % yield.

1H -NMR (600 MHz, CD_3CN): δ (ppm) 8.24 (d, $J = 4.98$ Hz, 2H), 8.00 (d, $J = 8.1$ Hz, 2H), 7.86 (t, $J = 8.1$ Hz, 2H), 7.64 (d, $J = 5.2$ Hz, 2H), 7.16 (t, $J = 6.54$ Hz, 2H), 6.83 (t, $J = 7.4$ Hz, 2H), 6.70 (s, 2H), 6.67 (t, $J = 7.4$ Hz, 2H), 6.61 (d, $J = 8.0$ Hz, 2H), 6.39 (t, $J = 8.0$ Hz, 2H), 6.17 (d, $J = 7.4$ Hz, 2H), 5.35 (s, 1H), 3.77 (s, 6H), 2.63-2.55 (m, 4H), 2.37-2.32 (m, 2H), 2.27-2.21 (m, 2H).

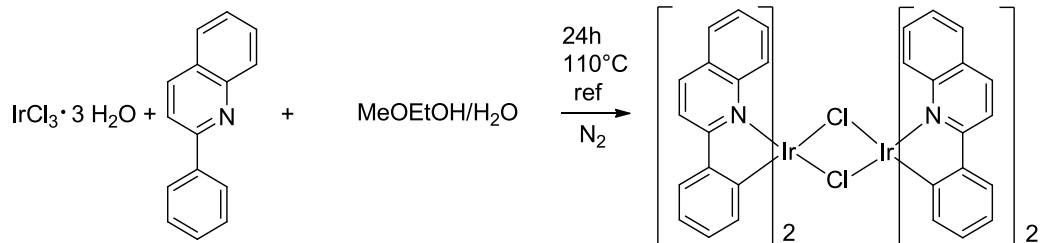
^{13}C -NMR (150 MHz, CD_3CN): δ (ppm) 186.8, 168.0, 148.2, 147.8, 147.6, 147.6, 144.1, 145.4, 137.6, 133.1, 128.6, 123.8, 122.1, 120.7, 120.7, 118.6, 114.4, 111.9, 99.8, 55.6, 42.8, 31.9.

Anal. Calcd.(%) for $C_{44}H_{43}IrN_2O_6$: C, 59.50; H, 4.88, N, 3.15 . Found: C 59.78; H 4.90, N 3.16.

3.2.6. Synthesis of the anionic heteroleptics Ir(III) complexes 60_1 – 65_1.

3.2.6.1. Synthesis of complex 60_1.

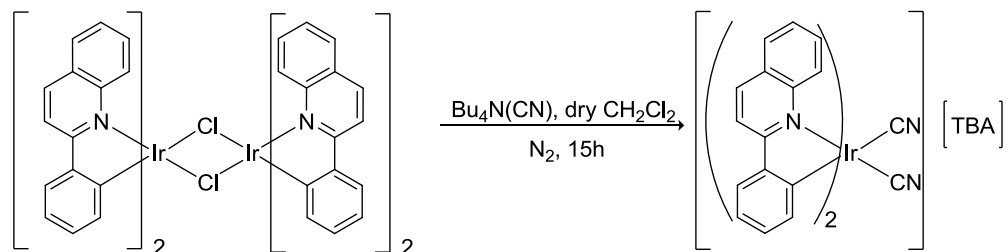
➤ *Synthesis of the dimer 60*



At room temperature, the Iridium trichloride (540.6 mg, 1.53 mmol) was dissolved in methoxyethanol (45 mL) and water (15 mL) under nitrogen. To this solution 2-phenylquinoline (691.7 mg, 3.37 mmol) was added. The reaction mixture was refluxed under stirring for 24 h. The precipitated solid was washed with methanol and ethyl ether. The solid was air dried. The final product appears as a red solid (yield 41%).

¹H-NMR (400 MHz, DMSO-d₆): δ(ppm) 8.52 (d, J = 8 Hz, 4H), 8.28 (d, J = 8 Hz, 8H), 8.19 (d, J = 8 Hz, 4H), 8.11 (d, J = 8 Hz, 4H), 8.04 (d, J = 8 Hz, 4H), 7.82 (t, J = 8 Hz, 4H), 7.65-7.51 (m, 12H).

➤ *Synthesis of complex 60_1*



Compound **60** (43.2 mg, 0.05 mmol) was dissolved in dry dichloromethane (30 mL) under nitrogen. To this solution tetrabutylammonium cyanide (161.09 mg, 0.60 mmol) was added.

The reaction mixture was refluxed under stirring for 15 h. Then, to the solution was added a 1:1 solvent mixture of diethyl ether and low-boiling petroleum ether (100 mL). The precipitated solid was collected and recrystallized from methanol and low-boiling petroleum ether.

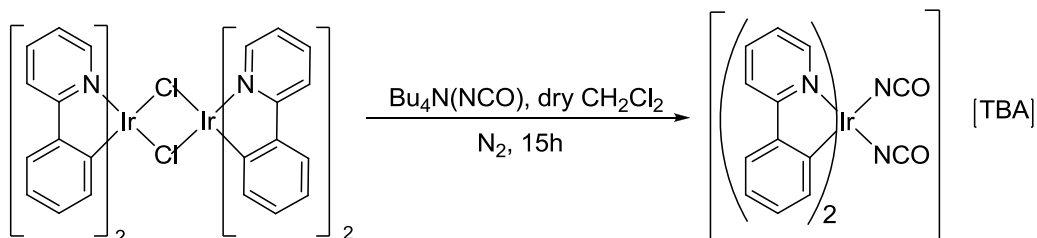
The final product appears as orange-red crystal solid (yield 58%).

¹H-NMR (300 MHz, DMSO-d₆): δ(ppm) 10.13 (d, J = 3 Hz, 2H), 8.46 (d, J = 3 Hz, 2H), 8.23 (d, J = 3 Hz, 2H), 8.02 (d, J = 3 Hz, 2H), 7.78 (d, J = 3 Hz, 2H), 7.67 (m, 4H), 6.72 (t, J = 2 Hz, 2H), 6.50 (t, J = 2 Hz, 2H), 6.50 (t, J = 2 Hz, 2H), 5.93 (d, J = 3 Hz, 2H), 3.17 (t, J = 4 Hz, 8H), 1.28 (m, 8H), 1.10 (q, J = 3 Hz, 8H), 1.01 (t, J = 3 Hz, 12H).

3.2.6.2. Synthesis of complex 61_1.

For the synthesis of the dimer see paragraph 3.1.4.

➤ *Synthesis of complex 61_1.*



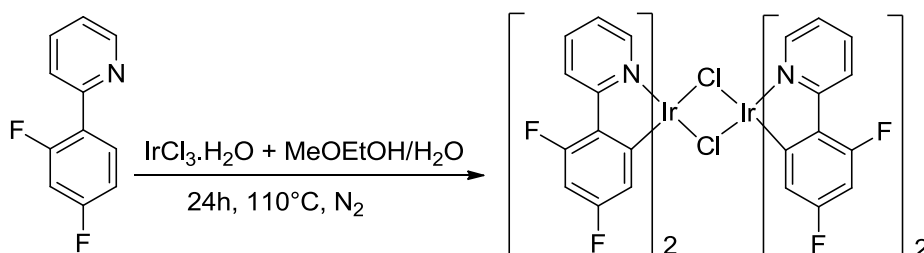
The dimer (200.00 mg, 0.187 mmol) was dissolved in dry dichloromethane (30 mL) under nitrogen. To this solution tetrabutylammonium cyanate (638.86 mg, 2.238 mmol) was rapidly added. The reaction mixture was refluxed under stirring for 15 h. Then, to the solution was added a 1:1 solvent mixture of diethyl ether and low-boiling petroleum ether (100 mL). An orange oil was formed and recrystallized from methanol and low-boiling petroleum ether.

The final product appears as yellow solid (yield 29%).

¹H-NMR (400 MHz, DMSO-d₆): δ(ppm) 9.77 (d, J = 2 Hz, 2H), 9.08 (d, J = 1.3 Hz, 2H), 8.26 (d, J = 5 Hz, 2H), 8.07 (t, J = 2 Hz, 2H), 7.78 (t, J = 2 Hz, 2H), 7.49 (t, J = 2 Hz, 2H), 6.89 (t, J = 2 Hz, 2H), 6.75 (m, 2H), 3.17 (m, 8H), 1.54 (m, 8H), 1.30 (m, 8H), 0.94 (t, J = 2 Hz, 12 H).

3.2.6.3. Synthesis of complex 62_1 and 62_2.

➤ *Synthesis of the dimer 62*

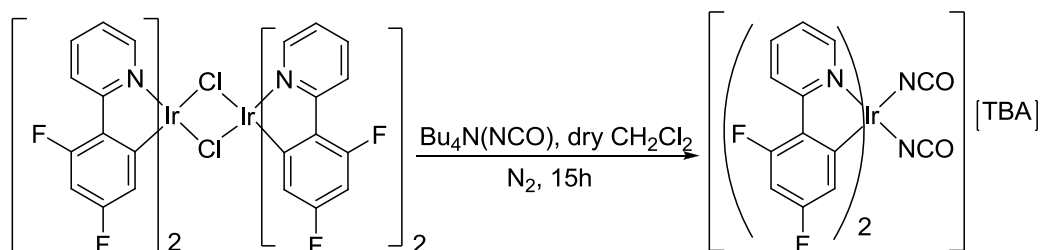


At room temperature the Iridium trichloride (359.4 mg, 1.01 mmol) was dissolved in methoxyethanol (60 mL) and water (20 mL) under nitrogen atmosphere. To this solution 2-(2,4-difluorophenyl)pyridine (454 μL, 2.979 mmol) was added. The reaction mixture was refluxed under stirring for 24 h. The solution was filtered and the precipitated solid was washed with methanol and ethyl ether. The solid was air dried.

The final product appears as a "fluorescent" yellow solid (yield 8%).

$^1\text{H-NMR}$ (400 MHz, DMSO-d_6): δ (ppm) 9.95 (d, $J = 1$ Hz, 4H), 9.55 (d, $J = 1$ Hz, 4 H), 8.21 (m, 4 H), 8.12 (m, 4 H), 7.63 (td, $J = 5$ Hz, $J = 2$ Hz, 4 H), 6.82 (m, 4 H).

➤ *Synthesis of complex 62_1.*



Dimer **62** (40.00 mg, 0.033 mmol) was dissolved in dry dichloromethane (17 mL) under nitrogen.

To this solution tetrabutylammonium cyanate (112.36 mg, 0.395 mmol) was rapidly added.

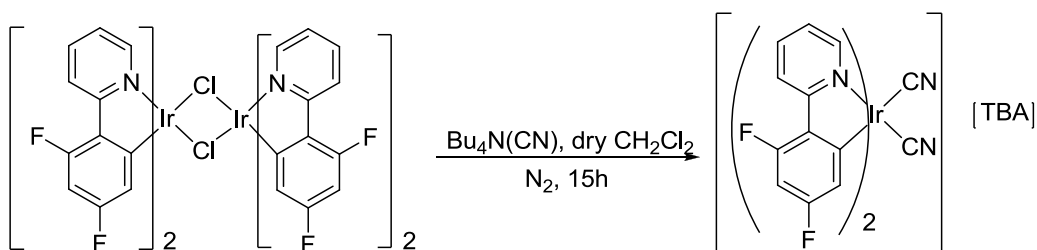
The reaction mixture was refluxed under stirring for 15 h. Then, to the solution was added a 1:1 solvent mixture of diethyl ether and low-boiling petroleum ether (100 mL). A yellow oil was formed and recrystallized from methanol and low-boiling petroleum ether.

The final product appears as small yellow crystal solid (yield 36%).

$^1\text{H NMR}$ (600 MHz, DMSO-d_6): δ (ppm) 9.29 (d, $J = 1$ Hz, 2H), 8.17 (d, $J = 1$ Hz, 2H), 8.02 (t, $J = 2$ Hz, 2H), 7.52 (t, $J = 2$ Hz, 2H), 6.56 (m, 2 H), 5.44 (dd, $J = 2$ Hz, $J = 1$ Hz, 2H), 3.17 (m, 8 H), 1.58 (m, 8H), 1.33 (m, 8 H), 0.94 (t, $J = 2$ Hz, 12H).

$^{13}\text{C-NMR}$ (150 MHz, DMSO-d_6): δ (ppm) 164.26, 160.20, 157.25, 151.07, 138.51, 128.76, 123.14, 122.67, 122.21, 113.24, 96.31, 58.07, 23.55, 22.01, 19.68, 13.39.

➤ *Synthesis of complex 62_2.*



Dimer **62** (42.20 mg, 0.035 mmol) was dissolved in dry dichloromethane (11 mL) under nitrogen atmosphere. To this solution tetrabutylammonium cyanide (112.76 mg, 0.420 mmol) was added.

The reaction mixture was refluxed under stirring for 15 h. Then, to the solution was added a 1:1 solvent mixture of diethyl ether and low-boiling petroleum ether (100 mL). An orange oil was formed and recrystallized from methanol and low-boiling petroleum ether.

The final product appears as dark orange oil (yield 97%).

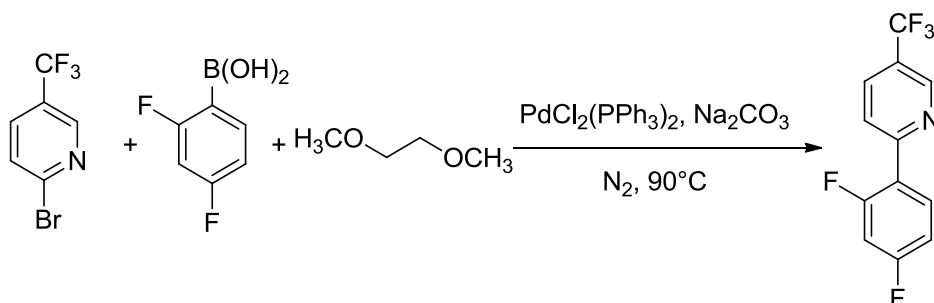
^1H NMR (600 MHz, DMSO-d_6): δ (ppm) 9.55 (d, $J = 1$ Hz, 2H), 8.20 (d, $J = 1$ Hz, 2H), 8.04 (t, $J = 1$ Hz, 2H), 7.44 (t, $J = 1$ Hz, 2H), 6.59 (t, $J = 1$ Hz, 2H), 5.54 (d, $J = 1$ Hz, 2H), 3.16 (t, $J = 3$ Hz, 8H), 1.58 (m, 8H), 1.32 (m, 8H), 0.94 (t, $J = 2$ Hz, 12H).

^{13}C -NMR (150 MHz, DMSO-d_6): δ (ppm) 110.02, 112.13, 123.14, 125.12, 126.08, 128.13, 137.15, 139.54, 155.65, 160.34, 165.15, 58.08, 23.56, 19.69, 13.94.

3.2.6.4. Synthesis of complex **63_1** - **63_3**.

➤ *Synthesis of the dimer **63***

➤ *Synthesis of 2-(2,4-difluorophenyl)-5-(trifluoromethyl) pyridine*

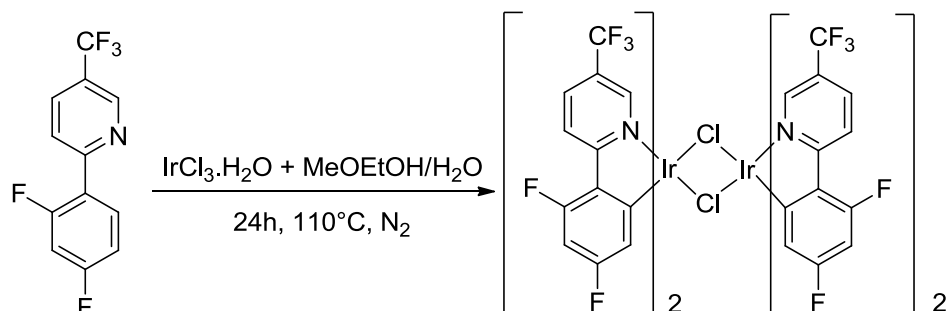


At room temperature, 2-Br-5(trifluoromethyl)pyridine (600.00 mg, 2.344 mmol), 2,4-difluorophenylboronic acid (555.20 mg, 3.516 mmol) and the catalyst $\text{PdCl}_2(\text{PPh}_3)_2$ (164.23mg, 0.234 mmol), was dissolved in dimethoxyethane (12 mL), with a solution 2M of Na_2CO_3 (795.00 mg, 7.501 mmol). The reaction mixture was heated at 90°C under stirring for 24 h. After the reaction was quenched with water and extracted with dichloromethane. The organic layer was washed with water, dried with Na_2SO_4 and the solvent was removed at reduced pressure. The crude product was purified by flash chromatography on silica gel (eluant: hexane/dichloromethane 7:3).

The purified product appears as a white solid (yield 85.3%).

^1H -NMR (400 MHz, CDCl_3): δ (ppm) 8.98 (s, 1H), 8.13 (m, 1H), 7.98 (m, 1H), 7.09 (m, 1H), 6.96 (m, 1H), 6.9 (m, 1H).

➤ *Synthesis of the dimer 63*

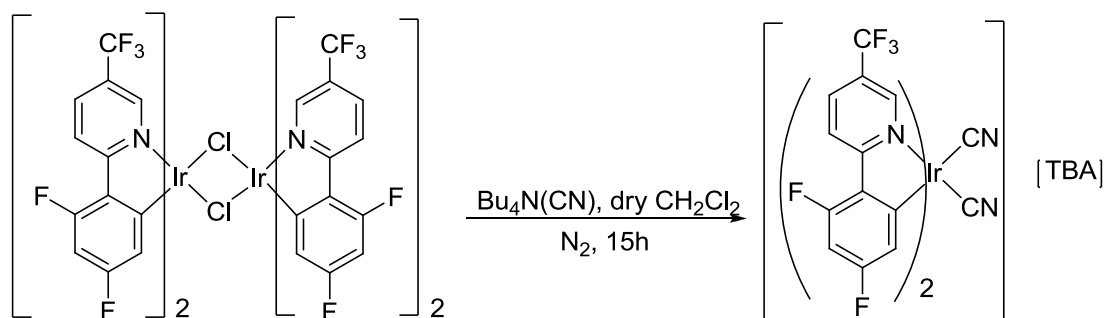


At room temperature, the Iridium trichloride (155.40 mg, 0.442 mmol) was dissolved in methoxyethanol (6 mL) and water (3 mL) under nitrogen atmosphere. 2-(2,4-difluorophenyl)-5-(trifluoromethyl) pyridine (258.45 mg, 1.00 mmol) was added to this solution. The reaction mixture was refluxed under stirring for 24 h. The solution was filtered and the solid precipitated was washed with water and recrystallized with dichloromethane and pentane.

The final product appears as a yellow solid (yield 10%).

¹H-NMR (400 MHz, CDCl₃): δ (ppm) 9.5 (d, J = 1 Hz, 4H), 8.45 (m, 4H), 8.04 (m, 4H), 6.4–6.47 (m, 4H), 5.07 (m, 4H).

➤ *Synthesis of complex 63_1.*



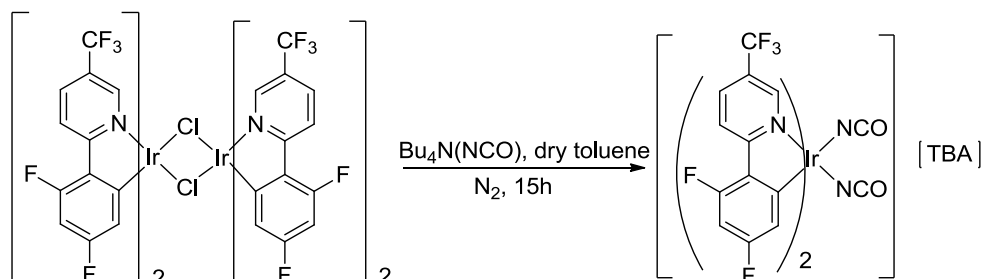
Dimer **63** (30.00 mg, 0.020 mmol) was dissolved in dry dichloromethane (6 mL) under nitrogen. To this solution tetrabutylammonium cyanide (64.44 mg, 0.240 mmol) was added.

The reaction mixture was refluxed under stirring for 15 h. After a 1:1 solvent mixture of diethyl ether and low-boiling petroleum ether (100 mL) was added to the solution.

The final product appears as dark orange oil (yield 96%).

$^1\text{H-NMR}$ (400 MHz, DMSO): δ (ppm) 9.86 (d, $J = 1$ Hz, 2H), 8.38 (m, 2H), 7.98 (m, 2H), 6.38 (m, 2H), 5.7 (m, 2H), 3.39 (8H, t), 1.7 (quintuplet, 8H), 1.5 (sextet, 8H), 1.12 (m, 12H).

➤ *Synthesis of the complex 63_2.*

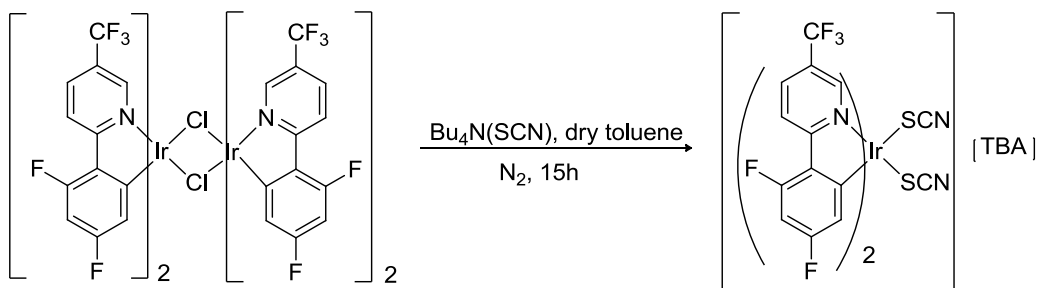


Dimer **63** (30.00 mg, 0.020 mmol) was dissolved in dry dichloromethane (3.8 mL) under nitrogen atmosphere. Tetrabutylammonium cyanate (68.28 mg, 0.240 mmol) was added to this solution. The reaction mixture was refluxed under stirring for 15 h. After, to the solution was added a 1:1 solvent mixture of diethyl ether and low-boiling petroleum ether (100 mL).

The final product appears as a brilliant orange oil (yield 98%).

$^1\text{H-NMR}$ (400 MHz, CDCl_3): δ (ppm) 9.70 (d, $J = 1$ Hz, 2H), 8.38 (m, 2H), 7.93 (m, 2H), 6.30 (m, 2H), 5.6 (m, 2H), 3.4 (8H, t), 1.65 (8H, quintuplet), 1.48 (sextet, 8H), 1.12 (m, 12H).

➤ *Synthesis of complex 63_3.*



Dimer **63** (30.00 mg, 0.020 mmol) was dissolved in dry dichloromethane (8 mL) under nitrogen atmosphere. Tetrabutylammonium thiocyanate (122.00 mg, 0.400 mmol) was added to this solution.

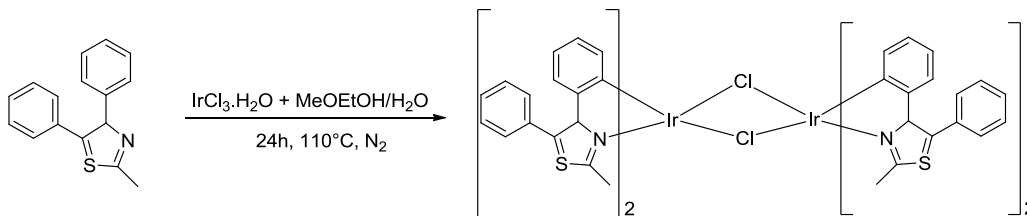
The reaction mixture was refluxed under stirring for 15 h. After, to the solution a 1:1 solvent mixture of diethyl ether and low-boiling petroleum ether (100 mL) was added. A yellow oil formed and the final product was recrystallized with dichloromethane/diisopropyl ether.

The final product appears as a yellow solid (yield 41%).

$^1\text{H NMR}$ (400 MHz, DMSO): δ (ppm) 9.86 (d, $J = 1$ Hz, 2H), 8.38 (m, 2H), 7.98 (m, 2H), 6.38 (m, 2H), 5.7 (m, 2H), 3.39 (m, 8H), 1.7 (quintuplet, 8H), 1.5 (sextet, 8H), 1.12 (m, 12 H).

3.2.6.5. Synthesis of complex **64_1**.

➤ *Synthesis of the dimer **64***

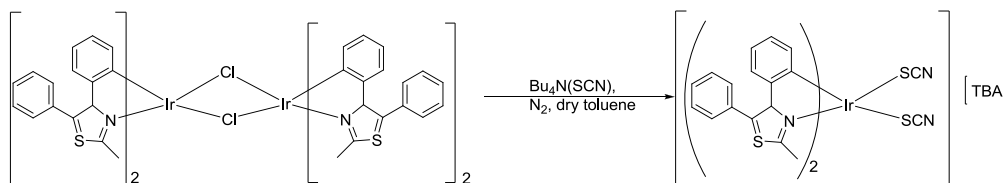


At room temperature, the Iridium trichloride (500.00 mg, 1.419 mmol) was dissolved in methoxyethanol (30 mL) and water (10 mL) under nitrogen atmosphere. 4,5-diphenyl-2-methylthiazole (848.00 mg, 3.35 mmol) was added to this solution. The reaction mixture was refluxed under stirring for 24 h. The solution was cooled down at room temperature and the yellow precipitate was filtered under nitrogen atmosphere. The precipitated was washed with 95% ethanol (60 mL) and acetone (60 mL) and then dissolved in dichloromethane (75 mL) and filtered. The desired product was obtained by evaporating the solvent.

The final product appears as yellow solid (yield 80%).

$^1\text{H-NMR}$ (400 MHz, DMSO): δ (ppm) 7.58 (s, 10H), 6.77 (d, $J = 6.55$ Hz, 1H), 6.59 (t, $J = 8.57$ Hz, 1H), 6.47 (t, $J = 7.64$ Hz, 1H), 6.17 (d, $J = 7.69$, 1H), 3.31 (s, 3H).

➤ *Synthesis of complex **64_1***



Dimer **64** (250.00 mg, 0.171 mmol) was dissolved in anhydrous dichloromethane (40 mL) under nitrogen atmosphere. Tetrabutylammonium thiocyanate (617.00 mg, 2.052 mmol) was added to this solution.

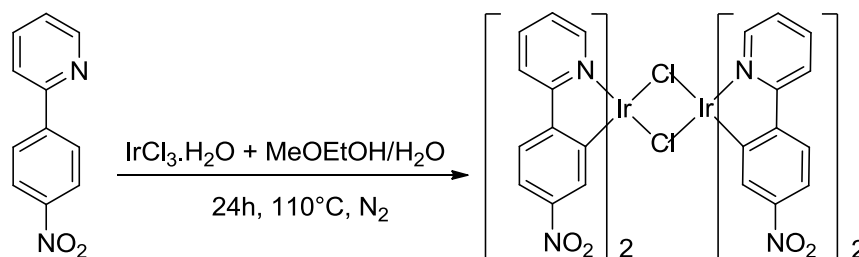
The reaction mixture was refluxed under stirring for 15 h. After, to the solution a 1:1 solvent mixture of diethyl ether and petroleum ether (100 mL) was added. A brown oil was formed, recrystallized with dichloromethane/diisopropyl ether.

The final product appears as a light brown solid (yield 8%).

$^1\text{H-NMR}$ (400 MHz, DMSO): δ (ppm) 7.58 (m, 6H), 6.77 (d, $J = 2$ Hz, 2H), 6.55 (td, $J = 2$ Hz, 2H), 6.43 (t, $J = 2$ Hz, 2H), 6.15 (d, $J = 2$ Hz, 2H), 3.18 (m, 8H), 3.05 (s, 3H), 1.58 (m, 8H), 1.32 (m, 8H), 0.94 (t, $J = 2$ Hz, 12 H).

3.2.6.6. Synthesis of complex 65_1.

➤ *Synthesis of the dimer 65*



At room temperature, the Iridium trichloride (73.55 mg, 0.209 mmol) was dissolved in methoxyethanol (60 mL) and water (20 mL) under nitrogen atmosphere. 2-(4-nitrophenyl)pyridine (125.20 mg, 0.626 mmol) was added to this solution. The reaction mixture was refluxed under stirring for 24 h. The solution was filtered off and the precipitated solid was washed with methanol and ethyl ether. The solid was air dried.

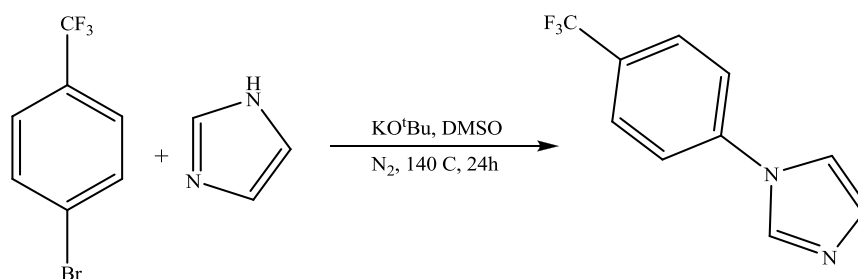
The final product appears as a red solid (yield 29 %).

¹H-NMR (400 MHz, DMSO): δ (ppm) 8.52 (d, $J = 8$ Hz, 2H), 8.50 (d, $J = 8$ Hz, 2H), 8.29 (dd, $J = 4$ Hz, $J = 2$ Hz, 2H), 8.27 (d, $J = 8$ Hz, 2H), 7.80 (m, 6H).

3.2.7. Synthesis of neutral homoleptic Ir(III) complex 59.

I report here the synthetic procedure of complex 59. The route for achieving complex 58, that I didn't do myself, is similar, but starting from 3-Bromobenzotrifluoride.

➤ *Synthesis of 1-(4-(trifluoromethyl)phenyl)-1H-imidazole.*



4-Bromobenzotrifluoride (1.00 g, 4.44 mmol, 1 equiv.), imidazole (0.36 g, 5.33 mmol, 1.2 equiv.) and anhydrous potassium *tert*-butoxide (0.59 g, 5.33 mmol, 1.2 equiv.) were added in nitrogen-degassed DMSO (10 mL). The mixture was purged with nitrogen by 10 evacuation-backfilling cycles of vacuum-N₂ and then heated to reflux at 140 °C for 24 h. The mixture was cooled down to room temperature and S-6 then filtered through celite. The residue was washed with DMSO (3 mL) and to the combined filtrate and the washings were added ice-cold distilled water (50 mL) and

DCM (100 mL). The organic layer was separated out and the aqueous layer was re-extracted with DCM (2 x 20 mL). The combined organic layers were evaporated to give a pale-yellow oil. The crude product was purified by silica column chromatography using 30% ethyl acetate in hexanes to afford the product as a white solid.

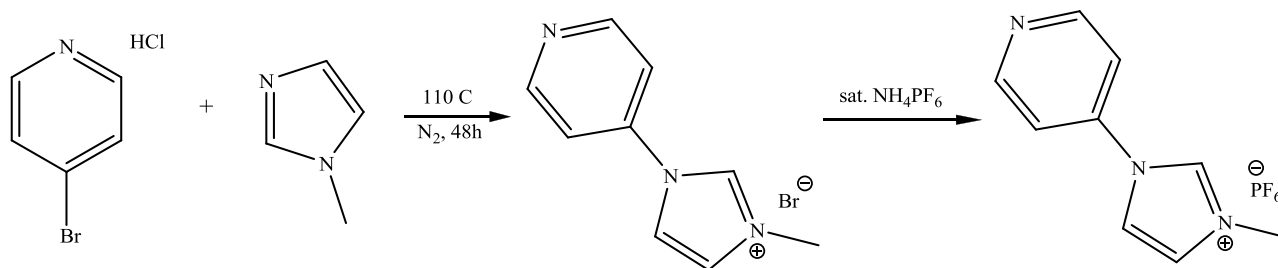
Yield: 0.414 g, 44%. Rf: 0.2 (30% EtOAc/hexanes on SiO₂). Mp: 69-71 °C.

¹H-NMR (500 MHz, CDCl₃) δ (ppm): 7.92 (d, *J* = 1.8 Hz, 1H), 7.76 (d, *J* = 7.9 Hz, 2H), 7.52 (d, *J* = 8.0 Hz, 2H), 7.33 (q, *J* = 1.4 Hz, 1H), 7.25 – 7.22 (m, 1H).

¹³C-NMR (126 MHz, CDCl₃) δ (ppm): 140.09, 135.55, 131.22, 128.76 (q, ²J_{C-F} = 34 Hz), 127.41, 123.78 (q, ¹J_{C-F} = 273 Hz), 121.45, 118.02.

¹⁹F-NMR (470 MHz, CDCl₃) δ (ppm): -62.49.

➤ *Synthesis of 3-methyl-1-(4-(trifluoromethyl)phenyl)-1H-imidazol-3-ium hexafluorophosphate.*



1-(4-(trifluoromethyl)phenyl)-1H-imidazole (2.00 g, 9.43 mmol, 1 equiv.) was suspended in MeCN (40 mL) and to it was added methyl iodide (4.01 g, 1.75 mL, 28.28 mmol, 3 equiv.). The mixture was purged with nitrogen by 3 evacuation-backfilling cycles of vacuum-N₂ and then heated to 40 °C under N₂ for 20 h while a clear pale-yellow solution was obtained. The mixture was cooled down to room temperature and the volatiles were evaporated to dryness under reduced pressure. To the resulting light brown solid an aliquot (60 mL) of saturated solution of NH₄PF₆ in water was added and the mixture was sonicated with hand-stirring for two minutes. The resulting light-brown microcrystalline precipitate was filtered out, washed with water (2 x 40 mL) and dried under vacuum to afford the product as a light-brown microcrystalline solid.

Yield: 3.29 g, 94%. Mp: 128-130 °C.

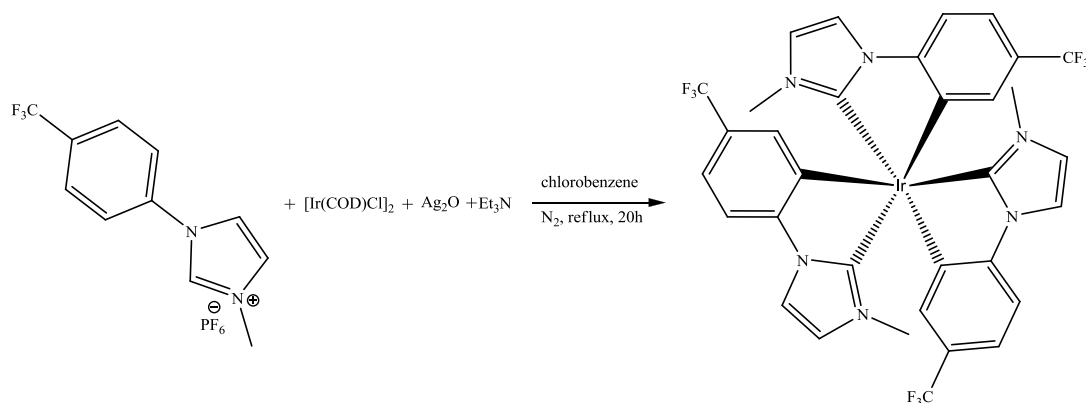
¹H-NMR (500 MHz, DMSO-*d*₆) δ (ppm): 9.86 (d, *J* = 1.7 Hz, 1H), 8.38 (t, *J* = 1.9 Hz, 1H), 8.10 (d, *J* = 8.5 Hz, 2H), 8.01 (d, *J* = 8.5 Hz, 2H), 7.98 (t, *J* = 1.8 Hz, 1H), 3.96 (s, 3H).

¹³C-NMR (126 MHz, DMSO-*d*₆) δ (ppm): 137.85, 136.57, 129.80 (q, ²J_{C-F} = 32 Hz), 127.51, 124.65, 123.66 (q, ¹J_{C-F} = 272 Hz) 122.71, 120.96, 36.28.

¹⁹F-NMR (470 MHz, DMSO-*d*₆) δ (ppm): -61.11, -70.13 (d, ¹J_{F-P} = 712 Hz).

HR NSI+ MS: $[M-PF_6]^+$ Calculated: $(C_{11}H_{10}N_2F_3)$ 227.0791; Found: 227.0789. Anal. Calcd. for $C_{11}H_{10}N_2PF_6$: C, 35.50; H, 2.71; N, 7.53; Found: C, 35.66; H, 2.73; N, 7.48.

➤ *Synthesis of complex 59.*



A mixture of 3-methyl-1-(4-(trifluoromethyl)phenyl)-1*H*-imidazol-3-ium hexafluorophosphate, (0.60 g, 1.69 mmol, 6 equiv.), silver(I) oxide (0.39 g, 1.69 mmol, 6 equiv.) and triethylamine (0.17 g, 0.24 mL, 1.69 mmol, 6 equiv.) in chlorobenzene (30 mL) was purged with nitrogen by 3 evacuation backfilling cycles of vacuum- N_2 and then heated to 60 °C under N_2 for 30 min to give a grey suspension. The reaction was cooled down to room temperature and to it was added $[Ir(COD)Cl]_2$ (COD = 1,5-cyclooctadiene) (0.19 g, 0.28 mmol, 1 equiv.) and chlorobenzene (10 mL) while an immediate colour change to yellowish-grey was observed. The mixture was again purged with nitrogen by 5 evacuation backfilling cycles of vacuum- N_2 and then heated to reflux under N_2 for 20 h, after which time, the solution was cooled down to room temperature. The reaction mixture was then filtered through a pad of celite and the residue was washed with DCM (2 x 30 mL). The combined filtrate and the washings were evaporated to dryness to give a brown oil. From this crude mixture of *mer*- and *fac*-isomers, the *mer*-isomer was purified by silica column chromatography using a mixture of DCM and hexanes (2:3, v/v) as the eluant. The *mer*-isomer was obtained as a white solid and can further be purified by bulk crystallisation using vapour diffusion of hexanes into a concentrated solution of the title compound, **59**, in ethyl acetate as colourless block crystals.

Yield: 0.413 g, 85%. Rf: 0.42 (1:1, v/v, DCM:hexanes on SiO_2). Mp: 348 °C (dec.).

1H -NMR (500 MHz, CD_2Cl_2) δ (ppm): 7.52 (dd, $J = 7.9, 2.1$ Hz, 2H), 7.45 (d, $J = 2.1$ Hz, 1H), 7.21 (qd, $J = 8.0, 3.4$ Hz, 4H), 7.15 – 7.12 (m, 2H), 7.03 (d, $J = 2.0$ Hz, 1H), 6.95 (d, $J = 2.1$ Hz, 1H), 6.86 (dd, $J = 6.3, 2.1$ Hz, 2H), 6.80 (dd, $J = 7.0, 1.9$ Hz, 2H), 3.09 (s, 3H), 3.00 (s, 3H), 2.94 (s, 3H).

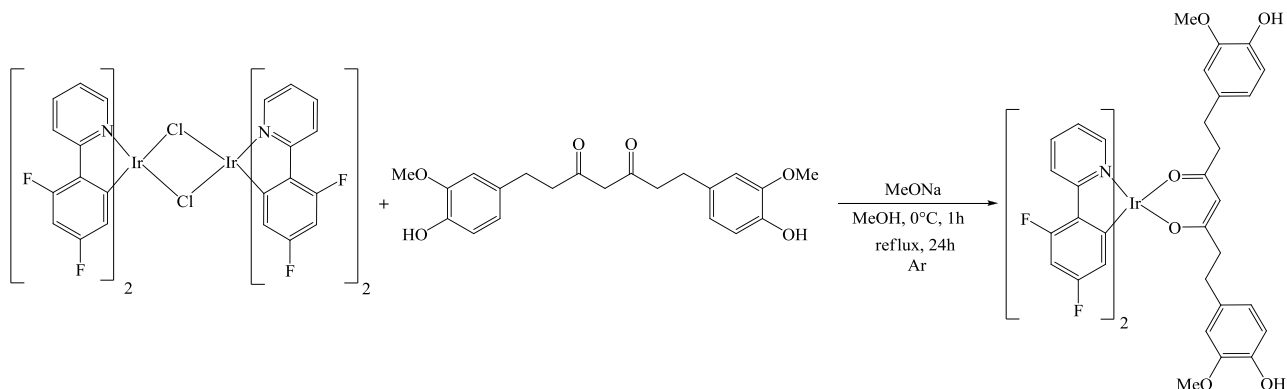
^{13}C -NMR (126 MHz, CD_2Cl_2) δ (ppm): 174.60, 172.88, 172.11, 151.29, 150.99, 150.64, 149.93, 149.89, 148.54, 135.54, 135.33, 133.51, 127-126 (m, overlapping CCF₃ signals), 122.16, 122.01,

121.64, 118.41, 118.38, 118.21, 115.20, 115.17, 115.10, 110.61, 110.51, 110.03, 37.40, 37.38, 36.45. CF₃ signals were not detected due to the weak signals resulting from coupling to ¹⁹F.

¹⁹F-NMR (470 MHz, CD₂Cl₂) δ (ppm): -61.54, -61.60, -61.76.

HR-ASAP+ MS: [M+H]⁺ Calculated: (C₃₃H₂₅N₆F₉Ir) 869.1626; Found: 869.1630. Anal. Calcd. for C₃₃H₂₄N₆F₉Ir.H₂O: C, 44.75; H, 2.96; N, 9.49; Found: C, 45.01; H, 2.83; N, 9.32.

3.2.8. Synthesis of the neutral heteroleptic Ir(III) complex **70**.



Tetrahydrocurcumin (37.25 mg, 0.1 mmol) was dissolved in methanol (3 mL) and NaOMe (5.40 mg, 0.1 mmol) was added. The mixture was stirred for 1 h at 0°C and then dimer **60** (see par. 3.2.6.3.) (60.00 mg, 0.05 mmol) was added. The resulting yellow solution was stirred at reflux for 24 h. The yellow precipitate was filtered and then was dissolved in the minimum amount of dichloromethane and precipitated with diethylether. The pure product was obtained as an orange precipitate in 51 % yield.

¹H-NMR (400 MHz, CD₃CN): δ (ppm) 8.24 (d, J= 8.2 Hz, 2H), 8.14 (d, J= 4.8 Hz, 2H), 7.93 (t, J= 8.2 Hz, 2H), 7.20 (t, J= 5.8 Hz, 1H), 6.81 (d, J= 8.7 Hz, 2H), 6.72 (d, J= 7.71 Hz, 2H), 6.68 (m, 4H), 6.60 (d, J= 8.7 Hz, 2H), 6.49 (dd, ¹J= 10.6 Hz, ²J= 2.4 Hz, 2H), 6.34 (dd, ¹J= 9.6 Hz, ²J= 1.9 Hz, 2H), 5.64 (dd, ¹J= 9.6 Hz, ²J= 2.4 Hz, 2H), 5.38 (s, 1H), 3.76 (s, 6H), 2.58 (m, 4H), 2.37 (m, 2H), 2.29 (m, 2H).

¹³C-NMR (100.6 MHz, CD₃CN): δ (ppm) 187.2.8, 164.3, 162.5, 162.2 (d, ¹J_{C-F} = 245 Hz), 160.9, 160.5 (d, ¹J_{C-F} = 245 Hz), 148.4, 146.9, 144.1, 138.7, 132.9, 122.7, 122.5, 120.4, 114.7 (d, ²J_{C-F} = 17 Hz), 114.4, 111.9, 110.1, 96.9 (t, ²J_{C-F} = 26 Hz), 56.5, 42.2, 31.5.

3.3. X-ray Crystallography of complexes **58** and **59**.

Single crystals were grown by vapour diffusion of petroleum ether into a concentrated dichloromethane solution of **58**, or by vapour diffusion of petroleum ether into a concentrated

ethyl acetate solution of **59**. Data were collected at 173 K using a Rigaku FR-X Ultrahigh brilliance Microfocus RA generator/confocal optics with XtaLAB P200 diffractometer [Mo K α radiation ($\lambda = 0.71075 \text{ \AA}$)]. Intensity data were collected using ω steps accumulating area detector images spanning at least a hemisphere of reciprocal space. Data for all compounds analysed were collected and processed (including correction for Lorentz, polarization and absorption) using CrystalClear. Structures were solved by either direct (SIR2004)⁸ or Patterson methods (PATTY)⁹ and refined by full-matrix leastsquares against F² (SHELXL-2018/3)¹⁰. Non-hydrogen atoms were refined anisotropically, and hydrogen atoms were refined using a riding model. The structure of **58** showed voids, 925 Å³, 12.9 % of the unit cell volume, and the SQUEEZE¹¹ routine implemented in PLATON¹² was used to remove the contribution of the unordered electron density in the void spaces. Additionally, disorder was found in several of the CF₃ groups, and restraints to bond-distances and angles, as well as enhanced rigid bond restraints and other restraints to thermal motion were required. In **59**, two of the CF₃ groups showed disorder. All calculations were performed using the CrystalStructure¹³ interface. Selected crystallographic data are presented in Table 16. CCDC 1852488-1852489 contains the supplementary crystallographic data for this paper. The data can be obtained free of charge from The Cambridge Crystallographic Data Centre via www.ccdc.cam.ac.uk/structures.

The Ir(III) ion in **58** and **59** exhibits a coordinatively saturated, distorted octahedral coordination environment, unambiguously showing the *mer*-geometry of the complexes. The C[^]C: ligands in both *mer*-**58** and **-59** are twisted from planarity around the bridging Caryl-C: bond (dihedral angles vary between 1.280 – 7.340 for **58** and between 1.700 – 3.990 for **59**). This variation in ligand distortion is most likely due to crystal packing effects. As a result of the five-membered structure of imidazole ring, CIm–Ir–Caryl angles are all less than 80° (Table 17). The average Ir–Ccarbene: bond distance (2.057 Å in **58** and 2.035 Å in **59**) was found to be slightly shorter than the average Ir–Caryl distance (2.087 Å in **58** and 2.091 Å in **59**) indicating that the carbenic-carbon atom of the imidazolyl group is a stronger donor than the cyclometalating C-atom of the aryl ring.¹⁴ The bond length of Ir–Caryl *trans* to imidazolyl (Ir1-C14 = 2.082(15) Å in **58** and Ir1-C22 = 2.084(5) Å in **59**) is greater than the bond length of Ir–Caryl *trans* to the pyrazolyl group in another deep blue emitter *mer*-Ir(ppz)₃ (Ir-C3 = 1.993(2) Å,) (ppz = 1- phenylpyrazolyl-*N,C2'*, *l*_{max} in 2-MeTHF = 427 nm at 77 K),¹⁵ illustrating the stronger *trans* influence of the carbene ligand over that of pyrazolyl.¹⁶ These Ir1-C14 in **58** and Ir1-C22 in **59** distances are very similar to the bond length of Ir–Caryl *trans* to benzimidazolyl group (Ir-C2 = 2.078(4) Å) in **66** (see Chapter 2, par. 2.3.1),¹⁶ suggesting similar *trans* effects of carbonic-imidazolyl and -benzimidazolyl groups. The lengths of the mutually *trans* Ir–Caryl bonds (Ir1-C4 and Ir1-C13, average (avg) = 2.089 Å in **58**; Ir1-C19 and Ir1-C30, avg = 2.095 Å in **59**) in **58** and **59** are slightly longer than

those in *mer*-Ir(ppz)₃ (avg = 2.040 Å) and similar to those in **66** (Ir-C1 and Ir-C3, average (avg) = 2.093 Å), indicating greater electron donation from the carbenic-imidazolyl group than from the pyrazolyl moiety and similar donation in comparison to carbenic-benzimidazolyl group.¹⁶ The bond length differences suggest that the cyclometalated carbenes are stronger field ligands than their pyrazolyl or pyridyl counterparts, and therefore, complexes **58** and **59** should have high energy ligand field states.

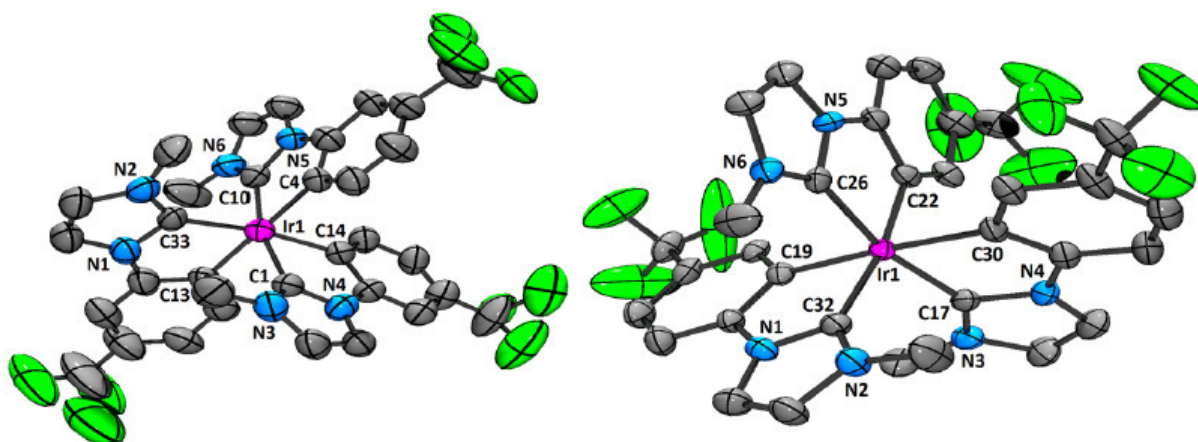


Figure 67. Representation of the molecular structures of molecule 1 of complex **58** (left) and complex **59** (right) with hydrogen and solvent atoms omitted to aid with clarity and ellipsoids drawn at 50 % probability. Key atoms are labelled and all atoms are color coded: grey – carbon, blue – nitrogen, green – fluorine, magenta – iridium.

compound	58	59
empirical formula	C _{33.25} H _{24.5} Cl _{0.5} F ₉ IrN ₆	C ₃₅ H ₂₈ F ₉ IrN ₆ O
FW	889.03	911.85
cryst syst	Triclinic	monoclinic
space group	P $\bar{1}$ (#2)	I2/a (#15)
a [Å]	17.8833(11)	18.0556(18)
b [Å]	18.0588(15)	20.6967(12)
c [Å]	23.0188(17)	21.1495(16)
α [°]	87.076(5)	
β [°]	74.304(4)	108.149(6)
γ [°]	89.485(5)	
vol [Å ³]	7147.3(9)	7510.2(11)
Z	8	8
ρ (calc) [Mg/m ³]	1.652	1.613
μ [mm ⁻¹]	3.863	3.646
F (000)	3460	3568
cryst	colorless, prism	colorless, prism
cryst size [mm ³]	0.12 × 0.03 × 0.01	0.21 × 0.07 × 0.06
θ range	1.684 – 25.400°	1.968 – 25.396°
reflns collected	143417	45592
indep reflns (R _{int})	26089 (0.0793)	6868 (0.0220)
Data/restraints/params	26089 / 1004 / 1868	6868 / 0 / 555
GOF on F ²	1.174	1.090

final R indices	R1 = 0.0908	R1 = 0.0213
[I > 2σ(I)]	wR2 = 0.2121	wR2 = 0.0643
R indices	R1 = 0.1186	R1 = 0.0241
(all data)	wR2 = 0.2883	wR2 = 0.0660
largest diff. peak/hole [e/ Å ³]	3.17 / -2.38	1.36 / -0.32

Table 16. Crystal Data and Structure Refinement.

Compound	Bond Length (Å)			Angle (°)		
		Obs. (X-Ray)	Calc. (DFT)		Obs. (X-Ray)	Calc. (DFT)
58	Ir1-C1 _{Im}	2.059(14)	2.060	C1 _{Im} -Ir1-C14 _{Ar}	79.0(6)	78.05
	Ir1-C14 _{Ar}	2.082(15)	2.102	C10 _{Im} -Ir1-C4 _{Ar}	77.8(6)	77.85
	Ir1-C4 _{Ar}	2.080(15)	2.126	C33 _{Im} -Ir1-C13 _{Ar}	78.1(7)	77.59
	Ir1-C10 _{Im}	2.029(14)	2.063			
	Ir1-C13 _{Ar}	2.099(16)	2.131			
	Ir1-C33 _{Im}	2.031(15)	2.096			
59	Ir1-C17 _{Im}	2.034(5)	2.064	C17 _{Im} -Ir1-C30 _{Ar}	77.80(19)	77.80
	Ir1-C30 _{Ar}	2.097(5)	2.126	C32 _{Im} -Ir1-C19 _{Ar}	78.17(19)	77.59
	Ir1-C32 _{Im}	2.051(5)	2.092	C26 _{Im} -Ir1-C22 _{Ar}	78.47(19)	77.94
	Ir1-C19 _{Ar}	2.093(4)	2.132			
	Ir1-C26 _{Im}	2.021(5)	2.058			
	Ir1-C22 _{Ar}	2.084(5)	2.103			

Table 17. Comparison of observed bond distances and angles in complexes 58 (molecule 1) and 59 with values calculated for these complexes [Restricted DFT calculations of 58 and 59 (B3LYP/SBKJC-VDZ[Ir]6-31G[C,H,N,F]), Ar = cyclometalating aryl group, Im = carbenic imidazolyl group].**

3.4. DFT calculations of complexes 58 and 59.

All calculations were performed with the Gaussian09, revision D.01[17] suite of programs employing the DFT method, the Becke three-parameter hybrid functional,[18] and Lee-Yang-Parr's gradient-corrected correlation functional (B3LYP).[19] Singlet and triplet ground state geometry optimizations and single point energy calculations for **58**, **59** and **66** were carried out at the (R)B3LYP and (U)B3LYP levels, using their respective crystallographic structures as starting points. All elements except Iridium were assigned the 6-31G(d,p) basis set.[20] The double- ζ quality SBKJC VDZ ECP basis set[21] with an effective core potential was employed for the Ir(III)-ion. Vertical electronic excitations based on (R)B3LYP optimized geometries were computed for **58**, **59** and **66** using the TD-DFT formalism[22] in dichloromethane using conductor-like polarizable continuum model (CPCM).[23] Vibrational frequency calculations were performed to ensure that the optimized geometries represent the local minima and there are only positive eigenvalues. The electronic distribution and localization of the singlet excited states

were visualized using the electron density difference maps (ED-DMs).^[24] *Gausssum 2.2* and *Chemissian v3.8*^[25] were employed to visualize the absorption spectra (simulated with Gaussian distribution with a full-width at half maximum (fwhm) set to 3000 cm⁻¹) and to calculate the fractional contributions of various groups to each molecular orbital. All calculated structures and Kohn-Sham orbitals were visualized with ChemCraft.^[26]

3.5. OLEDs fabrication.

- *Compounds synthesized in St. Andrews*

The OLED devices were fabricated in bottom-emitting architecture via vacuum sublimation in high vacuum at a base pressure of $2-5 \times 10^{-7}$ mbar. The organic layer sequence and the metal cathode were deposited onto pre-cleaned glass substrates coated with indium tin oxide (ITO) which has a sheet resistance of 30 Ω /sq. A pre-patterned ITO glass substrate was treated by ultrasonic cleaning in acetone and isopropanol consecutively and then treated by oxygen plasma before the transfer to the vacuum chamber. The general device structure was the following: ITO (90 nm)/HTL/EBL (10 nm)/DPEPO:*meta*-IrNHC (20 nm, 10 wt%)/TPBi (30 nm)/LiF (1 nm)/Al (100 nm). Here TPBi stands for (1,3,5-tris(1-phenyl-1H-benzimidazol-2-yl) benzene) and is used as an electron transporting layer.

HTL of devices I and II consists of 20 nm of N,N'-bis(naphthalen-1-yl)-N,N'-bis(phenyl)-benzidine (NPB) and 20 nm of tris(4-carbazoyl-9-ylphenyl)amine (TCTA). Device III uses 15 nm of CzSi doped with 15 wt% of molybdenum oxide (MoO₃) as a hole injection layer followed by 10 nm of hole transporting CzSi, similar to the structure used by Adachi.²⁷ 4,4'-Cyclohexylidene-bis[N,N-bis(4-methylphenyl)benzenamine] (TAPC) was used as HTL in devices IV and V, similar to the structure used by Adachi.²⁸ CzSi was used as EBL in Device I, while **58** was employed as EBL in devices II-IV. No EBL is used in Device V.

Organic layers were deposited at a rate of 0.3-0.6 Å/s, which was controlled in situ using the quartz crystal monitor. Doping of the emission layers was achieved through co-evaporation of the emitter and host materials. Electron injection layer LiF was deposited at a rate of 0.05 Å/s while the Al cathode was deposited at a rate of 2 Å/s through the shadow mask defining the top electrode. The spatial overlap of the anode and cathode electrodes determined the active area of the OLED which was estimated to be 2 mm². All the devices were encapsulated with UV epoxy resin inside the inert atmosphere. The luminance-current-voltage characteristics were measured in an ambient environment using Keithley 2400 source meter and Keithley 2000 multimeter connected to a calibrated Si photodiode. The external quantum

efficiency was calculated assuming Lambertian emission distribution. The electroluminescence spectra were recorded by an Andor DV420-BV CCD spectrometer.

3.6. Internalization studies.

- **Cell lines**

A549 cells were maintained in monolayer cultures in Dulbecco's Modified Eagle's Medium (DMEM, Lonza) containing 10% fetal bovine serum and 2 mM L-glutamine. HeLa and T98G cells were cultured in Minimum Essential Medium Eagle (MEM, Biowest) containing 10% fetal bovine serum, 2 mM L-glutamine, 1 mM NaPyruvate and 0.1 mM NEAA (non-essential amino acids). All cell lines were authenticated at each batch freezing by STR profiling (StemElite ID System, Promega). All cell lines were tested for mycoplasma at each batch freezing with PCR and with a biochemical test (MycoAlert, Lonza).

- **Cellular uptake and staining**

To examine the cellular permeability of the synthesized compounds A549 and HeLa cells were used. Cells were seeded in 6-well plates with coverslips and incubated at 37°C. After 24 h, medium was removed and cells were incubated with various compounds at different concentrations for 2 h. Once the incubation was completed, the cells were fixed with 4% paraformaldehyde for 10 min and then incubated with the nuclear staining DAPI for 10 min. Coverslips were mounted in a glycerol solution (20% glycerol, 50 mM, Tris pH = 8.4) to avoid mechanical deformation of the sample. Images were captured using a Leica inverted SP2 microscope with a laser scanning confocal system. Analysis was performed with ImageJ (<http://imagej.nih.gov/ij/>).

- **Time lapse experiments**

Cells were seeded into 12 or 24-well plates and incubated overnight at 37°C. Cells were then treated with the indicated compounds at different concentrations 2 h before the time-lapse recording. To set the conditions, cells were irradiated with different excitation filters (360-370 nm, 465-495 nm and 530-560 nm) and time (0.5s, 1s and 2s) using an inverted motorised microscope Olympus IX81, an illumination source MT20 with a 150 W xenon lamp and a 10x phase contrast objective UplanFL N 0.3 N.A. Images were acquired every 15 min for 24 or 48 h. Live-cell imaging was performed with the same microscope equipped with closed heating and CO₂

perfusion devices. In the subsequent experiments, cells were irradiated with the 465–495 nm filter for 2 s or for 10 or 20.

- **Cell viability (MTT and CCK8) assays**

Exponentially growing A549 or HeLa cells were seeded in 96-well plates (1250 cells/well) and incubated overnight at 37°C. The cells were then treated with different concentrations of the synthesized photosensitizers (in triplicates) for 2 h. Cells were either left untreated or irradiated with 465–495 nm filter using a timelapse microscope, illuminating the entire surface of each well for 2 s. The cells were then incubated for 48 h in the dark at 37°C.

To determine cell viability, a dehydrogenase-based assay (CCK-8 assay, Dojindo) was performed according to the manufacturer. After 2.5 h of incubation with the CCK-8 solution, measurement of O.D. at 450 nm was performed with Victor³ multilabel microplate reader (PerkinElmer). Absorbance is proportional to the number of viable cells. LD₅₀ was calculated as the concentration of the compound that determines 50% of the absorbance of the control cells. Experiments are repeated three times. Examples of the results obtained upon irradiation are reported in Figure 68.

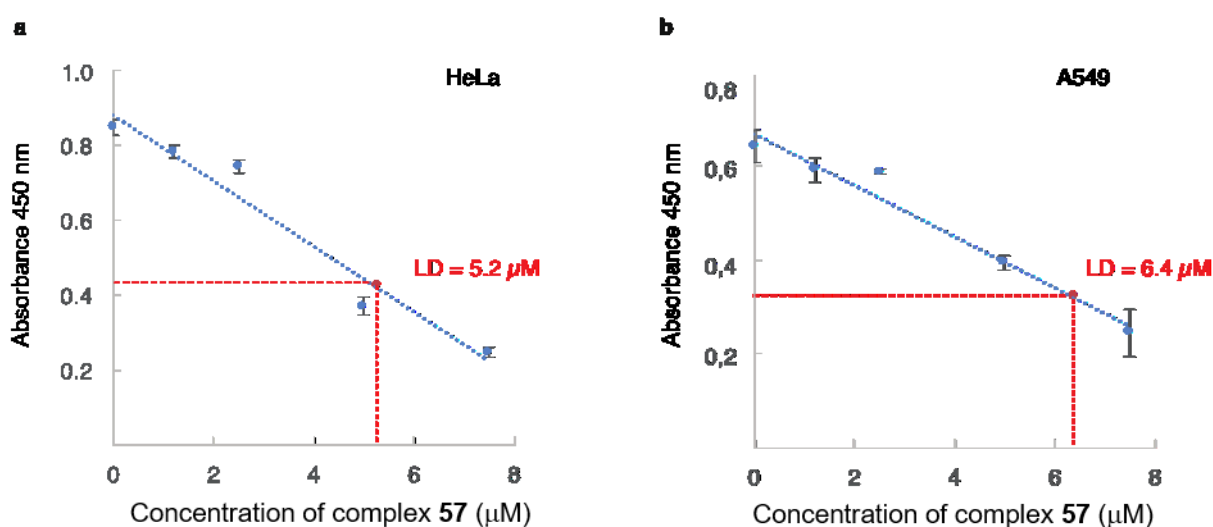


Figure 68. Examples of cytotoxicity assay (CCK-8 assay) performed in HeLa and A549 cells.

For toxicity evaluation of the synthesized compounds in the dark an MTT assay (Thiazolyl Blue Tetrazolium Bromide, Sigma) was also used. Briefly, cells were treated with different concentrations of the synthesized photosensitizers for 48 hours. MTT solution (5mg/mL in PBS) was added to the medium and cells were incubated at 37° C for 4 hours to allow the conversion of

the soluble MTT into water-insoluble MTT formazan by mitochondrial dehydrogenases of living cells. The medium was then removed and the blue crystals were solubilized by addition of DMSO. The plate was put on a shaker for 10 minutes and O.D. was measured at 570 nm.

3.7. References.

1. G. A. Crosby, J. N. Demas, *J. Phys. Chem.* **1971**, 75, 991.
2. W. H. Melhuish, *J. Phys. Chem.* **1961**, 65, 229.
3. N. C. Greenham, I. D. W. Samuel, G. R. Hayes, R. T. Phillips, Y. A. R. R. Kessener, S. C. Moratti, A. B. Holmes, R. H. Friend, *Chem. Phys. Lett.* **1995**, 241, 89.
4. V. V. Pavlishchuk, A. W. Addison, *Inorg. Chim. Acta* **2000**, 298, 97.
5. a) C. G. Bethea B. F. Levine, *Appl. Phys. Lett.* **1974**, 24, 445–447; b) C. G. Bethea B. F. Levine. *J. Chem. Phys.* **1975**, 62, 2666–2682; c) J. Zyss I. Ledoux, *J. Chem. Phys.* **1982**, 73, 203–213.
6. J. K. Groves, *Chem. Soc. Rev.* 1972, 1, 73.
7. N. Hogihara, K. Sonogashira, Y. Tohda, *Tetrahedron Lett.*, **1975**, 16, 4464.
8. M. C. Burla, R. Caliandro, M. Camalli, B. Carrozzini, G. L. Casciarano, L. De Caro, C. Giacovazzo, G. Polidori, R. Spagna, *J. Appl. Crystallogr.* **2005**, 38, 381.
9. H. Poisel, U. Schmidt, *Angew. Chem., Int. Ed. Engl.* **1971**, 10, 130.
10. G. Sheldrick, *Acta Crystallogr., Sect. C: Cryst. Struct. Commun.* **2015**, 71, 3.
11. A. Spek, *Acta Crystallogr., Sect. C: Cryst. Struct. Commun.* **2015**, 71, 9.
12. A. Spek, *Acta Crystallographica Section D* **2009**, 65, 148.
13. W. J. Hehre, R. Ditchfield, J. A. Pople, *J. Chem. Phys.* **1972**, 56, 2257.
14. T.-Y. Li, X. Liang, L. Zhou, C. Wu, S. Zhang, X. Liu, G.-Z. Lu, L.-S. Xue, Y.-X. Zheng, J.-L. Zuo, *Inorganic Chemistry* **2015**, 54, 161.
15. A. B. Tamayo, B. D. Alleyne, P. I. Djurovich, S. Lamansky, I. Tsyba, N. N. Ho, R. Bau, M. E. Thompson, *Journal of the American Chemical Society* **2003**, 125, 7377.
16. T. Sajoto, P. I. Djurovich, A. Tamayo, M. Yousufuddin, R. Bau, M. E. Thompson, R. J. Holmes, S. R. Forrest, *Inorganic Chemistry* **2005**, 44, 7992.
17. M. J. Frisch, G. W. Trucks, H. B. Schlegel, G. E. Scuseria, M. A. Robb, J. R. Cheeseman, G. Scalmani, V. Barone, B. Mennucci, G. A. Petersson, H. Nakatsuji, M. Caricato, X. Li, H. P.

Hratchian, A. F. Izmaylov, J. Bloino, G. Zheng, J. L. Sonnenberg, M. Hada, M. Ehara, K. Toyota, R. Fukuda, J. Hasegawa, M. Ishida, T. Nakajima, Y. Honda, O. Kitao, H. Nakai, T. Vreven, J. A. Montgomery, J. E. Peralta, F. Ogliaro, M. Bearpark, J. J. Heyd, E. Brothers, K. N. Kudin, V. N. Staroverov, R. Kobayashi, J. Normand, K. Raghavachari, A. Rendell, J. C. Burant, S. S. Iyengar, J. Tomasi, M. Cossi, N. Rega, J. M. Millam, M. Klene, J. E. Knox, J. B. Cross, V. Bakken, C. Adamo, J. Jaramillo, R. Gomperts, R. E. Stratmann, O. Yazyev, A. J. Austin, R. Cammi, C. Pomelli, J. W. Ochterski, R. L. Martin, K. Morokuma, V. G. Zakrzewski, G. A. Voth, P. Salvador, J. J. Dannenberg, S. Dapprich, A. D. Daniels, Farkas, J. B. Foresman, J. V. Ortiz, J. Cioslowski, D. J. Fox, Wallingford CT, **2009**, citeulike-article-id:9096580.

18. A. D. Becke, *The Journal of Chemical Physics* **1993**, *98*, 5648.
19. C. Lee, W. Yang, R. G. Parr, *Physical Review B* **1988**, *37*, 785.
20. A. D. McLean, G. S. Chandler, *The Journal of Chemical Physics* **1980**, *72*, 5639.
21. J. S. Binkley, J. A. Pople, W. J. Hehre, *Journal of the American Chemical Society* **1980**, *102*, 939.
22. a) M. E. Casida, C. Jamorski, K. C. Casida, D. R. Salahub, *J. Chem. Phys.* **1998**, *108*, 4439; b) R. E. Stratmann, G. E. Scuseria, M. J. Frisch, *J. Chem. Phys.* **1998**, *109*, 8218.
23. a) M. Cossi, N. Rega, G. Scalmani, V. Barone, *J. Comput. Chem.* **2003**, *24*, 669; b) M. Cossi, V. Barone, *The Journal of Chemical Physics* **2001**, *115*, 4708; c) V. Barone, M. Cossi, *J. Phys. Chem. A* **1998**, *102*, 1995.
24. W. R. Browne, N. M. O'Boyle, J. J. McGarvey, J. G. Vos, *Chem. Soc. Rev.* **2005**, *34*, 641.
25. F. Seel, W. Gombler, R. Budenz, *Liebigs Ann. Chem.* **1970**, *735*, 1.
26. Q. E. Thompson, *Quarterly Reports on Sulfur Chemistry* **1970**, *5*, 245.
27. Q. Zhang, B. Li, S. Huang, H. Nomura, H. Tanaka, C. Adachi, *Nature Photonics* **2014**, *8*, 326.
28. C.-Y. Chan, L.-S. Cui, J. U. Kim, H. Nakanotani, C. Adachi, *Adv. Funct. Mater.* **2018**, *28*, 1706023.

Ringraziamenti

Per avermi guidato in questi tre anni, per i suggerimenti, per essere stata una magnifica supervisor e per la possibilità concessami in primo luogo vorrei ringraziare la Professoressa Dominique Roberto. Da ringraziare sono anche la Claudia, l'Ale, la Stefi e Dani che in questi anni, oltre ad avermi supportato e sopportato hanno fatto sì che i miei giorni in Università fossero sempre piacevoli, soprattutto in quest'ultimo periodo. Degni di una menzione sono anche la Franci e il Gabri, del gruppo della Professoressa Pizzotti, grazie per i consigli e per aver contribuito ad alleggerire i periodi più difficili. Vorrei citare nei miei ringraziamenti anche il Professor Giordano Lesma, che con i suoi preziosi suggerimenti mi ha aiutato a districarmi tra la chimica organica e con il quali ormai si è instaurato anche un bel rapporto. Vorrei ringraziare anche gli altri colleghi-dottorandi Sofia Capelli, Stefano Gazzotti, Davide Gornati, Massimo Bernareggi, Stefano Racioppi e Andrea Jouve, che hanno condiviso con me questi anni. Ringrazio tanto Pasquale, che oltre ad aver contribuito al mio progetto con tutti i suoi NMR, si è rivelato un ottimo amico e compagno di allenamenti, sia in pista, sia a tavola e che mi ha introdotto a quella che da qualche anno è diventata la mia passione: il Dragon Boat! Di seguito dunque, vorrei ringraziare tutti i Dragoni della Statale, che ai tempi mi hanno accolto benissimo, facendomi sentire subito parte del loro simpaticissimo gruppo. Dopo i Dragoni della Statale, con cui iniziai il mio percorso, voglio ringraziare la mia squadra dell'Idroscalo Club, con cui sudo, mi diverto e vinco; tra loro una menzione speciale va a Nico e Fra, che oltre ad essere compagni di squadra e di allenamenti, si sono rivelati anche due ottimi amici, sia nei momenti di svago, che per fortuna sono stati molti (e in questi vorrei inserire anche la Pricca, grazie), ma soprattutto nei momenti difficili, nei quali mi hanno sostenuto. Ringrazio a questo punto gli amici Abruzzesi, quelli storici di quando eravamo bambini: Sofia, Matteo, Gian Marco, ML ed Eleonora. Che dire...siete stati al mio fianco da sempre (chi più, chi meno), avete reso veramente indimenticabile e insostituibile tutto fin'ora e ogni volta che torno in Abruzzo lo faccio con il sorriso grazie a voi!!!

Ringrazio a questo punto Alessandra, la mia splendida ragazza, che in questi ultimi due anni mi ha dato amore, buonumore e supporto morale...anche se non sono facile da gestire, lei non demorde e continua a stare imperterrita al mio fianco.

La famiglia costituisce la base ed il sostegno fondamentale per vivere una vita degna di tale nome. Ringrazio quindi zie, zii e tutti i cugini, che non elenco, perché essendo io orgogliosamente terrone, sono davvero tanti. Ringrazio il nonno Raffaello, la nonna Laura, il nonno Giovanni e la nonna Marietta che mi vegliano da lassù. Ringrazio Dario, mio fratello, con cui ho convissuto in questi ultimi anni a Milano e che ha contribuito a non farmi sentire troppo la mancanza del nucleo familiare. Infine i miei ringraziamenti più grandi e sinceri vanno di sicuro ai miei genitori, Rosanna e Flavio, che mi hanno offerto e trasmesso tutto quello di cui un figlio può avere bisogno e anche molto di più, facendo innumerevoli sacrifici. Se sono quello che sono oggi, lo devo in gran parte a voi e ai vostri preziosi insegnamenti; per questo non finirò mai di dirvi grazie.

Molte persone sono passate nella mia vita: qualcuno ha poi intrapreso strade diverse, qualcun altro mi sta ancora accompagnando; per ringraziare tutti decentemente non bastano di sicuro queste quattro righe. Quelli che non sono stati qui nominati non si sentano offesi o dimenticati; provvederò in altri modi.

Non sono mai stato molto bravo ad esprimere i sentimenti, né tantomeno a metterli per iscritto, tuttavia spero che tutti quanti abbiano recepito il messaggio: dal profondo, grazie davvero.